Field Study of Capture Zones in a Shallow Sand Aquifer

by

William R. Linderfelt

Submitted in Partial Fulfillment of the

Requirements for the Degree of

Doctor of Philosophy

New Mexico Institute of Mining and Technology

Socorro, New Mexico

December 1994

ABSTRACT

Two field tracer experiments were conducted in a shallow sand aquifer located at the Borden site in Ontario, Canada. The overall goal of the study was to improve our understanding of the zone of contribution, or capture zone, produced by a pumping well. Capture zone analysis is an integral part of well head protection and aquifer remediation. Experimental results, and associated model comparisons, were aimed at assessment of data requirements for field delineation of a capture zone and validation of predictive capture zone models. Both experiments involved a single pumping well extracting water from an essentially uniform ambient flow field. The well was fully penetrating in the first experiment and partially penetrating in the second experiment. Seven fluorinated benzoic acid tracers and bromide were injected at 15 locations within and near the anticipated capture zone. Tracer breakthrough was monitored in multiple levels at the well, at a down-gradient multilevel monitoring fence, and in the vicinity of the pumping well. Total mass recovered at the well for each injection site indicated capture zone boundaries. With tracer at some sites showing zero capture at the well and other tracers showing distinct and separate breakthrough from each injection site, it was possible to assign recoveries to individual sites with a high level of confidence for most of the tracers in both experiments. The estimated tracer recoveries provided a direct estimate of the capture potential at those sites. The maps of the relative recoveries at each site allowed direct delineation of the capture zone in the field.

The two experiments were significantly influenced by transient conditions. Hydraulic gradients, calculated from measured head data, showed large seasonal fluctuations with the directional component varying up to 90 degrees, and higher frequency fluctuations varying by as much as 20 degrees over a one week period. The highly transient nature of the flow field increased the fuzziness of the capture zone boundary and also caused significant uncertainty in capture zone prediction when data needed to describe these transients was not available. In the first experiment, the transient flow direction caused the capture zone to be oriented approximately N25E to N30E, while the mean flow direction was N15E to N20E. This

suggests that steady-state capture zone models which use the mean flow direction may be in error in predicting the true capture zone orientation in a transient system. The width of the capture zone in the first experiment was estimated at approximately 2.5–3.0 m, which is smaller than the 5 m width estimated during the design of the experiment. The narrower measured capture zone was due to the changing flow direction and also higher hydraulic conductivity than was used to originally estimate the capture zone width. Steady-state capture zone models would predict a wider capture zone which would be conservative in terms of wellhead protection.

The first experiment was designed to represent an essentially two-dimensional flow system, allowing comparison between measured and simulated results using simple two-dimensional flow and transport models. Mass recovered at the pumping well and at multilevel samplers during the first experiment indicated that tracer plumes migrated vertically downward in the range of 0.25 m to 0.94 m. The plume sinkage was attributed to pumping in a vertically stratified aquifer, with the well acting as a flux boundary, and buoyancy effects caused by density contrasts between the tracer plumes and surrounding aquifer water. Vertical breakthrough profiles at the pumping well and multilevel samplers also indicated a vertically non-uniform flow field, with tracer arrival times varying with depth. In some instances, tracer recovery at the well was affected with plumes showing partial recovery due to vertical plume splitting indicating a distinct lower conductivity zone at depth overlain by the more typical, higher conductivity Borden sand. In a real system without vertical resolution of breakthrough in the well, the vertical plume splitting could be incorrectly interpreted as lateral splitting, causing misconceptualization of the capture zone. The second experiment was designed to represent a partially-penetrating well located in an aquifer exhibiting largely two-dimensional flow characteristics. The well was screened over the upper portion of the aquifer. The capture zone for this system did not intercept the bottom of the aquifer, allowing injected tracer to migrate below the capture zone and to not be recovered by the pumping well. This loss of tracer was enhanced by density contrasts between the injected

tracer plume and the background aquifer water, causing the plume to partially or fully migrate outside the capture zone.

Modeling of the first experiment used both two- and three-dimensional transient transport models. The second experiment was simulated using only the three-dimensional model. The models were either partially or completely calibrated, with simulations giving the smallest errors considered representative of the 'best fit' model. Model input included hydraulic conductivity, ambient gradient, dispersivity, aquifer thickness, and porosity. In general, there was good agreement between observed and simulated tracer breakthrough and recovery behavior. The model results were assessed using two methods. Relative recovery error is the error in predicting overall tracer recovery normalized by the total tracer mass recovered, while relative breakthrough error indicates the inability of the model to predict the time-sequence of mass breakthrough at the well, and is an indication of the error in travel time prediction. The relative recovery error of two- and three-dimensional transient transport models ranged from 0.10 to 0.15 in Experiment 1 and was at least 0.50 in Experiment 2, depending on the input data set used. The relative breakthrough error was approximately 0.55 in Experiment 1 and 1.00 in Experiment 2. The relative breakthrough error was much larger than the relative recovery error due to the insensitivity of the models to input parameters when determining time-independent recoveries as compared to the time-sequence of mass breakthrough.

The model results for the first experiment were compared to purely predictive model results obtained from a simple capture zone model commonly used in capture zone prediction. Three simulations of the simple model, representing three *a priori* data sets, gave relative recovery errors of 0.22 for two data sets, and 0.60 for the third data set. The third data set giving the poorest result, obtained from the well known Waterloo-Stanford experiments conducted at the Borden site, was also the oldest data set and did not reflect the more recent trends in the highly transient flow field. Compared to the relative recovery errors of 0.10 to 0.15 for the calibrated models, the relative recovery error of 0.22 for the simple model

is considered a reasonably accurate prediction of the capture zone. While a purely predictive model was not used to simulate the second experiment, the relative errors associated with the calibrated model are significant, suggesting that a predictive model would provide an unreliable capture zone prediction. However, the large errors are associated with simulation of tracers located on the capture zone boundary, which is the source of the most significant error in all the models. A conservative application of the model would be obtained by assuming the capture zone to extend to the bottom of the aquifer.

ACKNOWLEDGEMENTS

The members of my Ph.D. committee deserve special thanks for their valuable criticisms and guidance while working on my dissertation. The committee consisted of John Wilson, Fred Phillips, Chia Chen, Robert Lee and William Haneberg. I would especially like to thank John Wilson, my advisor, for his guidance and support, and for helping make the field project at Waterloo both a reality and a success.

A larger number of people at both New Mexico Tech and the University of Waterloo contributed to the organization, implementation, and overall success of the project. At New Mexico Tech, Rob TerBerg was responsible for analyzing the large number of samples in the HPLC lab for the first experiment, as well as performing preliminary model simulations and writing the portions of this report on laboratory tracer analysis. Rob also contributed the information regarding the HPLC analysis methodology in the text and in Appendix 3 for this dissertation. Jinzhong Liu took over HPLC analysis responsibilities for the remainder of first experiment, as well as for all second experiment samples. Rob Bowman, also at Tech, acted as technical advisor in all aspects of tracer implementation and analysis. Edith Montoya helped with the administrative tasks. John Wilson was the overall project supervisor, and was instrumental in maintaining the status quo of the project and providing technical expertise when it was needed. At the Department of Earth Sciences and the Centre for Groundwater Research, University of Waterloo, the following people contributed to the project: Chuck Mase acted as project supervisor at Waterloo for the majority of the project. Youzhi Chen participated in the program during its early stages. He was responsible for setting up the original field installations and worked on startup of the first experiment. Murray Ostrander took over Youzhi's tasks for the the second experiment and was in charge of all field activities and field data retrieval and reduction. After the field experiments were completed, Murray joined the group at Tech for several months and was responsible for all gradient calculations and time series analysis of the head and gradient data. Raymond Hossick performed the invaluable task of overseeing the day–to–day operation of the experiment at

the site. Dave Thomas helped fill in gaps in field operations during the first experiment. Several technicians helped in design of the many components in the experiments, and were primarily responsible for all in-ground installations; these include Bob Ingleton, Paul Johnson and Chris Flowers. Bert Habicher also helped take water-table measurements during part of the second experiment. Dave Smyth was manager of all activities at the Borden site and was extremely helpful in coordinating technician help and overseeing the operation of the site and our experiments at all levels. In addition, Dave was the liaison between all Univeristy of Waterloo interests at Borden and the Borden base commander. During the course of the project, several people provided technical advise: Dave Rudolph, Ed Sudicky, Ron Nicholson, Jim Barker, Stephanie O'Hannesin, Greg Friday, and Rob McLaren. Ed Sudicky also graciously provided time and space on his computer network. Sandra Mayer was very helpful in dealing with the many administrative problems. Finally, our EPA Project Officer Stephen Kraemer provided timely council and criticism. I am grateful to all for their help and advise during the course of this project.

The research on which this report is based was financed in part by the U.S. Environmental Protection Agency, Robert S. Kerr Laboratory, through grant number CR 818019-091-0.

TABLE OF CONTENTS

LIST OF TABLES

LIST OF FIGURES

EXECUTIVE SUMMARY

Two multiple-tracer experiments were conducted in a shallow sand aquifer in order to determine the extent of the capture zone produced by an extraction well. The desired aquifer setting for the experiments was a homogeneous, isotropic aquifer with essentially horizontal regional flow and effectively no lateral boundaries. The aquifer that best fit the design criteria was the Borden aquifer in Ontario, Canada. The Borden site also has the favorable characteristics of a fairly well defined and horizontal lower impermeable boundary underlying the aquifer. In addition to meeting the above criteria, the Borden aquifer has been the focus of numerous experiments, providing an extensive data base from which to draw on (see Section II for a description of the field site and previous work conducted at Borden).

The design of the two experiments differed primarily in that the first experiment had a fully penetrating extraction well while the second experiment had a partially penetrating well in the upper portion of the aquifer (see Section II for descriptions of the experiment designs). In the first experiment, seven fluorinated benzoic acid (FBA) tracers were injected at 15 injection sites (see Tracer Description and Solution Preparation, and Tracer Injection, Section III, and Appendix 1-3, for descriptions of tracers and tracer injections). Thus, six of the tracer were injected at two injection sites each, and the seventh tracer was injected at 3 injection sites. An eighth tracer, bromide (Br^-) was injected along with four of the FBAs in order to evaluate any possible sorption or decay properties they may exhibit in the Borden aquifer. These comparisons indicated that the FBAs are conservative, such that Br- was used as a separate tracer in the second experiment. Tracer were injected over as a cylinder 3 meters long and approximately 0.20 m in diameter from 2 to 5 m below ground surface. Tracer was not injected at depth to prevent interaction with the leachate in the lower 2 m of the aquifer, since it was suspected that interaction of the tracers with the leachate would cause interference effects during laboratory analysis of water samples using high pressure liquid chromatography (HPLC). In the second experiment, a more complex injection pattern was used at

several of the injection sites in order to better evaluate the vertical flow induced by the partially penetrating well. At two sites, one tracer, which showed little interference effects from the leachate in the first experiment, was injected from 5 to 7 m to help delineate the lower capture zone boundary. At those same sites, Br– was injected at the upper part of the aquifer, in one case it was simply added to the water table, in order to evaluate the shallow region of the capture zone.

Spatially, tracer was injected both within and outside the predicted boundaries of the capture zone. The design of both experiments relied on a simple capture zone model based on potential flow theory, and *a priori* data. Tracer breakthrough was monitored at the extraction well, and tracer breakthrough and recovery data indicated travel times and capture zone boundaries. Tracer injected within the capture zone gave a relative recovery of 1.0; tracer injected outside the capture zone gave a recovery of 0.0. Injection sites located on the boundary of the capture zone produced extraction well recoveries between 0.0 and 1.0, indicating a fuzzy capture zone boundary. The fuzzy boundary was caused by the effects of dispersion, a fluctuating ambient flow field, and other possible causes. Vertical flow components, and vertical stratification of horizontal flow components, present in both experiments, made interpretation of the capture zone more difficult, especially for injection sites located near or on the capture zone boundary.

The two experiments were significantly influenced by transient conditions. Hydraulic gradients, calculated from measured head data, showed large seasonal fluctuations with the directional component varying up to 90 degrees, and higher frequency fluctuations varying by as much as 20 degrees over a one week period (see Water-table Measurements, Section II; and Hydraulic Gradient Calculation, Section III). The variable flow direction created problems from the start of the project. The initial design of the first experiment was oriented at an angle of N52E. After construction and installation of the individual components of the experiment (see Section II for the field site description), it became apparent that flow was in a more northerly direction than suggested by prior studies. This resulted in modification

of the original installation prior to start-up of the first experiment. Following the first experiment, and prior to start-up of the second experiment, additional modifications were made to account for the more northerly flow. Once the second experiment was under way, flow then rotated back to the northeast, so that, again, some of the injection sites and multilevel samplers in the downgradient monitoring fence were not optimally placed. The mean flow direction, based on data collected during the course of this study, was approximately N20E, which is substantially different than that observed in the intermediate scale natural gradient plume experiment conducted by Mackay et al. (1986).

The data collected during the two experiments allowed direct delineation of the capture zone in each experiment. In the first experiment (discussed in Section IV), interpretation of recoveries for individual injection sites was straightforward with a high degree of certainty for most of the sites. Assigning recoveries for 4 of the 15 injection sites was difficult due to overlapping breakthrough (for two tracers injected at two sites each) such that the individual breakthrough sequences could not be easily separated. Further analysis comparing model results to experimental results helped to better estimate recoveries for these four sites. The transient flow direction during the first experiment caused the capture zone to be oriented approximately N25E to N30E, while the mean flow direction was N15E to N20E. This suggests that steady-state capture zone models which use the mean flow direction may be in error in predicting the true capture zone orientation in a transient system. The width of the capture zone in the first experiment was estimated at approximately 2.5-3.0 m, which is smaller than the 5 m width estimated during the design of the experiment. The narrower measured capture zone was due to the changing flow direction and also higher hydraulic conductivity than was used to originally estimate the capture zone width. Steady-state capture zone models would predict a wider capture zone which would be conservative in terms of wellhead protection. In the second experiment (discussed in Section V), assigning recoveries to individual injection sites was again straightforward, however there was more uncertainty associated with interpretation of the second experiment than with the first experiment.

The source of this uncertainty arose from the more complex nature of the capture zone boundary associated with the partially penetrating well in the second experiment.

Results from the first experiment, which was designed to represent a two-dimensional flow system, supports conclusions from previous experiments conducted at the Borden site indicating that the aquifer is heterogeneous, with variability in vertical hydraulic conductivity suggesting a strongly layered system. The layering of the aquifer caused vertical splitting of the injected tracer plumes, which was evident from tracer concentrations determined from the individual pumping intervals within the well (see Extraction Well Installation, Section II, and Tracer Breakthrough and Recovery Analysis, Section IV). In both experiments, flux was specified for each well interval, making the well a prescribed flux boundary instead of a prescribed head boundary as is the case for most withdrawal wells. Imposing a flux boundary in an aquifer with lower hydraulic conductivity at depth, as was the case at Borden, created downward vertical flow. In addition, buoyancy effects, created by density contrasts between the tracer plume and the surrounding aquifer water, also caused the plumes to sink. The estimated vertical plume migration ranged from 0.25 m to 0.94 m (see appropriate parts of Tracer Breakthrough and Recovery Analysis, and Two-dimensional Model Analysis in Section IV) for tracers injected in Experiment 1. Model simulations gave similar results and suggested that buoyancy induced vertical flow was approximately one-half of the total vertical flow. In the second experiment, buoyancy effects most likely enhanced vertical plume splitting as the tracer plumes migrated downward across the capture zone boundary at depth.

Several models were used to simulate flow and transport, and to delineate capture zones, in the aquifer. The simplest model was based on two-dimensional, potential flow theory and has been used extensively in prediction of capture zones (Wilson and Linderfelt, 1991). This model was applied in a purely predictive fashion for Experiment 1 using three *a priori* data sets (as described in the Discussion part of Section IV). The accuracy of the model was determined by comparison to the observed tracer recoveries assigned to each in-

jection site. This "simple" model was also compared to more "complex" model results. The more complex models included transient effects, dispersion, and heterogeneous hydraulic conductivity, and were calibrated to various subsets of data collected during and prior to the experiments. The utility of the complex models was to determine the accuracy of different models, given various subsets of data, and to allow comparison of the simple, purely predictive model results to what is considered a best fit provided by the more complex models. This last feature is important in that it provided a check on the reasonable accuracy that can be expected for any given model in a practical sense.

The simple predictive model gave relative recovery errors of 0.22 to 0.60 in the first experiment, depending on what data set was used, and represents the fraction of tracer mass recovered at the well unaccounted for by the model (see Model Error Analysis, Section III, for a description of the error calculation method; see Section IV for the specific error results). The smaller error was for two data sets, one based on data collected during the project prior to the experiment, and one based on a plume migration study conducted approximately one year prior to the experiment. The larger error was for a simulation based on data from the Waterloo–Stanford experiment conducted in 1986, five years prior to the experiment conducted in the present study. The Waterloo–Stanford experiment represents the best known and most often cited data set of the three, and yet it produced the least desirable results. The primary difference between the three data sets was the direction of ambient flow, and the difference between the two error values reflects the transient nature of the flow system in the sand quarry at Borden.

The errors can be viewed from two perspectives. From the standpoint of the Borden aquifer, which is both well studied and considered a relatively simple aquifer, even 0.22 error may seem significant. The model errors can also be viewed from the standpoint of practical applicability. The error obtained by applying the more complex models was in the range of 10%–15%, regardless of which model was applied (i.e. two– or three–dimensional, homogeneous or heterogeneous), or the degree of calibration (calibrations were done for hydraulic

conductivity, dispersivity, aquifer thickness, and hydraulic gradient) (see the modeling analysis subsections in Section IV). If we directly compare the errors for the simple and complex models, then the prediction error for the simple model ranges from 0.12 (i.e. 0.22–0.10) to 0.50 (i.e. 0.60 – 0.10), depending on which *a priori* input data set is used in the predictive model. Clearly, if the older Waterloo–Stanford data is used then the error can be considered significant. However, by carefully evaluating the transient nature of the system, which has a large influence on the hydraulics of the flow system, then the resulting prediction error of 0.12 is much better.

Modeling of the second experiment gave relative recovery errors of at least 0.55 (see Section V). This is much higher than the 0.10–0.15 seen in the first experiment, and suggests that the larger error from incorrect specification of the hydraulic conductivity distribution in the model, since the transient nature of the system was handled in the same manner as in the first experiment. Virtually all tracer plumes interacted with the lower capture zone boundary. Had all the tracer been injected at the water table, which may better represent a contaminant spill, the error would have been much lower. In the first experiment, the largest source of error for an individual simulation was from interaction of several of the tracer plumes with the lateral capture zone boundary, and the boundary location was most largely influenced by the transient flow direction. In the second experiment, the capture zone had both a lower boundary, as well as a lateral boundary such that, not only was the lateral boundary affected by the transient, but the lower boundary was affected by the transient and the vertical variability in hydraulic conductivity. Since a purely predictive model was not compared to the second experiment results, we can not comment on the practical application of a predictive model in that case. However, even if a predictive three-dimensional model such as the one used in this study were used to predict the capture zone, it is expected that the error would be larger than the 0.55 obtained from the calibrated model.

Besides determining the error in mass recovered for each injection site, the error in the time–sequence of the mass recovery, or the breakthrough curve, was also calculated. In all cases, the error of the models in predicting the time–sequence of mass breakthrough was much larger than that for determining the mass recovery. In the first experiment, the relative breakthrough error ranged from 0.55 to 0.70. In the second experiment, the relative error was over 1.0 of the mass recovered at the well. It is clear that there would be significant error in predicting time–dependent fronts, and that the model is more robust in predicting the mass recovered independent of time, which results from the insensitivity of simulated recoveries to model input parameters except for sites located on the capture zone boundary.

I. INTRODUCTION

The quality of water pumped from water supply wells depends on the relative amounts of water drawn from different hydrologic units (Wilson and Linderfelt, 1991). The zone within each unit contributing water to the well is referred to here as the capture zone. This zone is also called a wellhead protection area, or WHPA, and is defined as the "surface and subsurface area surrounding a water well or well field, supplying a public water system, through which contaminants are reasonably likely to move toward and reach such water well or well field" (Environmental Protection Agency, 1987). A contaminant spilled within an aquifer capture zone will eventually enter the well.

Congress passed the Safe Drinking Water Act of 1986, which contains a wellhead protection provision in an attempt to protect public water supply wells and well fields from contamination. Once a wellhead protection area is defined, contaminant sources within it are to be assessed and appropriate control measures implemented. The Environmental Protection Agency's (EPA) Office of Ground-Water Protection (OGWP) was formed to provide administrative and technical guidance to the states. One of the most important technical questions facing OGWP and the states has been how to delineate a wellhead protection area. The OGWP responded to this question with a set of guidelines that were published shortly after the legislation became law (Environmental Protection Agency, 1987), and the development of more sophisticated mathematical models that presumably improved delineation capabilities (Environmental Protection Agency, 1990, 1991).

The work presented herein improves on capture zone delineation approaches by, first, conducting field experiments to assess data requirements for in-situ capture zone delineation and, second, using this data to validate and improve capture zone delineation techniques. This was a joint project of the Hydrology Program of the New Mexico Institute of Mining and Technology and the Waterloo Centre for Groundwater Research, affiliated with the University of Waterloo in Ontario, Canada.

Background

The first diagram of a extraction well capture zone in a two dimension uniform flow field was published by Slichter (1899) almost one-hundred years ago (Wang, 1987). Later theoretical work on capture zone analysis by Jacob (1950), Bear and Jacobs (1965), Bear (1972, 1979) and many others used stream functions and potential theory to describe the effects of wells in aquifers under steady state conditions in a two dimensional setting. Their work relied on studies of well hydraulics by Thiem (1906), Theis (1935), and Muscat (1937). In more recent times these techniques have been elaborated and applied to a variety of issues. Nelson (1978), considering radionuclide migration, developed methods of obtaining flow paths, travel times and outflow fluxes in the subsurface environment by using path, stream, and streak functions. These three kinematic functions, when combined with the potential distribution, gave the velocity of fluid throughout the flow system. Using similar principles, Keely and Tsang (1983) developed the RESSQ model for deriving streamlines, front locations and well breakthrough concentrations in a simple, two-dimensional flow system. Javandel and Tsang (1983) applied this model to develop a simple optimization approach for siting extraction wells and determining discharge rates for cleaning contaminated aquifers. In 1990, EPA released the WHPA code for use in delineation of capture zones (Environmental Protection Agency, 1990, 1991). It is based on principles developed in the previous studies, especially the RESSQ model.

Further modification and improvement of the above models take into account various boundary conditions, uncertainty effects, and three-dimensional effects. Capture zones intersecting head boundaries can reverse gradients and cause induced infiltration from the water body into the aquifer (Wilson, 1981, 1986, 1993; Lee, 1986; Lee and Wilson, 1986; Chow and Wilson, 1988; Newsom and Wilson, 1988; Wilson and Linderfelt, 1991). In the presence of local recharge the steady state capture zone cusps out along a barrier boundary or along a groundwater divide to possibly capture distant contamination sources (Lee, 1986; Lee and Wilson, 1986; Wilson and Linderfelt, 1991; Lerner, 1992). For a contaminant in

an aquifer with a uniform flow field, asymptotic approximations were derived for the rate and mean time at which the contaminant will enter the well (van Kooten, 1994). In systems where vertical flow components are important, a three-dimensional analysis is required. This may be the case for variable penetration of boundaries such as lateral, stream or well boundaries (Morrisey, 1989; Wilson and Linderfelt, 1991; Linderfelt and Wilson, 1991), or in a heterogeneous aquifer (Schafer-Perini, 1990; Schafer-Perini and Wilson, 1991a). Uncertainty analysis can also be added to the capture zone model. Treating parameters such as porosity and hydraulic conductivity as random variables leads to capture uncertainty based on stochastic theory (Varljen and Shafer, 1991; Bair et al., 1991c). Constant but uncertain input model parameters lead to uncertain capture zones which can be used in decision making applications (Wilson and Linderfelt, 1991).

There have been several field and model validation capture zone studies published in the literature. Bair and Roadcap (1992) compare CAPZONE/GWPATH (Bair et al., 1991a; Shafer 1987a,b, 1990), RESSQC, DREAM (Bonn and Rounds, 1990), and MODFLOW/MODPATH (McDonald and Harbaugh, 1983) in their application to a field study in a leaky-confined fractured, carbonate aquifer. A similar study was carried out by Springer and Bair (1992) on a stratified-drift buried-valley aquifer. Both of these studies relied on the head calibration to assess model performance of capture zone delineation. Accuracy of the models was determined by comparison of simulated heads to measured heads. Further comparisons were made using the one year capture zones, or fronts, determined by reverse-tracked pathlines for each model. These studies support the idea that the application of models based on incorrect conceptualization lead to erroneous results. Lerner (1992) compared ROSE to GPTRAC (Environmental Protection Agency, 1991) in the ability to delineate capture zones and fronts in a simple aquifer with vertical recharge.

Bair et al. (1991b) examined accuracy of simple calibrated models in estimating time dependent capture zones. Their findings point out the limitations of the models tested, and also the error associated with calibration to heads for these models. Teutsch and Hofmann

(1990) performed a forced gradient tracer test designed to validate wellhead protection zoning for a site near Karlsruhe, Germany. In their study five tracers were injected simultaneously into the aquifer. Samples were taken from the extraction well and from eight sampling tubes located in the well gravel pack at different levels. Their results suggest "... that transport predictions based on hydraulic data might be far off from reality, even in an aquifer environment of limited heterogeneity." They also state that point-source pollution migration seems unpredictable at the local scale (see also Teutsch, 1989), and that there is a large margin of error in delineation of wellhead protection areas depending on what type of data is used. However, they do not account for incomplete tracer recoveries seen in the experiment, making it difficult to determine whether their lack of success is due to sampling error, sample analysis error, or improper model conceptualization.

Objectives

The overall goal of the study was to improve our understanding of the zone of contribution, or capture zone, produced by a single extraction well located in a relatively simple aquifer. To accomplish this goal, pertinent questions regarding capture zones were formulated in the form of hypotheses. The field experiments provided a basis with which to test these hypotheses.

The initial focus of the experiments was to determine whether a capture zone actually exists in the field, and that it can be delineated based on collected data. Also, we know that the spatial distribution of the capture zone results from physical processes associated with subsurface flow, such that we are not only proposing that a capture zone exists, but that we also know something about the features of the capture zone such as it's shape and orientation. Our understanding of the capture zone is based on an understanding of both the processes governing flow, and on information regarding the associated flow parameters. The hypothesis regarding capture zone existence is stated as follows: *A zone of contribution, or capture zone, is produced when water is withdrawn from a well, with the shape and orientation of*

the capture zone reflecting the interaction of the radial flow field, induced by the extraction well, and the pre-pumping flow field. By conducting the experiments, we set out to collect data which will allow direct testing of this hypothesis. Based on previous investigations, both directly and indirectly aimed at capture zone analysis, we suspected that capture zones do exist, so the first hypothesis is worded such that testing will lead to a positive result. Should testing of the first hypothesis turn out negative, and a capture zone is shown to not exist, it may be that the type or amount of data collected, or both, was not adequate and the experiments could be redesigned and rerun. Should additional testing lead to a positive result, then further hypotheses, discussed below, can be tested. Should the testing of the existence hypothesis lead to a negative result regardless of the types or amounts of data collected, then our basic understanding of the governing flow processes comes into question and we must rethink our original conceptual model. Again, the experiments can be redesigned and rerun to reflect the new conceptualization. As a worst case scenario, the existence of a capture zone may never be established regardless of the conceptualization or the data available, leading to serious questions regarding current thinking and practices in hydrology.

Once a capture zone is delineated in the field, we will test additional hypotheses regarding mathematical capture zone delineation. The mathematical models which are to be tested include simple and commonly used delineation methods, as well as more complex models incorporating more detail about the flow and transport properties of the aquifer. It may turn out that we can adequately delineate a capture zone with data collected during an experiment, but that the predictive capabilities of the models, based solely on *a priori* data, are inadequate. It may also turn out that an impractical amount of information is required by a model to adequately delineate a capture zone. In either case, our approach to practical capture zone delineation is reduced to field experimentation which is time consuming and costly. In this study, the accuracy of various mathematical models in delineating capture zones will be examined, as well as the data requirements of these models in providing an accurate prediction.

Strategy and Approach

The two experiments were designed with a single extraction well located in a hydrogeologically simple aquifer with fairly homogeneous hydraulic conductivity, essentially horizontal and uniform regional flow, a horizontal basal aquitard, and a small saturated thickness. The first experiment was aimed at delineation of the capture zone for a fully penetrating extraction well, while the second experiment focused on the effects of a partially penetrating well. In order to experimentally delineate the boundary of the capture zone, defined by the dividing streamline in steady state systems, injection sites were located both within the estimated boundaries of the capture zone, ensuring capture by the extraction well, as well as outside of the capture zone, ensuring no capture. Figure 1–1 shows in plan view an idealized tracer–delineated capture zone, with tracer injection sites inside and outside the capture zone. When using tracers to delineate a capture zone in this way, it is preferable to obtain information from as many injection sites as possible. The number of sites is limited by the number of tracers. In addition to observing tracer breakthrough in the extraction well, multilevel bundle samplers were used to observe tracers not captured by the extraction well, shown in Figure 1–1 and Figure 1–2. The multilevel sampling locations included the vicinity of the stagnation point, where tracers injected near the edge of the capture zone may tend to collect, and along a transect of multilevel samplers downstream from the well through which all tracers not captured by the well must eventually pass. A final design feature of the experiment was its small scale, allowing for a fast response to pumping and fast tracer movement, ensuring that the experiment and subsequent analysis were completed and analyzed within the allotted time–frame of the project. The field test can be viewed as a scale model of real municipal well fields: what takes decades to observe at a larger scale we were able to observe in weeks or months.

A site that fits the above criteria is the well known Borden experimental site in Ontario, Canada. The Borden aquifer is an unconfined shallow sand aquifer located at Canadian Forces Base, Borden, Ontario, Canada. The quarry and vicinity has been the site of numer-

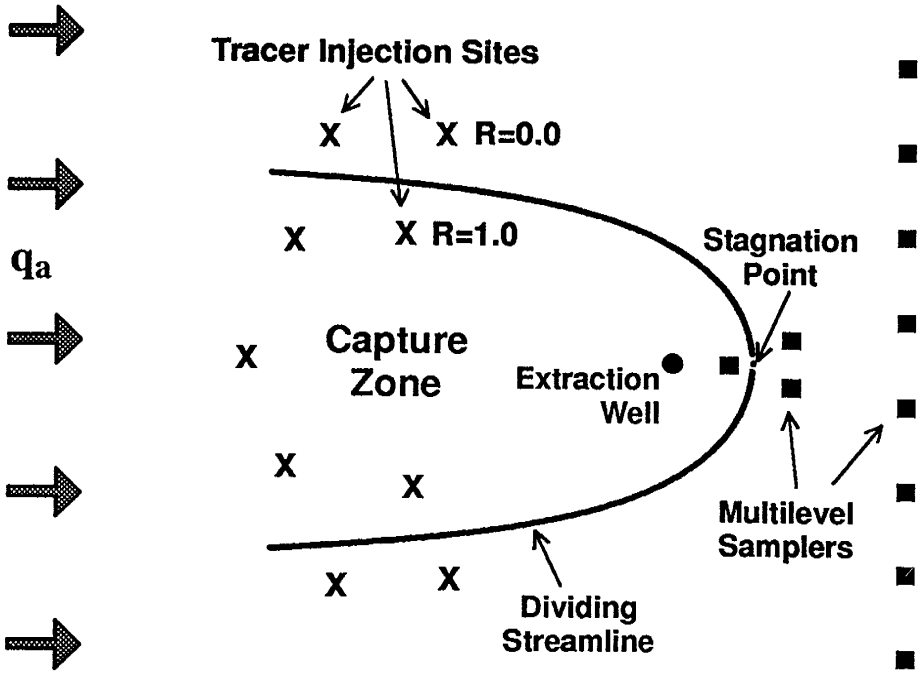

Figure 1–1. Plan view of an idealized tracer–delineated capture zone. R represents relative tracer recovery at the extraction well; q_a is ambient flow rate.

ous groundwater studies dating from 1979, and have provided extensive information regarding aquifer characteristics and flow and transport dynamics, including a landmark natural gradient plume study supported by EPA through Stanford University (Mackay et al., 1986). The tracer experiment presented here was within the study area of the Waterloo–Stanford experiment (Mackay et al., 1986), the transects used for estimating hydraulic conductivity by Sudicky (1986), and the recent forced gradient reactive tracer experiment conducted by Mackay et al. (1994).

Once the capture zone was established in the field, various models were compared to the field delineated capture zone. A variety of modeling approaches were examined, ranging from purely predictive models based on simple, two–dimensional mathematical formulations to complex, three–dimensional finite difference representations calibrated to all the available data. Comparison of predicted capture zones to measured capture zones tests the accuracy of the predictions. Comparison of the accuracy of capture zones delineated

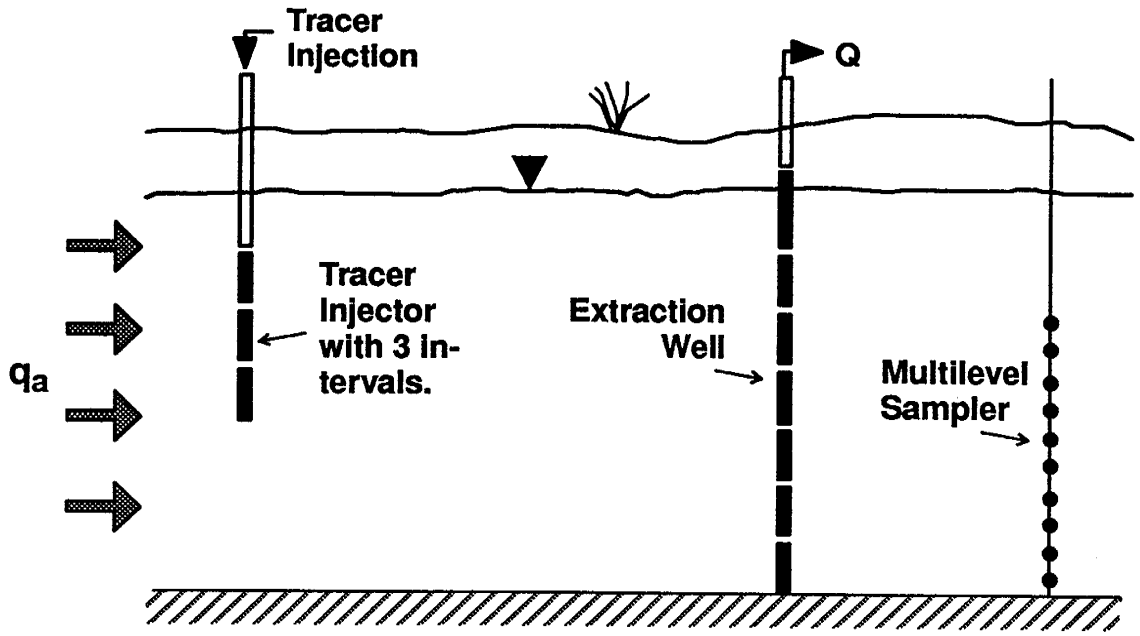

Figure 1–2. Schematic cross section of capture zone experiment with a partioned extraction well. All 7 intervals in the extraction well were used in the first experiment, only the top 2 intervals were used in the second experiment.

from calibrated models to those delineated from predicted models determines how practical it is to use a given model. For instance, if the error associated with the calibrated model is as large as that in the simpler predictive model, then there is no basis for using more complex models which require larger resources. On the other hand, if the error in the calibrated model is much smaller than that in the predictive model, then use of a more complex model with larger data requirements is substantiated. Results of this type will provide useful information to scientists conducting capture zone studies.

Scope

This report presents the design, experimental procedure, results and interpretation of the two experiments. Section II presents a description of the field site including: background information on the Borden aquifer including a review of previous studies, especially

those directly related to this work; descriptions of the installations used in the experiments including the extraction well, tracer injection wells, downstream multilevel samplers, water table measurements, and the electronics used in recording vibrating wire piezometer and pumping rate data. Section III provides information on methods and procedures used in the experiments including hydraulic gradient calculation, tracers, tracer injection, tracer monitoring and sampling, and laboratory tracer analyses. Also included is a short section on the capture zone modeling approaches used in the study. Section IV covers the experimental and modeling results and interpretation of the first experiment. Section V covers the experimental and modeling results and interpretation of the second experiment. Section VI presents summary and conclusions, with references and appendices following.

II. FIELD SITE DESCRIPTION

There is an extensive body of literature describing past experiments at the Borden Site. Some of this is cited below, in reference to site conditions and properties. Following this review is an outline of the monitoring system that was installed to observe the water-table configuration and hydraulic gradients during the capture zone experiments. The pumping well, multilevel sampler, and tracer injection well designs and locations complete the site description.

Borden Site

The two capture zone experiments were conducted in the unconfined aquifer underlying an inactive sand quarry at Canadian Forces Base Borden in central Ontario, Canada (Figure 2-1, a-c). The quarry and vicinity has been the site of numerous groundwater studies dating from 1979. These studies have provided extensive information regarding aquifer characteristics and flow and transport dynamics.

The physiography and climate of the site and vicinity have been described by MacFarlane et al. (1983). Elevations range from 232 m above sea level at the nearby landfill to 222.5 m in the sand quarry. The mean daily temperature ranges from 12.4° to 0.6° C, averaging 6.5° C, with extremes of +36.7° and -41.1° C. Mean total precipitation averages 82.8 cm/year, with 58.67 cm in the form of rain and 240.5 cm of snow. Typically there are 171 days of frost, 88 days of rain and 56 days of snow.

The aquifer extends about 8 m beneath the nearly horizontal quarry floor (see topographic map in Figure 2-2) and is underlain by a thick silty clay deposit (Mackay et al., 1986). A single core taken near the pumping well site of this study indicates silts and clays predominate at about 8 m below the quarry floor, and this depth was used as the lower aquifer boundary in this study. A leachate plume originating from a nearby landfill exists at the bottom 2-3 m of the aquifer (MacFarlane et al., 1983; Mackay et al., 1986). The water table depth ranges from about 1.5 m below the quarry floor to the ground surface, with occasional

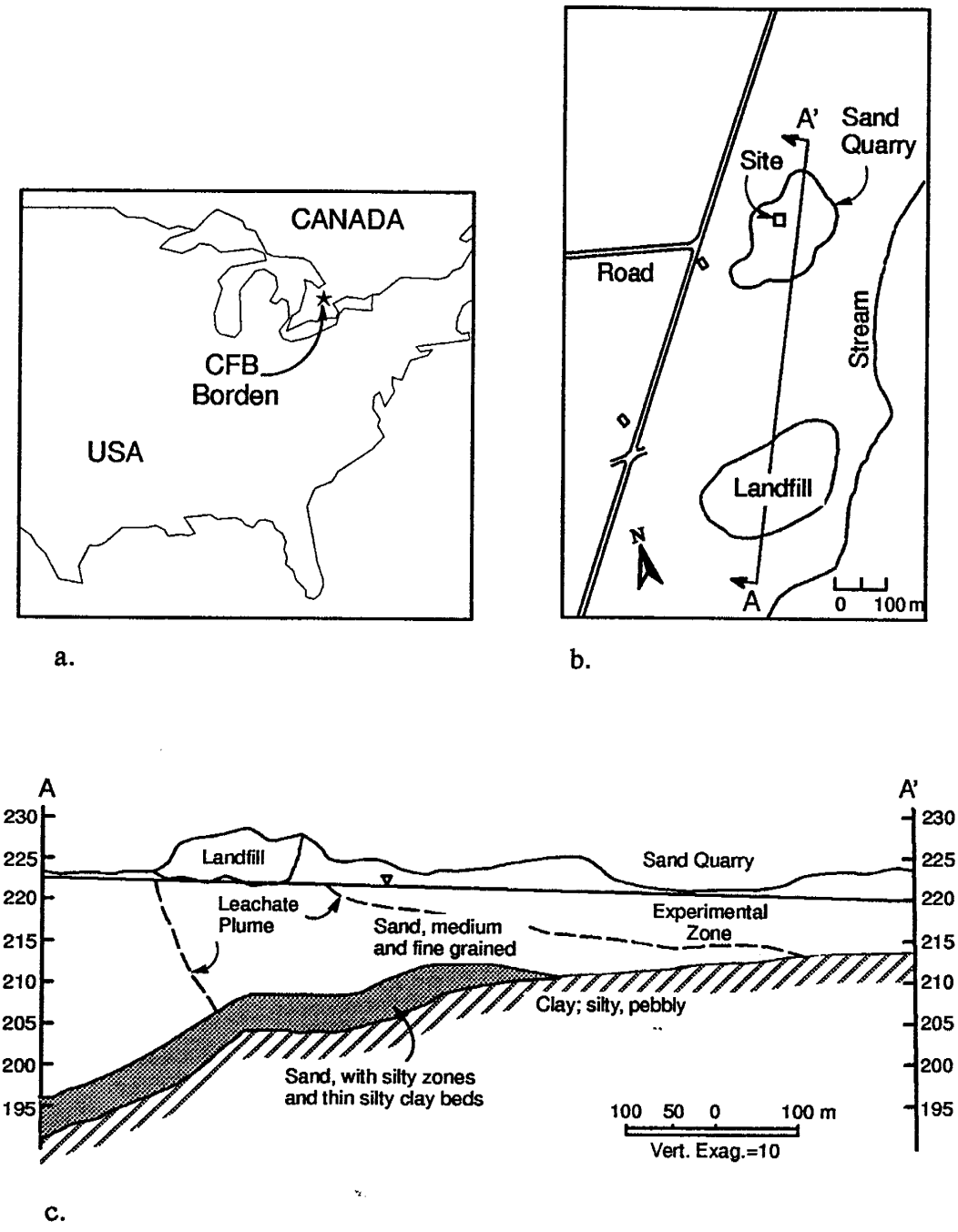

Figure 2–1. (a) Map of eastern USA and southern Ontario, Canada, showing Great Lakes region and location of CFB Borden; (b) Plan view of the experimental site in the sand quarry at Borden; (c) Site cross section (schematic) A–A' showing landfill, experimental zone, and local geologic features (b and c after Mackay et al., 1986).

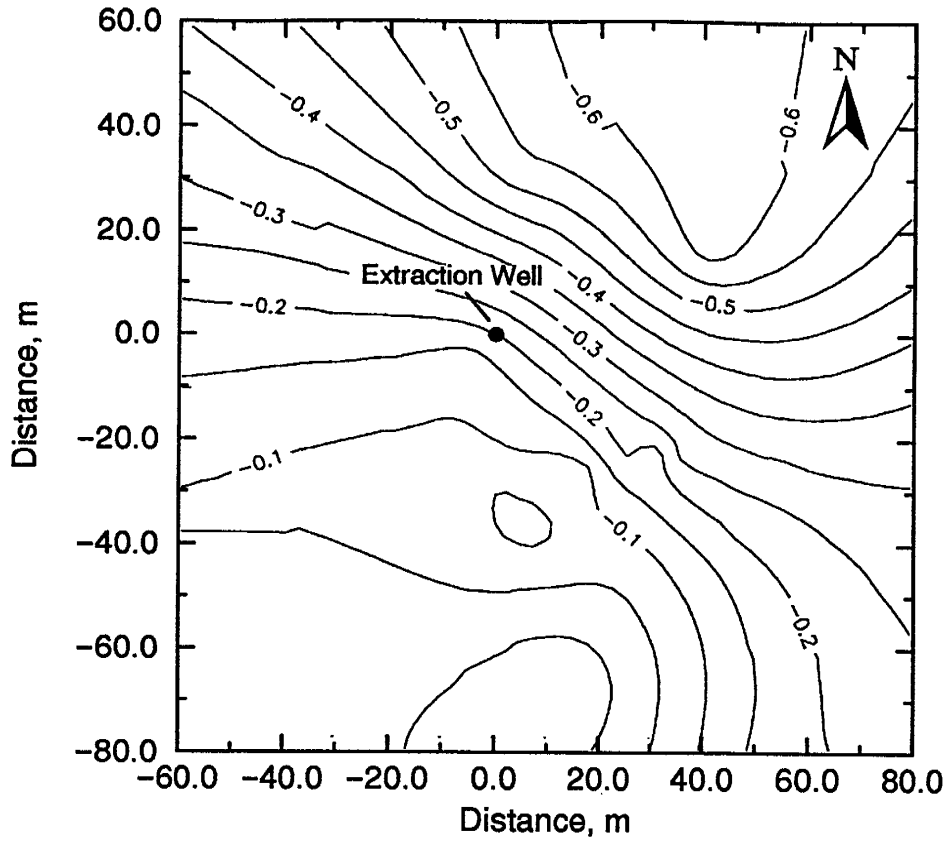

Figure 2–2. Rough ground elevation contour map in the vicinity of the experimental site, based on elevations measured at standpipes and piezometers used to observe water levels (see Figure 2–3). Kriged with a linear variogram; datum is the top of VWP1 piezometer shown in Figure 2–3. The location of the extraction well used in the two experiments is shown for reference.

ponding, and varies due to seasonal as well as short term fluctuations. Increases of 20–30 cm in water table elevations in response to precipitation events can occur within 1 hour of the onset of rainfall. Localized mounding in the aquifer region underlying the quarry is also seen in response to precipitation. Seasonal water table fluctuations are on the order of 1.0–1.5 m. The lowest water tables are generally in the summer and fall during periods of low rainfall. The highest water tables occur in winter and spring following seasonal recharge events, with a maximum typically occurring in March or April during periods of snow melt and spring rains.

Aquifer grain size ranges from 0.070 to 0.69 mm for 846 samples taken from 11 undisturbed cores (O'Hannesin, 1981, cited in Mackay et al. 1986). Ball et al., using dry sieve analysis of Borden bulk solids, report that approximately 57% of the sand falls in the 0.125 to 0.25 mm range, and 90% falls in the 0.075 to 0.42 mm range. Grain roundness ranges from subangular to well rounded for these samples. From 32 undisturbed cores taken at the location of the tracer tests, Sudicky (1986) reported the presence of coarse to silty fine-grained sand lenses embedded in a fine- to medium-grained sand. Thickness of individual beds varied from a few centimeters to a few tens of centimeters. Sudicky also noted that material within individual beds was relatively homogeneous with occasional fine laminations on the order of a millimeter to a few millimeters in thickness.

The water table surface generally slopes in a north-easterly direction with fluctuations in response to short term and seasonal precipitation patterns. Sykes et al. (1982) used a time averaged hydraulic gradient to predict the piezometric surface for an area encompassing the quarry and nearby landfill. However, measured data for 1979 indicate the direction of flow changes with time and that these changes "are anticipated to have a stronger effect on the flow system and contaminant migration (in particular, hydrodynamic dispersion) than the inclusion of spatial permeability changes." MacFarlane et al. (1983) conducted 11 monitoring episodes during 1979. Groundwater flow in a region including the landfill and the sand quarry was northward during the fall and winter months. During the spring and summer months, regional flow had a radial component emanating outward from the landfill due to water-table mounding near and beneath the landfill in the spring. In the vicinity of the quarry, flow is northeasterly during this time. The range in flow direction was approximately 13°, minimum and maximum gradient magnitudes were .0035 and .0054, respectively, and the fluctuation in the water-table elevation was about 1.0 m. This compares to a range in flow direction of 14°, and minimum and maximum gradient magnitudes of .0036 and .0056, respectively, estimated by Sudicky (1986) for the sand pit. Recent unpublished work, which was made available to us during the second experiment, indicated larger fluctuations and

tested the hypothesis that gradient fluctuations influence plume transport (originally published as Farrell et al., 1992; see also Farrell et al., 1994). Their water-table data was from a site approximately 100 m north of the site in this study, where the first so-called "emplaced source experiment" at Borden was conducted. The analysis included determination of a spatial trend in the water-table data, computation of the mean gradient magnitude and flow direction time series, geostatistical analysis of this time series in order to determine the variance and integral scales present, and computation of harmonics present in the gradient data. Results from their time series analysis show dominance of the north-south gradient component of the gradient magnitude time series at their site, while the east-west gradient component and flow direction time series are very similar in appearance. The maximum range in flow direction estimated at this site was 39° over approximately 250 days (Farrell et al., 1994) and was much larger than the estimates of previous studies. The flow direction varied from N5W to N35E. Minimum and maximum gradients were reported as 0.0033 and 0.0064, respectively, and the water table fluctuations were measured at 0.8 m. Detailed sampling of the water table within the sand quarry during the course of the present study indicate that the fluctuations in gradient direction are significant, and are larger than the fluctuations in gradient magnitude. These findings are discussed in depth beginning in Section III.

MacFarlane et al. (1983) estimated the horizontal hydraulic gradient as 0.0035 to 0.0054 near the experimental site. Data collected during the course of this study indicated gradients ranging from roughly 0.0025 to 0.0045. Vertical gradients determined from MacFarlane et al. (1983) are essentially zero. Sudicky (1986) used moment analysis of a natural gradient tracer test to estimate a downward vertical gradient of about 6×10^{-5}.

Hydraulic conductivity, K, has been measured by a variety of methods in several previous Borden site studies with values ranging from 0.09 to 19.0 meters per day (m/d). Sykes et al. (1982) used a multidimensional finite-difference flow and transport model to analyze the leachate migration from the landfill. In this study, a calibrated value of 6.2 m/d more closely approximated the hydraulic gradient both at the landfill and down gradient from the

landfill than a measured value of 5.0 m/d (Sykes et al., 1982). Furthermore, an anisotropy ratio K_h/K_v of 2 was assumed. Nwankwor et al. (1984) used slug and bail tests from deep piezometers and calculated hydraulic conductivity values ranging from 2.6 to 5.2 m/d. Using Boulton (1963) and Neuman (1972) type curves, Nwankwor et al. (1984) calculated transmissivity within a range of 86.4 to 132.2 m^2/d. Using 7 m as the saturated thickness, hydraulic conductivity was given as 12.3 to 18.9 m/d.

Of the previous field investigations conducted at the Borden site, two have been at the heart of much ongoing research into mechanisms controlling transport in aquifers. The first of these investigations is reported in McFarlane et al. (1983) and associated publications, especially Sudicky et al. (1983), and the second involves the Waterloo–Stanford experiment as reported in Mackay et al. (1986) and associated publications. The results of these investigations have led to numerous insights regarding the hydraulic conductivity and dispersivity (especially macrodispersivity) of the Borden aquifer, as well as in other aquifers.

MacFarlane et al. (1983) obtained values of hydraulic conductivity using grain–size analysis, water–level response test in piezometers, pumping tests and permeameter tests on two disturbed core samples. The range of K from all of these methods was 2.6 to 8.6 m/d for the fine– and medium–grained sand and 0.04 to 1.7 m/d for the silty fine–grained sand at depth. Hydraulic conductivity for a site near the sand quarry was reported by Sudicky et al. (1983) for a fast and a slow zone using a falling–head permeameter method. The slow zone K ranged from 4.14 to 6.13 m/d while the fast zone K ranged from 4.49 to 6.57 m/d. Sudicky (1986) performed falling head permeameter tests on 0.05 m sections of 32 cores, each approximately 2 m in total length, taken along two transects in the sand pit. With this data, Sudicky (1986) estimated the geometric mean hydraulic conductivity as K_g=6.19 m/d, effective horizontal conductivity as $\overline{K}_{11}=\overline{K}_{22}$=7.09 m/d, and effective vertical conductivity as $\overline{K}_{33}$=5.47 m/d. The capture zone experiments were located very near the intersection of these two transects, which were sampled from 2.5 to 4.5 meters in depth.

A significant amount of the work resulting from Sudicky's 1983 experiment (Sudicky et al., 1983) and the experiment conducted with Stanford University (Mackay et al., 1986; Freyberg, 1986; Sudicky, 1986) has dealt with the stochastic representation of hydraulic conductivity. Results from the Waterloo–Stanford experiment indicate two important points regarding the hydraulic conductivity of the Borden site, 1) a strong vertical trend in conductivity does not exist in the data, suggested by Figure 4 of Mackay et al. (1986) and Figure 5 of Sudicky (1986), and 2) the local hydraulic conductivity field has a complex, lenticular structure, as can be observed in Figures 6 and 7 in Sudicky (1986). Furthermore, using permeameter data, Sudicky (1986) arrived at an exponential covariance model for Y=lnK, with variance σ_Y^2=0.29, and correlation lengths $\lambda_1=\lambda_2$=2.8 m in the horizontal, and λ_3=0.12 m in the vertical, which agree well with natural gradient plume analyses results obtained from Freyberg (1986) of σ_Y^2=0.24 and λ=2.7 m. Thus, the aquifer exhibits a strongly layered character. Woodbury and Sudicky (1991) re–evaluated the original permeameter data from the two transects A–A' and B–B' of Sudicky (1986) using a nonlinear least squares approach. Woodbury and Sudicky's estimates are noticeably different than Sudicky's results, with the horizontal correlation scale larger for the Woodbury and Sudicky (1991) study. Also, the fitted parameters for the two transects, AA' and BB', were different as determined by Woodbury and Sudicky (1991). Results from Freyberg (1986), Sudicky (1986) and Woodbury and Sudicky (1991) are tabulated in Table 2–1.

Table 2–1. Estimated hydraulic conductivity spatial statistics.

Parameter	A–A'[1]	B–B'[1]	Sudicky[2]	Freyberg[3]
σ_Y^2	0.24	0.37	0.38	0.24
σ_0^2 (= nugget)	0.07	0.11	0.10	-
λ_h (m)	5.14	8.33	2.8	2.7
λ_v (m)	0.21	0.34	0.12	-

[1] Woodbury and Sudicky, 1991; [2] Sudicky, 1986; [3] Freyberg, 1986

Dispersion of tracers or contaminants in the Borden sand has been examined in several studies. Sykes et al. (1982) conducted steady state numerical simulations of the landfill leachate plume using a variety of longitudinal and transverse dispersivities, with longitudinal dispersivities on the order of 5.0 m and transverse dispersivities on the order of 0.1 m providing the best fit between measured chloride and potassium data and simulation results. In addition, sensitivity analysis conducted in this study indicated that a transient flow system can have a significant effect on contaminant migration, and that changing velocity directions may be largely responsible for much of the lateral transverse dispersion evident in the leachate plume. However, these simulations were effected by potentially significant numerical dispersion. Using a different modeling approach, Frind et al. (1985) calculated a longitudinal dispersivity of 10.54 m for the landfill leachate plume, and suggested that the actual value is less since transverse dispersion was neglected in the calculation. Sudicky et al. (1983) conducted a small–scale natural gradient tracer experiment in the Borden sand. For a distance of 0.75 m from the injection wells, longitudinal and lateral transverse dispersivities of 0.0125 m and 0.005 m were estimated, respectively. For a travel distance of 11.0 m and travel time of 121 d, they estimated longitudinal dispersivity at 0.08 m, horizontal transverse dispersivity at 0.03 m, and suggested that vertical dispersion was described by a diffusion coefficient equal to $1.0 \times 10^{-10}\ m^2 s^{-1}$. For smaller travel distances, it was suggested that scale or time–dependent dispersion parameters are necessary to better describe the dispersion process. Their dispersivity values are also reasonable considering that the scale of their study is much smaller than the landfill plume. The Stanford natural gradient experiment followed, at a scale intermediate between the landfill plume and Sudicky's original experiment (Mackay et al., 1986). Freyberg (1986) performed a moment analysis of the Bromide tracer plume in this experiment to calculate macro–dispersivities, A_{ij}. Freyberg's first–cut analysis assuming a constant dispersivity and linear temporal growth of the plume's second moment yielded:

$$\begin{bmatrix} A_{11} & A_{12} \\ A_{21} & A_{22} \end{bmatrix} = \begin{bmatrix} 0.36\ \text{m} & 0.023\ \text{m} \\ 0.023\ \text{m} & 0.039\ \text{m} \end{bmatrix} \tag{2-1}$$

where the subscript 1 is the mean longitudinal direction of the plume, and 2 is the mean horizontal transverse direction. Using similar assumptions calibrated to snapshots of the plume at different times, he found the value for longitudinal macrodispersivity increased from 0.06 to 0.43 m over a period of about 1000 d. The horizontal transverse apparent macrodispersivity showed no similar increase in magnitude, with the value similar to that given above for the average fit. Finally he applied scale-dependent stochastic theories to estimate an asymptotic (large travel distance) longitudinal dispersivity of 0.49m. Sudicky (1986) used his permeameter data and a general integral expression proposed by Gelhar and Axness (1983) to estimate the asymptotic macrodispersivity tensor, calculating the following values:

$$\begin{bmatrix} A_{11} & & A_{13} \\ & A_{22} & \\ A_{13} & & A_{33} \end{bmatrix} = \begin{bmatrix} 0.61\ \text{m} & & \sim 0 \\ & \sim 0 & \\ \sim 0 & & \sim 0 \end{bmatrix} \tag{2-2}$$

where 3 is the vertical direction. These were considered to be principle values. Sudicky (1986) also applied a vertically integrated theory developed by Dagan (1982, 1984) for determining macrodispersivity. This approach lead to $A_{11} = 0.45$ m and $A_{22} = 0$ for large times. In a related study Frind et al. (1987) examined scale dependent transport processes and the travel distance required to reach asymptotic conditions in the Borden aquifer using micro-scale modeling technique. Local- or micro-scale dispersion is handled in the governing equation while macro-scale dispersion is "represented through the advective-diffusive interaction between zones of contrasting velocity which are represented explicitly by the high-resolution flow field." Using a local pore-scale longitudinal dispersivity of 0.01-0.02 m, a vertical transverse dispersivity of 0.0, and an effective molecular diffusion coefficient of $D_d = 1.17 \times 10^{-4}$ m^2/d, they found that molecular diffusion can have a significant impact on the development of longitudinal macrodispersivity. They also show that asymptotic conditions may require numerous correlation lengths, up to 50 in their study, and that plume split-

ting due to velocity variations at the source can have important consequences in plume migration.

The intermediate scale natural gradient test conducted by Mackay et al. (1986) and the related analysis of transect data by Sudicky (1986) has been examined in many subsequent journal papers by other authors in an attempt to better understand the transport phenomenon. These include Barry et al. (1988), Naff et al. (1988), Dagan (1989), Naff et al. (1989), Barry and Sposito (1990), and Rajaram and Gelhar (1991). Barry et al. (1988) use the two–dimensional Dagan model (Dagan, 1982, 1984), which is based on the stochastic–dispersion equation, to predict the ensemble–mean tracer concentration within the Borden aquifer, and compare them to the measured data of Mackay et al. (1986). Their comparisons are generally quite good, however they conclude that the sparse data sets available did not provide the needed accuracy for proper comparison, and that a fully three–dimensional stochastic model could reduce some of the uncertainties associated with the data analysis. Barry and Sposito (1990) compare estimates of the low–order statistical properties of the Waterloo–Stanford data to the predictive model of Dagan (1988), with the analysis being performed in three–dimensions to remove the vertical averaging. The agreement between the model prediction of Dagan (1988) of total plume variance and that determined from the data was considered excellent, even though the assumptions contained in the model were not satisfied (Dagan, 1988). Barry and Sposito (1990) cite as one of the sources of uncertainty the lack of characterization of the local flow field at the Borden site. Rajaram and Gelhar (1991) also conducted a three–dimensional analysis of the bromide data from the Waterloo–Stanford experiment. Their approach uses more detailed methods of data interpolation and extrapolation. Based on what they term the fairly accurate prediction of the longitudinal macrodispersivity, they conclude that existing stochastic theories are partially validated. However, they estimate that the horizontal transverse macrodispersivity is larger than the vertical macrodispersivity, which they point out is contrary to the theories put forth by Gelhar and Axness (1983) and Dagan (1989) for steady flow. The value they predict for vertical

macrodispersivity is about twice the molecular diffusion coefficient, and was estimated at 0.0022 m which is typical of local dispersivity values. As with many other studies, Rajaram and Gelhar (1991) point out that an accurate prediction of the transverse second moment may depend on the transient nature of the flow field at the Borden site, but that suitable data for such an analysis was not yet then available.

Incorporation of unsteady flow effects into the stochastic theories proposed for the Borden site have been developed by Naff et al. (1988, 1989) and Rehfeldt and Gelhar (1992). Results from Rehfeldt and Gelhar (1992) indicate that the value for longitudinal macrodispersivity was not affected by the variable gradient direction, but that the transverse dispersivity value was estimated at 0.009 m which was considered similar to the observed value of 0.05 m and is larger than the molecular diffusion coefficient. The accuracy of their results suffered from limited data and large uncertainty in the covariance of the hydraulic gradient. Naff et al. (1988, 1989) also carried out studies to examine the variance of the plume from the natural gradient tracer test at Borden (Mackay et al., 1986). Their earlier model allows for three–dimensional flow, a highly stratified medium, and looks in particular at the time modeling of the second moment of the plume. They had success in fitting the two–dimensional model based on the model by Dagan (1984, 1987) but had limited success in fitting their three–dimensional model. Naff et al. (1989) assumed the time–dependent and spatial processes were independent, and used a deterministic approximation of the temporal variation to determine the transverse second moment of solute mass. Dagan (1988) points out that the data do not support the basis of the three–dimensional model. The fit of the model to the data is good, indicating that it is possible that small transient fluctuations in the gradient could explain the unexpectedly large transverse moments at the Borden site.

Finally, a tracer test conducted less than one year prior to the present study, and just recently published, reveals several key features of the Borden aquifer which are directly applicable to the work conducted in the present study. Thorbjarnarson and Mackay (1994, this is part 2 of 3, see Mackay et al. 1994) conducted a forced gradient tracer test in the vicinity

of the present study and at the site of the Sudicky transects (Sudicky, 1986). They discuss the concept of a strongly stratified aquifer, and present results which more or less support this supposition and the results from Sudicky (1986). Estimates for dispersivities, derived from fits to a one-dimensional model, ranged from 0.01 to 0.11 m. Dispersivities were not seen to be time-dependent. The average longitudinal dispersivity, determined from 3 multi-level samplers located at varying distances from the injection well, was estimated at 0.02 m, which they noted is representative of a local dispersivity.

A porosity of 0.38 was calculated by Sudicky et al. (1983) for a site near the sand quarry, based on the difference between saturated and air-dried weight of relatively undisturbed cores. Porosity was determined by Mackay et al. (1986) using values of bulk density and solid density for 36 samples from 4 cores. The volume-weighted arithmetic mean was reported as 0.33 with the standard deviation of the spatial distribution as 0.0165, which is small compared to the spatial variability of hydraulic conductivity (Mackay et al., 1986). Nwankwor et al. (1984) reported saturated and residual volumetric water contents to be 0.37 and 0.07, respectively. These values suggest an upper limit for porosity of 0.37 or 0.38, but effective porosity may be closer to 0.30.

The specific yield, S_y, of the aquifer was evaluated by Nwankwor et al. (1984) using the methods of Boulton (1963), Neuman (1972), a volume-balance approach, and gravity drainage. Gravity drainage gave S_y=0.30 and the volume-balance approach gave S_y=0.25, after 65 hours of pumping. Both Boulton's and Neuman's method gave lower values of 0.08 and 0.07, respectively. Nwankwor et al. (1992) revisited the 1984 site, and conducted a more detailed drawdown test, measuring heads in both the saturated and unsaturated zoned. Their results indicate that the simplifying assumptions used by Boulton (1954) and Neuman (1972), to derive analytical solutions to the flow equations, do not accurately represent the drainage processes actually occurring in a pumped unconfined aquifer. Akindunni and Gillham (1992) applied a numerical approach to validating the conceptual model of Nwankwor et al. (1992). Their results agree with the model proposed by Nwankwor et al. (1992), and

their results also support the volume–balance method (see Nwankwor et al., 1984) in representing the trends in apparent specific yield during pumping of unconfined aquifers.

Sykes et al. (1982) used an annual average infiltration rate of 0.366 m/year for the landfill area and 0.305 m/year for non–landfill areas. Sensitivity to seasonal variations in infiltration was not investigated. Calibration of the potential and stream function model used by Frind et al. (1985) estimated the basic recharge value at 0.20 m/year and a maximum recharge value directly under the landfill of 0.80 m/year.

The aquifer water quality was a special consideration since interference effects by background anions in tracer samples can affect tracer analysis using HPLC analytic methods. Nicholson et al. (1983) found that overall TDS varied from 380. mg/L in uncontaminated water, to 3800. mg/L in the leachate plume, moving northeastwards from the abandoned landfill, along the bottom 2.5 m of the aquifer. Chloride and nitrate varied from 1.1 and 0.6 mg/L, respectively, in the uncontaminated water, to 347. and 5.3 mg/L, respectively, in the plume. Other contaminants included reduced iron, which varied from 2.2 mg/L in uncontaminated water to 30.–300. mg/L in the plume. In the tracer experiments described in this report, reduced iron from the portion of the pumping well within the leachate caused significant pump and pump–line clogging problems when it was brought to the surface and oxidized. Nicholson et al. (1983) reported the aquifer water pH at 6.8–8.0, and Ball et al. (1990) reported organic carbon for Borden bulk aquifer material at 0.021%, both factors which help to minimize the sorption of the FBA tracers used in this study on to the aquifer material.

The inorganic carbon content was estimated by Ball et al. (1990) at 1.73%. Assuming the source of inorganic carbon to be calcium carbonate, the calcium carbonate content of the bulk Borden solids is estimated to be 15.4% (Ball et al., 1990). Further analysis by Ball et al. (1990) has shown that the carbonates in the the larger size fractions occur largely as very fine micrite or biomicrite crystals, and that these are part of larger aggregated structures. The specific surface area of the bulk Borden solids is one to two orders of magnitude

greater than expected for nonporous spherical particles (Ball et al., 1990). This large surface area results from the aggregated particles in the form of intraparticle porosity, with total intraparticle porosities ranging between 0.004 and 0.020 cm^3/g (Ball et al., 1990). Brusseau (1993) points out that this is a very small portion of the total porosity, and that intraparticle diffusion is most likely negligible in the Borden sand.

As its absence from the record indicates, no site specific comprehensive hydrogeologic study has ever been conducted. Each time data was collected, analyzed and reported it was aimed at supporting a single relatively narrow experimental objective. As a result there are gaps and inconsistencies in the record that have never been resolved.

Water-Table Measurements

Head measurements for the capture zone experiments were taken using a manual water–table measurement device and vibrating–wire piezometers (VWP), or pressure transducers. The VWPs (Model 4500sL, Geokon Inc, Lebanon, NH) had a range of 0–10 psi, resolution of 0.025% full scale minimum and accuracy of $\pm 0.2\%$ full scale. The location of the seven VWP hydraulic head piezometers and the barometric pressure piezometer are shown in Figure 2–3. The VWPs were scanned by the data logger (Model CR–10, Campbell, Chatam, Ontario) once every 10 minutes. This data was stored in the data logger until downloaded to the on–site computer on a daily basis Monday through Friday. Downloading to the computer was initiated interactively. Roughly once a week (when manual water–table measurements were taken) data in the raw data set on the computer was saved to three files, one on the e:\archive partition of the hard disk, one on the c:\archive partition, and one on the a: drive, or floppy. This floppy was kept at the site until full, at which time it was replaced with a new one, the full one being returned to the office and stored. Also, at the same time, a copy of the dated data set was made on a separate floppy which was used to transport the data to University of Waterloo, (UW) where it was down loaded to an IBM RISC/6000, and then reduced using data reduction codes. Raw data was reduced by the following procedure:

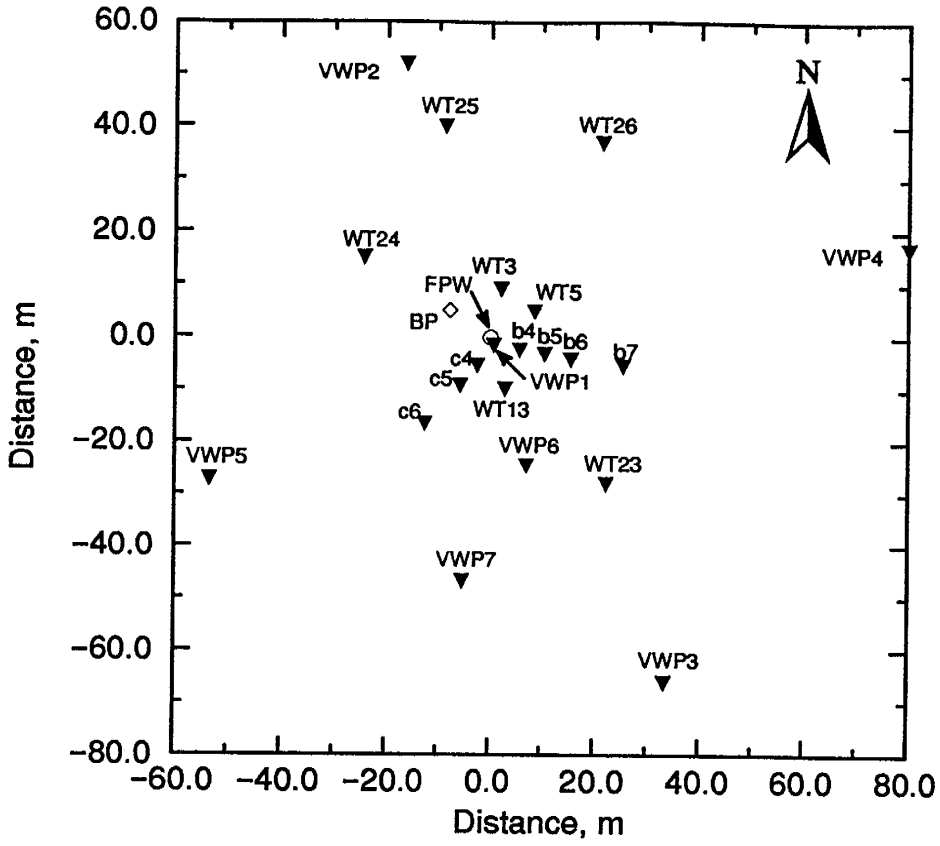

Figure 2–3. Plan view of Borden sand quarry showing location of pumping well (FPW), vibrating wire piezometers (VWP#), barometric pressure vibrating wire piezometer (BP) and water–table standpipes (WT#, b#, c#).

- the raw pressure data was converted to total pressure;
- the total pressure was corrected for temperature effects;
- gauge pressure was calculated by subtracting the atmospheric pressure;
- pressure head was calculated by dividing gauge pressure by the specific weight of water; and
- hydraulic head was calculated from pressure head and elevation head.

Reduced data was then in a form of {time,head} for each VWP piezometer. At the time of data reduction, manual head measurements (described next) were also entered onto

the RISC/6000 for use in the data reduction code and also for use in the determining a water-table map of the site.

In addition to pressure readings, water-table measurements were also recorded manually once per week. These measurements were used to act as a calibration data set for the VWPs and to also provide a larger data set with which to more accurately map the water table. Due to the degradation of the VWP system over the duration of this project, the weekly water-table measurements are the most reliable data and were used in essentially all subsequent analyses involving head in this project. Water-table measurements were taken at the 7 VWP stations as well as at an additional 15 sites, designated by WT#, b# and c# in Figure 2-3. The additional sites consisted of standpipes 2 inches in diameter and completed at various depths. Several different devices have been used to measure the head in the standpipes including an electric water-table tape, a flashlight and standard tape measure, and an electric water-table 'stick'. The flashlight and tape measure method proved adequate and was feasible since water tables were never more than 1.5 m below ground surface. The electric stick was the most accurate and easy to use and was used primarily during the second experiment while the first two methods listed were used prior to the start of the second experiment.

Figure 2-4 shows the water-table elevations for 5 measurement locations for the time period encompassing the project. The general trend is for the water table to drop during the summer and rise in the winter and spring. Also evident are perturbations about the trend, representing short-term fluctuations due to individual precipitation events.

Extraction Well Installation

The design of the extraction well is shown in Figure 2-5. It was constructed of PVC center stock with 1/4" polyethylene pump tubing connected to the outside. Seven pump intervals, each of 1 m length, fully penetrated the aquifer and provided vertical resolution of the breakthrough curves. The bottom 6 intervals extended from 8 to 2 m below ground sur-

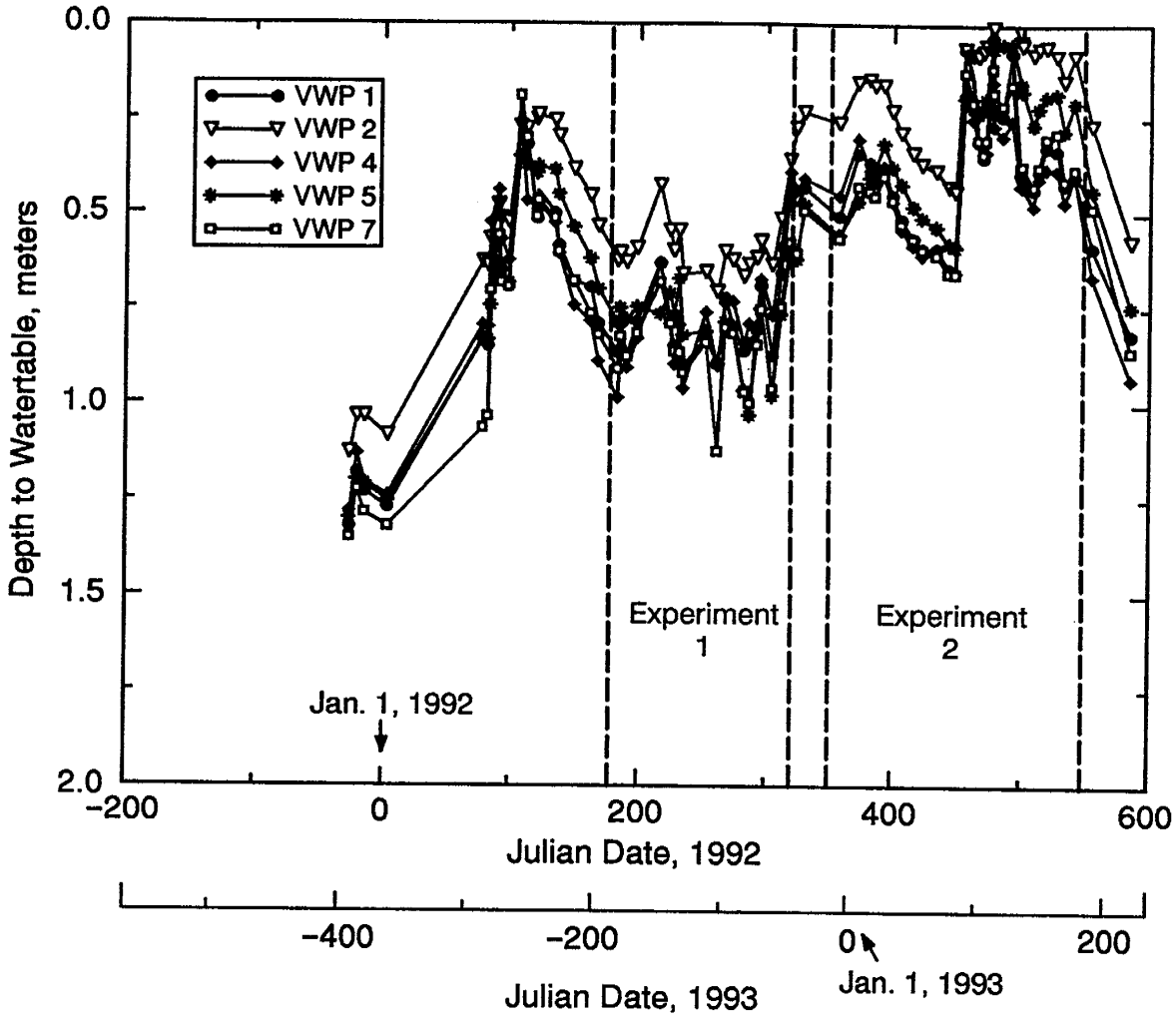

Figure 2–4. Depth to water table versus time for 5 of the 21 measurement locations in the Borden sand quarry.

face. Each interval was composed of 1/4" polyethylene tubing with holes drilled at 10 cm intervals over the 1.0 m distance. Starting at the bottom of an interval, the tubing had one set of holes (note: 1 set of holes constitutes 1 hole drilled through the entire tubing, or 2 holes in the tubing wall at that point) at 1 cm from the bottom. This set of holes constituted the bottom of the interval with the holes and bottom 1 cm being filled with silicon caulking which acted as a plug. The next set of holes was 0.5 cm above the first hole with successive holes at 10 cm intervals. Special care had to be taken for the uppermost pumping interval since the pump would be compromised if the water table dropped below the upper most

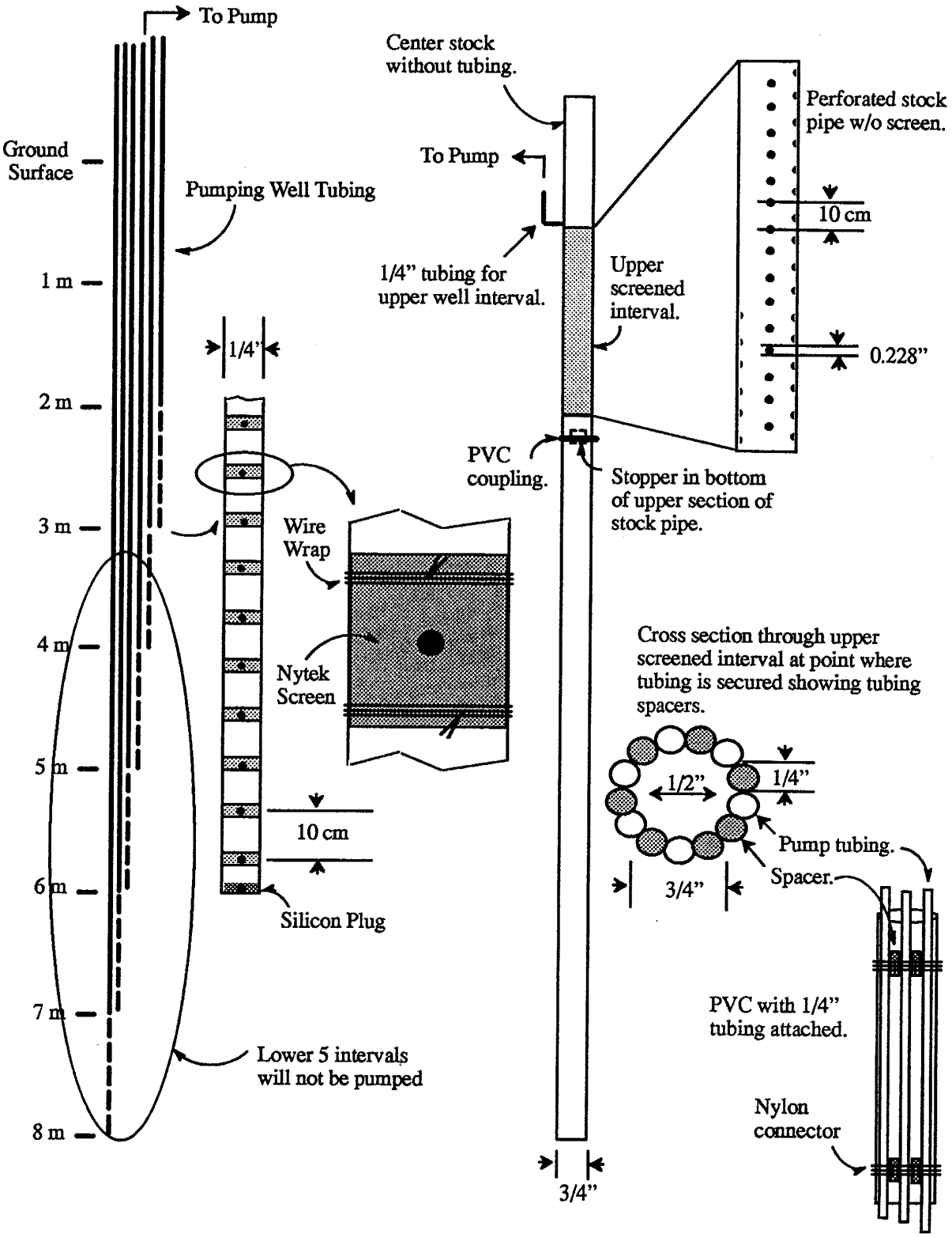

Figure 2–5. Schematic of extraction well.

screen and air was pumped. For the upper interval, a water table well was constructed. The center stock of the well was cut at 2.2 m below ground surface. A separate 3.0 m length of center stock was used for the upper interval, allowing 0.8 m to extend above ground surface. This portion of the well was connected to the lower portion with a PVC coupling. A rubber stopper sealed with silicone caulking was placed in the bottom of the connection to seal off the lower portion of PVC pipe. From a distance of 2.0 m to 0.5 m below ground surface, the pipe was perforated with sets of 0.228" diameter holes drilled 5.0 cm apart. Successive sets of holes were rotated 90 degrees to allow radial access of the aquifer to the inside of the pipe. This section of pipe was fully screened with 3 wraps of Nytek screen and wired at roughly 30 cm intervals. It was securely cemented to the lower portion using a standard coupling. The tubing from the lower intervals was evenly spaced around the PVC pipe using small (about 4 cm) lengths of 1/4" tubing at intervals along the pipe where the tubing was secured. Finally, a piece of 1/4" tubing was placed into the bottom of the top interval with which to draw water with. In Experiment 1, the fully penetrating well was used as shown in Figure 2–5. Experiment 2 was aimed at the effects of pumping well partial penetration. The same well installation was employed, but with only the top 2 intervals (the top tubing interval and the water table interval) being pumped.

The pump, along with accessory components, was housed in a 10' by 10' shed approximately 30 feet to the north of the pumping well. Figure 2–6 shows the schematic of the pump, filters and sampling manifold. The water from the well was brought into the shed in the 7 lines from the well, past spinners used to adjust the flow of individual lines visually. Water then flowed into the sample manifold where it was controlled by two sets of valves for each line. With both valves turned in one direction (up), water flowed from the first set of valves, through the sample vials, and then out through the second set of valves. With the valves turned a second direction (down), flow bypasses the sample vials and flowed directly to the second valves. When samples were taken, both valves for a single line were turned down, allowing the sample vials to be removed and a sample collected without disturbing

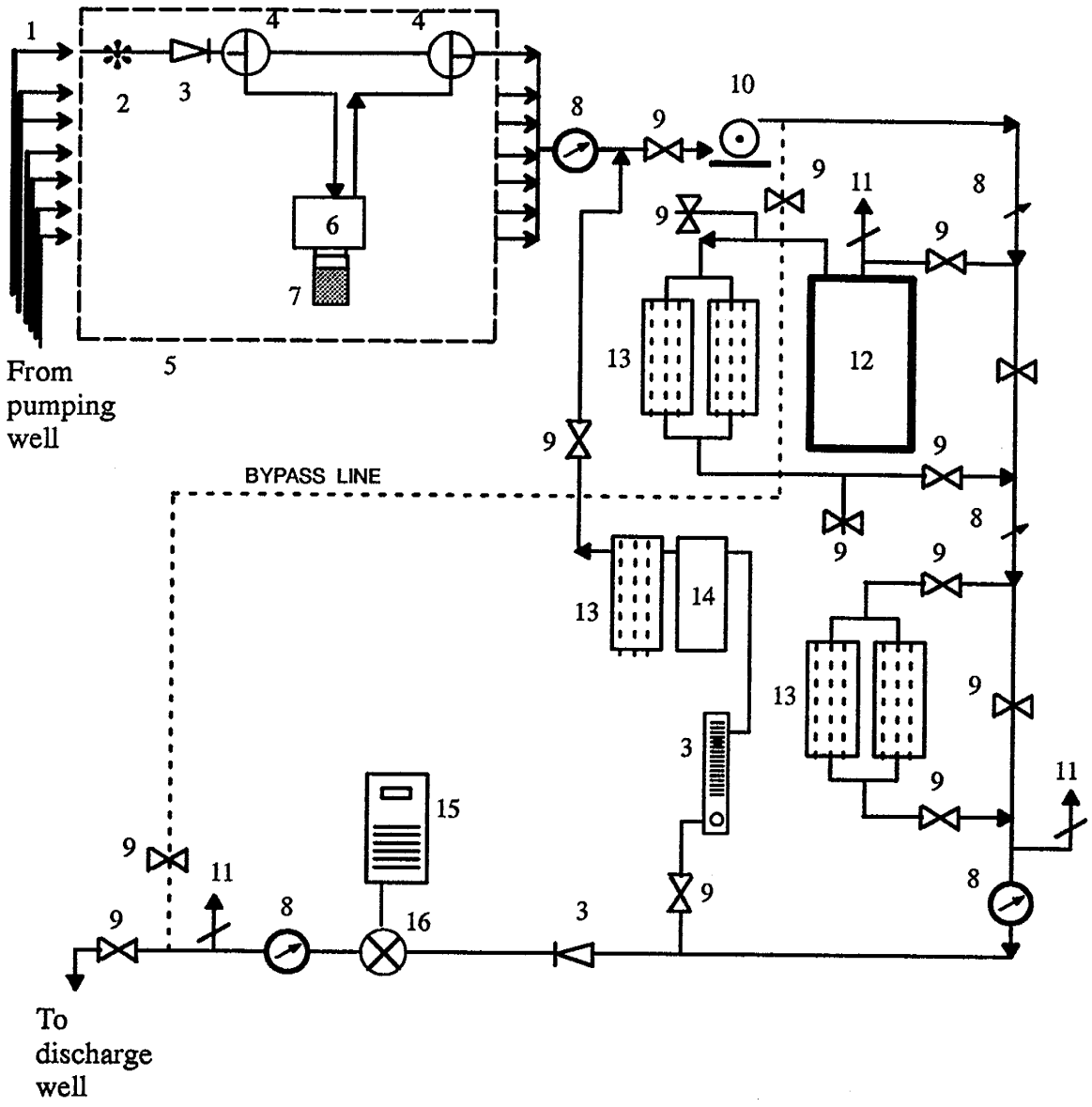

1. 1/4" tubing from well
2. Visual flow indicator
3. Flow regulating valves
4. Three-way stopcock
5. Sample manifold
6. Sampling device
7. Collected sample
8. Pressure gauge
9. On/Off valves
10. Centrifugal pump
11. Air release valve
12. Residence tank
13. In-line filter
14. Calcium hypochlorite feeder
15. Datalogger
16. In-line flow meter

Figure 2-6. Schematic of pump assembly.

the flow. A third valve setting (horizontal) allowed flow through a particular line to be shut off, which was required when cleaning a portion of a line. Once through the second set of valves, all pump lines flow into a single main pipe which was connected to the pump. Prior to the pump, a small diameter 1/8" line was connected to the pump line to introduce a small, continuous stream of calcium hypochlorite solution to the pump water which was thoroughly mixed in the pump. The calcium hypochlorite solution helped flocculate any iron oxide present in the water. After leaving the pump, the water flowed into a large settling tank. From there it flowed through two sets of filters, first through two 70 μm filters and then through four 50 μm filters. After the filters, the water flowed past a small diameter outlet pipe which circulated water through a canister containing calcium hypochlorite crystals and a single 50 μm filter, after which it was introduced into the flow system just prior to the pump. The main flow of water continued through the main flow-rate adjustment valve and then past a flow sensor (Model L-05621-54, Cole-Parmer Instrument Company, Niles, IL). The flow sensor was connected to a signal conditioner which converted the 'clicks' of the flow sensor into a voltage which was downloaded to the CR-10 data logger. An analog flow volume accumulator (Model L-05625-30, Cole-Parmer Instrument Company, Niles, IL) provided a backup record of cumulative flow. Once past the flow sensor, the water discharged into an underground pipe which transported the water 55.4 meters north and 101.0 meters east of the pumping well, where it was recharged back into the aquifer through an injection well. Additionally, five pressure gauges were connected in-line in the system, as shown in Figure 2-6. These helped to establish proper functioning of the system and to determine when filters were becoming clogged and needed replacing.

As with the VWPs, flow readings were recorded every 10 minutes by the CR-10 datalogger. The process of collecting and downloading the data was identical. The recorded flow rate for the first experiment is shown in Figure 2-7. The average flow rate for Experiment 1 was Q_{ave}=1.47 L/min. Figure 2-7 indicates that there were some small fluctuations in the pumping rate. This was caused by the large amount of iron oxide in the leachate which

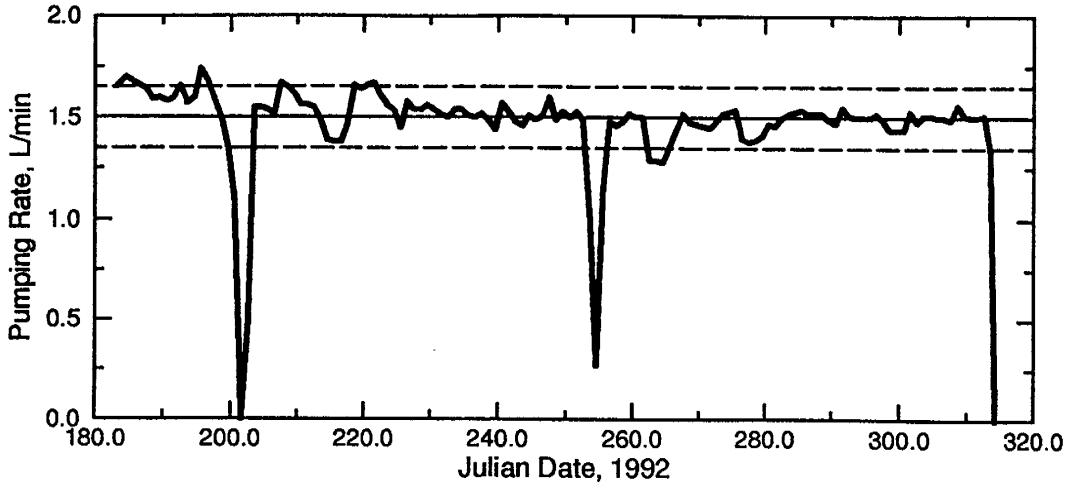

Figure 2–7. Daily average pumping rates versus Julian Date, 1992, for Experiment 1. Also shown is desired pumping rate of 1.5 L/min (solid horizontal line) and $\pm$10% of the desired rate (dashed lines).

clogged the filters relatively quickly and required daily flow rate adjustment. The pumping rate fluctuated within $\pm$10% of this rate. There were two brief periods when the pump system malfunctioned and shut off, or pumped at a significantly lower rate. Considering that the pump ran continuously for over 130 days this is a remarkable record of reliability.

Significant problems were caused by clogging of the sample collection manifold and downstream pump assembly and plumbing. Clogging was primarily caused by iron oxidation and precipitation. The leachate plume had concentrations of 20. to 30. mg/L of reduced iron (Nicholson, 1983) which was oxidized within the pump tubing due to diffusion of oxygen directly through the polyethylene, and due to mixing with oxidized, upper aquifer water at the downstream end of the sampling manifold. Two agents for clogging are possible. The oxidized iron can precipitate directly onto the inside of the tubing and pipes. Also, the presence of the iron reducing bacteria Leptothrix sp. and possibly Thiobacillus in the uppemost region of the aquifer (C. Richardson, pers. comm., 1992) would create colonies of these microbes within the plumbing system when they are mixed with the oxidized leachate water. Leptothrix sp. is known to derive metabolic energy principally from oxidation of ferrous iron

(Atlas and Bartha, 1987). The complex filtering and hypochlorite injection system was required to minimize clogging of the plumbing and subsequent damage to the flow control valve and especially the flow sensor.

The pumping rate during Experiment 2, shown in Figure 2–8, was 1.0 L/min during the first 120 days, and was then increased to 1.25 L/min for the remainder of the test. In the second experiment, the well was located in the upper region of the aquifer and did not intercept the leachate while the pump rate was 1.0 L/min. Consequently, there was no problem with iron oxide clogging of the plumbing and the pumping rate remained remarkably constant, as evident in Figure 2–8. However, there were still some problems with bacterial growth in the upper pump interval during the latter stages of the experiment following the spring thaw, especially noticeable during the period when the pumping rate was increased to 1.25 L/min as shown in Figure 2–8.

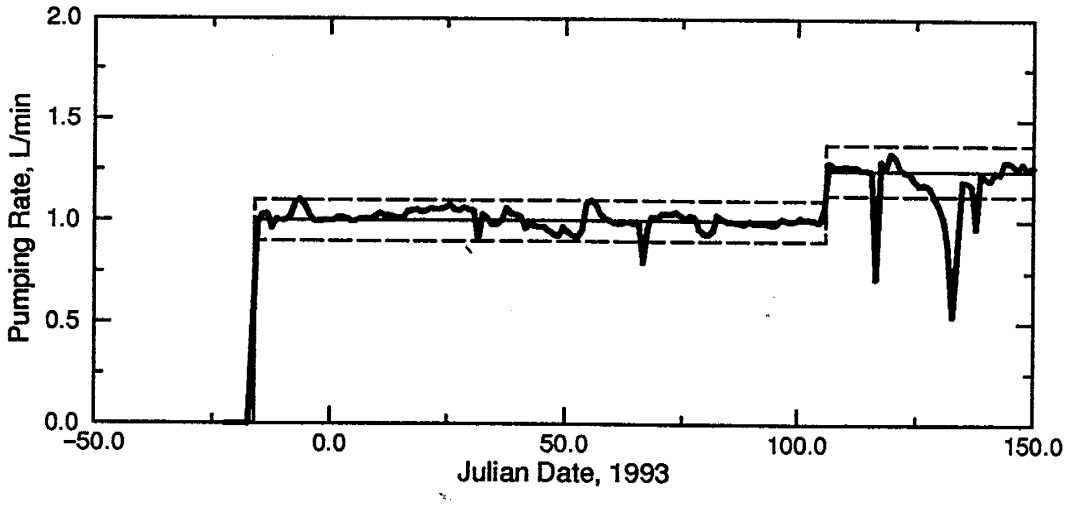

Figure 2–8. Daily average pumping rates versus Julian Date, 1993, for Experiment 2. Also shown is desired pumping rate of 1.0 (from t=–16 to t=106) and 1.25 L/min (from t=106 to t=187) (solid horizontal lines) and ±10% of the desired rate (dashed lines).

Multilevel Monitoring Samplers

Tracer concentrations in the aquifer were monitored with multilevel bundle–type samplers, constructed of 1/2" PVC center stock and 1/8" OD polyethylene tubing. There were 11 sampling intervals per bundle. The lowest interval was 8.0 m below ground surface and the others were spaced every 0.5 m above, with the top interval 3.0 m below ground surface. The 11 sample lines extended a short distance above ground and were connected to a sample manifold for sampling. Samples collected for Experiment 1 were taken from all levels for all samplers For Experiment 2, samples were only taken from the 3.5, 5.0 and 6.0 m intervals. The reduced sampling of the second experiment resulted from information gained during the Experiment 1 indicating: 1) the tracer plumes were large enough to be intercepted by fewer ports vertically, 2) the number of samples taken during the Experiment 1 was more than the tracer analysis laboratory could manage, 3) even at the higher density sampling, the ports were not close enough to give adequate information regarding tracer mass recovery, and fewer ports would give a similar amount of qualitative information, and 4) sampling in the middle of winter was harsh and difficult.

Locations for sample bundles are shown in Figure 2–9 for Experiment 1 and in Figure 2–10 for Experiment 2 and are designated by MW#–# and SW#. There was no difference in design for piezometers labeled MW or SW. The SW samplers were placed in the estimated vicinity of the stagnation point whereas the MW samplers were arranged in a "picket fence" structure downgradient of the capture zone. The horizontal spacing between samplers along the MW fences was 1.0 m, such that the maximum spacing perpendicular to these fences was 0.5 m. For flow at an angle to the fences, the spacing perpendicular to flow would be less than 0.5 m. The difference between positioning of some of these structures for the two experiments reflects information gained during the first experiment regarding the direction of ambient flow.

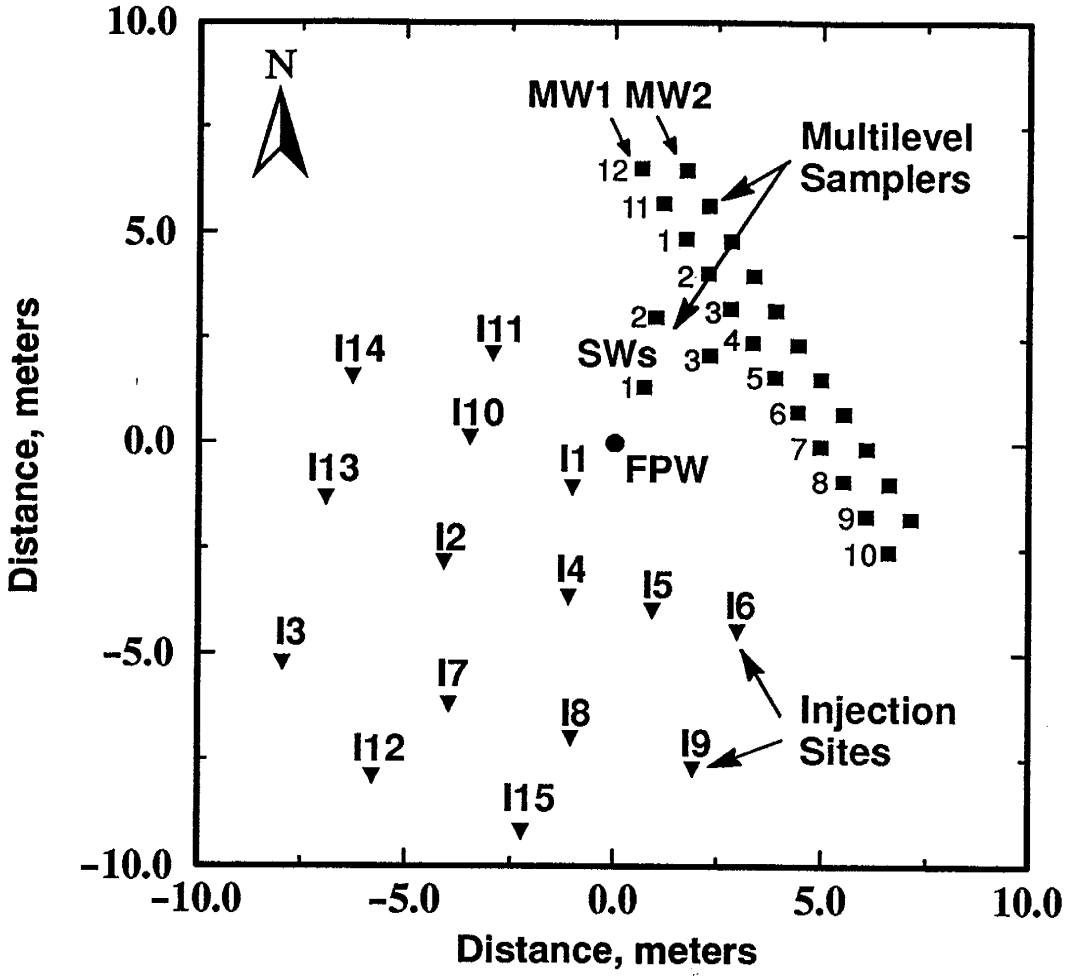

Figure 2–9. Plan view of Experiment 1 site showing location of injection sites (I#), multilevel sampling wells (MW#–#; SW#) and the fully penetrating extraction well (FPW).

Tracer Injection Sites

The injection wells were of a design similar to the extraction well, although significantly shorter. In Experiment 1, each injection well had 3 injection intervals of 1 meter each extending from 2 m to 5 m below ground surface. Experiment 2 had a similar system except 3 wells were modified such that injection well I3 had 2 intervals from 2 to 4 m and 2 intervals from 5 to 7 m. Well I14 had 2 intervals from 5 to 7 m. Well I12 had 3 intervals from 2 to 5 m, but only the top two intervals were used. A schematic of an injection well with 3 levels

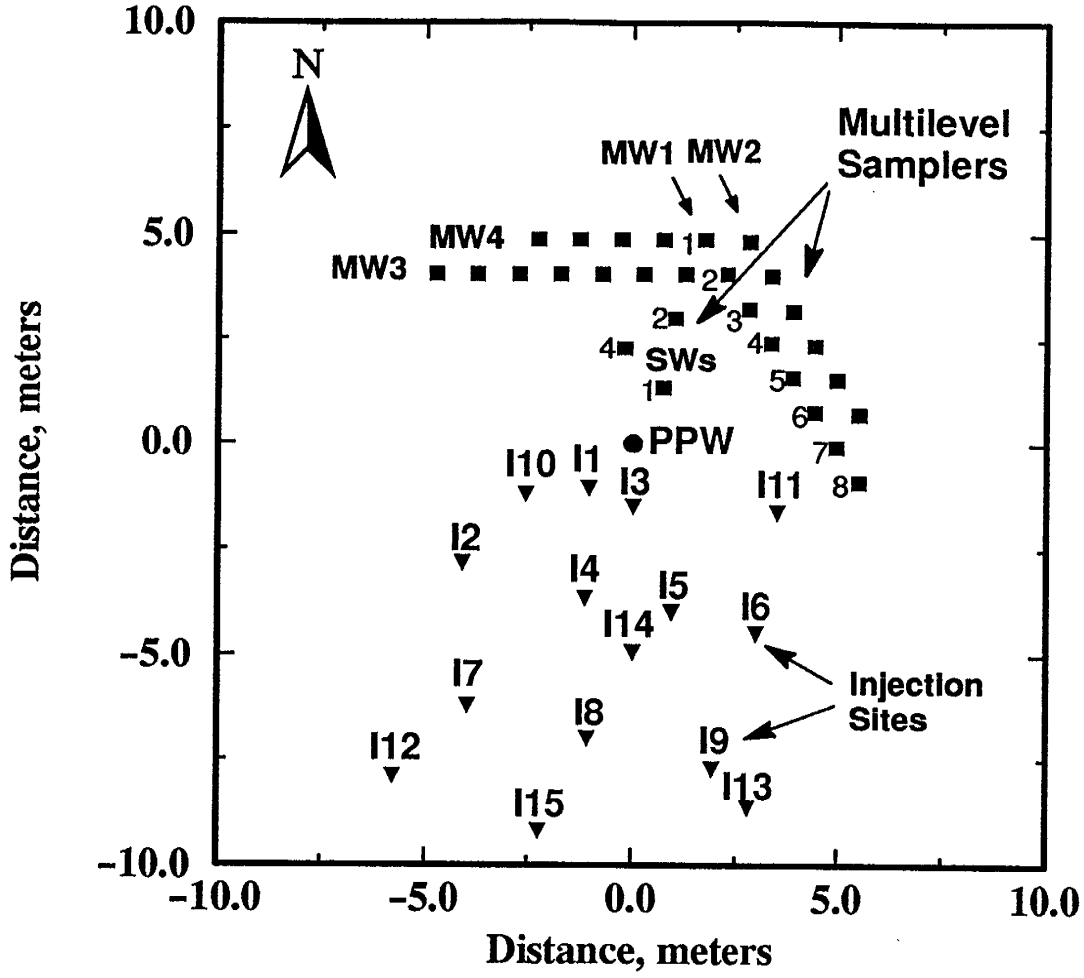

Figure 2–10. Plan view of Experiment 2 site showing location of injection sites (I#), multilevel sampling wells (MW#–#; SW#) and the partially penetrating extraction well (PPW).

of injection is shown in Figure 2–11. The injection well perforations were designed to insure uniform distribution of the tracer, and tested in a water tank in the lab prior to installation.

The location of injection wells for Experiment 1 is shown in Figure 2–9. The first experiment was oriented parallel to the estimated flow direction, N52E, based on data from previous experiments in the sand pit, and initial water–table measurements and gradient calculations made prior to starting the experiment. The MW sampling fences were aligned perpendicular to the flow direction. Tracer injection sites were chosen so as to delineate various aspects of the capture zone. In order to inject tracer at locations relative to the capture zone,

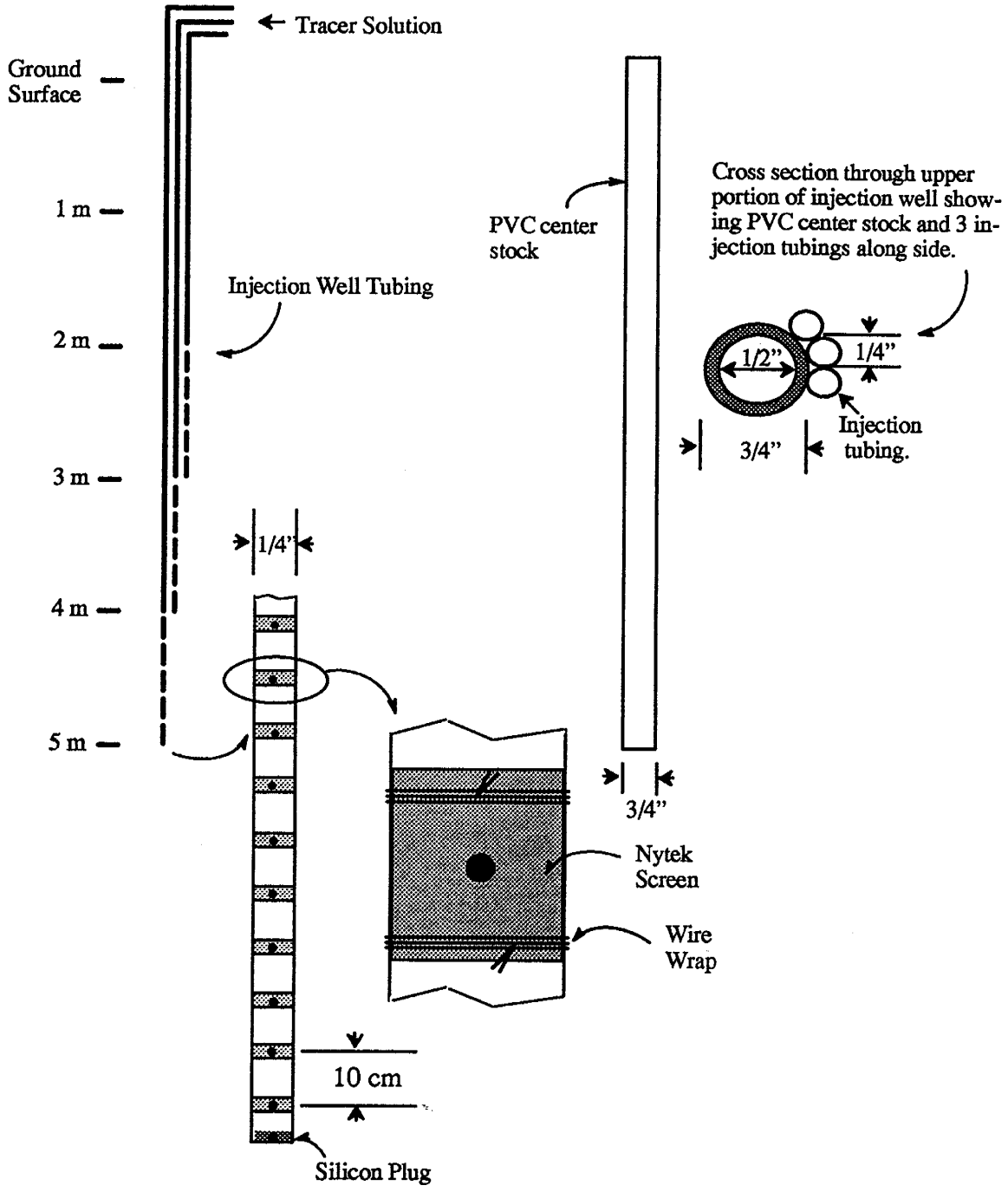

Figure 2–11. Schematic of injection well.

the location of the capture zone itself must be estimated. This was done with the aid of a simple predictive model of the capture zone, given design criteria such as pumping rate, and estimates of porosity, hydraulic conductivity and hydraulic gradient based on data collected during previous ground-water studies in the vicinity of the experimental site, and data collected during the study prior to experiment startup. To delineate the capture zone boundaries, tracer injection sites were arranged with sites inside the capture zone boundary, ensuring capture, outside the capture zone boundary, ensuring no capture, as well as in the vicinity of the boundary itself, possibly producing partial capture. Other injection sites were located inside the capture zone, away from the boundaries, to evaluate time-dependent capture fronts. If each FBA was injected at one site, only seven sites could be specified. Since this is a relatively low number of injection sites with which to delineate a capture zone, each tracer was injected at more than one site. Six of the FBAs were injected at two sites and one was injected at three sites, for a total of 15 injection sites. The arrangement of injection sites is shown in Figure 2-9. Injection sites used to evaluate time-dependent fronts were located along the estimated center axis of the capture zone, shown as sites I1, I2 and I3 in Figure 2-9. Four transects of 3 injection sites each were used to delineate the boundary of the capture zone. Two of these transects, used to delineate the southeast boundary of the capture zone, are I4, I5 and I6, and I7, I8 and I9, shown in Figure 2-9. The transects on the northwest boundary were originally I10, I11 and I12, and I13, I14 and I15. However, with the flow direction changing towards the north, I12 and I15 were considered to be too far outside the capture zone to be of any use, and so were relocated to the positions shown in Figure 2-9 before the experiment was started. Also, two additional multilevel samplers were added to the northwest end of fence MW1 (MW1-11 and MW1-12 in Figure 2-9) and one additional sampler was added to the northwest end of fence MW2, to accommodate the changing flow direction. Finally, the furthest injection distance from the well was constrained by the estimated time it would take for the tracer to reach the well. For a mean seepage velocity of approximately 0.091 m/day (Freyberg, 1986) and a desired experiment time of 90-120 days, 10 m was set

as the maximum injection distance. This was reduced to 9.5 m, for site I3, due to the location of nearby surface infrastructure. The transects were at an angle to the predicted capture zone boundaries to allow for shorter travel times to the extraction well for tracer injected at sites within the capture zone, and longer travel times for tracer injected at sites near the capture zone boundaries.

With each tracer injected at more than one site, there was the potential problem of differentiation of tracer breakthrough from multiple injection sites using identical tracers. To minimize potential overlap of breakthrough, injection sites using identical tracers were carefully spaced. For example, two tracers could be injected along the same estimated path-line, but spaced far enough apart that their breakthrough at the extraction well didn't overlap. This was the case for 2,3 DFBA injected at I5 and I8. It was also possible to inject tracer along two separate pathlines, with one site located on a longer travel time flow path than the other. This was the case for o-TFMBA injected at I1 and I13. Taking this to the extreme, some sites were considered to be outside the capture zone, such that tracer injected at those sites would not be expected to breakthrough at the well, and not interfere with breakthrough from the same tracer injected at other sites.

The tracer injection sites for Experiment 2 are shown in Figure 2-10. The injection pattern in the second experiment was essentially the same as in the first experiment, with the chief differences reflecting knowledge gained about the flow field during the first experiment, and the different pumping rate and extraction well aquifer penetration in the second experiment.

III. METHODS AND PROCEDURES

The general approach to conducting the capture zone experiments was to first design the experiment using simple mathematical models. Input into the models was primarily in the form of prior information from previous experiments in the vicinity of the sand quarry, and also data collected during the course of the study. Following the design phase, the next step was to install the experiment, which included design and fabrication of necessary equipment and materials. Once installation was complete, the experiment was initiated and the necessary data collected. Reduction, interpretation and modeling of the data was carried out during the course of, and following termination of the experiment. These steps are shown schematically in Figure 3-1 for both experiments. Implementation of the second experiment benefited from knowledge of the system gained during the first experiment.

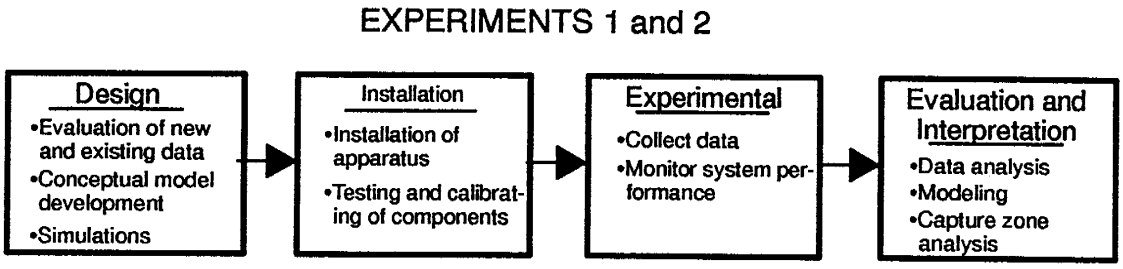

Figure 3-1. Flow chart showing 4 phases of each experiment.

Seven fluorobenzoic acids (FBAs) and potassium bromide were used for tracers, including four difluorobenzoic acid isomers, two trifluoromethyl-benzoic acids and pentafluorobenzoic acid. These particular tracers were chosen for their collective attribute of being simultaneously analyzable by the HPLC separation developed by Bowman (1984a; Bowman and Gibbens, 1992). Furthermore, the FBAs are noted for indeterminately low toxicity (as by U.S. federally mandated Material Safety Data Specifications), detectability at low concentrations, absence in nature, and conservativeness outside of areas with high organic carbon contents (Bowman, 1984; Bowman and Gibbens, 1992; Boggs and Adams, 1992). The tracers are listed in Table 3-1, along with some of their properties, and diagramed

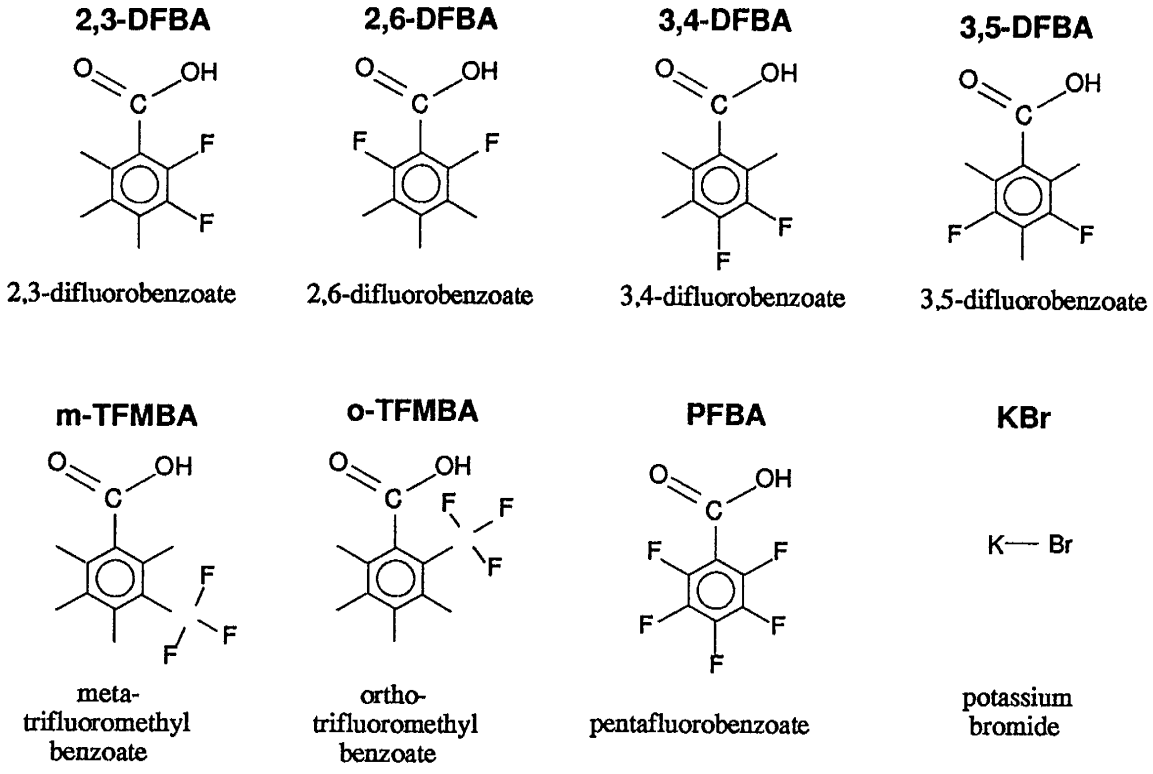

Figure 3–2. Molecular structure of tracers.

in Figure 3–2. The FBAs were obtained from Yarsley Fluorochemicals Ltd. (UK), while Br^-, in the form of KBr, was obtained from Aldrich Chemical Co. (Milwaukee, WI). The compounds were used without further purification from stock purity, which was 97%. The acid dissociation constants were determined for 0.01M solutions using base titration. Aqueous diffusion coefficients were estimated (Bowman and Gibbens, 1992; Benson and Bowman, 1994) from molecular structure using the Hayduk and Laudie method (Tucker and Nelken, 1982). Molar mass, melting point, and cost, are specifications from 1991 literature of Yarsley Fluorochemicals Ltd. and Aldrich Chemical Company. The dipole moments in Table 3–1 were calculated for the undissociated acid molecules by the Nelken and Birkett (1982) method. No data was available for the dissociated acid molecules. Hence, the dipole moments are only for purposes of relative comparison in subsequent discussion.

Tracer Description and Solution Preparation

Bowman (1984), and Bowman and Gibbens (1992) found that all the tracers used in this investigation have limited sorptive tendencies in batch sorption studies and field experiments involving sandy soils. Boggs and Adams (1992) and Benson and Bowman (1994) further qualified the sorptive tendencies with the caveat that acidic environments rich in humus, peat, or coal may produce hydrophobic sorptive interaction with the fluorobenzoic acids. The specific retention mechanisms appear to be similar to those in the HPLC column used to analyze the samples (later in this section), in that an acidic environment inhibits deprotonation in the fluorobenzoic acid tracers thereby preserving their neutral character. No batch sorption testing with Borden sand was undertaken as part of these experiments. The experiments were in a former sand quarry, aquifer pH was 6.8 to 8.0 (Nicholson et al., 1983), and injections entered the subsurface at 2 to 5 m depth and left the subsurface from pumping well intervals at 2 to 6 m of depth. There is no reason to expect FBA sorption, but further confirmatory batch tests may be warranted.

Each tracer solution was composed of tracer chemical and 10.67 liters of deionized water. Potassium hydroxide was added to all of the fluorinated benzoic acid tracer solutions, to neutralize the acidity of the tracer solution and to facilitate dissolution. The amounts of chemical used for each sample are listed in Appendices 1 and 2. All chemicals were measured by weight ($\pm$ 0.0005 grams). The 10.67 liter volume of water was also measured by weight, with an accuracy of $\pm$ 0.125 1b., and stored in individual plastic containers.

Table 3-1. Overview of tracer properties.

Tracer	pK_a	Dipole Moments	Aqueous Diffusion Coefficient ($10^{-10}m^2/s$)	Molecular Weight (g/mol)	Melting Point (°C)	Cost (US$/100g) July, 1991
2,3-DFBA	3.29**	3.05	7.6	158.11	161.5-162.5	236.84
2,6-DFBA	2.85**	3.16	7.6	158.11	158.5	22.35
3,4-DFBA	3.83**	3.05	7.6	158.11	120.0	346.68
3,5-DFBA	3.59**	0.24	7.6	158.11	120.0-122.0	236.84
KBr	N/A	N/A	18.7	119.01	734.0	9.50
m-TFMBA	3.8*	1.93	7.4	190.12	111.0	105.62
o-TFMBA	3.0*	3.30	7.3	190.12	103.0	170.10
PFBA	2.72**	1.59	7.2	212.07	103.0	90.72

* Gibbens, 1989; ** Benson and Bowman, 1994

To make an injection solution, approximately 1 liter of de-ionized water was removed from a container and mixed with the chemical tracer, along with an equivalent molar amount of potassium hydroxide. For almost all solutions, the additional potassium hydroxide had to be added to bring the pH up to 7.0. Potassium bromide was also added to the solution for 4 injection site solutions (see Table A1-1). When a pH of 7.0 was achieved and the solution visually appeared to be free of particulate matter, the tracer was considered dissolved. The measuring and combining of chemicals with the de-ionized water took approximately 30 minutes. The mixing process took between 30 minutes and 20 hours. After mixing was completed, the 1 liter solution was poured back into the original container. Additional mixing took place during transport of the solutions to the field site by vehicle, which took approximately 2 hours.

Tracer Injection

There were several design criteria and constraints used in determining the choice of tracer and its mass for each tracer injection site:

- Predicted tracer breakthrough concentrations and recoveries;
- HPLC interference effects;

- Detectable HPLC concentrations;
- Density effects causing downward tracer migration;
- Simultaneous well breakthrough of identical tracers from different injection sites;
- Well bore dilution;
- Aquifer transport properties: dispersion, sorption, degradation;
- Injected tracer volume;
- Tracer cost.

For an injected tracer mass to produce adequate well breakthrough, the concentration at which the mass is injected must provide adequate breakthrough resolution, minimize density effects, and be of a small enough volume to approach a point source in both space and time. The two dimensional, random walk, particle tracking, mathematical model described above was used to assess injection strategy. In the model "100 grams" of particles were released at each injection well location and observed as they arrived at either the pumping well or the downstream picket fence. Expected concentration breakthrough curves were computed and used to design the injection mass, as described below, and to minimize the probability of the joint arrival of a single tracer or interfering tracers from different injection locations.

Adequate breakthrough resolution at the well determined the minimum mass of tracer injected. As a rule-of-thumb peak breakthrough concentration should be about 10 to 100x the lower detectable limit (LDL) in order to be quantitatively identified. Under ideal conditions, the LDL for the tracers using HPLC analysis is about 0.005 mg/l. With background noise, the practical LDL is roughly 1 to 2 orders of magnitude higher. This implies that sufficient tracer should be injected to result in a peak concentration, in at least one of the pumping well intervals, of something like 5. mg/l (in practice the actual observed peak values were

in the range 1 to 5 mg/l). The model simulation suggested about 120. g should be injected at the farthermost injection site to achieve this goal.

The maximum amount of tracer injected is limited mostly by density effects, and secondarily by injected tracer volume and tracer cost. Sensitivity analysis with the model indicated that, for a fixed injection mass, breakthrough concentrations at the well were not effected by injection concentrations when the injection volume occurred within a radius of about 50 cm around the injection well (this assumes a cylindrical input volume based on injection well structure). Density effects were then the controlling factor, given a reasonable injection volume. A cylinder of fluid with a radius of 10 cm and height of 3 m was considered a reasonable volume of fluid which wouldn't adversely affect the flow field and could be injected relatively quickly. For an aquifer porosity of 0.33, a 32. L injection volume was calculated. The 3 m injection length, from 2 to 5 m below ground surface, allowed for some vertical migration of the plume while preventing it from either 'bottoming out' at the base of the aquifer, or migrating into the leachate which has an upper range of 5 to 6 m below ground surface. In addition, a three-meter long cylinder of fluid would ensure complete breakthrough over two of the one-meter long pumping well intervals.

Density effects were estimated using a simple analytical expression. The vertical density sinkage rate of a non-dispersing cylinder of dense fluid in a porous media is described by: $V_v=0.5K\Delta\varrho/\varrho n$, where K is hydraulic conductivity, n is porosity, ϱ is a reference density, in this case the density of the background aquifer water, and $\Delta\varrho$ is the density difference between the tracer solution and the aquifer water (Yih, 1965; see also Bear, 1972). The random walk model indicated a "minimum" injection mass of 120 g. This leads to an injection concentration of 120 g/32 L, or 3.75 g/L, resulting in a vertical, density induced velocity of $V_v=0.036$ m/d, for typical Borden parameters (including ambient density due to the background dissolved solids concentration). At this rate a tracer plume would sink 4.3 m for a travel time of 120 days. This is clearly too much, although this is a conservative estimate and

the actual sinkage would be significantly less. It ignores the fact that as the tracer plume disperses over time tracer concentrations, and the concentration gradient, will decrease. Less importantly the total dissolved solids within the aquifer increases with depth, especially near the leachate plume, further reducing the concentration gradient. This value is also conservative when compared to vertical migration of the plume in an experiment conducted by Sudicky et al. (1983). In their experiment, the plume dropped only 0.75 m in 121 days with a similar density contrast (approximately 1.8 g/L). Sudicky suggested that the vertical migration was due to both density contrast and vertical aquifer gradients. Mackay et al. (1986) had an injection density of roughly 1.2 g/L, and observed some initial plume sinkage.

Based on the above density considerations, total mass injected at each site was reduced to approximately 60 g, for an injection concentration of about 1.9 g/L, depending on the type of tracer, and whether more than one tracer was injected at a site. This concentration had an initial, maximum vertical, density induced velocity of V_v=0.016 m/d. Even at this rate the total sinkage would be less than 2 m, ignoring attenuation by dispersion. The mass was also reasonable in terms of tracer cost. The masses injected, along with location and time of injection for each tracer, are shown in Table 3-2 and Table 3-3, for Experiments 1 and 2, respectively, with additional details in Appendices 1 & 2. Injection well numbers refer to the numbered locations show in Figure 2-9 and Figure 2-10. All masses for the FBAs are given as measured in the lab prior to dissolution. The actual purity of the FBAs was 97%, and all remaining analyses used 0.97 of the measured mass listed in Figures 2-9 and 2-10.

The procedures for dissolving the tracer in the lab, and the injection procedure for the two experiments were given above. The tracers were dissolved in de-ionized water and solutions were neutralized with KOH in order to facilitate dissolution of the acid compounds, and to help match the ionic strength of the solution with that of the aquifer. The pH of the aquifer water was within a range of pH=7 to 8. Originally, $Ca(OH)_2$ was chosen as the neutralizing base since it may have better preserved the chemical balance of the aquifer wa-

ter. However, initial laboratory experiments indicated dissolution of this compound was too slow considering the large number of dissolutions needed.

Table 3-2. Tracer injection sites, dates and masses for Experiment 1. Injection sites correspond to the locations shown in Figure 2-9. All injections were from the 2-5 meter depth. See Appendix 1 for details. Masses for FBAs represent laboratory measurements and do not account for 97% purity.

Injection Site	Injection Date 1992	Julian Date 1992	FBA; mass, g	Bromide mass, g	KOH mass,g
I-1	July 1	183	o-TFMBA; 30.2	30.2	10.0
I-2	July 1	183	m-TFMBA; 30.2	32.8	9.6
I-3	July 6	188	3,4-DFBA; 60.4	-	24.5
I-4	July 1	183	PFBA; 60.3	-	19.0
I-5	July 1	183	2,3-DFBA; 60.4	-	23.4
I-6	July 3	185	2,6-DFBA; 60.4	-	23.8
I-7	July 6	188	3,5-DFBA; 60.3	-	24.4
I-8	July 3	185	2,3-DFBA; 60.4	-	24.5
I-9	July 3	185	PFBA; 30.2	29.3	9.3
I-10	July 1	183	3,4-DFBA; 60.8	-	23.8
I-11	July 3	185	3,5-DFBA; 60.4	-	24.2
I-12	July 6	188	PFBA; 60.3	-	18.5
I-13	July 3	185	o-TFMBA; 60.4	-	20.4
I-14	July 6	188	m-TFMBA; 60.3	-	20.5
I-15	July 6	188	2,6-DFBA; 30.2	29.9	12.6

In addition to the criteria mentioned above, two additional factors affected tracer injection and the resulting distribution of tracer in the system: vertical distribution of tracer along the injection well and disturbance of the flow field during injection. The vertical distribution of tracer during injection was assumed uniform. However, injection rates were quite low for I3 and I15 at the 2-3 m level for Experiment 1. Injection of tracer for Experiment 1 used gravity feed as the means of injection. Injection time for most Experiment 1 injections was 10-45 minutes, with the majority taking about 20 minutes. The two slow injections took about 2 hours to complete. It is impossible to determine the reason for the increased injection time, but it may have been due to clogged screens and injection ports, or

due to higher silt and clay content in the aquifer near I3 and I15. Injector I3 was pulled out and reinstalled prior to the start of the second experiment. At this time it was examined and checked for clogging or improper functioning but was found to be operating normally. Both injectors I3 and I15 were used again in Experiment 2 without any noticeable difference in injection times from other injectors.

Initially, gravity drainage was used to inject tracer in Experiment 2. However, it appeared injection would take considerable time, if it was at all possible. Consequently, the majority of the tracer injections for Experiment 2 were done using peristaltic pumps. This provided for short injection times of roughly 20 minutes and also gave more uniform injection rates than were seen for Experiment 1 injections. It is unclear why gravity drainage did not work for Experiment 2. It is worth noting that the only observed difference in conditions between Experiments 1 and 2 at injection time was the ambient air temperature. Experiment 1 injections were in the summer, Experiment 2 injections were in the winter with the temperature near freezing during the day and below freezing during the night. At this time, there was 15–20 cm of frozen soil at the ground surface. Tracer solution temperatures were well above freezing when injected in Experiment 2.

Disturbance of the flow field was not quantified in any way. However, it was noted that there was a build up of head in the injection tubing following completion of injection at several sites during Experiment 1 injections. Head buildup was not noticed as much or at all for Experiment 2 injections and may have been a result of using peristaltic pumps for injection. It should be noted that for all injections, there was disturbance of the head field. However, due to the small volume of injection, the short injection time and the high permeability of the Borden sand, it is assumed the disturbance was of short duration and equilibrium conditions were re-established quickly compared to the estimated travel time for tracer to migrate to the well.

Table 3-3. Tracer injections for the second experiment. Injection well locations given in Figure 2-10. Unless otherwise noted all injections took place over the 2-5 meter depth. See Appendix 2 for details. Masses for FBAs represent laboratory measurements and do not account for 97% purity.

Injection Site	Injection Date 1992	Julian Date 1992/1993	Tracer; mass, g	KOH mass, g	Inj. Depth Notes 2-5m unless noted
I-1	Dec. 18	352/-15	2,6-DFBA; 60.5	23.9	-
I-2	Dec. 23	357/-10	PFBA; 60.3	18.4	-
I-3	Dec 21	355/-12	Br^-; 19.5	0.0	2-4m
	"		3,4-DFBA; 40.2	17.2	5-7m
I-4	Dec. 21	355/-12	m-TFMBA; 60.3	20.1	-
I-5	Dec. 18	352/-15	3,5-DFBA; 60.4	23.9	-
I-6	Dec. 21	355/-12	o-TFMBA; 60.3	20.4	-
I-7	Dec. 23	357/-10	3,5-DFBA; 60.4	24.1	-
I-8	Dec. 28	362/-5	m-TFMBA; 60.4	20.3	-
I-9	Dec. 28	362/-5	2,3 DFBA; 60.4	16.4	-
I-10	Dec. 23	357/-10	2,3 DFBA; 60.4	16.2	-
I-11	Dec. 21	355/-12	2,6 DFBA; 60.4	24.0	-
I-12	Dec. 28	362/-5	2,6 DFBA; 40.3	24.1	2-4m
I-13	Dec. 28	362/-5	PFBA; 40.2	12.4	2-3 & 4-5m
	"		3,4 DFBA; 20.1	8.7	3-4m
I-14	Dec. 21	355/-12	3,4 DFBA; 40.3	17.1	5-7m
	"		Br^-; 20.0	0.0	@ the water table
I-15	Dec. 28	362/-5	o-TFMBA; 60.3	20.6	-

Tracer Monitoring and Sampling

Water samples for HPLC analysis were taken at the pumping well and at the multilevel sampler bundles. Pump samples were taken on a daily basis from Monday through Friday, and generally not taken during the weekend. The availability of personnel and the cost of collecting samples made weekend sample collection infeasible. Daily sampling, versus a higher frequency sampling, was considered adequate since plume breakthrough was estimated to take one or more weeks in most cases. This was verified by actual breakthrough data. Interpolation was used to in-fill where data was missing. This is reasonable since breakthrough curves are generally smooth in nature over a time period of several days.

Multilevel bundle samples were taken on a weekly basis. The multilevel samples were used as a check to determine whether tracer had bypassed the well and migrated down gradient or had migrated into the stagnation zone. These samples could only provide information on the general location of tracers at particular times since the sampling frequency in both space and time was inadequate to resolve plume breakthrough characteristics. Preliminary modeling indicated that a 10–25 cm spatial resolution would be required instead of the 50 cm spacing employed, and samples would need to be collected several times a week. This would have unrealistically increased the number of samples produced by the first experiment alone to over 30,000.

For the first experiment, an entire suite of bundle samples was taken per sampling period. This involved taking 286 samples which took roughly 8–10 hours to complete. The maximum amount of water extracted from each sampling port was approximately 50 ml and included both the purged volume and the 20 ml sample volume. Multiplied by 286 gives 14.3 L of water extracted during each sampling session. The volume of water flowing through the fence was approximately 18,326. L/week and the water extracted was 0.07% of this amount, which was reasonably small to be considered negligible. A total of 3146 samples were collected from the multilevel samplers during the first experiment. This large number of samples was more than the tracer analysis laboratory could manage such that, after preliminary screening, only the samples from the 4.0, 5.0 and 6.0 m depths were analyzed. Since the sample ports were not spaced close enough to allow for mass balance calculations, the fewer depths analyzed gave a similar amount of qualitative information.

Fewer numbers of bundle sample ports per sampling period were sampled during the second experiment. Based on plume behavior observed during the first experiment, only the 3.5, 5.0 and 6.0 meter intervals were sampled from all bundle piezometers during the second experiment. This sampling was not initiated until mid–March due to problems with sampling in sub–zero temperatures. This lower number of sampled intervals is considered reasonable since at 0.5 m spacing, resolution of plumes was not possible, rendering fence data

useful only as a general check on plume location at certain times. The reduced number of samples was also reasonable from an analysis standpoint. A similar calculation as above for 3 ports per bundle per week leads to 4.2 L, or about 0.02% of water flowing through the fence, extracted from the aquifer for Experiment 2. The upper 9 ports for all injectors were sampled prior to increasing the pumping rate during Experiment 2, which leads to a similar volume of extracted water as for Experiment 1 sampling sessions. A total 924 samples were collected from the multilevel samplers during the second experiment.

Once samples were collected and properly labeled, they were either stored in a refrigerator at the site until retrieved and shipped to New Mexico Tech (NMT), as was the case for pump samples, or they were immediately transported to UW and from there shipped to NMT. Usually samples were stored in a refrigerator at UW for one or sometimes more nights prior to actual shipment. Samples were shipped in coolers packed in ice packs. A packing list indicating destination, the number of samples, and a listing of the individual samples, times collected and the sampler identification was also included. Samples were refrigerated once received at NMT.

Laboratory Tracer Analysis

Samples from the pumping well and multilevel samplers were analyzed for tracer using an HPLC separation technique developed by Bowman (1984; see also Bowman and Gibbens, 1992; Benson and Bowman, 1994). The separation mechanism uses mobile phase pH, ionic strength, and organic modifier content, to differentiate tracer retentiveness on an anion exchange column, based on the degree of deprotonation, or acid dissociation constant, of each tracer. Several of the basic features and important considerations of HPLC analysis are discussed next. A more complete description of HPLC technique used during this study is presented in Appendix 3.

Prior to HPLC analysis, samples were filtered to remove particles in excess of 0.45 μm, which is the maximum threshold permitted in HPLC analysis. The chromatograms were

analyzed using peak height, which gave more reliable and consistent results than peak area. Single component tracer standards were tested before each mobile phase was used. In addition, the HPLC analysis used external calibration: detector response to a standard calibration suite under one mobile phase condition was applied to the five samples directly preceding and following that suite.

Accuracy of HPLC Analysis Table 3–4 is a compilation of statistics for three different eight–component standards. Standards 2 and 3 were derived from 1:1 and 1:10 dilutions, respectively, of Standard 1. Three standards were analyzed in triplicate for each of four mobile phases used (see Appendix 2, Table A2–4). The coefficient of variation for each tracer for each mobile phase for a particular standard, was used to calculate an average coefficient of variation for each tracer for all mobile phases. Its this value that is reported in the table. The coefficient of variation is larger for smaller concentrations, but is still less than 5%. Differences in the statistic can be attributed to slight temporal and spatial variations of sorptive properties, within the column, as functions of temperature and mobile phase properties. The relatively higher coefficient of variation for 3,4–DFBA and m–TFMBA is a reflection of how close the two tracers elute, causing interference in the signals.

Biodegradation To inhibit bacterial growth the principal consideration for sample storage was cooling. Syringe filtering of the samples prevented bacterial contamination of HPLC equipment. Leptothrix sp. is nonacidophilic, suggesting a weak predisposition to degradation of the fluorobenzoic acid tracers. This was confirmed in long-term testing of bacteria–rich aquifer water tracer standards. Although there were some deviations induced by a centrifugal filtering technique used initially, subsequent testing with low dead-volume disposable filters showed no tracer degradation over a period of three months.

Misidentification of Tracers Possible misidentification of tracers were attributed to two main causes: interference effects and column retention time drift. Interference resulted from non–target ion elution overlapping with desired tracer elution. This was especially a

concern with ions such as nitrate and chloride which have a potential to interfere with both the FBAs and bromide. Retention time drift was due primarily to increased anion concentration. This could result from either increased mobile phase anion concentration, or variable background TDS of the aquifer water. The TDS concentration for background samples ranged from 300 mg/L, in the uncontaminated upper intervals, to 3800 mg/L in the leachate plume at the base of the aquifer (Nicholson et al., 1983)

Bromide Recoveries In the first experiment, the mass of bromide recovered at the pumping well was 355% of that injected. Part of this discrepancy was attributed to interference effects from the leachate in the lower 2 m of the aquifer. Removing the apparent mass recovered from the lower 2 intervals of the aquifer gives a mass recovery of 154% of that injected for the upper 5 well intervals. From the analysis presented in Section IV, it is estimated that the recovery should be less than 100% of the mass injected. Some of the mass recovered from the fifth well interval (the third from the bottom) may also be attributable to interference from the leachate since the leachate most likely extends above the 5 m depth, however this amount is thought to be small compared to the actual Br^- recovered for this interval. Also, the mass recovered in Experiment 2 was 233% of the mass injected, and it was assumed that the capture zone did not intersect the leachate during most of the experiment. A partial solution was found when it was discovered that Br^- was being reported as KBr following HPLC analysis, while the injection masses were reported as Br^-. This correction was 0.6714 of the original amount, however, concentrations were still too high. It was then noticed that another correction of 0.6714 would give reasonable results for concentrations reported in both experiments. The total correction used was 0.4507, and all Br– concentrations reported herein reflect this correction. It is currently not known why the second correction is necessary, yet its use provides for reasonable results. The second correction is also supported by an independent check of Br^- values in selected samples conducted by New Mexico Bureau of Mines and Mineral Resources. Using ion chromatography, the values they re-

ported were consistently 50–60% lower than the HPLC results. It should be noted that there analysis was not able to resolve the interference effects attributed to the leachate.

Table 3–4. Average coefficient of variation, $\overline{C.V.}$, for each tracer.

Tracer	Standard 1 (mg/L)	$\overline{C.V.}$ %	Standard 2 (mg/L)	$\overline{C.V.}$ %	Standard 3 (mg/L)	$\overline{C.V.}$ %
2,3-DFBA	20.4	0.7	10.2	0.4	2.04	0.7
2,6-DFBA	20.4	0.6	10.2	0.4	2.04	0.7
3,4-DFBA	28.8	1.1	14.4	1.0	2.88	0.9
3,5-DFBA	20.2	0.8	10.1	0.2	2.02	1.6
m-TFMBA	21.2	2.3	10.6	0.7	2.12	4.3
o-TFMBA	21.6	0.5	10.2	0.5	2.16	0.7
PFBA	34.4	0.9	17.2	0.7	3.44	1.2
Br^-	15.0	0.6	7.5	0.3	1.50	1.3

Hydraulic Gradient Calculation

Hydraulic head measurements taken with vibrating wire piezometers were initially designed to provide detailed time profiles of the water table. However, due to lightening damaging the piezometers and the data logger just before Experiment 1 startup, VWP data is both incomplete and often unreliable even when data does exist. The most reliable source of head data is the set of weekly hand taken water-table measurements.

Hydraulic gradient was calculated from hand taken water-table measurements using a least-squares multiple linear regression method (trend surface analysis) which provides a planar fit to the head data at each measurement time:

$$h_k = a + bx + cy \qquad k=1,2,...,K \qquad (3-1)$$

where x and y are horizontal coordinates, origin at the pumping well (see Figure 2–9 and Figure 2–10) with positive x pointing east and positive y pointing north, k is the index of the measurement time, t_k, and K is the number of measurements. Head residuals were generally on the order of several centimeters, with maxima of approximately 10 cm. The water table gradient can be represented by

$$\mathbf{J}_k = \mathbf{i}J_{xk} + \mathbf{j}J_{yk} \quad . \tag{3-2}$$

with components J_{xk}=b and J_{yk}=c in (3-1). The magnitude J of the gradient is given by

$$J_k = \left(J_{xk}^2 + J_{yk}^2\right)^{1/2}, \tag{3-3}$$

where $J_x = -\partial h/\partial x$ and $J_y = -\partial h/\partial y$. The direction of flow is described by the angle θ_k, measured from north, the y-axis, in the geographically conventional clockwise direction (east is at 90°)

$$\theta_k = \text{Arctan}\left(\frac{J_{xk}}{J_{yk}}\right). \tag{3-4}$$

Between measurements, the magnitude and direction of the gradient were linearly interpolated providing piecewise continuous, time-dependent estimates:

$$J(t) = J_k + m_{Jk}(t - t_k), \qquad t_k < t \leq t_{k+1} \tag{3-5}$$

and

$$\theta(t) = \theta_k + m_{\theta k}(t - t_k), \qquad t_k < t \leq t_{k+1} \tag{3-6}$$

where m_{Jk} and $m_{\theta k}$ are the slopes of the linearly interpolated curves between the k and k+1 time steps for the gradient magnitude and direction, respectively. Figure 3-3 and Figure 3-4 present the magnitude and direction components of the hydraulic gradient estimates. Figure 3-6a illustrates a typical contour plot of the linear fit to the measured heads for day 393 (January 26, 1993). Gradients were also estimated using kriging, as shown in Figure 3-6b, but this did not appear to offer any advantages over trend surface analysis for this spatial pattern of water level measurements. Saturated thickness was also used in the computations, and was estimated from water table data at VWP1 using an aquitard depth of 8 meters below ground surface (see Figure 3-5).

Although higher frequency changes in the water table may exist, the weekly measurements are thought to provide a relatively good estimate of the changing flow field. This

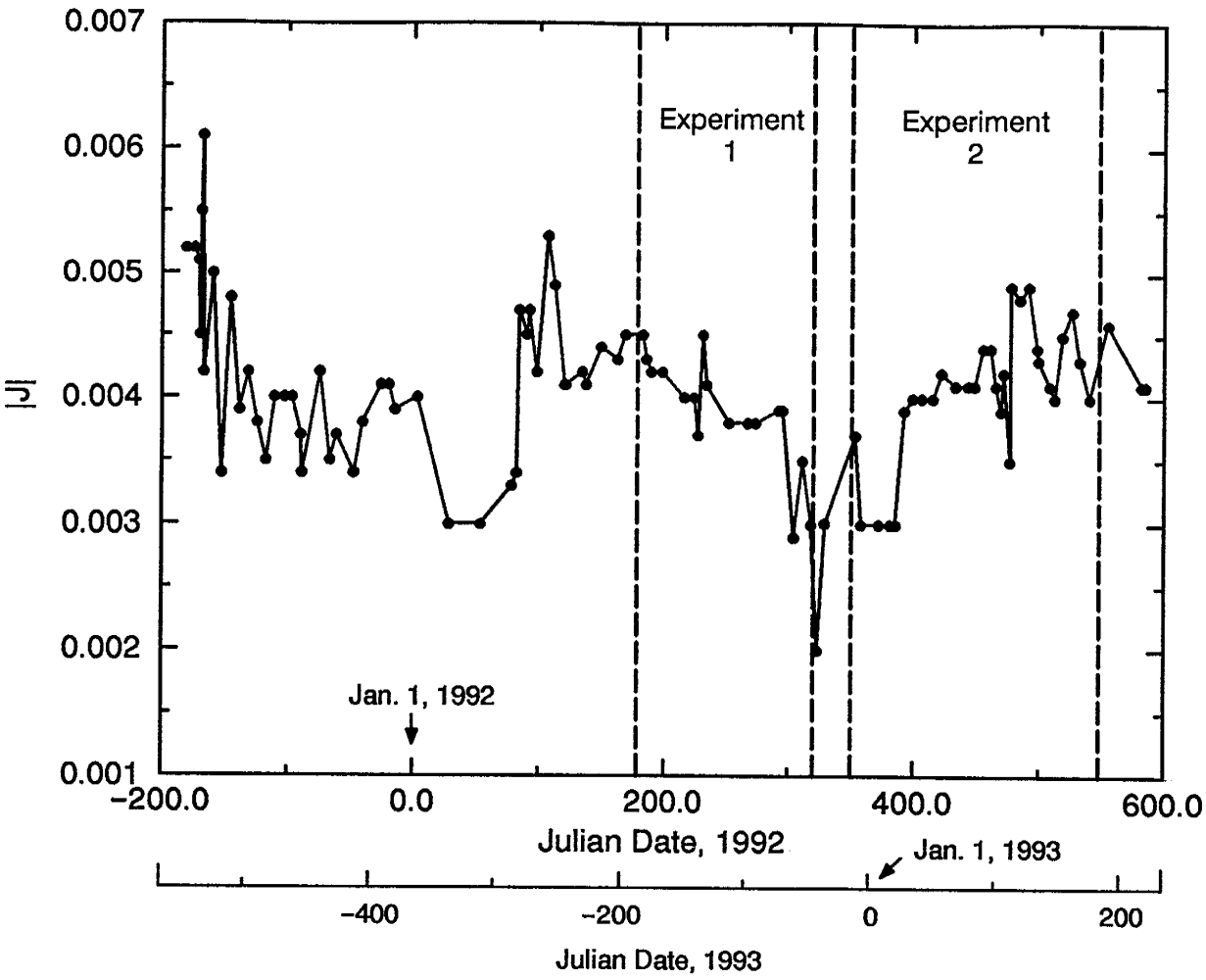

Figure 3–3. Magnitude of hydraulic gradient as a function of time.

is supported by preliminary frequency analysis of the VWP1 data set from t=234 to 329 d which indicates the highest observed frequency is 0.1/d. This frequency is observable using either the VWP or the hand measurement data sets. This suggests that hand measurements taken every 2 or 3 days would have provided more accurate time profiles of the gradient. However, the magnitudes of the higher frequency fluctuations and random perturbations about this trend would probably not have affected the fuzziness of the caputre zone significantly, such that the weekly measurements appear to adequately represent the mean flow field for that one week period with only small error.

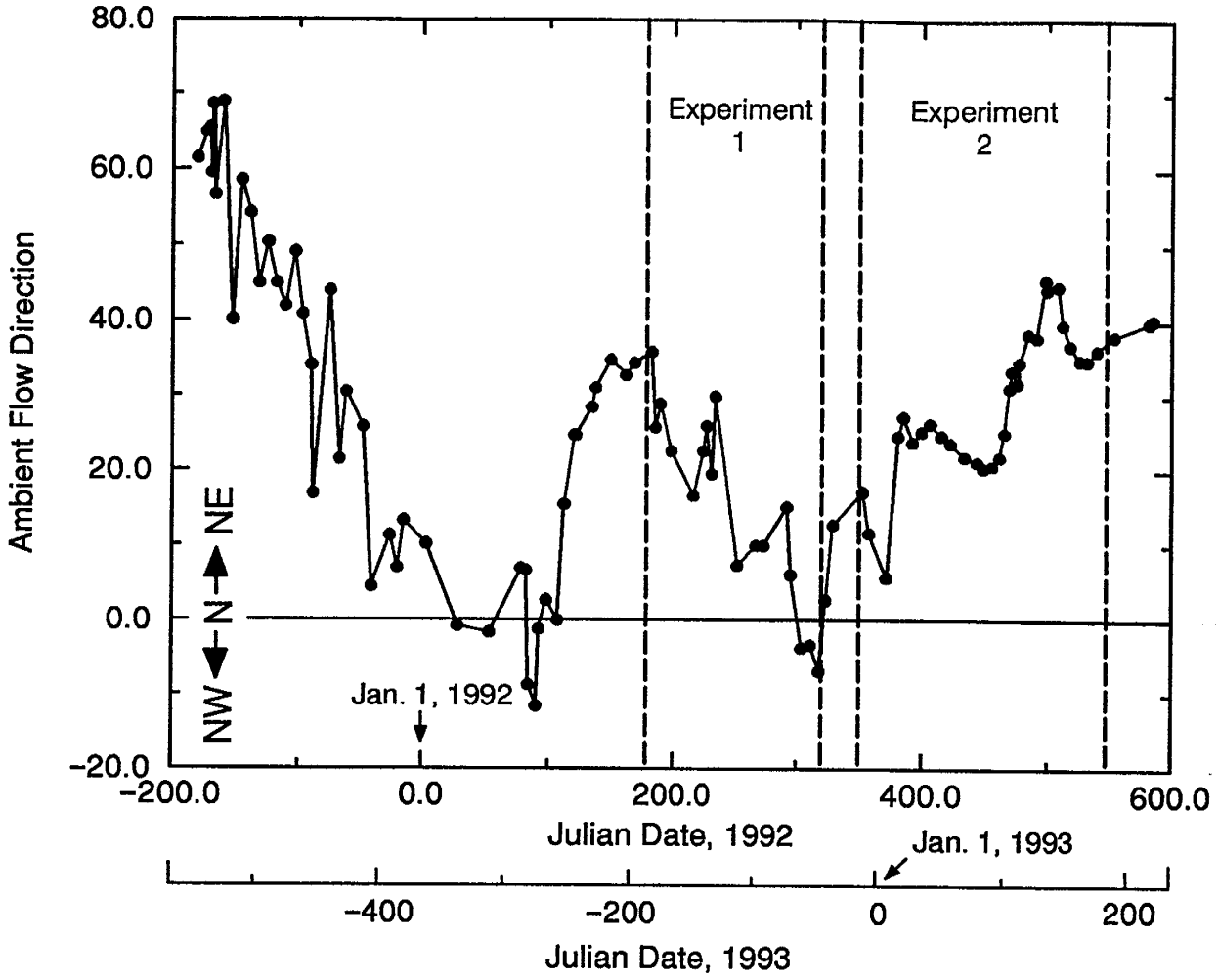

Figure 3–4. Directional component of hydraulic gradient as a function of time.

Capture Zone Modeling

With a single tracer injected at more than one injection site, and with possible interferences between different tracers during laboratory analyses (discussed later in this section), flow and transport modeling was used to assist with both the design and interpretation of the experiments. The modeling simulated tracer plume transport and breakthrough at the pumping well and the downstream monitoring fence of multilevel samplers. Using the model during the experimental design phase, tracer injection was simulated at candidate injection sites, and the best available information at the time was used to characterize aquifer properties and conditions. After the experiment, during interpretation of observed tracer break-

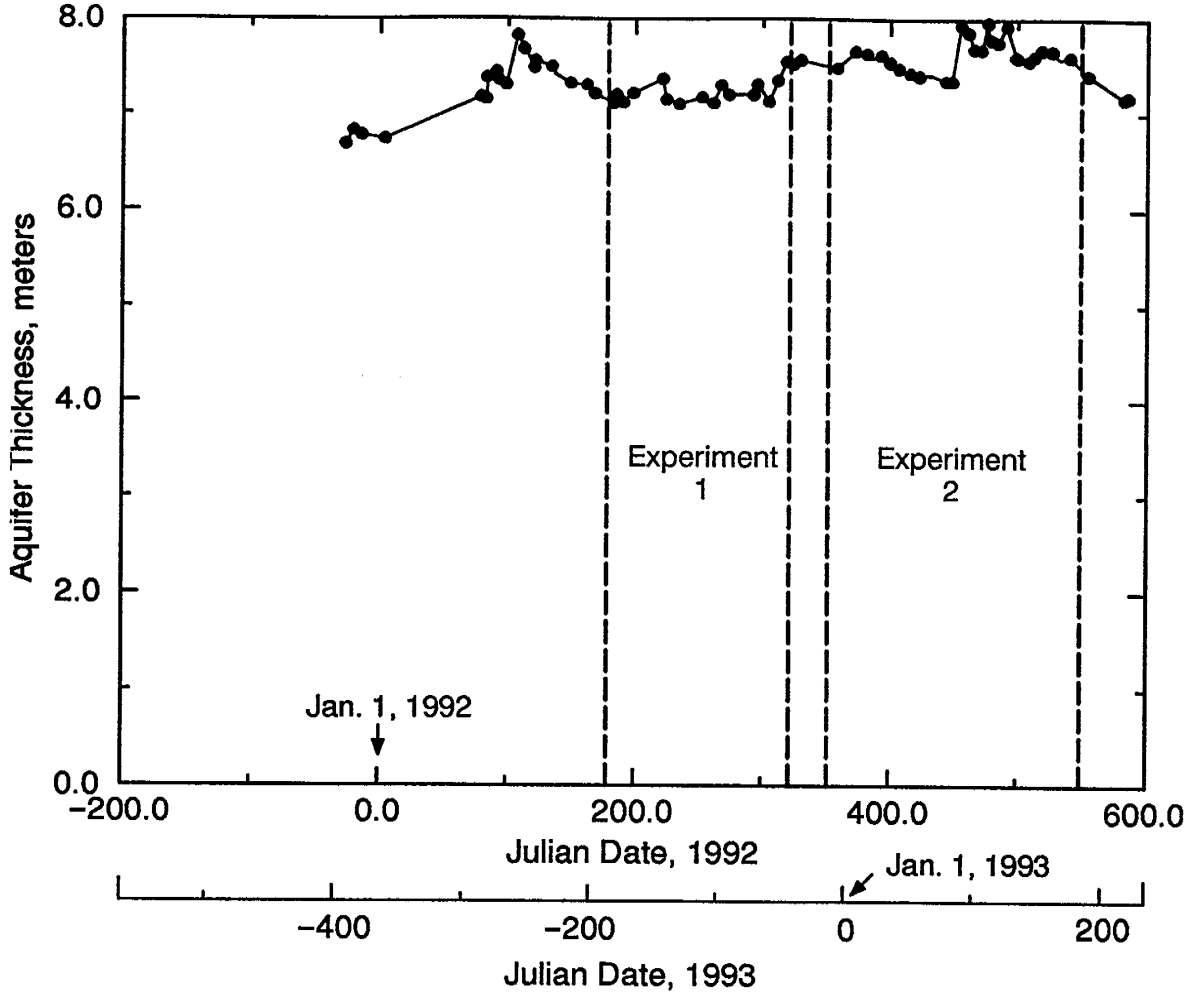

Figure 3–5. Aquifer thickness versus time measured at VWP1.

throughs, this was supplemented by all of the new information collected on actual tracer injections, water table elevations, and pumping rate. The values for hydraulic conductivity, dispersivity and porosity were estimated from previous work conducted at and near the study site (see Section II). The first experiment was designed using hydraulic gradients estimated in this previous work (MacFarlane et al, 1983; Mackay et al., 1986), supplemented by the water table measurements made the previous summer and fall (the first 200 days in Figure 3–3 and Figure 3–4). The second experiment was designed using a hydraulic gradient record based on the first 12 months of water level measurements (the first 400 days on Figure 3–3 and Figure 3–4).

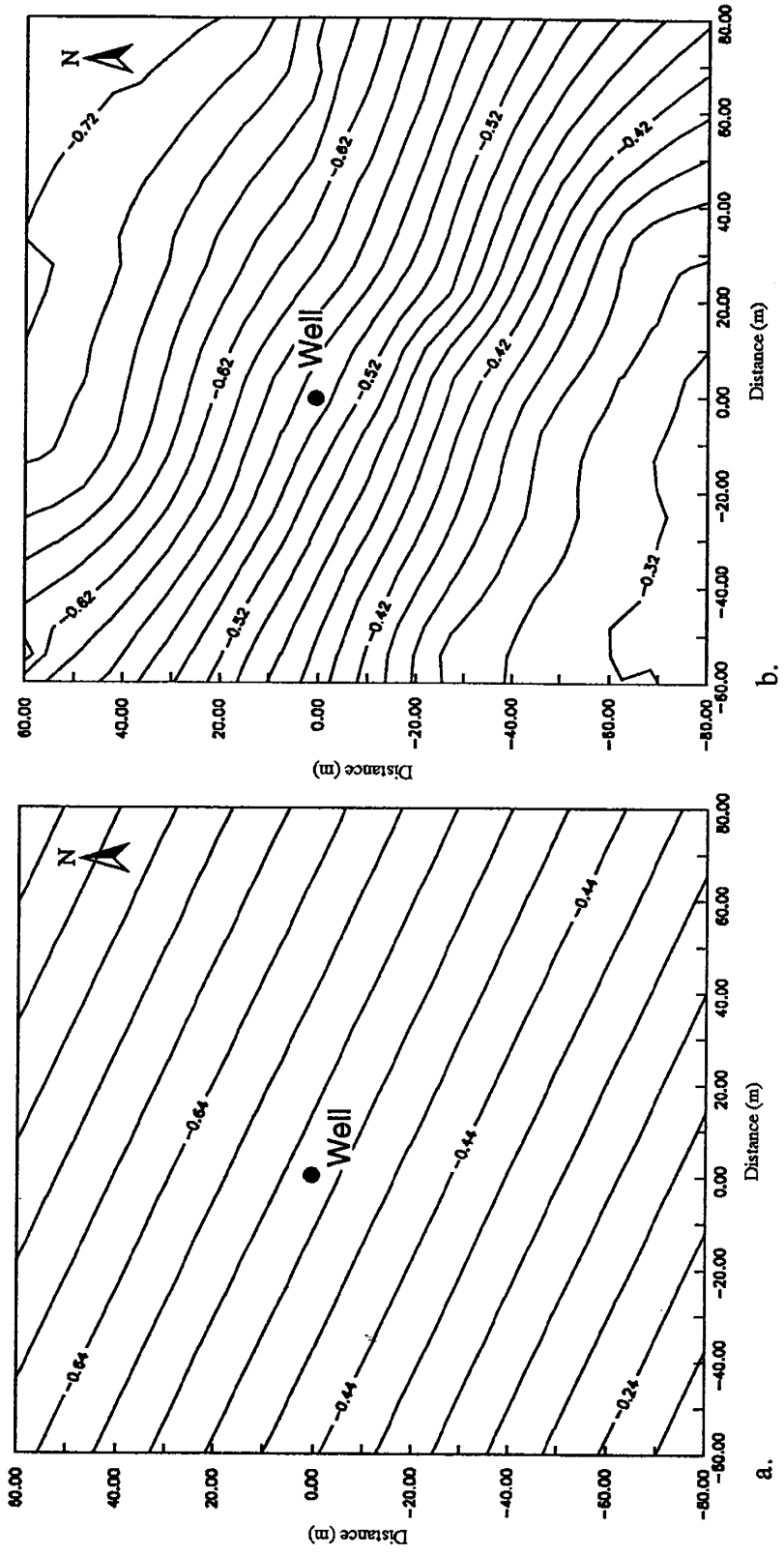

Fiugre 3-6. Contour plots of (a) linear fit to heads, (b) kriged heads using a linear variogram. Contour interval is in meters relative to VWP1 datum, time is Jan 26, 1993 (t=26, Julian Date, 1993).

A variety of modeling approaches were available to assist with the interpretation. Simple models are easier to use, but may not allow for certain types of behavior. More sophisticated models require greater understanding of the system. They also require a larger time investment in their development, necessary to obtain reliable results. The vertically integrated modeling approach described in this report used simple mathematical solutions to design both of the experiments, and as a first cut in the interpretation of the first experiment. These interpretation results, presented in the next section, provide direction for further modeling work and the construction of more sophisticated models as needed. They also provide a test of the applicability of simple models to capture zone delineation. Three-dimensional modeling was also employed and was essential for the interpretation of both the first and second experiments.

Vertically Integrated, Two-dimensional Model

The first-cut model was a linear, quasi-steady state, vertically integrated, two-dimensional flow and transport model with dispersion represented by the random walk method (Uffink, 1988; Kinzelbach, 1990). The random walk method has been used to solve groundwater flow and transport problems in previous studies (eg. Tompson and Gelhar, 1990; Tchelepi and Orr, 1993). The random walk method can be viewed as an analogue process to solving the governing advection-dispersion equation. Since it is not a direct numerical solution of the governing equation, it does not suffer from numerical dispersion (Uffink, 1988). The method handles sharp fronts well, and large Peclet numbers which typically cause problems in convential methods. Problems with using random walk typically have to do with statistical uncertainties associated with the number of particles used to define concentrations (Kinzelback, 1990). Concentrations may fluctuate, or appear 'spiky', limiting the precision with which the simulation results can be compared to measured data, especially when considering parameters with low sensitivity. These potential drawbacks are generally only a problem when local concentrations are of interest. Other problems are related to the selection of a

suitable particle step size, such as defining a suitable radius of capture at a withdrawal well so as to not influence breakthrough concentrations.

The modeled flow system consists of a single pumping well in an infinite flow domain with time varying uniform ambient flow. The solution to the flow field can be represented in its entirety by the complex function Ω (Bear, 1972) given by

$$\Omega = \Phi + i\Psi \tag{3-7}$$

where Φ is the complex potential function, Ψ is the complex stream function, and under steady state conditions Φ satisfies the Laplace equation, $\nabla^2\Phi = 0$. The state variable Φ [L^3/T] takes on different definitions in confined and phreatic aquifers,

$$\Phi = \begin{cases} Th & , \text{ confined or linearized Dupit phreatic aquifer,} \\ \frac{Kh^2}{2} & , \text{ Dupuit type phreatic aquifer,} \end{cases} \tag{3-8}$$

where h [L] is depth averaged head (also water table elevation in the phreatic aquifer case), K [L/T] is horizontal hydraulic conductivity, and T [L^2/T] is transmissivity. Using superposition, Φ is shown to be (Newsom and Wilson, 1988)

$$\Phi = \Phi_o - q_a(x \sin\theta + y \cos\theta) - \frac{Q_w}{4\pi}\ln(x^2 + y^2) \tag{3-9}$$

where Φ_o is the reference potential, q_a [L^2/T] is the ambient flow rate per unit aquifer width, and Q_w [L^3/T] is the pumping rate. Recall that x is positive to the east, y is positive to the north, and θ is the compass angle. The magnitude of q_a is found from Darcy's Law, $q_a = K\bar{h}J$ using a linearized Dupuit model and $\bar{h}$ is the constant saturated aquifer thickness. The magnitude and directional component of hydraulic gradient are given by J(t) and θ(t), respectively. This is an adequate model for the first experiment, because the ambient flow across the 15 meter long site is essentially horizontal, and there is almost no variation of saturated thickness with distance or due to pumping (maximum drawdowns were less than 10 cm.). Since the model neglected vertical flow, it was a crude design model for the second, partially penetrating well experiment.

In these simulations imaginary particles were injected into the system and tracked as they moved through the calculated velocity field. The velocity field was modeled by taking the derivative of (3–9) with respect to x and y space coordinates to obtain Darcy velocities. These were then divided by the porosity, n, and the aquifer thickness, $\bar{h}$, to obtain seepage velocities, V:

$$-\frac{\partial \Phi}{\partial x} = q_x = + q_a \sin\theta - \frac{Q_w}{2\pi}\frac{x}{x^2 + y^2}; \qquad V_x = \frac{q_x}{n\bar{h}} \tag{3–10}$$

$$-\frac{\partial \Phi}{\partial y} = q_y = + q_a \cos\theta - \frac{Q_w}{2\pi}\frac{y}{x^2 + y^2}; \qquad V_y = \frac{q_y}{n\bar{h}}\ . \tag{3–11}$$

Particle tracking was accomplished using the Euler method with a constant time step (Schafer–Perini and Wilson, 1991b). Proper step size was determined by running preliminary simulations at various step sizes to find the maximum allowable step size without introducing unreasonable error. The aquifer thickness, $\bar{h}$, was taken from data presented in Figure 3–5, and also from Mackay et al. (1986) when an estimated *a priori* value was used.

In the simulations, the tracers were considered non–sorbing and non–degrading, and density effects were assumed negligible. Aquifer storage effects were neglected and the response of the aquifer to changes of pumping and the ambient flow field were assumed instantaneous.

Breakthrough curves (BTCs) were generated in the following manner: Estimates for input parameters were taken from the data which, along with coordinate location, were fed into (3–10) and (3–11) to obtain seepage velocities. At each time step, the particle was first advected, then randomly perturbed (the random 'walk') to incorporate the mechanism of dispersive transport. Monte Carlo simulations were conducted to simulate the entire advective–dispersive transport process for tracer injected at a single site. Preliminary simulations were run with a small number of particles and a larger step size in order to get a rough indication of the results. Typically, 100 to 200 particles were used with a time step size of 0.1 d. Final simulations were conducted with 500 to 2000 particles depending on characteristics of the

particular simulation. Most two-dimensional simulations used 1000 particles. Important parameters considered in determining the number of particles were the dispersivities and whether plume splitting occurred (thus the preliminary runs). For a time step size of 0.1 d and an ambient velocity of 0.09 m/d, the spatial step size is 0.009 m. This is considered sufficiently small to preserve the statistical representation of the dispersion phenomena, yet large enough to provide for reasonably small simulation time requirements. When combining simulation results from two different injection sites that used the same tracer, the number of particles employed for each site was either the same, to ensure equal statistical representation from each site, or if a different number of particles were used, the particles were weighted according to the number of particles representing a given tracer mass.

Breakthrough at the pumping well or the monitoring fence of multilevel samplers was determined by recording the time when a particle passed within a critical radius. In the case of breakthrough at the pumping well, the particle breakthrough time was recorded when the remaining distance between the well and the particle's new location, calculated for the deterministic advective move segment, was less than the advective distance moved for that time step. Otherwise the particle would begin to jump across the well in a random manner as it neared the well. The error in this approach was small since the non-recorded time segment was less than the time step. Following the random walk simulation, post-processing was conducted on the breakthrough data which grouped particles into equal time histogram bins. Based on the mass each particle represented, and the volume pumped for that time interval, concentrations were calculated:

$$C = \#\ \text{particles} \times \text{particle mass} \times Q_w \times \Delta t_{cell} \qquad (3\text{-}12)$$

where Δt_{cell} is the histogram time interval. Breakthrough curves determined using the random walk method tend to be spiky. The smoothness of the BTC is largely controlled by and the number of particles in the simulation, the time-step size and the histogram bin size. Larger bins and more particles, as well as smaller step sizes, give smoother curves. However,

large numbers of particles cost more to run, and larger cells tend to average out spikes which may be important. The method employed in this study used a moderate number of particles, 1000, and 1-day bin size in time for well breakthrough analysis.

Breakthrough along multilevel sampling fence was determined using a slightly different method. A linear breakthrough fence was constructed, recording the time and position of particles as they crossed the fence. Fence intersection was tabulated when a particle first intersected the fence. This prevented particles from being counted more than once due to their nature of randomly moving about, or following pathlines that cross the fence more than once. Histograms were then constructed in space and time, with concentrations determined as above for the well BTC. A 5-day bin size in time, and 0.25 m bin size in space, were employed for fence breakthrough analysis. Simulated concentrations for individual samplers could then be read from the data output, or from a graph of the data, for a particular sampler location. Simulated breakthrough at individual multilevel samplers was also mapped. A 0.05 m capture radius about a sampler was used along with a 1-day bin size in time.

During the design of the experiments and in the initial model analysis for Experiment 1, the values for hydraulic conductivity, dispersivity, porosity and aquifer thickness were estimated from the literature (see Section II, this report): $K=\overline{K}_{11}=\overline{K}_{22}=7.09$ m/d, $\alpha_L=0.08$ m, $\alpha_T=0.001$ m, n=0.33 and $\overline{h}=7.0$ m. Some of these values were modified during the course of the analysis during model calibration. The average saturated aquifer thickness, $\overline{h}$, for Experiment 1 was based on data collected during the experiment and was estimated at 7.3 m. The transient nature of aquifer thickness, as well as hydraulic gradient, was incorporated into the model using two different methods. The simplest approach was to assume these parameters were constant from the measurement time to a time half-way between adjacent values, representative of a point-distributed discretization (see Aziz and Setari, 1979). The second approach was to incorporate more of the transient nature of the system into the model by al-

lowing for linear interpolation between measured parameter values. These two approaches are shown schematically in Figure 3-7.

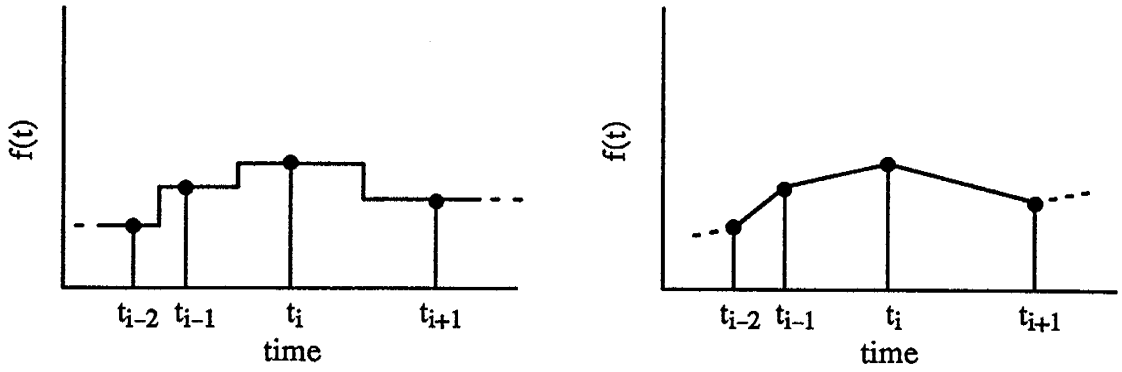

Figure 3-7. Point-distributed discretization (left) and linear interpolation (right) of time-varying parameters.

The longitudinal and transverse dispersivity used in the preliminary simulations were considered lower bound estimates, based on the 10 meter scale of the experiment. The effective longitudinal dispersivity is probably largest for tracers injected at the greatest distance from the pumping well, and could possibly be best represented by a linearly increasing value over the course of the experiment, as suggested by Mackay et al. (1986) and Thorbjarnarson and Mackay (1994). The majority of the simulations were conducted assuming constant dispersivities, however, simulations were occasionally run using a linearly increasing dispersivity to test this hypothesis. Simulations conducted using a constant value always compared more favorably to the measured data. A larger (horizontal) transverse dispersivity is reported by Mackay et al. (1986) and many other researchers (see review of previous work, Section II), yet Sudicky (1986) suggests that horizontal transverse dispersion may be represented by a value on the order of the vertical transverse dispersion coefficient and that larger values result from the time varying gradient.

The magnitude and direction of the hydraulic gradient were derived from multiple regression, linear least-squares fit of water-table measurements taken during the course of this study, as represented in Figure 3-3 and Figure 3-4. Linear interpolation between calculated gradient magnitude and direction provided continuous, time-dependent values. The pumping rate was also modeled as a time-dependent variable. Values were obtained from daily averages of the 10 min data logger readings, shown in Figure 2-7.

Three-dimensional Model

Simulations were performed using a three-dimensional, block centered finite difference flow code to generate velocity fields, and a three-dimensional random walk code to simulate transport. The random walk code was similar to the two-dimensional version used in Experiment 1 simulations, with the addition of 1) a third direction of flow and dispersion, 2) breakthrough at the well was determined for each well interval vertically, and 3) velocity fields were generated numerically. Heads and velocities were generated taking into consideration the thickness of the aquifer and the orientation and magnitude of the gradient. Vertical block dimension in the upper portion of the aquifer was 0.10 m (see Figure 3-8) An aquifer thickness of 8.0 m was used as the maximum vertical grid (and aquifer) dimension. The time varying depth to the water table below ground surface at VWP1 was used as the simulated aquifer thickness. For a thickness less than 8.0 m, the appropriate number of blocks at the top of the grid, representing the desaturated portion of the aquifer, were turned off. Aquifer thickness as a function of time, shown in Figure 3-5, was thus rounded off to the nearest 0.1 m in the simulations.

The estimated hydraulic gradient computed from hand measurements of water table elevation was used to prescribe heads along all four lateral boundaries of the grid, and for all nodes vertically at those boundaries. Since the magnitude of the gradient was small, the top of the aquifer was assumed relatively flat. The temporal variation of water table elevation was mimicked by turning off (or on) layers of blocks at the top of the aquifer. The as-

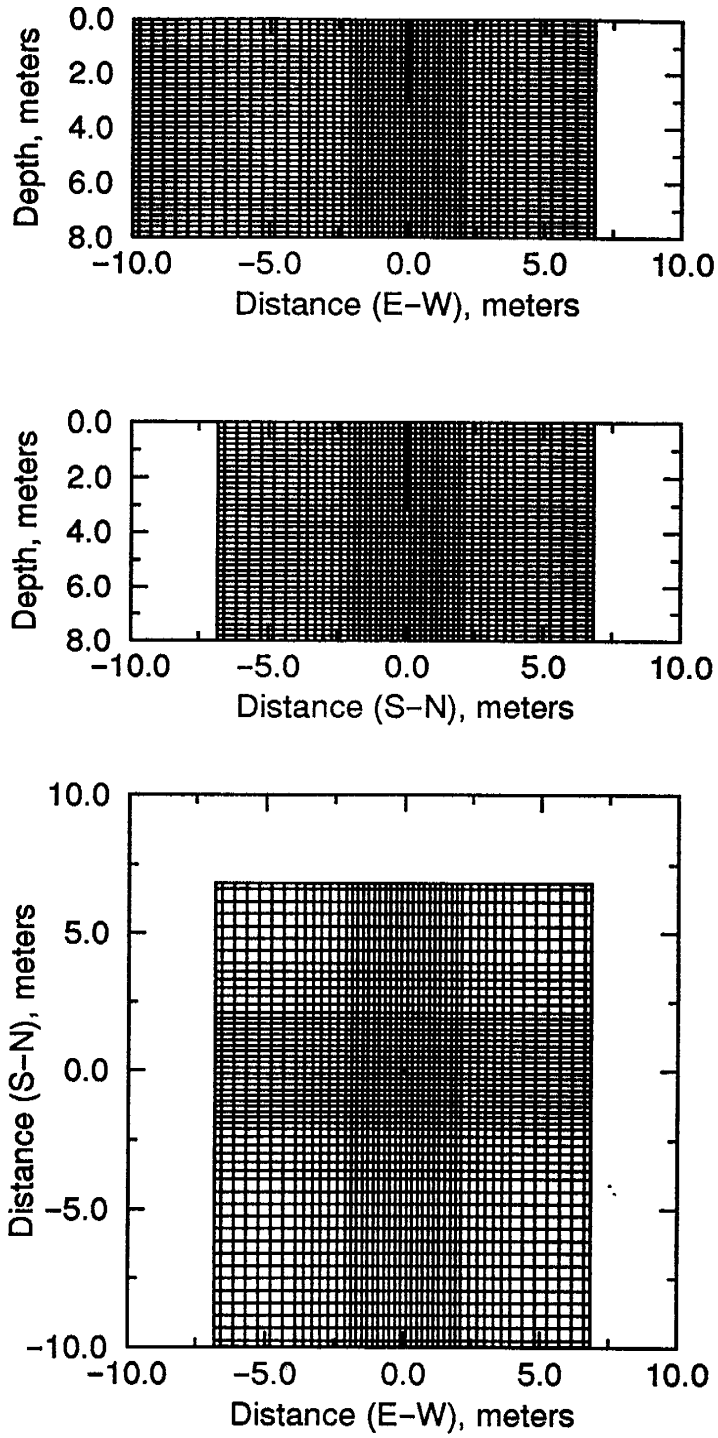

Figure 3-8. Grid used in three-dimensional, finite difference modeling.

sumption of an essentially flat upper surface is supported by use of a vertical block dimension of 0.10 m since the change in water-table height across the experimental site is generally less than this thickness. It is also similar to aspects of the Dupuit assumption used in the two-dimensional model analysis for Experiment 1. In order to vary water table elevation over the grid horizontally, the vertical block dimensions would have to have been approximately 0.01-0.02 m thick, which would have increased the number of blocks past a reasonable number, causing disk storage to become an issue. In essence, the vertical flow model was designed to address issues of aquifer heterogeneity and well partial penetration, not the minor effects of natural water table slope or the minimal water table drawdown due to pumping.

The transient nature of the aquifer was simulated in a similar fashion as for the two-dimensional model (see Figure 3-7). The time steps were based on the 24 hand measurements of water table elevation taken over the period of this test. Most simulations were done with the point-distributed discretization which greatly reduced the computational requirements as compared to linear interpolation of velocities. Particles were moved through the system for each time period, with their final location stored in an array. If a particle reached a boundary, including the well, its exit location and travel time were stored in a separate array. Once all active particles had moved through the system for the duration of a time period associated with a particular velocity field, a new velocity field was loaded into the velocity array and the stored particles re-activated into the system. Two stopping criteria were used for particles reaching the pumping well. One was similar to that used in the two-dimensional simulations, and employed an analytic velocity solution, where particles were removed if the distance between the last particle location and the well was smaller than the distance to be moved in the next advective-move step. A second criterion employed was for the particle to be removed once it moves to within a specified radius from the well, given by

$$s = \sqrt{\Delta x^2 + \Delta y^2} \qquad (3\text{-}13)$$

where Δx and Δy are the horizontal well-block dimensions in the x and y directions, respectively. For all simulations, $\Delta x=\Delta y=0.1$ m and s=0.14 m. With seepage velocity on the order of 0.1 m/d, the error in travel time is determined from 0.14 m/0.1 m/d=1.4 d, which is a maximum time since velocities are much larger near the well. Travel times are much larger than this for almost all of the tracers such that the error in calculating the total particle travel time by neglecting this small distance was considered negligible.

Well breakthrough was carried out as in the two-dimensional model. Fence breakthrough analysis was carried out by first checking whether a particle crossed a fence in the x-y plane. If yes, then the vertical location, along with the horizontal coordinate, was stored. Once all particles had been transported, histograms of the fence breakthrough were constructed, first in time, then in space, both horizontally and vertically, with bin sizes of 0.25 m in both horizontal and vertical directions. The data was then stored as s-z data (s being the horizontal distance along the fence from one end) for each particular time, or, alternatively, an s-t image could be viewed for any particular depth.

Breakthrough at individual multilevel samplers was handled in a similar fashion to that for breakthrough along a horizontal fence in the two-dimensional model discussed above. In this case however, the initial breakthrough criteria was a horizontal capture radius of 0.05 m. Once a particle intersected the sampler, the vertical location and time of intersection were stored for that particular sampler location. A two-dimensional, t-z, image could then be constructed.

There was a concern during the design phase of the experiment that high injection solution densities, relative to background fluid densities, would cause significant vertical migration of the tracer plumes. Based on previous experiments conducted at this and other sites, and on work by Yih (1965), injection densities of 1.89 g/L would not cause enough downward migration for the plumes to enter into the leachate zone or otherwise intersect the aquitard at depth. However, it appeared that densities would be large enough to cause signifi-

cant vertical migration of the plumes which would affect characteristics of the tracer breakthrough. To consider buoyancy effects in groundwater flow, the equation for flow in a non-deformable medium with constant porosity, is given by (Bear, 1972)

$$\nabla \cdot \varrho \mathbf{q} = -n \frac{\partial \varrho}{\partial t}, \tag{3-14}$$

where the assumption can often be made that $\mathbf{q} \cdot \text{grad}\, \varrho \ll n\, \partial\varrho/\partial t$ and that spatial variations in ϱ are much smaller than the local temporal variations. With this assumption, (3-14) becomes

$$\varrho \nabla \cdot \mathbf{q} = 0, \tag{3-15}$$

which is the form of the equation used to derive velocities in the three dimensional aquifer. However, transient flow due to density contrasts must still be addressed. To get around having to solve (3-14), a simple correction term for vertical velocities is derived and added to the velocities obtained from (3-15). This correction is based on Darcy's Law, given by

$$\mathbf{q} = \mathbf{q}_h + \mathbf{q}_b \tag{3-16}$$

where $\mathbf{q}_h$ is flow resulting from piezometric head differences and $\mathbf{q}_b$ is flow resulting from a buoyancy force acting on a fluid particle of density ϱ_f imbedded in a fluid of density ϱ_o. These two fluxes are given by (Bear, 1972)

$$\mathbf{q}_h = -K_{ij} \frac{\partial}{\partial x_j} \left(z + \frac{P}{\varrho_0 g} \right), \tag{3-17}$$

and

$$\mathbf{q}_b = -\frac{k_{ij} g (\varrho_f - \varrho_0)}{\mu} \frac{\partial z}{\partial x_j}. \tag{3-18}$$

The representation of buoyancy-induced flow given by (3-18) contains the assumption that density deviations from a standard ϱ_0 are small, which implies two things (Turner, 1973). First, the vertical scale of the mean motion must be much smaller than the scale height, and second, the fluctuating density changes due to local pressure variations must also

be negligible. The scale height is the distance over which the density falls off by a factor of 1/e. Turner (1973) suggests that an additional simplification is possible for incompressible fluids by not taking into account inertial effects of density variations initially, then calculating these effects after the fact from the solution of the corresponding Boussinesq problem. This is the approach essentially taken by Tchelepi and Orr (1993), and is applied in this study as well, and allows for direct application of (3–15).

Parameters used in the three-dimensional model are discussed in the appropriate parts of Sections IV and V.

Model Error Analysis

The error for overall tracer recoveries R is given as

$$\varepsilon_{R,i} = R_i - \hat{R}_i \ , \qquad i=1,2,...,8 \tag{3–19}$$

where R is the actual tracer mass recovered, $\hat{R}$ is the simulated recovery, and the subscript i refers to one of the 8 tracers. The error derived from comparison of breakthrough curves is given by

$$\varepsilon_{BTC,i} = \sum_{k=1}^{K} \left| R_k - \hat{R}_k \right|_i \ , \qquad i=1,2,...,8 \tag{3–20}$$

where R_k, k=1,2,...,K are the experimental mass recoveries for each time increment, t_k, and $\hat{R}_k$ is the recovery estimate from the model for each time increment. For observed and simulated BTCs that coincide perfectly, the error is zero. If the same two curves do not overlap at all, the residual is roughly twice the recovered mass. The error calculated above will give the total error between the simulation and the experiment for all tracers, in terms of mass. Estimation of error using this method depends on the number of injection sites and the mass of tracer being injected. In order to remove this dependence, the error in (3–19) and (3–20) can be divided by the tracer mass recovered giving the normalized error, or the error per unit mass recovered. Equations (3–19) and (3–20) become

$$RRE_i = \frac{\left|R_i - \hat{R}_i\right|}{R_i}, \qquad i=1,2,...,8 \tag{3-21}$$

and

$$RBE_i = \frac{\sum_{k=1}^{K} \left|R_k - \hat{R}_k\right|_i}{R_i}, \qquad i=1,2,...,8 \tag{3-22}$$

respectively. RRE and RBE, the relative recovery error and the relative breakthrough error, give the error per unit measured mass recovered for all tracers. Assuming the injections sites sample all aspects of the capture zone evenly, including points inside and outside, as well as on the boundary of the capture zone, then the best guess for breakthrough and recovery error per unit mass recovered for any injection site is given by RRE and RBE. These measures of relative error are useful tools in determining the error of the model since, for any mass recovered at the pumping well, the relative error represents the ability of the model to estimate the actual mass recovered.

IV. RESULTS AND INTERPRETATION: FIRST EXPERIMENT

The data available for direct delineation of the capture zone in each experiment is in the form of breakthrough curves and mass recoveries for each tracer at the pumping well and at the multilevel samplers. Assuming no other mass losses, well recoveries determined for each injection site represent a measure of capture zone at that site. For a relative mass recovery of 1.0 (i.e. mass recovered/mass injected for a particular tracer), the site is located entirely within the capture zone. For a relative recovery of 0.0, the site is "outside" the capture zone, that is, tracer injected at that site was not captured by the well. For relative recoveries between 0.0 and 1.0, the site is located on the boundary of the capture zone which is fuzzy due to the effects of dispersion, the fluctuating flow field, or other causes.

Interpretation of the experimental results was carried out first without the assistance of model comparisons, followed by analysis using two- and three-dimensional models. Initially, the two-dimensional simulation results were compared to the measured breakthrough and recovery data. Once the two-dimensional model was tested, additional interpretation using a three-dimensional model focused on discrepancies between the observed and simulated capture zone, taking into account aquifer heterogeneity, vertical flow and dispersion.

Tracer Breakthrough and Recovery Analysis

Six of the FBAs were each injected at 2 of the 15 sites while PFBA was injected at 3 sites. Br^- was injected along with 4 of the FBAs (see Table 3-2 and Figure 2-9). The breakthrough curves (BTCs) for all tracers for all well intervals that showed substantial well breakthrough are shown in Figure 4-1. The vertically-integrated BTCs for each tracer are also shown in Figure 4-1, and will be discussed in the modeling sections below. The curves represent daily measured concentrations. For periods when samples were not taken, concentrations were linearly interpolated from adjacent concentrations in time. Integration of the BTCs for each tracer gives the total mass recovered for that tracer. Using trapezoid-rule integration, daily concentrations were multiplied by the volume of water pumped over that

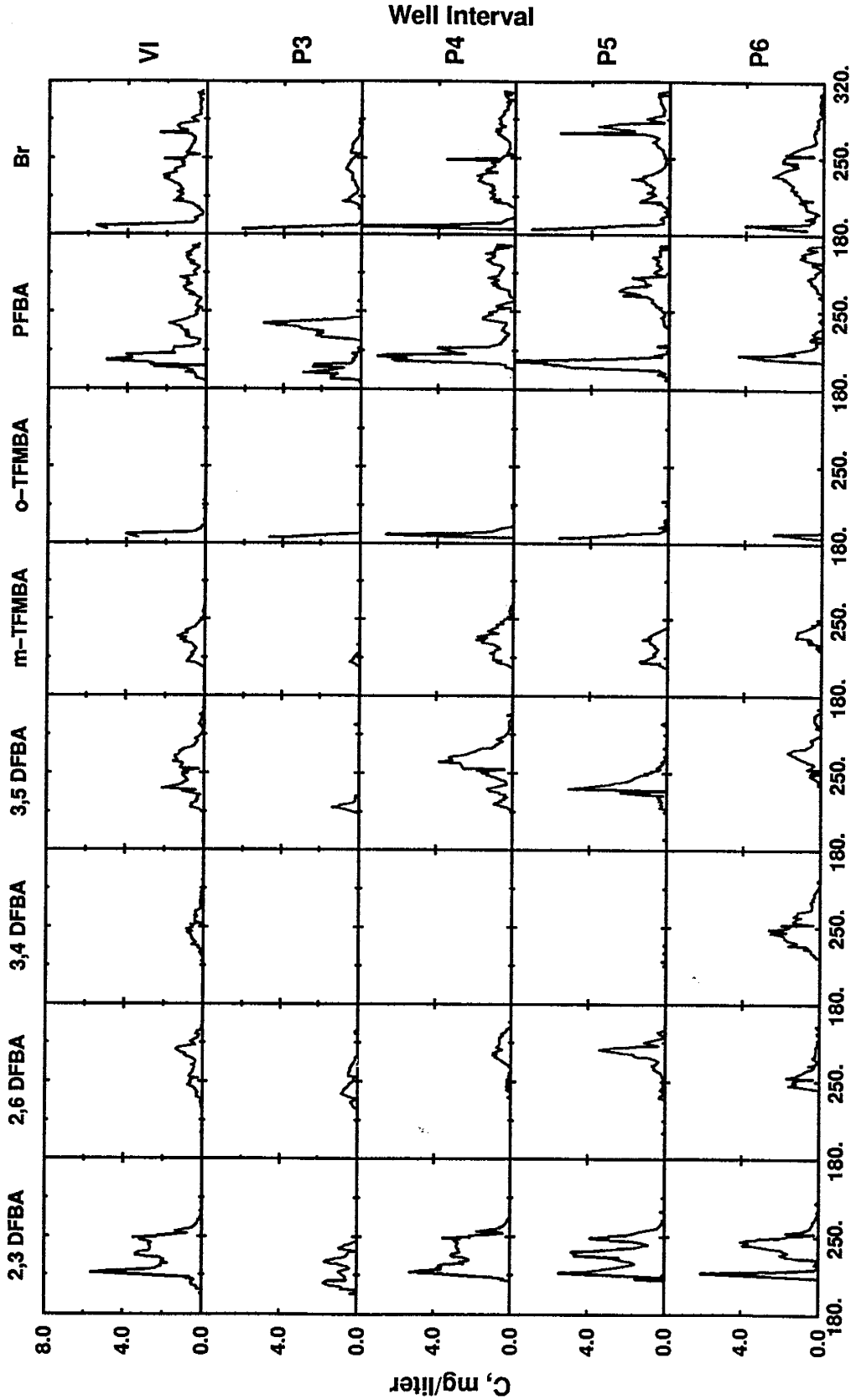

Figure 4–1. Experimental breakthrough curves for extraction well intervals P3–P6, and the vertically–integrated breakthrough curves (denoted by VI) for the 8 tracers used in Experiment 1.

24 hour period to obtain the mass recovered. Masses calculated for each day were summed to give total mass recovered for each well interval, r_j:

$$r_j = \sum_{k}^{K} c_k \forall_k \ , \tag{4–1}$$

where K is the number of time intervals, c_k is the daily concentration for time k and $\forall_k$ is the volume pumped for the kth day. Mass recoveries for each well interval, r_j, were summed to give total mass recovered for the ith tracer, R_i:

$$R_i = \sum_{j}^{J} r_j , \qquad i=1,2,...,8 \tag{4–2}$$

where J, the number of pumping well intervals, is equal to 7 for Experiment 1. Table 4–1 gives the mass released, the total mass recovered, R, and the relative mass recovered (mass recovered/mass injected) for the 8 tracers. Figure 4–2 shows the normalized cumulative mass recoveries for the 8 tracers as a function of time. From Figure 4–2, it is apparent that Br^- and PFBA are still arriving at the well at the end of the experiment since the slope of the cumulative curves for these tracers are not zero at the time the experiment ended. This could be due to tracer injected at distant injection sites from the well not reaching the well within the experiment run time, or due to tracer injected along the capture zone boundary. In both cases, travel times would be large. These issues will be discussed in more detail in the interpretation that follows.

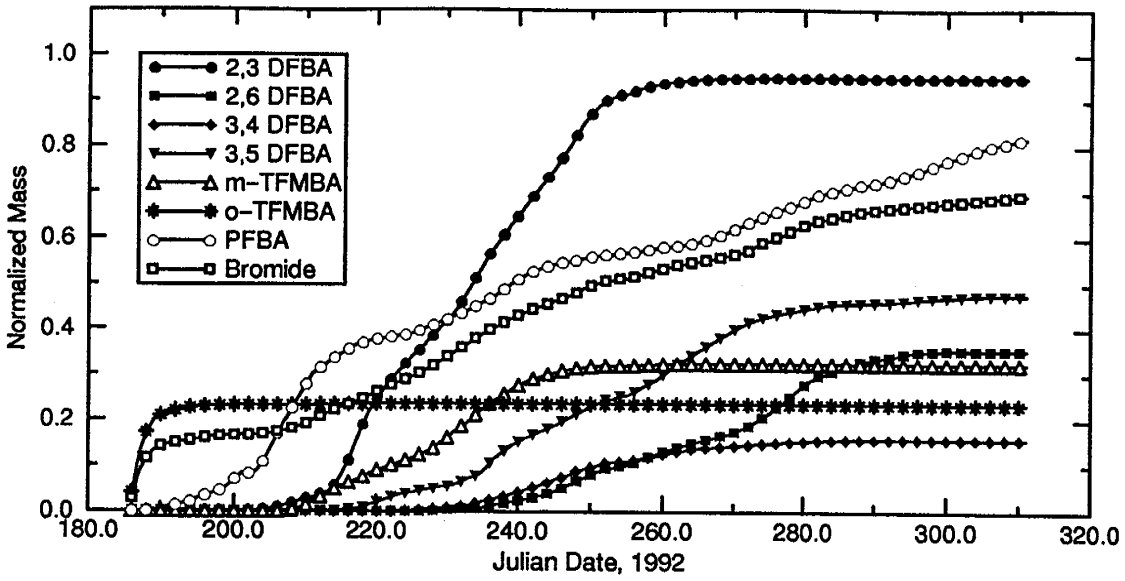

Figure 4–2. Normalized cumulative mass recoveries for the 8 tracers used in Experiment 1.

Table 4–1. Mass released, mass recovered, and relative recovery for each tracer. Injection masses account for 97% purity to allow for direct comparison to the mass recovered.

Tracer	Mass Injected, gm	Mass Recovered R, gm	Relative Recovery (Recovered/Injected)
2,3 DFBA	117.2	111.3	0.95
2,6 DFBA	87.9	31.1	0.35
3,4 DFBA	117.6	18.6	0.16
3,5 DFBA	117.1	55.7	0.48
o-TFMBA	87.8	20.5	0.23
m-TFMBA	87.8	38.3	0.42
m-TFMBA*	87.8	28.4	0.32
PFBA	146.3	137.4	0.91
PFBA*	146.3	119.6	0.82
Br (2–8)	123.1	201.7	1.64
Br (2–6)	123.1	85.5	0.69

* Smoothed data.

The estimated mass recovered for Br^- for all 7 well intervals is much larger than what was released (shown as Br^- (2–8) in Table 4–1). The discrepancy for Br^- resides primarily in levels 7 and 8 which are both in the leachate. Level 7 contributes the largest error and

accounts for 40.2% of the recovered mass. If these levels are completely removed from the calculation, then the mass balance is more reasonable, as shown in Figure 4–2, and reported in Table 4–1, as Br^- (2–6). It is likely that the leachate extends above the 6 m level, the possible consequences of which will be discussed below. All analysis which follows makes use of the Br^- (2–6) data set. There were some reported concentrations that appear as anomalous spikes when compared to adjacent data points in time and space for m–TFMBA and PFBA. These values were set to the average of adjacent values in time for that interval. Recoveries for the smoothed data sets are reported as m–TFMBA* and PFBA*. The analysis which follows uses only the smoothed data sets for m–TFMBA and PFBA.

Figure 4–3 gives the proportion of total recovery for each tracer by pumping well interval for all tracers except Br^-, in which case recoveries for only well intervals P2–P6 are shown. Each 1 m long interval is referred to by its greatest depth in this table and in the following figures and text; thus, the 2–3 m interval is called interval 3. From Figure 4–3, it is clear that the tracers have migrated vertically downward, evident by breakthrough in the 2–3 m interval which is smaller than the one–third of the total mass injected, and breakthrough in the 5–6 m interval which wouldn't be there had tracer only migrated horizontally and not migrated downward from the upper intervals. For a plume without any vertical migration, the breakthrough would be predominantly in the 2–5 m interval, which are equivalent to the zone of tracer injection.

Determination of the origin of tracers detected at the pumping well is straightforward for virtually all of the tracers. From Table 4–1, it is apparent that the only two tracers with relative recoveries (i.e. mass recovered/mass injected) close to 1.0 are 2,3 DFBA and Br^-. The remaining FBAs all exhibit partial recovery at the well, and we will examine each of these in turn. Important considerations to keep in mind are the ambient flow direction, as shown in Figure 3–4, the injection site locations, shown in Figure 2–9, and mass injected at

each site, shown in Table 3-2. Initially, we will only concentrate on the 7 FBAs and leave Br^- for last.

2,3 DFBA

The tracer 2,3 DFBA was injected at sites I5 and I8, with 58.6 g injected at each site. Relative recovery at the well was 0.95, which is very close full recovery for tracer injected at both sites. The small discrepancy between injected and recovered mass may be due to tracer not recovered at the well, or it may be a result of error in estimating the mass based on HPLC determined concentrations and subsequent data reduction used in calculating recovered tracer masses. Breakthrough curves for 2-3 DFBA are shown in Figure 4-1. It shows two distinct peaks, the earlier one is from breakthrough of tracer injected at I5, the second one is attributed to I8. In the individual well intervals, breakthrough is earliest in P3. BTCs for P4, 5, and 6 have similar first arrivals and tails, but show progressively more character with depth. P5 is tri-modal and may be influenced by vertical and horizontal K variations, buoyancy effects, and variable flow path for I5 and I8. It is likely that tracer injected

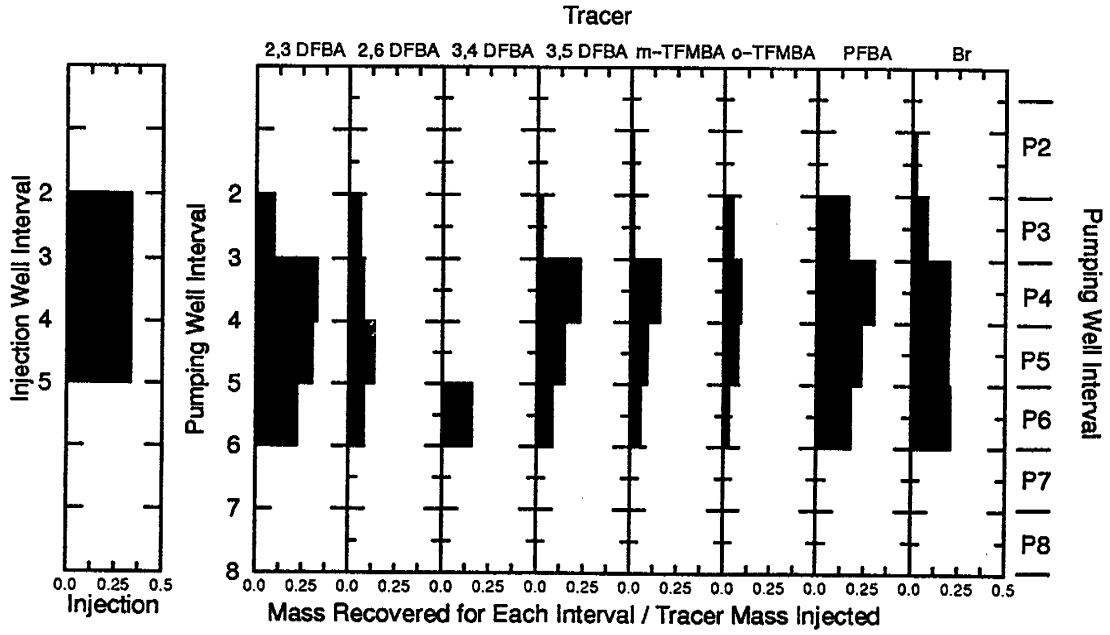

Figure 4-3. Vertical profile of injection mass and mass recoveries for 8 tracers used in Experiment 1.

at both of these sites would have recovery ratios of 1.0, or close to 1.0, based on gradient direction and site coordinates (see Figure 3–4 and Figure 2–9, respectively), so we can assign equal relative recoveries to each site. Estimated relative recoveries: I5: 0.95, I8: 0.95.

It is thought that variations in hydraulic conductivity are responsible for splitting of the plumes. Sudicky's (1986) transect data for the 2.5 to 4.5 m depths at this location confirms such heterogeneity (see his Figures 5, 6 and 7). Although he did not recognize any trends in the heterogeneity (nor did Mackay et al., 1986) the published data suggest a higher conductivity for our 3 and 4 m intervals, relative to the 5 m interval.

2,6 DFBA

Tracer 2,6 DFBA was injected at site I6 (58.6 g) and I15 (29.3 g). The mass recovered is estimated at 31.1 g, or 0.35 of the total mass injected. The breakthrough curves are shown in Figure 4–1. The mass recovered is very close to that injected at I15. It is likely that there was complete recovery for I15 and zero recovery for I6, with I6 being just outside the boundary of the capture zone. The total mass recovered is 1.06 of the mass injected at I15, however the discrepancy is within the nominal 10% error associated with the HPLC analysis and mass recovery estimation. It is also possible that both I15 and I6 had partial recoveries at the pumping well. It is improbable that all mass recovered was from I6 and none from I15 since it is clear that I8, which was near I15, had a recovery close to 1.0 (see *2,3 DFBA* above).

If we consider the changing gradient direction, we can hypothesize that tracer injected at I6 was outside the capture zone when injected, and then proceeded to flow in the general direction of MW1–8 or –9 (see Figure 2–9). 2,6 DFBA was detected along both of the monitoring fences, but not in any of the stagnation point multilevel samplers (SWs in Figure 2–9). Figure 4–4 shows the measured and simulated breakthrough at the 4, 5, and 6 m levels along the multilevel sampling fence MW1 (refer to Figure 2–9 for locations). Note that there is effectively no measured breakthrough at the 6 m level. For the other two

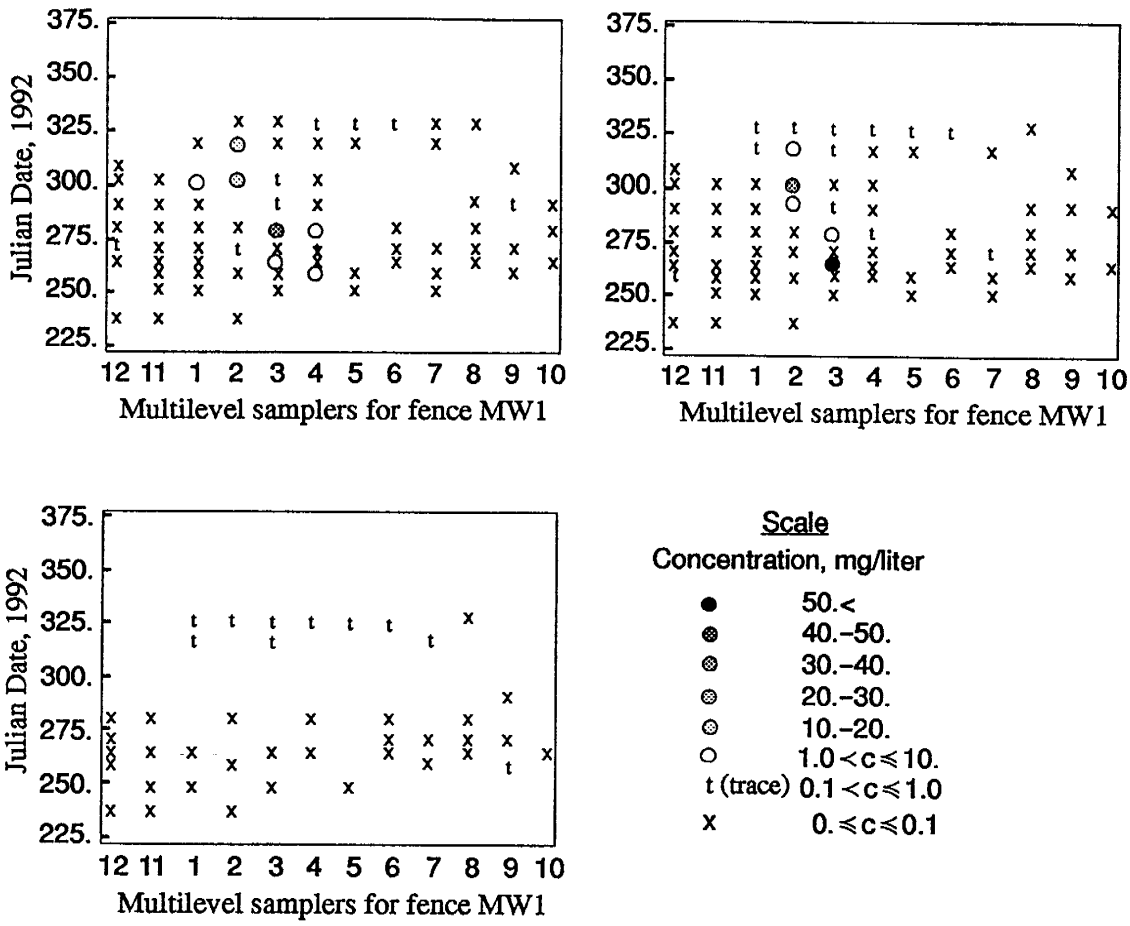

Figure 4–4. Measured concentrations of 2,6 DFBA along monitoring fence MW1.

levels, the plume intersects the fence at about 6 m from the southeast end, in the vicinity of sampler MW1–4. As the direction of flow became more northerly, the plume has migrated along the fence towards the northwest. Samples taken from the SW multilevel samplers were analyzed for the same sample time and depths, with no significant breakthrough occurring. This further indicates that the majority, if not all, of the tracer from I6 was not captured by the well, and that the well breakthrough for 2,6 DFBA is due largely, if not entirely, to I15. However, it is possible that tracer from I15 was not entirely captured by the well, based on the distance of I15 from the well. It may be that travel times were large enough such that the plume from I15 was not completely recovered at the well prior to turning off the pump.

Based on these arguments, we propose that I15 has recovery of 1.0, or very close to 1.0, and I6 has partial recovery at the well. Estimated relative recoveries: I6: 0.03, I15: 1.0

Based on the plume splitting evident at the MW1 sampling fence, the core taken near the pumping well, and the analysis carried out on 3,4 DFBA (see *3,4 DFBA*, below), it is clear that the hydraulic conductivity in the lower portion of the aquifer is less than that in the upper part of the aquifer. This would account for splitting of the tracer plume from I6, and would account for the lack of breakthrough along the fence for the 6 m interval.

3,4 DFBA

Tracer 3,4 DFBA was injected at sites I3 (58.6 g) and I10 (59.0 g). A recovery of 18.6 g indicates that one or both of the injected tracers from these two sites was on the capture zone boundary, and that the there was plume splitting. If we look at the location of I3, and consider the changing gradient direction, we speculate that tracer injected at I3 was injected outside the capture zone, remained outside the capture zone over the duration of the experiment and was not captured by the well. Also, if there was breakthrough from I3, it would reasonable to expect a later breakthrough, which isn't seen in the BTCs for 3,4 DFBA shown in Figure 4–1. This means that only about one–third of the tracer from I10 was captured at the well. For a homogeneous aquifer, this would place site I10 towards the outer edge of the capture zone boundary. However, if we look at the vertical breakthrough profile for I10, shown in Figure 4–3, we see that the recovered mass comes almost entirely from the 5–6 m interval. This strongly suggests that the aquifer has a layered structure, and that the plume split vertically and not horizontally, with the upper two–thirds of the plume migrating off towards the north or northeast. This is in agreement with results from the Waterloo–Stanford study by Freyberg (1986; see also Figure 14b in Rajaram and Gelhar, 1991), showing that the plume split at about the 5 m depth. Sudicky et al. (1983) also reported a similar occurrence, as shown in their Figure 4. Estimated recoveries: I3: 0.0, I10: 0.32

3,5 DFBA

Recovery of 3,5 DFBA was 55.7 g, or roughly 0.50 of that injected. The BTCs is shown in Figure 4–1. Injection sites were I7 (58.5 g) and I11 (58.6 g). From the gradient direction (Figure 3–4) and the location of the injection wells (Figure 2–9), it is reasonable to assume that I11 was not recovered at the well and that I7 was captured, with a relative recovery of 0.95. Estimated recoveries: I7: 0.95, I11: 0.0.

As illustrated in Figure 4–3, almost 50% of the breakthrough was in the 4 m interval, with about one–third recovered in the 5 m interval. Also evident in this set of figures is the difference in time of breakthrough for the different intervals. Breakthrough in P3 and P5 were earlier than breakthrough in P4 and P6. There are two early peaks in P4, one of which is very close in time to the breakthrough in P3, suggesting that the vertical separation of the plume is sharp, and that the depth of the separation does not coincide with the depth of the boundary between the two well intervals.

m–TFMBA

Tracer m–TFMBA was injected at I2 (29.3 g) and I14 (58.5 g). Recovery was estimated at 28.4 g. Following along with previous tracer analyses, we discount any breakthrough from I14 due to location and flow direction history. The relative recovery for I2 would be 28.4/29.3, or 0.97. This is close to 1.0 and is a reasonable recovery estimate for I2 given its location with respect to the pumping well. From examination of the BTC for m–TFMBA, shown in Figure 4–1, we see that there is only one period of breakthrough which is fairly early in time. If tracer from I14 were to be captured, the recovery would probably be much later in time. A relative recovery of 0.97 indicates a loss of mass which may result from error in estimating the concentrations using the HPLC, or in estimating masses from the concentrations. The loss may also be due degradation of the tracer which has been noticed in previous studies (Bowman, 1984; Bowman and Rice, 1986). This hypothesis is

tested using the two- and three-dimensional model analysis, which will be published in a sequel paper. Estimated relative recoveries: I2: 0.97, I14: 0.0.

Almost one-half of the recovered mass was recovered in P4, with most of the remaining mass split nearly equally between well intervals 5 and 6, as shown in Figure 4-1 and Figure 4-3. The order of breakthrough is similar to 3,5 DFBA which is assumed entirely due to I7, located roughly two meters further upgradient (see Figure 2-9). There is a single, small, early peak in P3, while BTCs for P4 and P5 are generally bimodal. The BTC for P6 is uni-modal and comes in later than for the other intervals. The later arrival times for P6 may be due to the lower conductivity at this depth of the aquifer. Figure 4-3 shows a smaller proportion of recovery for P3 than do the other tracers, except perhaps 3,5 DFBA.

o-TFMBA

Breakthrough of o-TFMBA, shown in Figure 4-1, is attributed to site I1. Tracer injected at I13 would not have had a chance for well capture, given the flow direction history. With a recovery of 20.5 g, and injection mass at I1 of 29.3 g, the relative recovery is 0.7. The reason for the low recovery is due to missed sampling early on in the experiment such that the leading edge of the plume was captured but not sampled. This is clear from inspection of the breakthrough curves for the individual well intervals, shown in Figure 4-1, where the early part of the plumes for o-TFMBA were not sampled for well intervals P3 and P5. Estimated recoveries: I1: 0.70 (1.0), I13: 0.0

PFBA

The tracer PFBA was injected at three sites; I4 (58.5 g), I9 (29.3 g) and I12 (58.5 g). By examining the various locations of these three sites in Figure 2-9, and applying the reasoning used in determining injection site breakthrough for 2,6 DFBA, we speculate that I4 and I12 are in locations favorable for well capture, while I9 may be on, or outside, the boundary of the capture zone, as was suggested for I6. This supposition is supported by breakthrough of PFBA along the northwest ends of both fences MW1 and MW2 (shown in

Figure 4–5 for MW1), as well as in SW3, shown in Figure 4–6. Complete well capture of

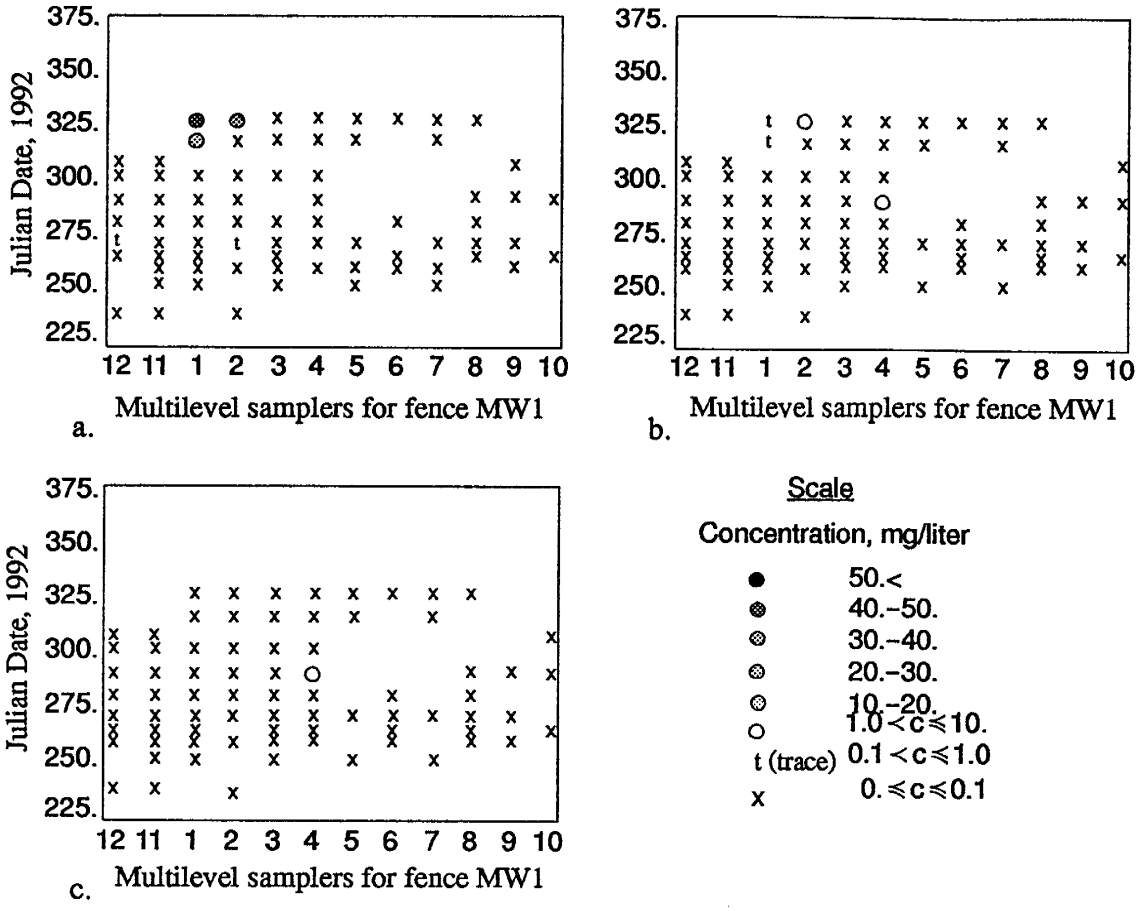

Figure 4–5. Measured concentrations of PFBA in Experiment 1 along multi-level sampling fence MW1 for Experiment 1 at the 4, 5 and 6 m depths (a–c, respectively).

I4 and I12 would give a recovered mass of 117.0 g, close to the measured recovery of 119.6 g and within the error associated with mass recovery estimation. However, it is possible that I9 had a small relative recovery of 2.6/29.3, or 0.09, or larger depending on the actual recoveries of I4 and especially I12. Site I12 may have had partial recoveries due to travel times to the well being larger than the experiment run time. Examining BTCs for PFBA in Figure 4–1 doesn't help to clarify the issue since there are at least three distinct peaks for well intervals P4, P5 and P6. Estimated relative recoveries: I4: 1.0, I9: 0.09, I12: 1.0.

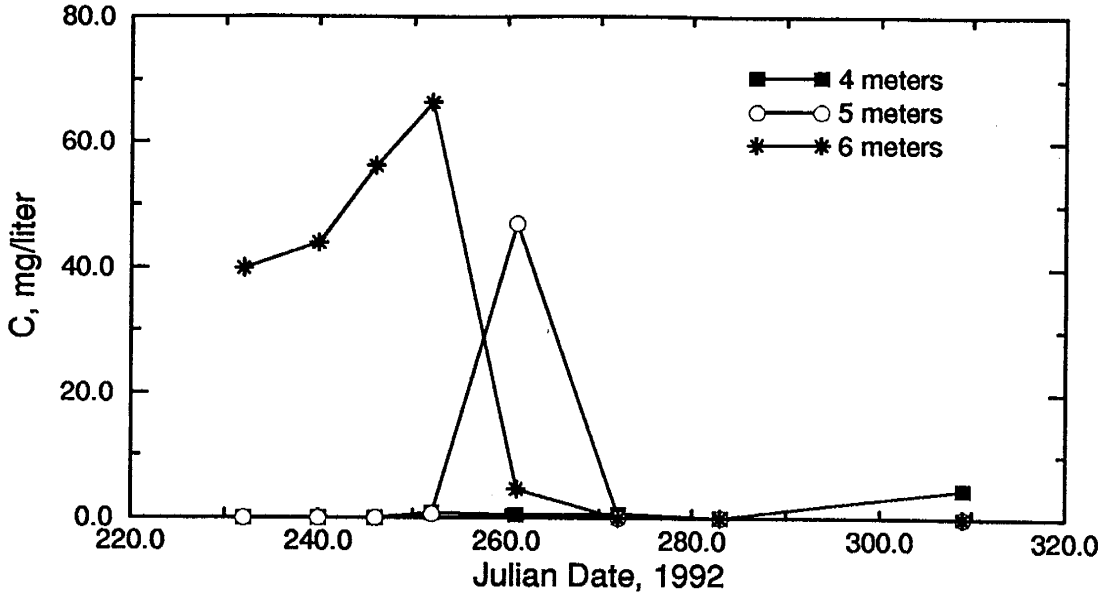

Figure 4–6. Breakthrough of PFBA at SW3 for three depths in Experiment 1.

Br^-

Estimation of recovery for Br^- is perhaps the most complicated since it was injected at four injection sites: I1, I2, I9, and I15 (roughly 30. g each of Br^-). The mass recovered for Br^- is 85.5 g, or 0.69 of the total mass injected (see Table 4–1 and Figure 4–2). Based on the previous analyses, it is likely that tracer from all 4 injection sites was either completely or partially recovered at the well. Figure 4–7 compares the vertically–integrated Br^- breakthrough (for well intervals P2–P6 only) to the breakthrough of the four FBA tracers it was injected with. Figure 4–7b compares the composite BTCs of m–TFMBA, o–TFMBA and 2,6 DFBA to Br^- while Figure 4–7c compares the BTC of PFBA to that of Br^- separately. The separate BTCs of m–TFMBA, o–TFMBA and 2,6 DFBA are shown in Figure 4–1. Comparison to PFBA was made separately since there is recovery of PFBA from several injection sites whereas the source of breakthrough for the other 3 FBAs were only from the sites where Br^- was also injected. From inspection of Figure 4–7b, it is clear that there is strong correlation in time between breakthrough of Br^- and the other 3 tracers, however con-

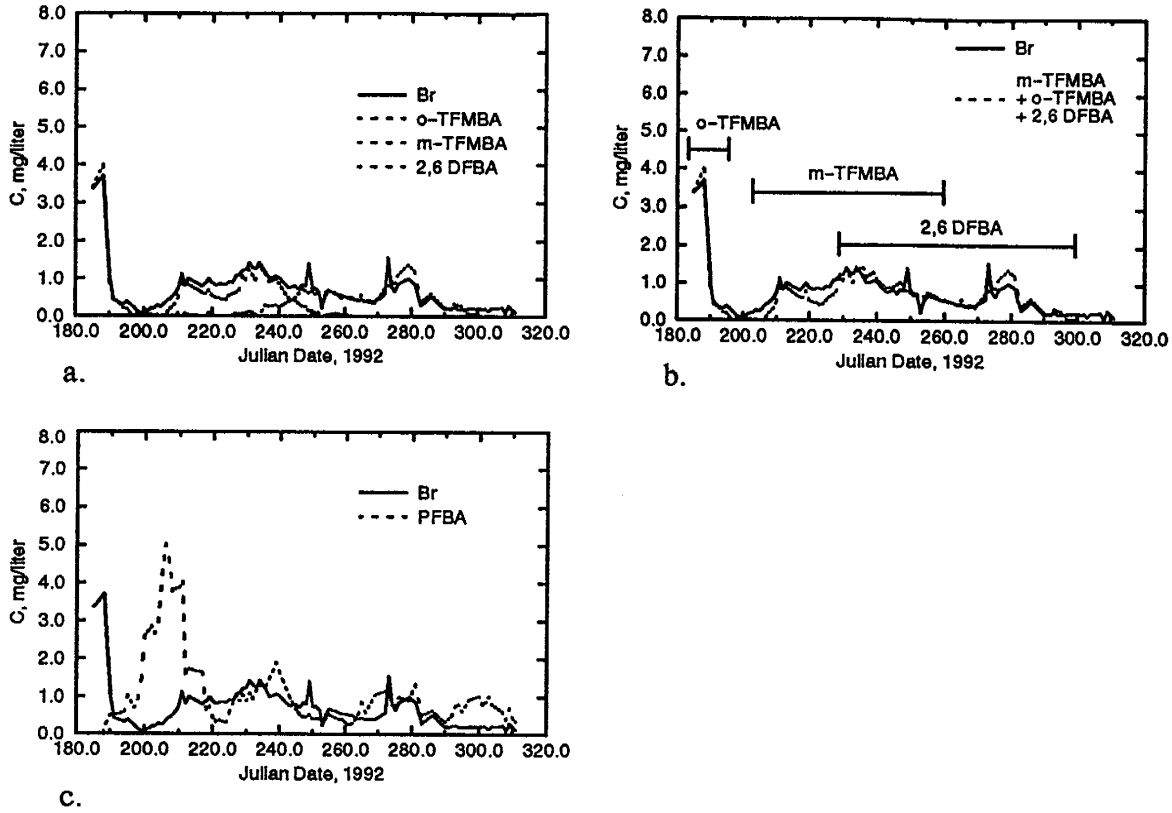

Figure 4–7. (a) Comparison of vertically–integrated BTC for Br^- to breakthrough of m–TFMBA, o–TFMBA and 2,6 DFBA separately;; (b) Comparison to composite of m–TFMBA, o–TFMBA and 2,6 DFBA; (c) Comparison to PFBA.

centrations for Br^- are higher than those for m–TFMBA, while concentrations of 2,6 DFBA are higher than those for Br^- over a portion of the breakthrough sequence (i.e. from approximately 275 d to 282 d). The strong correlation of Br^- arrival times with the FBA arrival times that it was injected with supports the claim made earlier that the FBAs are non–sorbing in an environment such as the Borden aquifer. The higher Br^- concentrations may be an artifact of HPLC analysis (Robert Bowman, pers. comm.). Also, m–TFMBA and o–TFMBA have both shown degradation behavior in other studies (Bowman, 1984; Bowman and Rice, 1986), however, this should not affect o–TFMBA since travel times are on the order of days for injection at I1, and travel times for I2 are also short. It should also be noted that Br^- was also detected at very low concentrations in the 2 m interval (not shown in Figure 4–1),

compared to zero breakthrough of o-TFMBA for this interval. Higher Br^- concentrations may also arise from interference effects caused by the leachate at depth. Earlier it was pointed out that the mass recovered for Br^- was much too high if the lower 2 pumping intervals were used in the mass balance. Most likely there was also some leachate in the 5–6 m well interval which increases the apparent mass recovery for Br^-. This is substantiated by Figure 4–3 where it is seen that there is a relatively large recovery in P6 for Br^-, especially when compared to recovery in P6 for m-TFMBA and 2,6 DFBA.

At 295 d in Figure 4–7a, concentrations of 2,6 DFBA drop off to zero, while Br^- concentrations remain at about 0.25 mg/L. This portion of the bromide BTC may be attributable to Br^- injected at I9 along with PFBA. However, from comparison of Br^- with PFBA in Figure 4–7c, it appears that there is lack of strong correlation between Br^- and PFBA breakthrough for these late arrival times. The higher concentrations for PFBA could be from tracer injected at I12 recovered at this time. If one looks closely at the very end of the BTC for both Br^- and PFBA, in Figure 4–7c, both curves show a similar trough and a peak in the BTC, just prior to concentrations dropping off at 313 d when the experiment was terminated. Using 295 d as the point in time when the influence of 2,6 DFBA begins to disappear and concentrations begin to drop to zero, the difference between the cumulative mass for Br– and 2,6 DFBA between 295 and 311 d can be attributed to breakthrough of PFBA from I9. This calculation gives a total mass of 2.75 g, which when divided by 29.29 g of Br^- injected at I9, yields a relative recovery of 0.094 which is essentially identical with the previous estimate of 0.09. However, it must be cautioned that there is uncertainty associated with this estimate.

The data further suggest that PFBA injected at I12 was still being recovered at the well when the experiment was terminated, and that the relative recovery for PFBA injected at I9 may be higher than the estimated value of 0.09, and relative recovery for 2,6 DFBA injected at I12 may be lower than 1.0. This is most clearly seen by comparing well interval P4 for PFBA and Br– in Figure 4–1 where the concentrations for these tracers are greater

than zero and not equal to each other when the experiment is terminated. The total estimated recovered mass of the four FBA tracers injected along with Br^- is 82.6 g (see Table 4–2). The total mass injected at these sites for the FBA tracers was 117.2 g, giving a relative recovery of 0.70, which compares very well with the relative recovery of 0.69 estimated for Br^-. This comparison further supports the estimated recoveries for PFBA given above, and suggests that most, if not all, of the PFBA from I12 was recovered at the well when the experiment ended.

Estimated Injection Site Recoveries

The estimated injection site recoveries based on the measured data are shown in Table 4–2. A map of relative recoveries for each injection site, shown in Figure 4–8, provides the desired map of the capture zone. Tracer injected at four of the sites (I3, I11, I13 and I14) was not recovered at the well indicating these sites were outside the capture zone for the locations and times considered. There are also several sites with relative recoveries of 1.0 (I4, I12 and I15), indicating that these sites were located completely within the capture zone. Finally, there are several sites with recoveries between 0.0 and 1.0 indicating that these sites were on the capture zone boundary.

The orientation of the capture zone based on the recovery data is approximately N25E to N30E. From comparison to Figure 3–4b, the capture zone orientation is similar to the direction of flow at the start of the experiment, while the mean flow direction during this time period was approximately N15E to N20E. The more easterly capture zone orientation results from the nearly linear change in flow direction. Tracer injected at sites further from the well, along the axis of the capture zone, migrated in a direction which kept it within the capture zone as the capture zone itself changed orientation. Other tracer injections closer to, or outside, the capture zone boundary either didn't remain in the capture zone, or never had a chance to be captured due to the dynamics of the system. This means that the injection sites indicating the capture zone with a relative recovery of 1.0 did not represent the mean

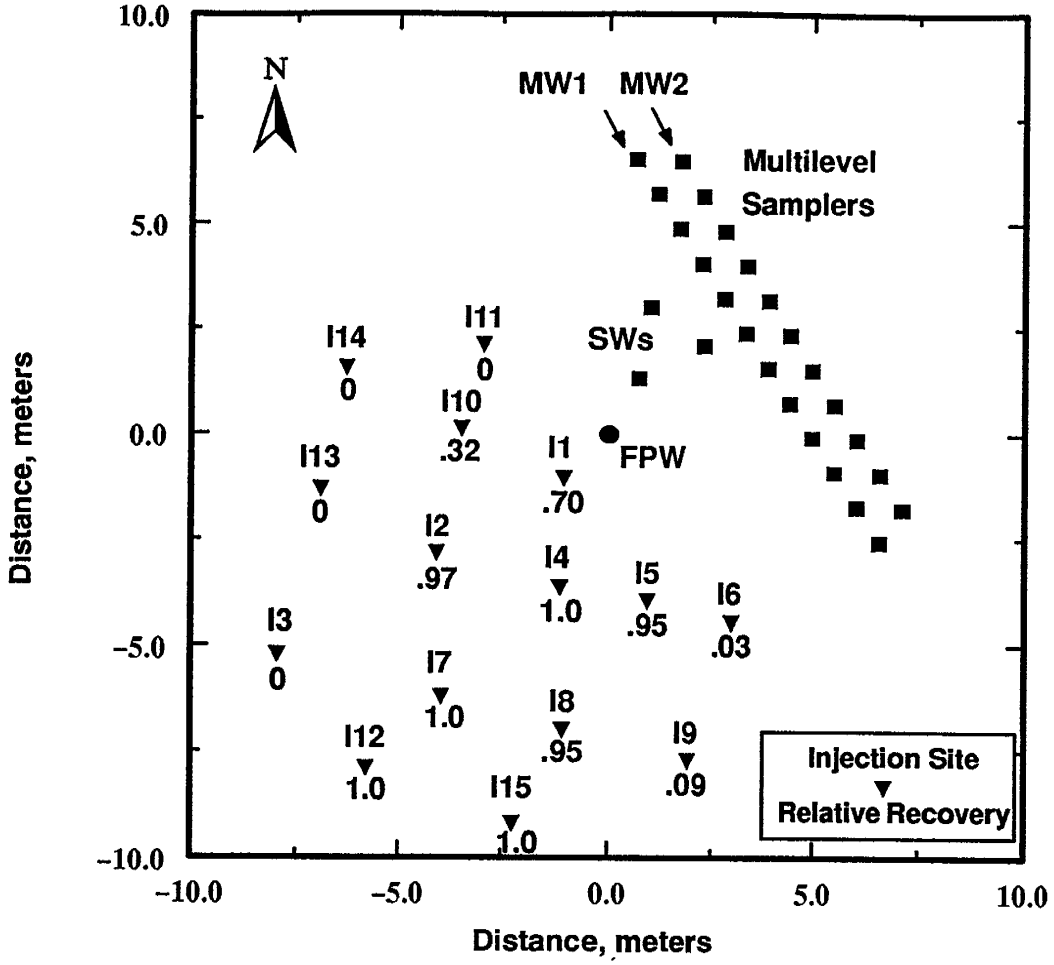

Figure 4–8. Experiment 1 capture zone map, based on relative recoveries for 15 injection sites. For each site, the top number is injection site location, the bottom number is the estimated relative recovery (tracer mass recovered at the pumping well / tracer mass injected at that site).

flow direction, but instead represented the flow direction at the time the experiment started. Steady–state capture zone models which use the mean flow direction may be in error in predicting the true capture zone orientation.

The width of the capture zone is estimated from the map in Figure 4–8 at approximately 2.5–3.0 m, which is smaller than the 5 m width estimated during the design of the experiment. This may be due to the changing flow direction and also higher hydraulic con-

ductivity than was used in originally estimating the capture zone width. It is apparent from the tracer breakthrough curves that hydraulic conductivity is higher in the shallow part of the aquifer, which would exhibit a higher Darcy velocity than what was used in the original estimate. Capture zones are narrower when Darcy velocities are higher. The changing flow direction would reduce the number of injection sites remaining within the region of complete capture. In a continually changing flow field, and with tracer injected at a point in space (horizontally) and in time, fewer sites will exhibit capture than in a steady state system. Steady-state capture zone models would predict a wider capture zone which would be conservative in terms of wellhead protection.

The estimated injection site recoveries based on the measured data are shown in Table 4–2. We can also map the relative recoveries for each injection site to give a capture zone map for the experiment, shown in Figure 4–8. Based on this map, tracer injected at four of the sites was not recovered at the well indicating these sites were outside the capture zone for the locations and times considered. There are also several sites with relative recoveries of 1.0, indicating that these sites are located completely within the capture zone. Finally, there are several sites with recoveries between 0.0 and 1.0 indicating that these sites are on the capture zone boundary. The orientation of the capture zone is roughly N20E to N30E. The width of the capture zone can be estimated from the map at approximately 4–4.5 m, and is close to the 5 m width estimated prior to conducting the experiment.

Table 4–2. Interpretation of tracer recovery at the extraction well in terms of injection site location. Injection masses account for 97% purity to allow for direct comparison to mass recovered.

Injection Well	Tracer	Mass Injected, gm	Mass Recovered, R, gm	Recovery error, ε_R
I1	o-TFMBA	29.3	20.5	0.70
I2	m-TFMBA*	29.3	28.4	0.97
I3	3,4 DFBA	58.6	0.0	0.0
I4	PFBA*	58.5	58.5	1.0
I5	2,3 DFBA	58.6	55.7	0.95
I6	2,6 DFBA	58.6	1.9	0.03
I7	3,5 DFBA	58.5	55.7	0.95
I8	2,3 DFBA	58.6	55.7	0.95
I9	PFBA*	29.3	2.6	0.09
I10	3,4 DFBA	59.0	18.6	0.32
I11	3,5 DFBA	58.6	0.0	0.0
I12	PFBA*	58.5	58.5	1.0
I13	o-TFMBA	58.5	0.0	0.0
I14	m-TFMBA*	58.6	0.0	0.0
I15	2,6 DFBA	29.3	29.3	1.0

* Smoothed data.

Plume Sinkage

Vertical movement of tracer was estimated using two methods, both of which are based on the assumption that if flow were purely horizontal, then tracer would breakthrough predominantly in the 2–5 m region of the well. As the cylinder of injected tracer moves vertically, the 2–3 m interval, P3, loses mass while the 5–6 m interval, P6, gains mass. One estimate was obtained by subtracting the mass remaining in P3 from one–third of the mass recovered, and normalizing by the one–third mass recovery. A second estimate was obtained by assuming the mass recovered in P6 directly represents the mass vertically lost from P5. Normalizing this mass by the one–third mass recovered provides the second estimate. The estimates were done for individual tracers and not each injection site, and as such represent an integrated value for tracers recovered from more than one injection site. It isn't possible

to use the first of these methods with 3,4 DFBA since the upper portion of the plume is not recovered at the well. The mass balance for Br^- is off probably because of error associated with determining the mass in P6 due to the leachate, so the sinkage estimates for Br– are suspect, especially for the lower well interval.

The results of these different calculations are shown in Table 4–3. For several of the tracers, the estimates are consistent using each method, e.g. 2,3 DFBA and PFBA. The estimates for the remaining tracers varies depending on which interval is used. It could be reasoned that the lower interval would show a smaller sinkage, since the total dissolved solids in the lower part of the aquifer, especially near the leachate, would be expected to increase, reducing the density contrasts assumed to be partially driving the sinkage. This trend is seen for several tracers, including 3,5 DFBA, m–TFMBA and o–TFMBA, but the other tracers show either no effect or the opposite effect. The largest sinkage, 0.94 m, is for 3,4 DFBA. This may due to the location of I10 along the boundary of the capture zone near the well which is the strongly convergent region of the capture zone. Dispersive effects would be minimal in this region, with concentrations and density–dependent velocities maintained at a relatively high value. The estimate for Br– using P6 is also relatively high, but may be due to the previously mentioned interference effects caused by the leachate. The estimate of vertical migration for o–TFMBA, which is for injection at I1, only 1.5 meters from the well, is moderately large for the P3 estimate, and small for the P6 estimate. These values suggest that a large portion of the sinkage occurred soon after injection due to high initial tracer concentrations and to downward vertical flow resulting from injection of the tracer solution.

Table 4–3. Estimation of the extent of vertical plume migration during Experiment 1.

Tracer	Vertical Flow, m	
	From P3	From P6
2,3 DFBA	0.70	0.70
2,6 DFBA	0.50	0.68
3,4 DFBA	–	0.94
3,5 DFBA	0.86	0.52
m-TFMBA	0.88	0.54
o-TFMBA	0.68	0.25
PFBA	0.41	0.44
Br^-	0.70	0.91

Two-dimensional Model Analysis

Both two-dimensional and three-dimensional models were developed, with the results compared to measured breakthrough and recovery. From inspection of Figure 4–3 and Figure 4–1, it is clear that the aquifer exhibits three-dimensional flow properties. Following the two-dimensional modeling analysis, the three-dimensional modeling phase of the Experiment 1 will be discussed.

The two-dimensional model was discussed in Section 3. Velocities were derived for a aquifer which had the following features:

- Simple geometry;
- Infinite lateral extent;
- Dupuit assumptions apply;
- Homogeneous, isotropic;
- K=7.09 m/d;
- α_L=0.08 m; α_T=0.001 m;
- Gradient derived from linear fit to heads;
- porosity=0.33;

- no vertical recharge.

Transport was handled by the random walk method. All simulations were conducted with 1000 particles, using a time step of Δt=0.1 d. In the aquifer without the pumping well, this time step gives a travel distance of 0.1 m/d x 0.1 d = 0.01 m. This distance is considered sufficiently small with respect to the dimensions of the plume. Bin sizes in time were 1.0 d for breakthrough at the well and 5.0 d for breakthrough at the multilevel sampling fences. A bin size of 1.0 d was used at the stagnation point samplers or stagnation wells (SWs).

Measured and simulated vertically–integrated breakthrough curves for the 8 tracers are presented in the discussion for each respective tracer that follows. Experimental, or measured, BTCs are shown as solid lines, the simulated BTCs as dotted lines. They can be compared in two ways. Total mass recovered indicates how much of each tracer was captured by the well. Recoveries provide a less constrained comparison since they are not very sensitive to capture zone parameters except for injection sites located at the capture zone boundary. For instance, for an injection site with observed recovery of 1.0, variation of simulation aquifer parameters within a reasonable range of values will still, in most cases, produce recoveries of 1.0. Comparison of breakthrough curves, on the other hand, allow direct comparison of breakthrough structure over time by comparing recoveries at individual times over the breakthrough period. Thus we would expect the error derived by comparing recoveries to smaller than the error derived from comparison of the breakthrough curves.

Comparisons between simulated and experimental recoveries and BTCs for each tracer are shown in Table 4–4 using the above measures for error. Only the smoothed data sets for m–TFMBA and PFBA, and well intervals 2 through 6 for Br^-, are used.

Before examining model results for each tracer, we can examine the simulated location for the stagnation point, and the capture zone width, for each set of input parameters for the model. In this case there were 17 times when gradient was calculated and used as input into the model. Aquifer thickness and pumping rate for these times were used as well.

Figure 4–9a shows capture zone width as a function of time and Figure 4–9b shows the stagnation point location for all 17 measurement times. The width, w, (total capture zone

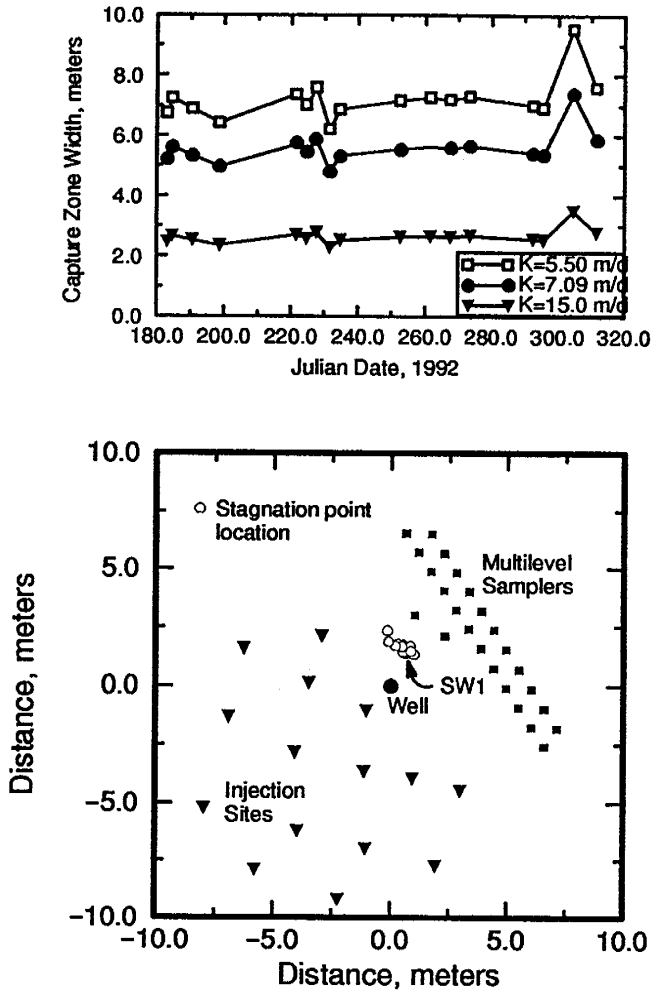

Figure 4–9. Capture zone width (top) and stagnation point location (bottom) for 17 measurement times during Experiment 1. Input included aquifer thickness, pumping rate and hydraulic gradient; K=7.09 m/d for stagnation point calculation.

width = 2w) varies from about 5 to 6 meters. As a rough estimate, if we take w=5.5 m as a mean width, then if we use half of the 1 m variation as the fluctuation either side of this mean value, then we can estimate the variation in capture zone width over the course of the experiment as 0.5 m/5.5 m = 0.09, or roughly 9% variation in w for K=7.09 m/d. As discussed above, the conductivity varies with depth, being higher in the upper portion of the aquifer. The width of the capture zone is inversely proportional to the ambient flow rate,

and this is proportional to the conductivity. For K=5.5 m/d in the upper part of the aquifer, using this same approach, the variation for w is about 0.6/6.75 =0.088, or again about 9% variation in w. For K=15.0 m/d, the variation in w is 0.5/2.6 = 0.192, or almost 20% variation in capture zone width. From this it is clear that not only is the capture zone sensitive to the changing flow direction, but as the capture zone narrows, the boundary of the capture zone has a much larger role in the overall capture zone structure.

The stagnation point location for the 17 measurement times was plotted for K=7.09 m/d only. From Figure 4–9b, it can be seen that the stagnation point location does not vary much. For K=5.5 m/d, the distance of stagnation point from the well would increase, and the arc distance along which it moved would also increase. Thus, for higher conductivities, the capture zone width becomes less certain, but the stagnation point location would be more confined. For lower conductivities, the opposite is true. Based on these arguments, for a layered system, as is proposed here, the lower portion of the aquifer has less uncertainty associated with it relative to the upper portion of the aquifer, assuming that the upgradient boundary of the capture zone is of more interest than the stagnation point location.

2,3 DFBA

The best match between measured and simulated breakthrough for all of the tracers is for 2,3 DFBA (see Figure 4–10a). Figure 4–10b shows the breakthrough of mass for both the experiment and the simulation, and it is apparent that the two types of breakthrough curves are similar in shape. The difference in mass breakthrough is used to determine the model fit. The simulated breakthrough for 2,3 DFBA is very similar to the measured BTC in both time of breakthrough and in magnitude of mass and concentration. The main difference in the measured and simulated BTCs are at the leading and trailing edges where the simulated curve arrives early. This could be due to an overestimate of K for this interval of the aquifer, increased travel time due to vertical flow not accounted for in the model, porosities being lower than estimated, error in estimated dispersivity, or there may be error in deter-

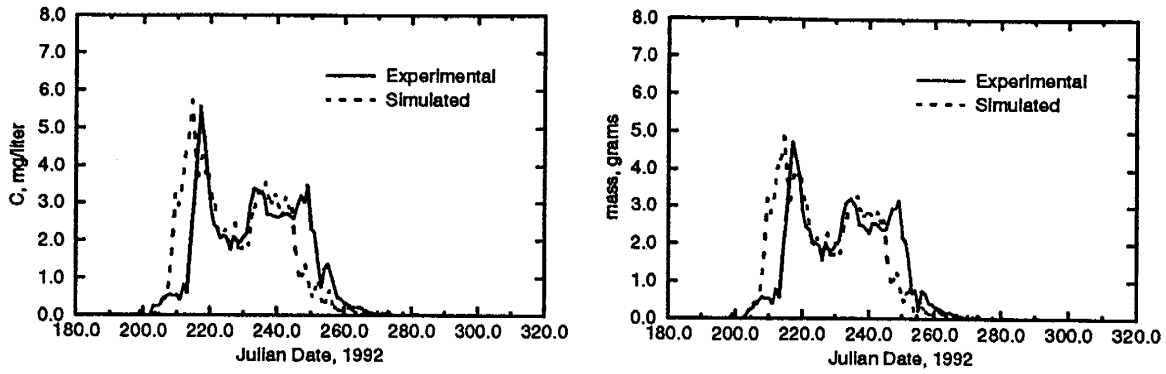

Figure 4–10. Comparison of experimental and simulated, vertically integrated concentration (left) and mass (right) BTCs for 2,3 DFBA.

mination of the gradient. Most likely, all of these factors contribute to the discrepancy in varying degrees. Misrepresentation of hydraulic conductivity and vertical flow are thought to be two of the primary contributing factors.

The simulated breakthrough best fits the measured BTC for the 4 m interval, shown in Figure 4–1. It is very similar in shape to the observed breakthrough, with the main difference again being arrival times.

Experimental and simulated recoveries are shown in Table 4–4, along with error in recovery and breakthrough for this particular model. The difference in mass recovery for 2,3 DFBA is 5.0 g, while the difference in mass from comparison of breakthrough curves is 47.0 g. The error relative to the total mass recovered during the experiment is also given, and can be taken as the accuracy of the model. As is seen, the RRE is much smaller than the RBE. This is largely due to the criteria for these two measures of error. The recovery error is only dependent on total mass recovered, and reflects only the position of the injection site with respect to the capture zone at the time of injection. The breakthrough error is a direct comparison of the sequence of recovery over time, and, as such, is much more sensitive to the model parameters being used.

Table 4–4. Comparison of experimental and simulated mass recoveries and breakthrough curves for Experiment 1; vertically integrated results.

	Tracer Mass Recovery				Tracer Breakthrough	
Tracer	*Experimental* R_E, g	*Simulated* R_S, g	Recovery Error, ε_R	Relative Recovery Error, RRE (Absolute value)	Breakthrough Error, ε_{BTC}	Relative Breakthrough Error, RBE
2,3 DFBA	111.3	116.3	5.0	0.05	47.0	0.42
2,6 DFBA	31.2	29.1	-2.1	0.07	25.7	0.82
3,4 DFBA	18.6	7.0	-11.6	0.62	15.3	0.82
3,5 DFBA	55.7	58.1	2.4	0.04	52.0	0.93
m-TFMBA*	28.4	29.0	0.6	0.03	23.3	0.82
o-TFMBA	20.5	32.5	12.0	0.58	17.2	0.84
PFBA*	119.6	103.1	-16.5	0.14	82.2	0.69
Br (2–6)	129.9	97.34	-32.6	0.25	71.0	0.55

* Smoothed data.

2,6 DFBA

Measured and simulated BTCs for 2,6 DFBA are shown in Figure 4–11. The simulated BTC matches the time of the measured breakthrough, but the breakthrough profile is not the same. The simulated curve is more symmetric, while the measured BTC is almost bimodal in shape. The difference in the shapes of the two curves most likely reflects the com-

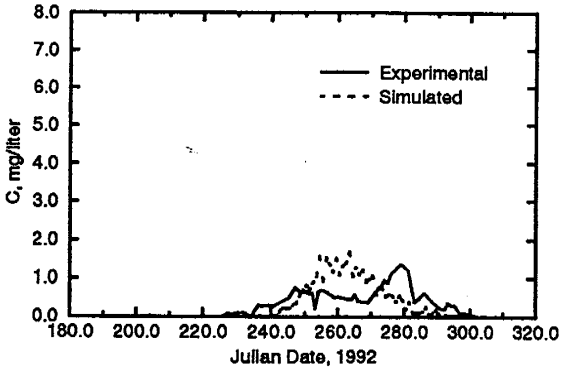

Figure 4–11. Experimental and simulated, vertically integrated BTCs for 2,6 DFBA.

plexities in the aquifer which are not incorporated in the model, such as heterogeneities and a more complicated transient flow field than what was modeled. Table 4–4 shows a small RRE, but the RBE is large. As discussed before, injection site I6 is thought to be on the outer edge of the capture zone boundary, which will make if very sensitive to model parameterization. As an example of the sensitivity, a second simulation was carried out with K=6.09 m/d (compare to K=7.09 m/d for the original simulation), while all other parameters were kept the same. Figure 4–12 shows the difference in the fate of the injected plume for these two scenarios. For K=7.09 m/d, the plume migrates past SW3 at t=245 d, and then towards the sampling fences at t=305 d. For K=6.09 m/d, at t=245 d the plume mostly misses SW3 and is migrating between it and the well. At 305 days, the plume intersects SW1 and SW2, with some of the plume being captured by the well. For K=6.09 m/d, there is a simulated relative recovery of 0.05 at the well, and all three SW wells are being intersected by the plume. It is interesting to note that 2,6 DFBA was not detected at any of the SW samplers during the course of the experiment.

Figure 4–13 shows measured and simulated fence breakthrough along fence MW1 for K=7.09 m/d. Measured data is presented for the 4, 5 and 6 m depths at the various multi-level samplers. The fit is good for the 4 and 5 m levels. However, the model cannot resolve vertical flow variations, and so does not reflect the measured 6 m fence profile which shows little if any breakthrough. We can look at the sensitivity of the simulated fence breakthrough for different conductivities. Figure 4–14 shows simulated fence breakthrough along fence MW1 for different conductivities. For all the conductivities examined, breakthrough along the fence was roughly in the same location at the same times. For K=6.79, we begin to see the simulated plume intersecting the SW samplers, mostly SW3 with some intersecting SW2. For K=6.09 m/d, the fence breakthrough is late in time and towards the left end of the fence (all simulations were stopped at 360 days). Compare this to Figure 4–12, for K=6.09 m/d, where the same plume was seen to first migrate towards the well where it was partially captured, then migrate towards the fence. A simple sensitivity analysis can help

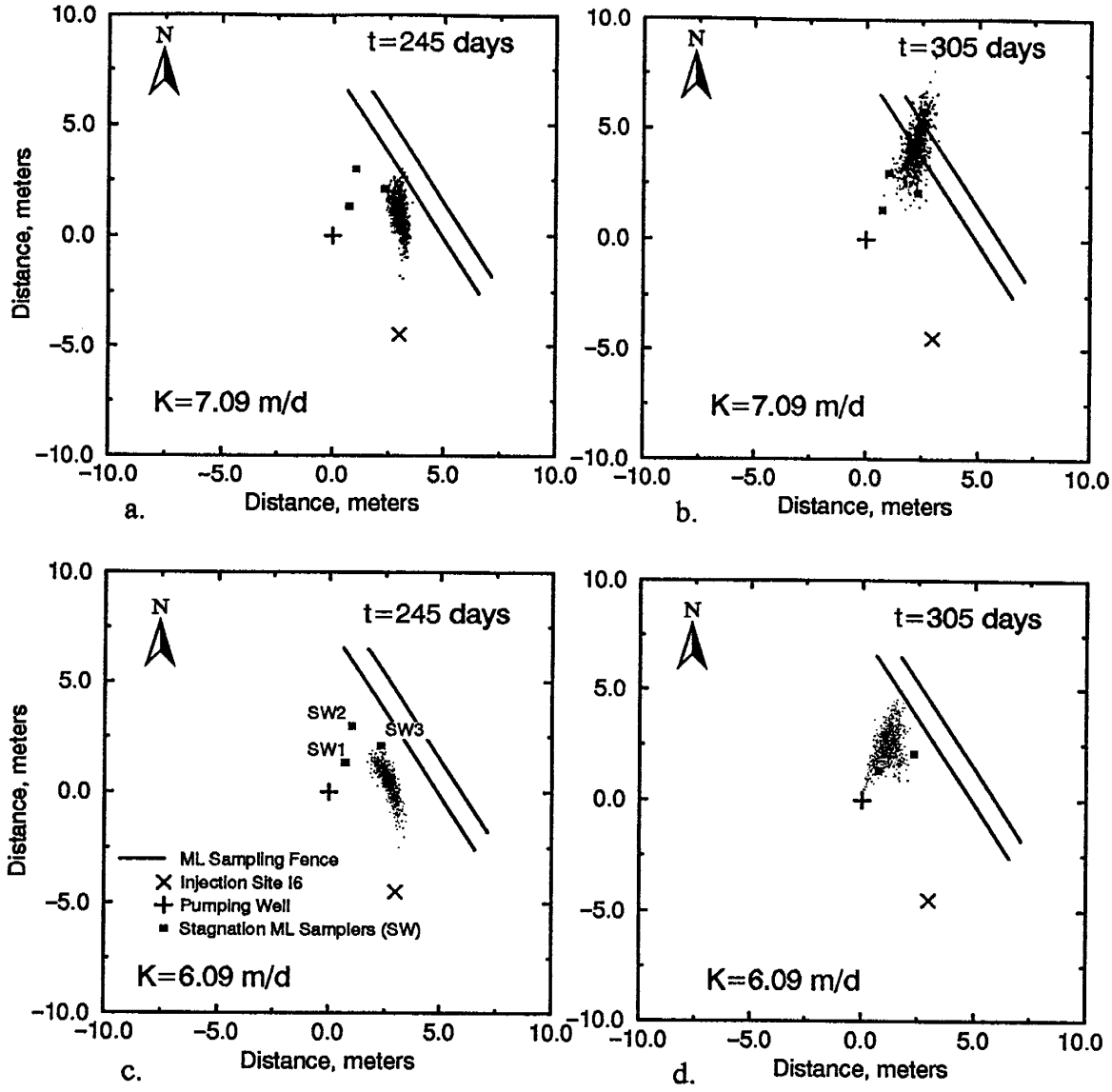

Figure 4–12. Scatter plots showing simulated plume locations for tracer injected at site I6 for K=7.09 (a and b) and K=6.09 (c and d) for Julian Dates 245 and 305 (60 and 120 days following injection, respectively).

to clarify these results. Table 4–5 gives fence and well recoveries for four different values of conductivity. The low simulated fence recovery for K=6.09 m/d shows that the plume had not entirely crossed the fence as of t=360 d. If tracer injected at I6 was partially captured at the well during the experiment, it was probably from the lower portion of the plume based on these simulations and the relatively lower hydraulic conductivity at depth.

In general, the direction of flow is changing and the simulated plume is swept across the fence at an angle. This is seen in Figure 4–14 where the plume intersects the fence further to the left (northwest) with increasing time. The plume is approximately 2 m wide. Had the plume intersected the fence perpendicularly, the width would have been even less, reducing the chances of intersecting the multilevel samplers which were place 1 m apart along each fence.

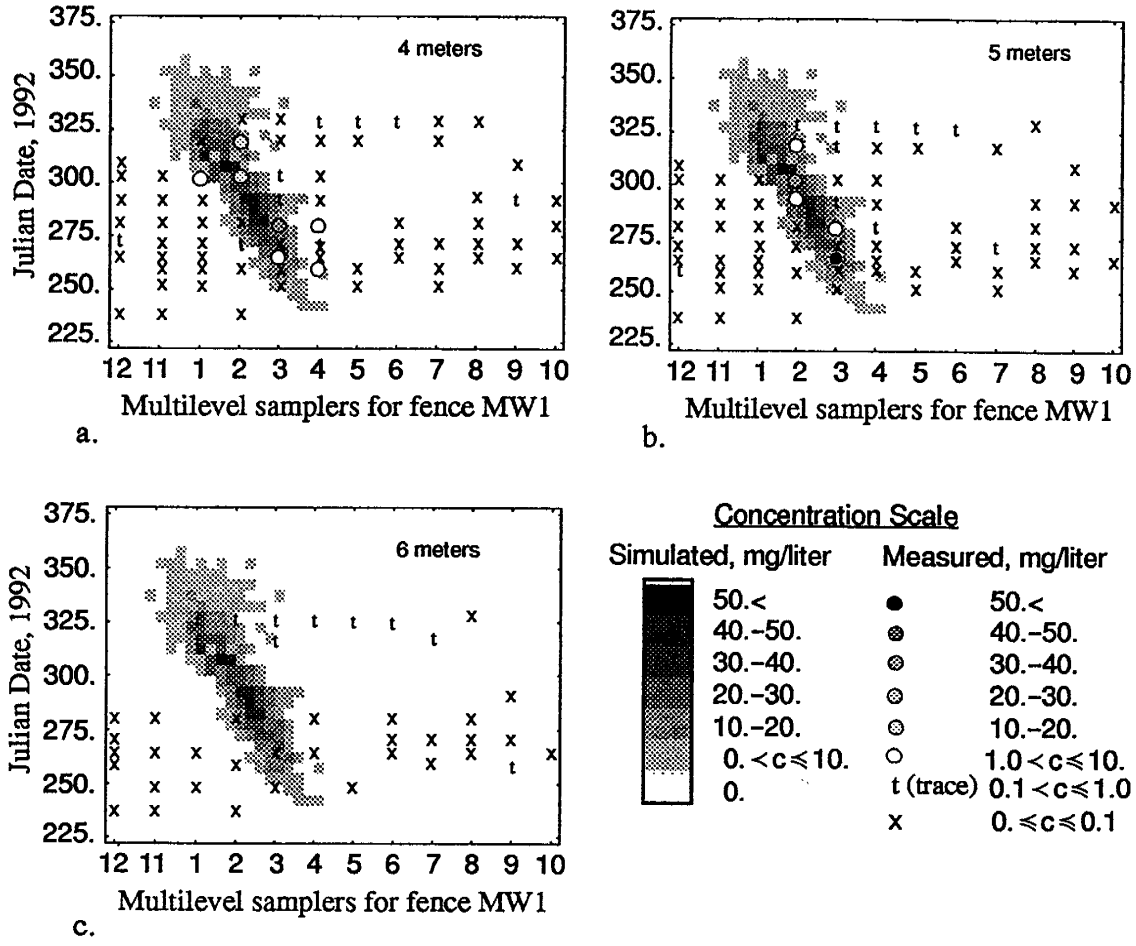

Figure 4–13. Comparison of measured and simulated breakthrough of 2,6 DFBA along monitoring fence MW1 in Experiment 1 for 4, 5 and 6 m depths (a–c, respectively).

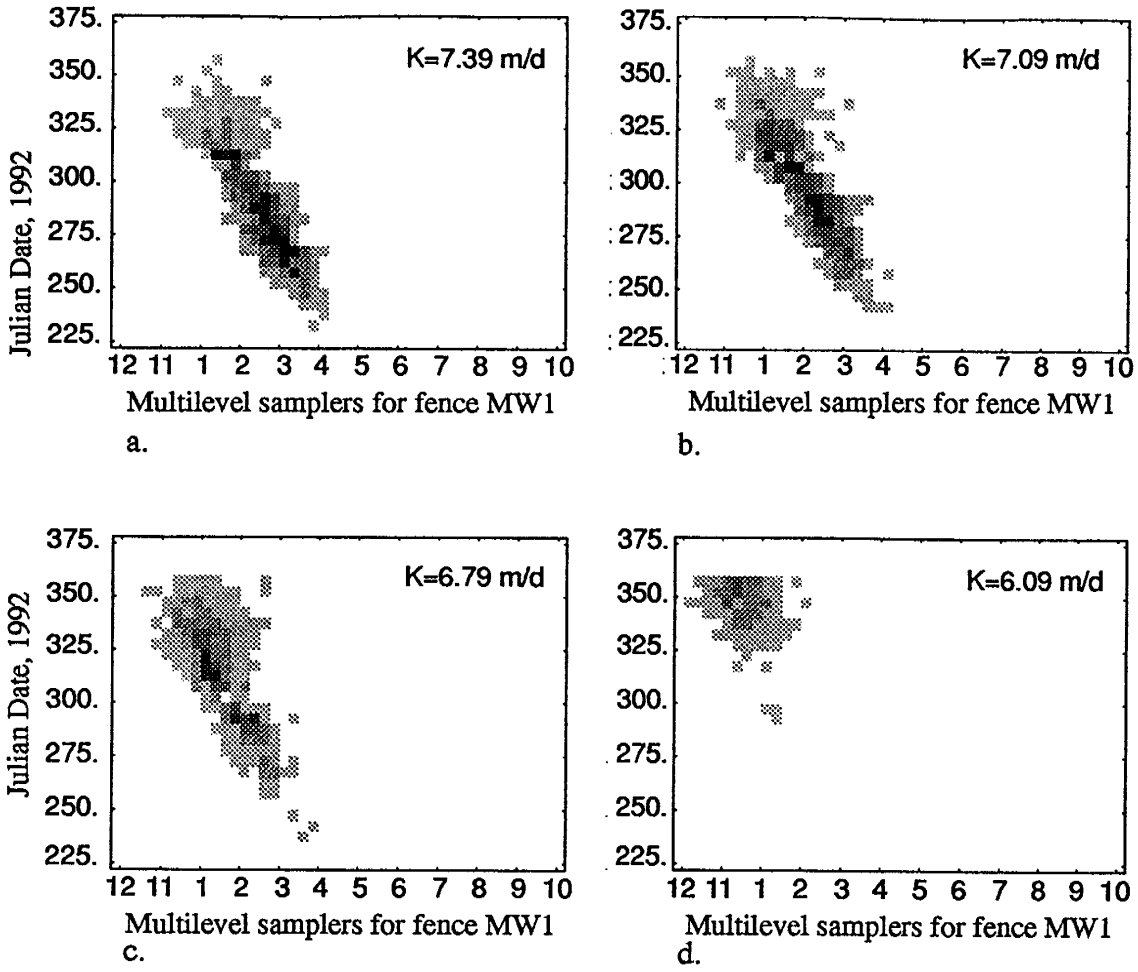

Figure 4–14. Comparison of simulated breakthrough along fence MW1 for injection at I6 for four different conductivities: (a) K=7.39; (b) K=7.09; (c) K=6.79, (d) K=6.09 m/d. The scale is the same as that for the simulations shown in Figure 4–13.

Table 4–5. Proportion of total mass breaking–through at respective sites for different values of hydraulic conductivity from injection of 2,6 DFBA at site I6.

Injection Site	BTC Site	Simulation Hydraulic Conductivity, K, m/d			
		7.39	7.09	6.79	6.09
I6	MW1	1.0	1.0	0.97	0.42
	MW2	0.96	0.90	0.69	0.04
	WELL	0.00	0.00	0.00	0.04

3,4 DFBA

Figure 4–15 shows measured and simulated BTCs. The relative recovery and BTC error, given in Table 4–4, are both large. As discussed previously, I10 is thought to be on the capture zone boundary, and this could account for the large recovery error since, as stated before, recovery for sites on the boundary are very sensitive to model parameters.

We hypothesized earlier that vertical plume splitting occurred for the tracer injected at I10, and that the splitting was caused by the combined effects of a flux–controlled pumping well located in a layered system with decreasing conductivity at depth, and the fluctuating hydraulic gradient. Prior to turning the pump on, flow was essentially horizontal and equipotentials were vertical. Darcy flux was higher in the upper portions of the aquifer, and lower at depth, due to the layered conductivity structure of the aquifer. Superposing a flux boundary at the well on the ambient flow system, and assuming no vertical flow, the capture zone would have a larger horizontal extent in the lower conductivity zone at depth than in the upper, high conductivity zone. However, with a layered system and a fully penetrating flux boundary, flow would be induced downward from the upper to the lower portions of the aquifer, attenuating the differences in capture zone size with depth.

The layered concept is supported by two simulations for tracer injected at I10, one with K=5.47 m/d and one with K=7.50 m/d. They span the range of sensitive conductivities

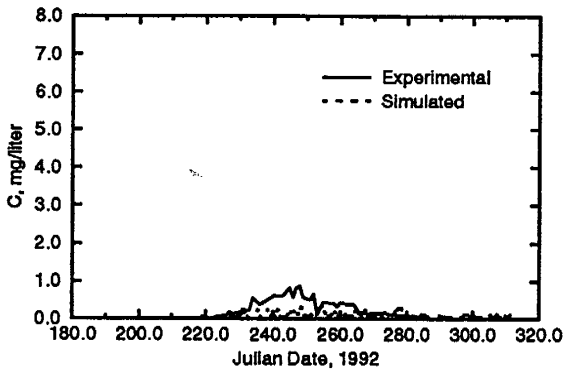

Figure 4–15. Experimental and simulated, vertically integrated BTCs for 3,4 DFBA.

for this injection point. The lower of these values were determined by running a sequence of simulations, starting with a very low K value that gave a recovery of 1.0, and increasing K until recovery began to drop below 1.0 indicating some of the plume was not being captured. Thus the value K=5.47 m/d represents the largest K value that ensures full recovery for tracer injected at I10, in the model. A similar sequential procedure was used to determine the upper K value, 7.50 m/d. Starting with a very high K resulting in no recovery, K was decreased until some of the tracer particles were captured by the well. For all K's higher than 7.50 m/d, there is no capture, while for all K's lower than 5.47 m/d, capture is 1.0. With vertical variation of hydraulic conductivity, it is quite possible that the tracer plume splits vertically in the manner just described, with part being captured and part eventually moving away from the well.

The above approach gives a feel for the sensitivity of the system to hydraulic conductivity. The two values of K give a ratio for the difference in upgradient capture zone width of 1.37 (for a steady state capture zone). For J=0.004, the difference in boundary locations is about 1.32 m on either side of the capture zone (at least for a simple capture zone in a steady state flow field). The width would be smaller near the well and when vertical flow components are considered, and is also modified by the transient nature of the system. The 30 d simulated plumes for these K values are shown in Figure 4–16. For this small difference in conductivity, 5.47 to 7.50 m/d, there is a large difference in the fate of the plume. It should be noted that the sensitivity also depends on the value for dispersivity. If a larger value for dispersivity were used, the fuzziness of the capture zone boundary is increased and so too is the range of K to which the capture zone is sensitive.

A simulation using the lower value of conductivity, K=5.47 m/d, and injection at I10 alone, gives the breakthrough shown as the dashed line in Figure 4–17. It has the same general shape as the observed BTC (solid line), but the arrival time is about 20 days sooner and the maximum concentration is slightly higher. Simulated breakthrough at the well for injection at I10 is very sensitive to the value of conductivity. For larger values, recoveries drop

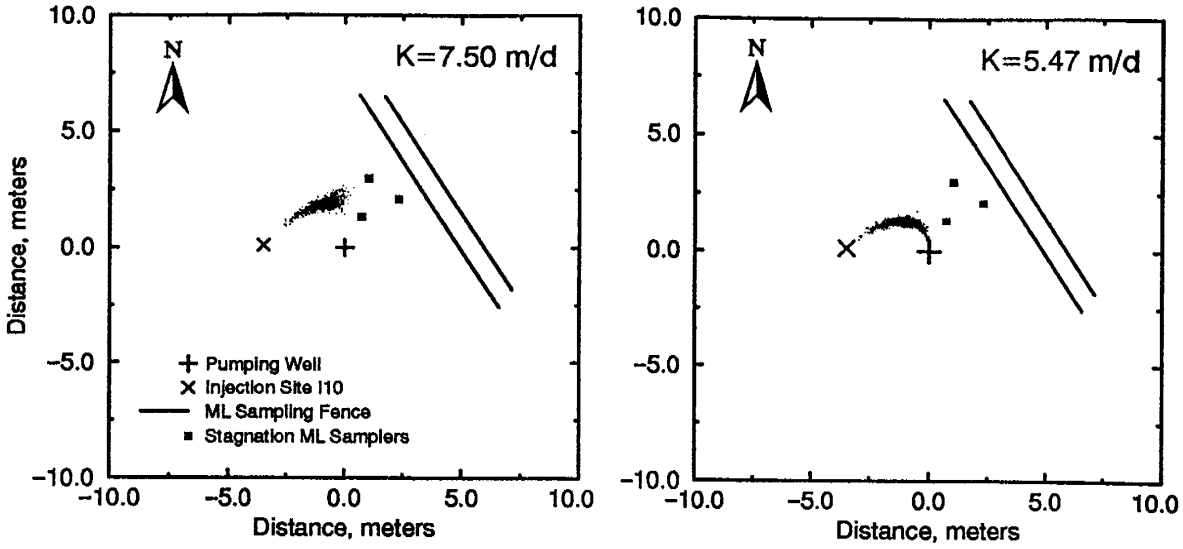

Figure 4–16. Scatter plot of 30 day plume (Julian Date 213) for site I10, K=7.50 m/d (left), and K=5.47 m/d (right).

below 1.0, while for smaller values, the travel time to the well actually decreases. This last effect results from a more direct pathline taken to the well as conductivity is decreased and the capture zone size increases. The end result is that calibration based on conductivity alone does not provide a reasonable fit of this simple model to the observed breakthrough. It should also be pointed out that the value of dispersivity used in the simulations will also affect these results.

Possible explanations for the larger measured arrival time are longer flow paths and/or larger travel times due to vertical flow of the plume, and possibly a higher porosity, larger saturated thickness, or tracer retardation. It was earlier suggested that downward vertical flow would be induced by lower hydraulic conductivity at depth and a prescribed flux boundary condition at the well. Since the vertical flow would satisfy part of the pumping demand at depth, the resulting horizontal velocities in the aquifer at this depth would be less than anticipated in this simple model. Retardation, or a different porosity or saturated thickness can also explain the delay. Time of travel for the peak of the observed breakthrough is about 70 days, the peak for the simulated curve is about 50 days. The ratio of observed to simulated peak times is 1.4. Using this as a retardation value in the model yields the breakthrough rep-

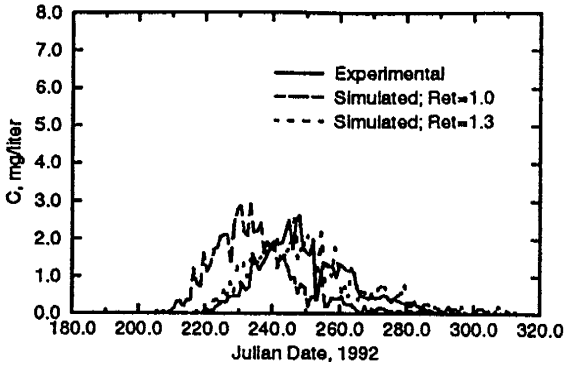

Figure 4–17. Experimental and simulated BTCs, simulations with K=5.47 and retardation factors of 1.0 and 1.4.

resented by the dotted line in Figure 4–17. This BTC is very similar to the observed curve with only minor differences, mainly in the peak concentrations. It has been assumed that the FBAs, as a group, do not exhibit sorption, although this assumption has only been tested for some FBA's on some soils (Bowman and Gibbens, 1992). Increasing model porosity to 0.46 or saturated thickness to 9.8 m would have the same effect, yet the magnitudes of these values are not reasonable.

Tracer not captured by the pumping well will have migrated downgradient, with the opportunity to intersect the SW samplers or the fences. However, 3,4 DFBA was not recorded at any of the multilevel samplers (for the 4, 5 and 6 m depths) at any of the sampling times. Simulations conducted with various conductivity values indicate the possibility of fence intersection, as shown in Table 4–5. With higher K values, indicative of the upper region of the aquifer, intersection of the plume with MW1 increases, while the recovery at the well shows the opposite trend keeping with the concept of vertical plume splitting. The reason for the discrepancy between measured and simulated concentrations at the multilevel samplers again may be due to heterogeneities or transients in the system unaccounted for by the current model. Also, tracer injected at sites that would be expected to be seen at the SW samplers are most likely located near the capture zone boundary, making simulated transport for these sites very sensitive to model input parameters. The lateral radius of capture used

in the model for the SW samplers was 0.05 m. This is a small target to hit, which would make a very useful point for model calibration since matching breakthrough at this point would require accurate model parameters, yet at the same time it requires calibration techniques beyond the scope of this study.

Table 4–6. Proportion of total mass breaking–through at respective sites for different values of hydraulic conductivity from injection of 3,4 DFBA at site I10.

Proportion of simulated total tracer mass from injection sites passing through sampling fences MW1 and MW2, and recovered by the pumping well through Julian Date 360.				
		Simulation Hydraulic Conductivity, K, m/d		
Injection Site	BTC Site	7.39	7.09	6.79
I10	MW1	0.74	0.55	0.17
	MW2	0.00	0.0	0.0
	WELL	0.02	0.12	0.40

3,5 DFBA

Measured and simulated BTCs for 3,5 DFBA are shown in Figure 4–18. The simulated BTC has similar overall arrival times, yet it is much more symmetric than the measured BTC. The difference results from the non–uniformity of the experimental breakthrough with depth. As can be seen in Figure 4–1, the time of breakthrough varies with depth, and this causes the non–symmetric nature of the measured BTC. From Table 4–4, the RRE is

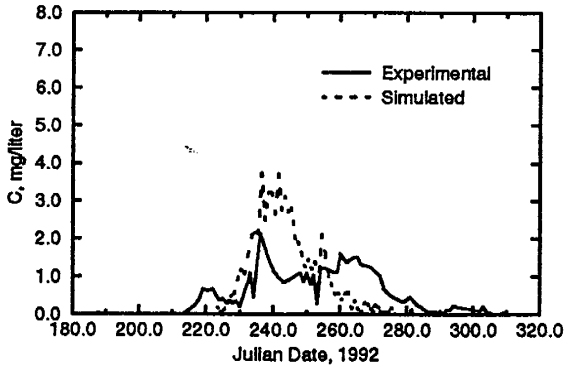

Figure 4–18. Experimental and simulated, vertically integrated BTCs for 3,5 DFBA

small, indicating the injection site is correctly modeled with respect to the capture zone boundaries. But, the RBE is large, which reflects the poor match between the BTCs, probably because of the inability of the model to resolve non-uniformity of aquifer properties with depth.

m-TFMBA

Measured and simulated BTCs are shown in Figure 4-19. The arrival times of the two BTCs match well, but the shape of the two curves is different and is reflected in the RBE. The RBE is large, probably because of the inability of the model to resolve non-uniformity of aquifer properties with depth. The simulated curve is symmetric, while the measured curve is bimodal. The differences are explained by variation in arrival times vertically, shown in Figure 4-1, as well as multi-peaked breakthrough in P4 and P5. The BTC for P6 is unimodal and exhibits the same general shape as the simulated peak, but the simulated peak arrives approximately 2 weeks earlier. The RRE is small, as shown in Table 4-4, indicating that the injection site is located within the capture zone boundary, the prediction of which is handled fairly well by the model. The simulated recovery was estimated at 1.0. However, as was suggested earlier, the discrepancy between the measured and simulated recovery could possibly be attributed to decay of the tracer. From data presented in Bowman and Rice (1986), a first-order decay constant of λ=0.0007 per day was calculated for m-

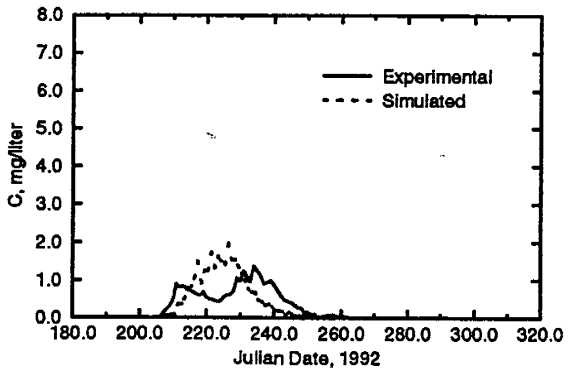

Figure 4-19. Experimental and simulated, vertically integrated BTCs for m-TFMBA.

TFMBA. Using this value in the simulation code, we see a recovery of R=0.962, which compares to the measured value of R=0.969. This suggests that it is possible that we are seeing some loss of m-TFMBA to decay processes.

o-TFMBA

Measured and simulated BTCs are shown in Figure 4-20. The simulated BTC has a later arrival time, and higher concentrations. This is partially due to missed pumping well samples at the beginning of the test. There is also noticeable variation in measured breakthrough vertically, as shown in Figure 4-1, which will also account for some of the discrepancy. Again, as in the previous tracer discussions, the P4 and P6 breakthroughs are later in time than the P3 and P5 BTCs. The RRE for o-TFMBA, shown in Figure 4-20, is large at 0.58. This is due to the missed samples. The RBE is also large, at 0.84, and reflects both the missed samples and the vertical non-uniformity of the system.

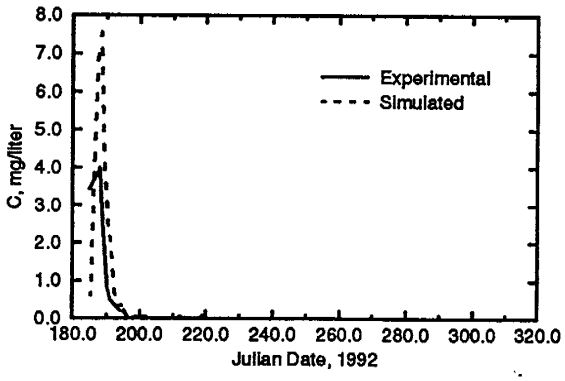

Figure 4-20. Experimental and simulated, vertically integrated BTCs for o-TFMBA.

PFBA

The measured and simulated BTCs are shown in Figure 4-21. The overall fit is not unreasonable, except for the unmatched, experimental breakthrough from t=225 to 250 d. From Figure 4-1, we see that the breakthrough in P5 most strongly resembles the simulated breakthrough. The mis-matched portion of the curve in Figure 4-21 is seen to arise mostly

in P3, and partially in P4 (refer to Figure 4–1). The BTC for P3 is earlier than for the other intervals, with breakthrough from I12 arriving from approximately t=220 to 250 d. Again, the two–dimensional model cannot handle the vertical flow component.

As discussed earlier, I9 is thought to be on, or very near, the boundary of the capture zone. Simulations confirm this and predict that tracer injected at I9 will have approximately 0.17 relative recovery at the well which is close to the measured value of 0.09. Plume configurations at t=245, 275, 305 and 335 d for simulated injection at I9 are shown in Figure 4–22. This sequence of snapshots shows partial plume capture with the majority of the particles not captured by the well, but moving down gradient across the end of the monitoring fence. Simulation results for tracer injected at I12 show that the plume was not completely recovered when the well was turned off. This result supports the conjecture made above (see the measured data analysis section for *PFBA*), regarding the matching of the bromide curve with the FBAs, that tracer from both I9 and I12 may still be entering the well when it was shutdown. In support of this notion, simulated first arrival time is about t=295 d for I9 and about t=250 d for I12, making it difficult to separate contributions from these injections. The measured recovery for PFBA may have been larger had the well continued pumping and more samples collected. Based on these arguments, the recovery for I12 may be less than initially estimated while recovery for I9 may be higher than initially estimated.

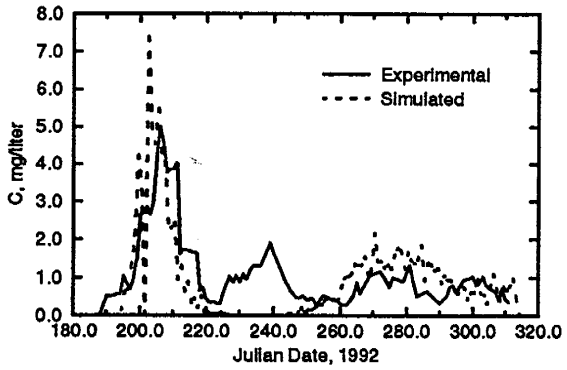

Figure 4–21. Experimental and simulated, vertically integrated BTCs for PFBA.

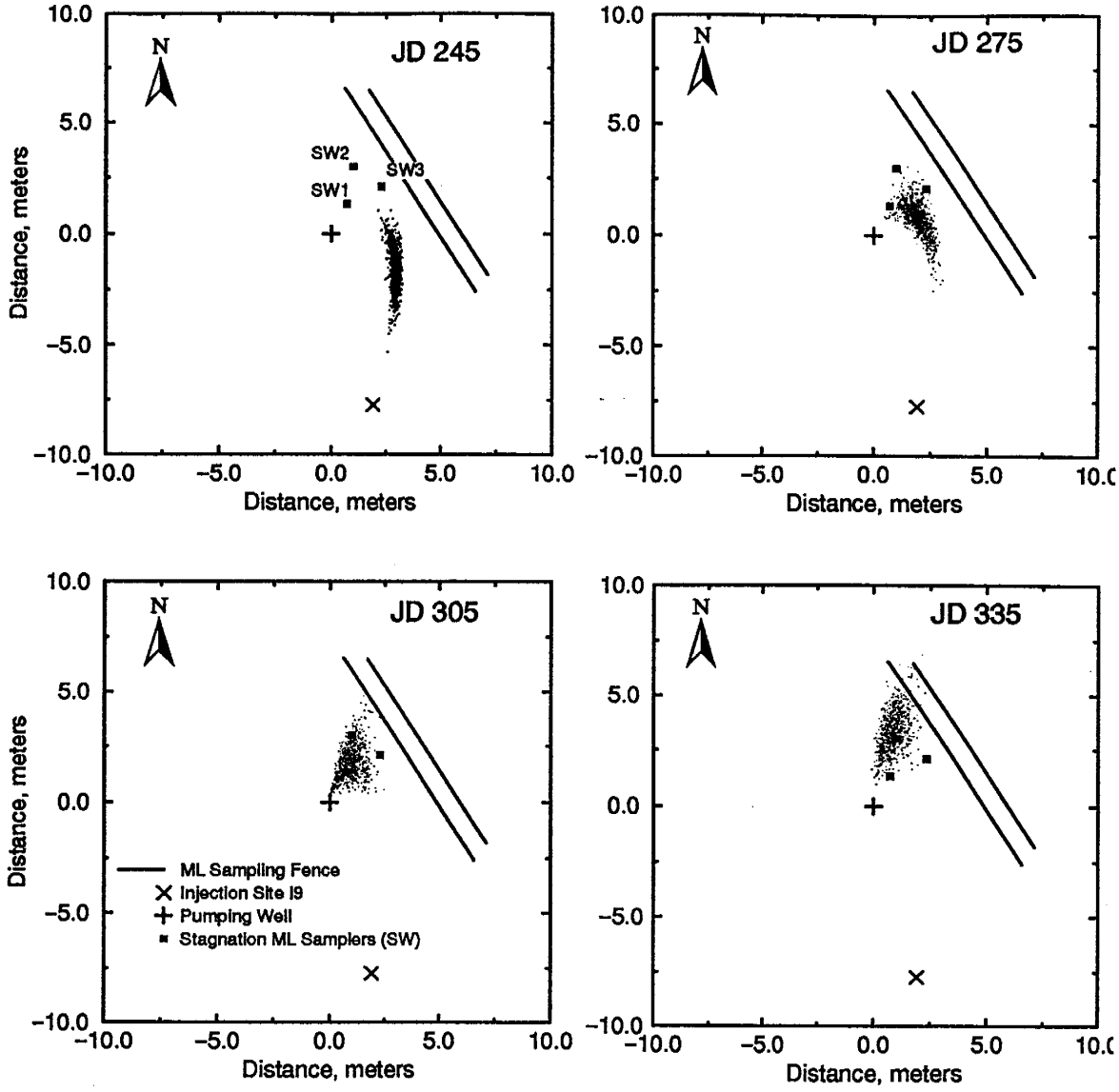

Figure 4–22. Scatter plots showing plume migration of tracer injected at I9 for Julian Dates 245, 275, 305 and 335 (60, 90, 120 and 150 days following injection, respectively).

The sensitivity of breakthrough to hydraulic conductivity is shown in Table 4–7 for three different values of K. For the current model, with K=7.09 m/d, the simulated mass recovery at MW1 is 0.29, and the well recovery is 0.17. The remainder of the plume migrated past the end of the fence and wasn't detected in the simulation. By varying K by 0.3

m/d, we see that recoveries are very sensitive to the value of K, which indicates that the injection site is on the capture zone boundary. The current model, however, shows a reasonable RRE of 0.14 (see Table 4–4), and also an improved RBE when compared to some of the previous tracers (compare 0.69 to e.g. 0.82).

Table 4–7. Proportion of total mass breaking–through at respective sites for different values of hydraulic conductivity from injection of PFBA at site I9.

Proportion of simulated total tracer mass from injection sites passing through sampling fences MW1 and MW2, and recovered by the pumping well through Julian Date 360.				
		Simulation Hydraulic Conductivity, K, m/d		
Injection Site	BTC Site	7.39	7.09	6.79
I9	MW1	0.62	0.29	0.09
	MW2	0.19	0.03	0.00
	WELL	0.03	0.17	0.40

Scatter plots of simulated plume migration shown in Figure 4–22 for K=7.09 m/d indicate Simulated stagnation well breakthrough for SW1 and SW2. From analyzed samples for the SW samplers, we see measured breakthrough across SW3 only, indicating that the conductivity we used in the simulation may be too low for the upper portion of the aquifer. A higher K value would reduce plume capture and keep the plume closer to the boundary of the capture zone.

We can also compare the measured and simulated breakthrough at the sampling fences, as shown in Figure 4–23. There is good agreement for the measured data at the 4 m depth and the simulated breakthrough. For the measured data at a time of 325 d along MW1–1, breakthrough is roughly 10 days earlier than the simulation, and about 1 m further to the right (i.e. the southeast on Figure 2–9), indicating the conductivity should be higher for the simulation at this depth in the aquifer. Data for the 5 m depth may be very close to the simulated breakthrough, but we can only speculate what concentrations would look like had more samples been collected at later times. Figure 4–23c indicates that there was no measured breakthrough for the 6 m depth, which agrees with earlier conjecture that the lower

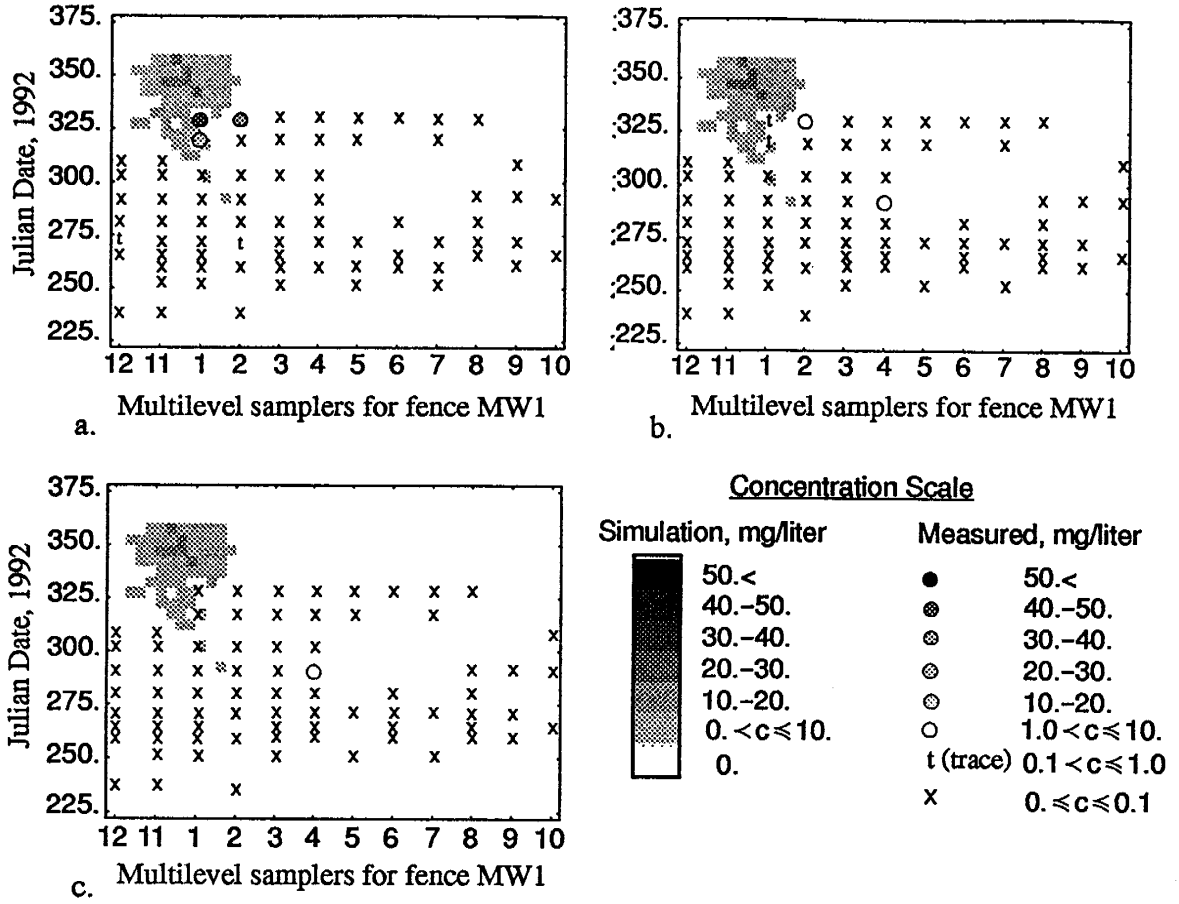

Figure 4–23. Comparison of measured and simulated breakthrough of PFBA in Experiment 1 along multilevel sampling fence MW1 for Experiment 1 at the 4, 5 and 6 m depths (a–c, respectively).

portion of the aquifer has lower conductivity. This idea will be tested in the three-dimensional modeling section below.

Br^-

Comparison of measured and simulated breakthrough of Br^- is shown in Figure 4–24. The RRE is larger than for the other tracers at 0.25, while the RBE is smaller than all the other tracers except 2,3 DFBA. The recovery error is probably large since measured mass recovery was 1.10 of the mass injected, while the simulation doesn't overestimate the injected mass. The RBE may be smaller than the other tracers since it reflects vertical

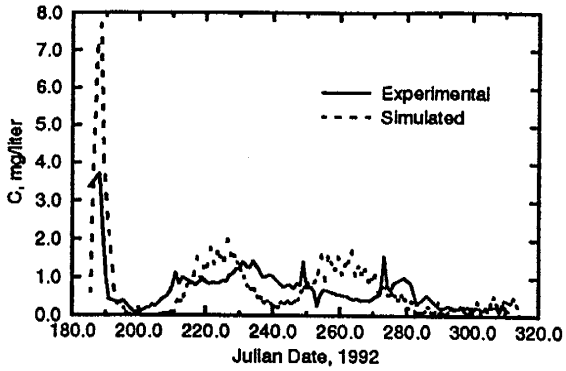

Figure 4–24. Experimental and simulated, vertically integrated BTCs for Br^-.

integration of the largest number of tracers injected and recovered at the well. This would have the effect of filling in gaps and smoothing the BTCs, thereby reducing the differences between the two curves.

Discussion

A cursory inspection of the measured and simulated BTCs above shows fairly good agreement between the time of breakthrough. The most notable exception is for PFBA (see Figure 4–21) which has a measured peak in the 230 to 240 d range without any simulated counterpart. In general, the simulated BTCs also appear to be better behaved than the measured BTCs. For instance, in Figure 4–11 and Figure 4–19 the simulated BTCs have an almost symmetric shape, whereas the experimental BTCs have two distinct peaks.

Comparing recovery and BTC residuals in Table 4–4, it becomes clear which sites demonstrate a good fit between simulated and observed results. If the percent differences are both small, then the overall fit is good. If one or both values are unreasonably large, then there is a discrepancy between the two results. For example, ε'_R for 2,3 DFBA is 0.04, indicating good mass recovery. However, ε'_{BTC} is 0.42 indicating that the BTC fit is not as good, as illustrated by Figure 4–10. The general shape of the simulated curve is reasonable, yet the arrival times are off by about 10 days at the leading and trailing edges of the simulated BTC.

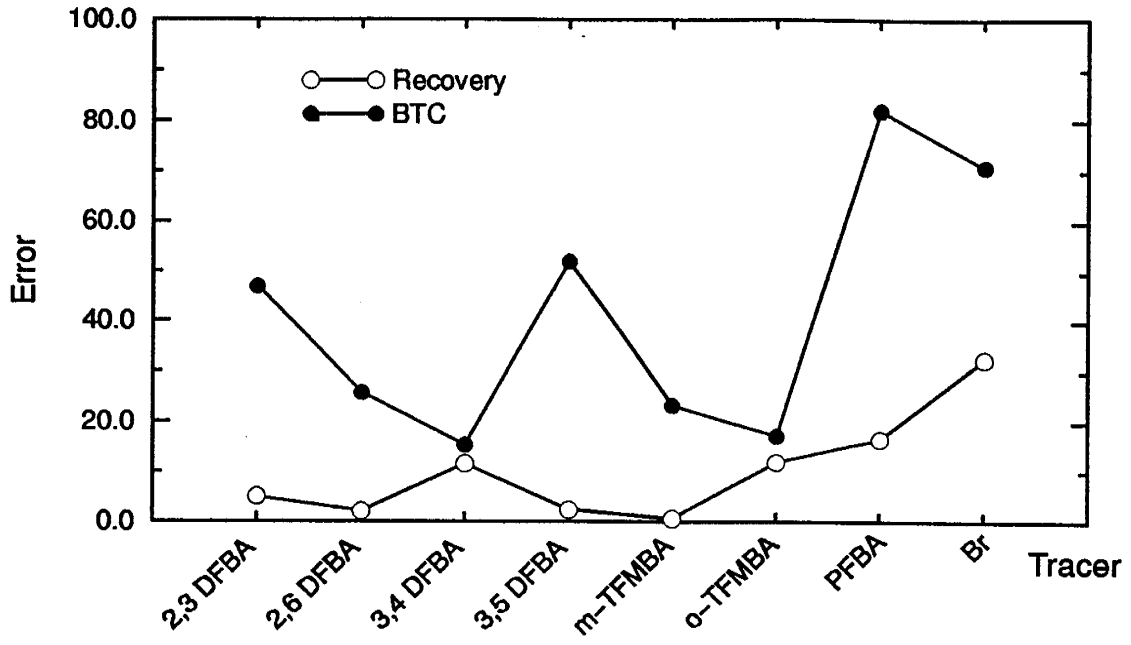

Figure 4–25. Model error for 8 tracers used in Experiment 1, derived from vertically integrated model.

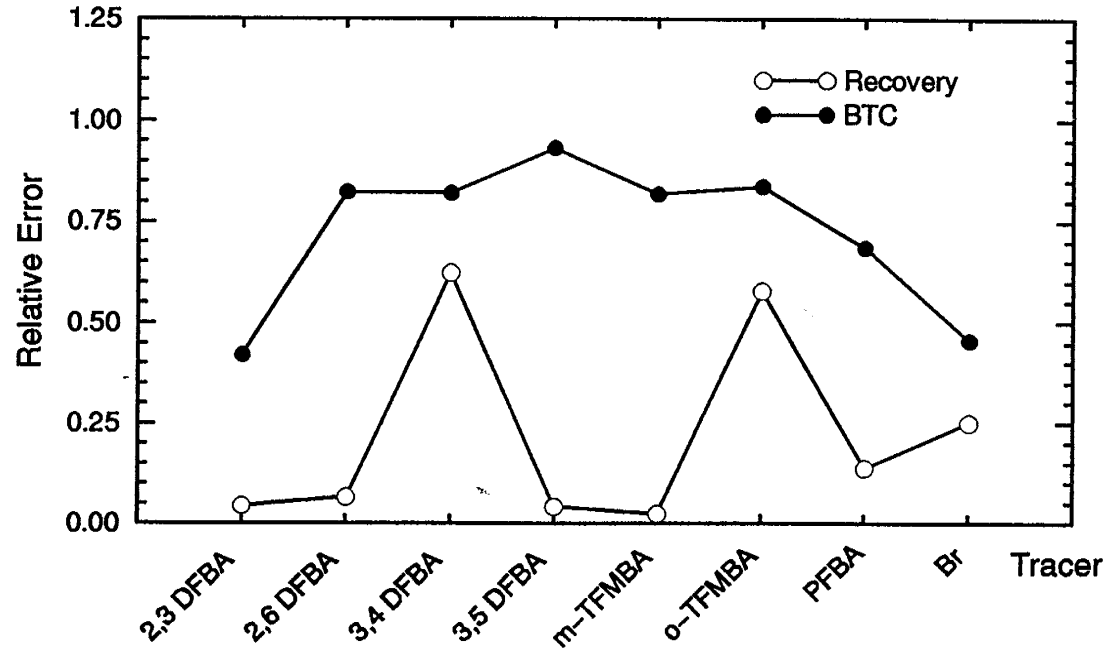

Figure 4–26. Relative model error for 8 tracers used in Experiment 1, derived from vertically integrated model.

Both the recovery and BTC error for all 8 tracers is shown in Figure 4–25. As discussed in Section 3, the error determined by (3–19) and (3–20) suffer from being dependent on how much mass was injected. In Figure 4–25, the error for PFBA and Br are the highest. Also note that the recovery and BTC errors for 3,4 DFBA and o–TFMBA are very close to being equal and are small. If we now look at the relative errors, shown in Figure 4–26, we see that the relative errors for PFBA and Br are no longer the largest and that the error term was representative of the larger injection mass for these two sites. On the other hand, the relative errors for 3,4 DFBA and o–TFMBA are large, and the relative recovery error is especially large for both. In the case of 3,4 DFBA, the large RRE reflects the sensitivity to the injection site location. For o–TFMBA, the large relative error reflects the missed samples which have affected the mass balance for this tracer. The moderately large RRE for Br^- is due mostly to mass balance error associated with injection at I1 due to missed samples early in the experiment.

A simple calibration study was performed by first finding a best fit BTC for a single tracer by first varying K, then adjusting values for α_L and α_T to improve it. The simulations for all tracers were then rerun using these parameters, and results compared for all injection sites and tracers as before. For 2,3 DFBA the selected best fit parameters were K=6.70 m/d, α_L=0.10 m and α_T=0.005 m. The new parameter values led to a total recovery error of 59.9 g and BTC error of 287.5 g. This compares to a recovery error of 82.9 g and BTC error of 334.0 g for the error results presented in Table 4–4. New recoveries and BTC residuals were calculated for all tracers and are reported in Table 4–8, along with the RBE, ε'_{BTC}. The recovery error shows varying levels of improvement for individual tracers with some fits improving and some staying the same, but none getting worse. The '(I)' next to the number for relative error indicates relative error terms that improved for the calibrated simulation. The error for 3,4 DFBA for the original model was negative whereas the error following calibration is roughly of the same magnitude, but positive. This is due to I10 being on the capture zone boundary and makes simulated recovery at the well very sensitive to input parame-

ters. The BTC error, ε_{BTC}, was reduced by the calibration for all tracers. This can be most clearly seen from comparison of the RBE in Table 4–4 and Table 4–8. The tracer 2,6 DFBA, 3,5 DFBA, m–TFMBA and o–TFMBA all showed fairly large improvement, while the reduction in error for PFBA was the smallest.

Table 4–8. Comparison of experimental and simulated mass recoveries and breakthrough curves for Experiment 1; calibrated simulations based on matching 2,3 DFBA BTC.

	Tracer Mass Recovery				Tracer Breakthrough	
Tracer	*Experimental* R_E	*Simulated* R_S	Recovery Error ε_R	Relative Recovery Error RRE (Absolute value)	Breakthrough Error ε_{BTC}	Relative Breakthrough Error RBE
2,3 DFBA	111.3	116.3	5.0	0.04 (I)	41.0	0.37 (I)
2,6 DFBA	31.2	29.04	-2.1	0.07	19.7	0.63 (I)
3,4 DFBA	18.6	26.9	8.3	0.45 (I)	14.7	0.79 (I)
3,5 DFBA	55.7	58.1	2.4	0.04	41.1	0.74 (I)
m–TFMBA *	28.4	29.0	0.7	0.03	16.8	0.59 (I)
o–TFMBA	20.5	31.7	11.2	0.55 (I)	13.3	0.65 (I)
PFBA*	119.6	114.7	-4.9	0.04 (I)	80.2	0.67 (I)
Br (2–6)	129.9	104.7	-25.3	0.19 (I)	60.7	0.47 (I)

* Smoothed data.

The RBE for all tracers for the first simulation is 0.65, the RBE for the simulation with parameters calibrated to the fit for 2,3 DFBA is 0.56. The improvement in BTC error in terms of mass is about 52. g, which is a 10% reduction in this error. This is a substantial improvement in model fit, although a relative error of 0.56 is still fairly large. The decrease in recovery error between the two simulations is 23. g, or about a 5% improvement. The RRE dropped from 0.16 to 0.12. A relative error of 0.12 is reasonable, and can be considered a good fit, yet it must be remembered that this is for what is considered to be a very simple and extensively studied aquifer. These facts suggest that there are complexities in the system not accounted for in the current model that need to be included if a better fit is to be achieved.

Next, we will look at the error for a series of simulations to examine sensitivity of the model and also evaluate some alternatives for parameterization. The relative error for eight different simulations are shown in Figure 4–27. The parameters used in each simulation are given in Table 4–9. For hydraulic gradient, two different data sets were available. The so–called entire data set refers to gradient generated using heads from all the 21 measurement locations within the sand pit. The local data set refers to gradients calculated from 14 measurement locations within the vicinity of the experiment. It was thought that the local measurements may better reflect the gradient at the experiment site, giving better results. Aquifer thickness was either held constant throughout the simulation, or allowed to vary with time to reflect water–table measurements made during the experiment. The two different constant values, 7.3 and 7.0, reflect different states of knowledge about the system. The value of $\bar{h}$=7.0 was determined prior to the experiment startup and was used in the design of the experiment. The value of $\bar{h}$=7.3 is the mean value taken from the time–varying distribution of $\bar{h}$ over the course of the experiment. The constant velocity interpolation means that all time–varying parameters were held constant for the period of time half–way between

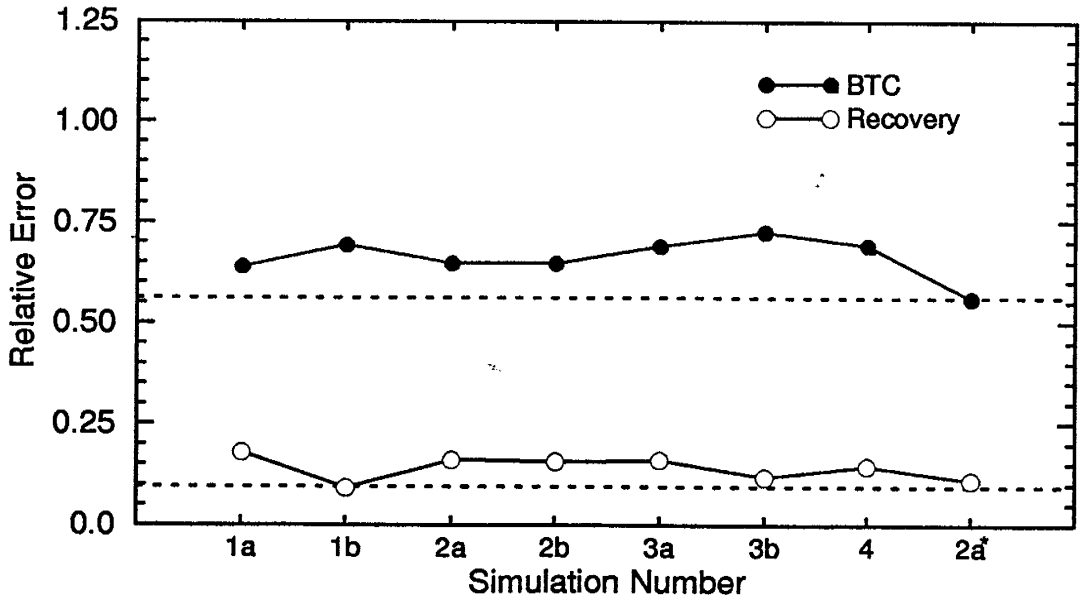

Figure 4–27. Relative error for various vertically integrated two–dimensional simulations.

neighboring measurement times. This would look like a step function. The continuous velocity-interpolation allows for linear interpolation between each measurement point taken at specific times. Simulation 2a was the simulation used in the two-dimensional analysis above. Simulation 2a* uses parameters calibrated to the breakthrough of 2,3 DFBA.

Table 4-9. Aquifer parameters used in two-dimensional modeling.

Simulation Number	K_x (=K_y), m/d	Hydraulic Gradient, J	Aquifer Thickness, b, m	α_L, m	α_T, m	Velocity Interpolation
1a	7.09	Entire	7.3	0.08	0.001	Cont.
1b	7.09	Entire	7.0	0.08	0.001	Cont.
2a	7.09	Entire	variable	0.08	0.001	Cont.
2b	7.09	Entire	variable	0.08	0.001	Step
3a	7.09	Local	7.3	0.08	0.001	Cont.
3b	7.09	Local	7.0	0.08	0.001	Cont.
4	7.09	Local	variable	0.08	0.001	Cont.
2a*	6.70	Entire	variable	0.10	0.005	Cont.

From Figure 4-27, it is apparent that regardless of what model is used, the recovery error remains near 0.10 and the BTC error is about 0.55 to 0.70. It is safe to say that, the error in predicting the mass recovered at a pumping well is about 10% of the mass recovered. If more information is desired, such as the timed sequence of mass breakthrough and recovery, then the error goes up to above 50%, that is, there would be 50% error in predicting the breakthrough of mass over time. This is significant considering that the predictions made so far all used history matching for time dependant parameters measured over the course of the experiment, in addition to substantial information regarding the hydraulic conductivity of the site. The following section on three-dimensional modeling of the experiment attempts to improve on the error present in the two-dimensional model, and to account for some of the complexities not addressed by the two-dimensional model.

Three-Dimensional Model Analysis

A three-dimensional modeling study was carried out to determine if certain discrepancies in the two-dimensional models could be addressed by taking into account vertical heterogeneities, buoyancy effects, and non-uniform pumping over the vertical extent of the pumping well. Buoyancy effects were handled using the method described in Section III.

To review, the three-dimensional model was quasi-steady state. As in the two-dimensional model, two different input parameter time dependencies were considered. One method treated time varying parameters as constant over a given time interval, which gives a stepwise-continuous treatment of the parameters. This is the approach for values of magnitude and direction of hydraulic gradient, aquifer thickness and pumping rate shown in Figure 4-28. The second method was to linearly interpolate over time between the measured values. For both methods, 28 velocity fields over time were used as input to the random walk code in the three-dimensional analysis.

Table 4-10 shows the parameters used in the various simulations. Simulations numbered less than 5 are reserved for the two-dimensional simulations. The differences in the simulations focus primarily on hydraulic conductivity, with the conductivity fields becoming more complex with each additional simulation. Simulations 5 and 6 represent the simplest three-dimensional aquifer model, homogeneous with a horizontal to vertical anisotropy ratio of 1.3 (Sudicky, 1986). Simulations 5 and 6 are the same except 6 allowed for vertical plume transport due to density contrast between the tracer plume and the surrounding background water. The same relationship holds for Simulations 7 and 8. Results of error analysis (discussed below) indicate that the model was more accurate when buoyancy effects were included, so all simulations after 8 included buoyancy effects. Simulations 7 and 8 use the parameters determined from applying the two-dimensional model to the upper and lower zones of the aquifer, as shown in Figure 4-16. Simulations 7, 8 and 10 (there were several renditions of 8, as well as 9, not reported here) focused on the vertical plume splitting of 3,4

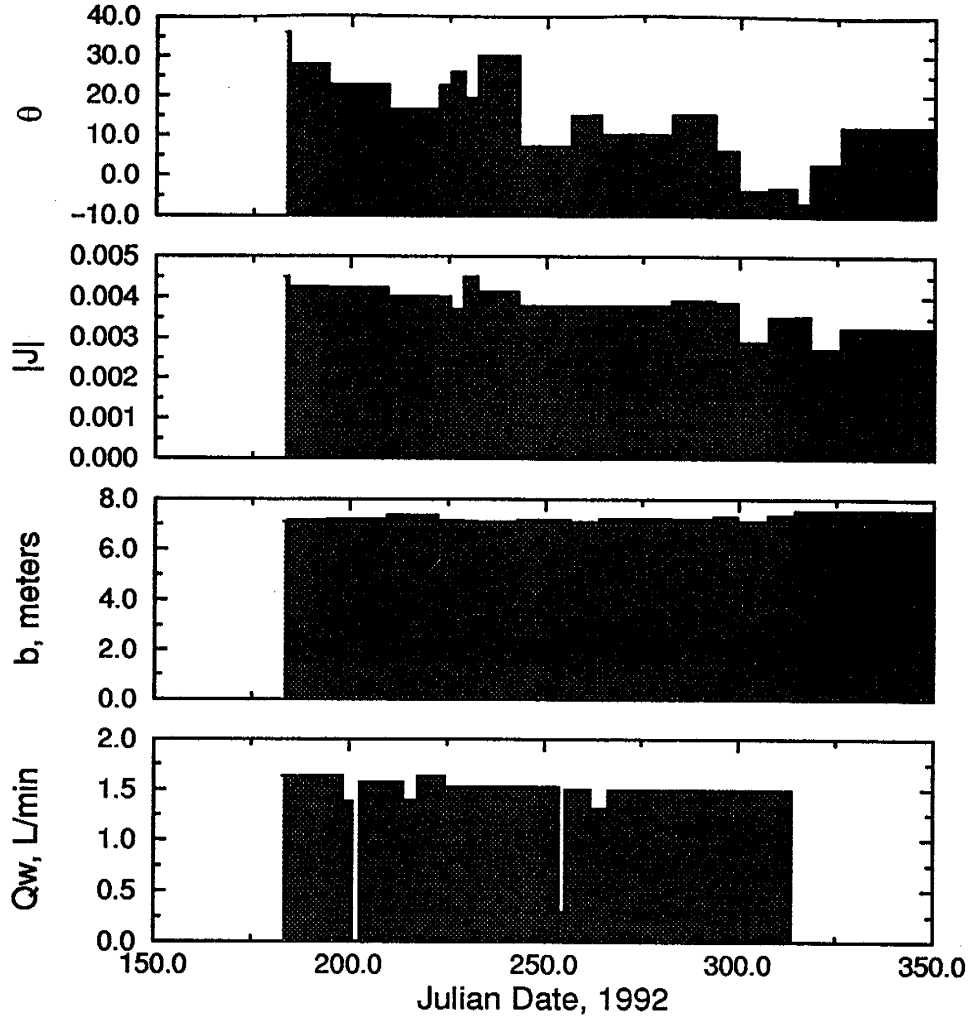

Figure 4–28. Time varying input parameters for three–dimensional analysis of Experiment 1. Q_w is pumping rate, b is aquifer thickness, |J| is magnitude of hydraulic gradient, and θ is directional component of hydraulic gradient.

DFBA injected at I10. Simulation 10 represents the two layer model derived from adjusting the hydraulic conductivity in the two layers to obtain a best fit for injection at I10. Sensitivity of the fit to longitudinal dispersivity was also tested for α_L=0.04, 0.06, 0.08 and 0.10 m.

Simulations 7, 8 and 10 optimized the model fit for only one tracer injected at a single injection site. To provide an overall comparison of model results to experimental results, the simultaneous fitting of BTCs and recoveries for all sites had to be taken into consider-

ation. The remaining simulations were attempts at maintaining the character of the plume splitting observed for 3,4 DFBA, while also improving the fit for upper intervals by taking into consideration the higher conductivities in the upper part of the aquifer as indicated later in Figure 4–40, for all tracer injections. Simulation 11 has 6 layers of conductivity based on data presented in Sudicky (1986) for Thorbjarnarson and Mackay (1994) the upper region of the aquifer, and on results from simulations 7, 8, and 10. The hydraulic conductivity in the 6–8 m region of the aquifer had to be lowered, and the contrast between conductivities above and below the 5 m depth had to be lessened, to compensate for the higher conductivity values specified in the upper region of the aquifer. Sensitivity of model results to longitudinal dispersivity were also tested. Simulation 12 was an attempt to improve on the results from simulation 11. Simulation 13 was of a 9 layer model. Since simulations 11 and 12 did not show improvement of the model fit, simulation 13 was an attempt to supply a more detailed conductivity field based on information from all previous simulations, and from Sudicky (1986) and Thorbjarnarson and Mackay (1994). Sensitivity to longitudinal dispersivity was also tested, and the values giving the best results for each tracer were used in deriving the resulting model error.

Table 4–10. Aquifer parameters used in three-dimensional modeling.

Simulation Number	Buoyancy Effects	K_x (=K_y), m/d	K_z, m/d	α_L, m
5	no	7.09	5.45	0.08
6	yes	7.09	5.45	0.08
7	no	0<z<5 : 7.50 5<z<8 : 5.47	5.77 4.21	0.08
8	yes	0<z<5 : 7.50 5<z<8 : 5.47	5.77 4.21	0.08
10	yes	0<z<5 : 8.50 5<z<8 : 5.00	6.54 3.85	0.08 (except I10: 0.04)
11a	yes	0<z<2.8 : 15.0 2.8<z<3.0: 12.5 3.0<z<3.2: 10.0 3.2<z<5.0 : 7.50 5<z<6 : 5.00 6<z<8 : 4.00	11.54 9.62 7.69 5.77 3.85 3.08	0.08
11b	yes	same as 11a	same as 11a	0.04
11c	yes	same as 11a	same as 11a	0.06
11d	yes	same as 11a	same as 11a	0.10
12	yes	0<z<2.8 : 14.0 2.8<z<3.0: 12.0 3.0<z<3.2: 10.0 3.2<z<5.0 : 7.50 5<z<6 : 5.00 6<z<8 : 4.00	10.77 9.23 7.69 6.15 3.85 3.08	0.08 (except I10: 0.04)
13	yes	0<z<2.8 : 12.0 2.8<z<3.0: 15.0 3.0<z<3.2: 12.0 3.2<z<3.4: 6.50 3.4<z<3.6: 10.0 3.6<z<3.8: 6.50 3.8<z<5.0 : 7.50 5<z<6 : 5.00 6<z<8 : 4.50	9.23 11.54 9.23 5.00 7.69 5.00 5.77 3.85 3.46	site dependent: I1,6,7,11,13,15: α_L=0.10 I2,4,5,8,9,12,14: α_L=0.08 I3,10: α_L=0.04
13a	Same as 13, except linear interpolation between velocity fields was used to produce continually changing velocities.			

As mentioned above, simulation 10 was based on a best fit of the two layer model for injection at I10, which is shown in Figure 4–29. The RREs for 3,4 DFBA injected at I10 are 0.18, 0.04, 0.49 and 0.20 for simulations 6, 10, 12 and 13, respectively (BTCs for these simulations are shown in Figure 4–29). Clearly, simulation 10 has the best fit when considering recovery of 3,4 DFBA alone. However, simulation 13 provides the best overall fit considering all tracer injections and recoveries. Figure 4–30 shows comparisons of the mea-

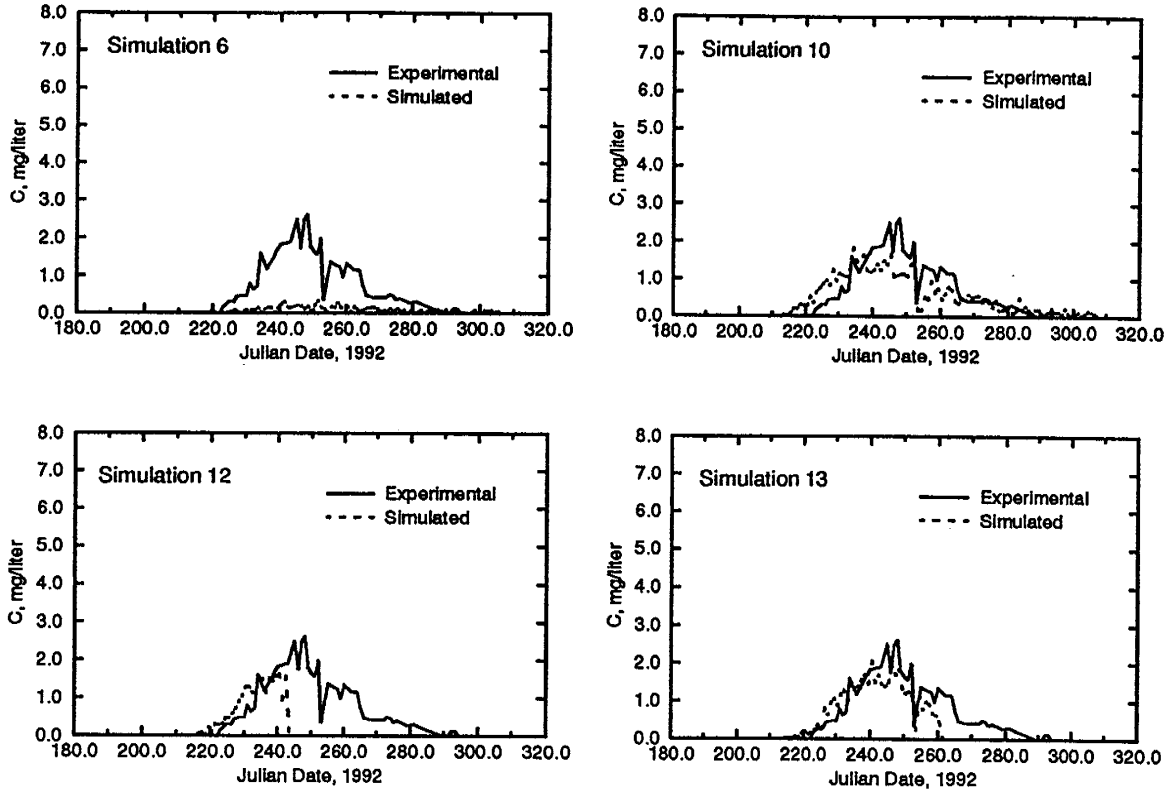

Figure 4–29. Comparison of 4 simulation BTCs to measured breakthrough of 3,4 DFBA for Experiment 1 for simulations 6, 10, 12 and 13. See Table 4–10 for description of parameters used in the simulations.

sured breakthrough of PFBA to BTCs from simulations 6 and 13, where simulation 6 is a homogeneous system and simulation 13 is a heterogeneous system with 9 layers. As can be seen, the measured peak at 240 d has no counterpart for simulation 6 (this is essentially the same as simulation 2a in the two–dimensional model, except for the horizontal to vertical hydraulic conductivity ratio of 1.3 in the three–dimensional model). Once we include higher conductivity layers in the upper portion of the aquifer, we begin to see this peak in the simulated breakthrough. The model fit for the remainder of the measured BTC in Figure 4–30b has also improved. The vertically–integrated, RBE for simulation 13 has improved to 0.55 from that of 0.65 for simulation 6. Three–dimensional model results for breakthrough of PFBA at the 4 meter depth of sampling fence MW1 are shown in Figure 4–31 for simulations 10, 12, 13 and 13a. All of the simulated breakthrough occurs much earlier than the measured

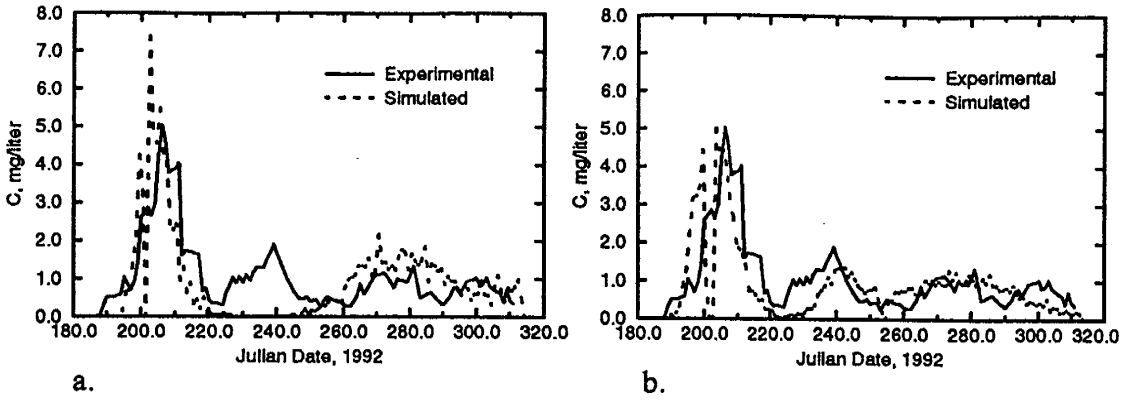

Figure 4–30. Comparison of vertically–integrated, simulated model BTC (a, simulation 6) and simulated three–dimensional model BTC (b, simulation 13) to measured BTC for Experiment 1.

breakthrough. This indicates that conductivities are too high in the upper part of the aquifer in the simulations. Interestingly, simulation 13a has a slightly better fit than the other 3, perhaps hinting at the need to conduct further simulations using continuous velocity interpolation. Figure 4–32 shows measured and simulated breakthrough of 2,6 DFBA at fence MW1 for simulation 13. Again the simulated breakthrough is earlier than the measured breakthrough. Also, Figure 4–31 and Figure 4–32 should be compared to Figure 4–23 and Figure 4–13 for simulated, two–dimensional fence breakthrough of PFBA and 2,6 DFBA, respectively.

It should be noted here that the simulated relative recovery from I12 was approximately 0.96 for simulations 10, 11, 12 and 13 while relative recovery from I9 was about 0.01 for the same simulations. For simulation 13a, simulated relative recoveries were 0.94 and 0.05 for sites I12 and I9, respectively. In the analysis of PFBA in the two previous subsections, it was hypothesized that tracer from I12, and perhaps from I9, was still being recovered by the well when it was shutdown. Both two– and three–dimensional analysis supports the view that I12 was still being recovered. But, for the simulated and measured recoveries to balance and with a relatively recovery of 0.96 from I12, the simulated recovery from I9 should be about 0.17. It may be that the hydraulic conductivity is too high in the three–di-

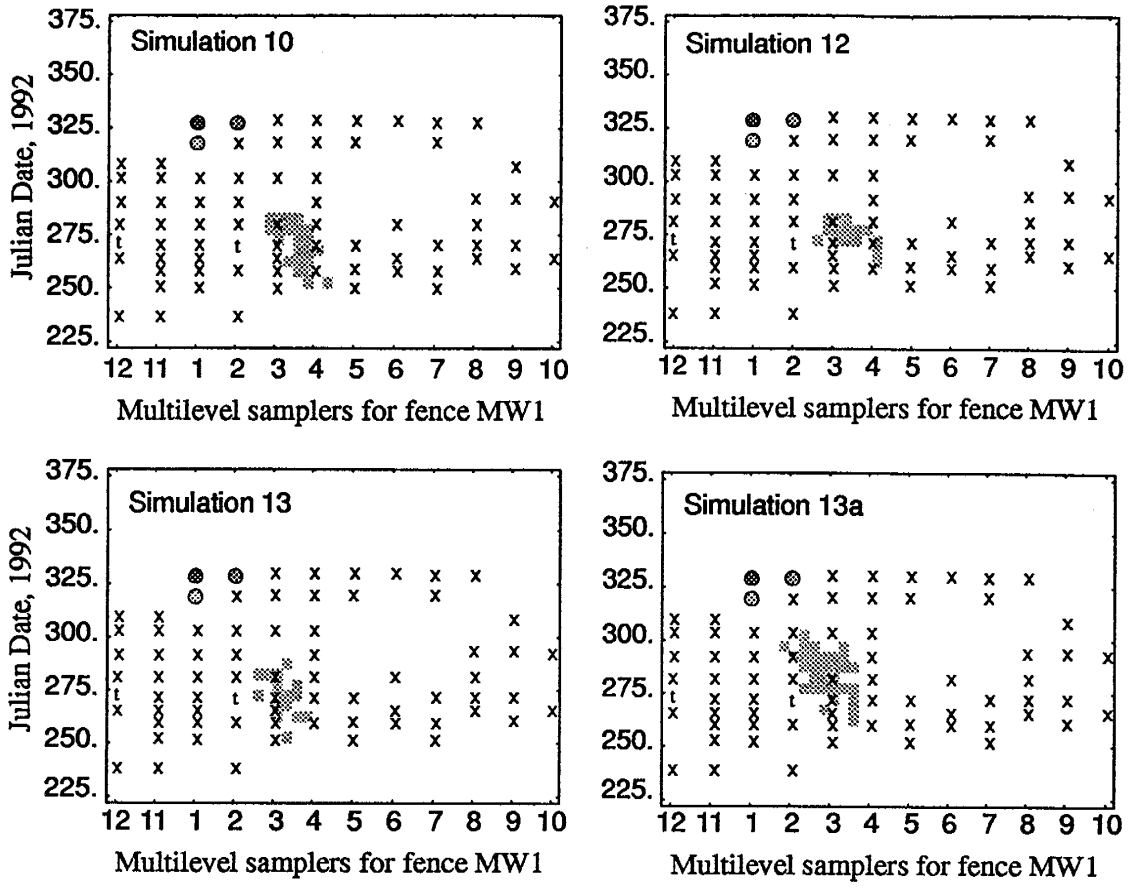

Figure 4–31. Comparison of measured and simulated breakthrough of PFBA along fence MW1 at the 4 m level for simulations 10, 12, 13 and 13a.

mensional simulations. Lower conductivities would possibly increase capture of tracer from I9, but they may also retard the arrival time of the plume from I12 such that the masses will still not balance.

Another explanation may come from re-examination of Sudicky's data. So far only a layered system has been discussed. Even though the horizontal correlation length is relatively large (see Section II), it may be entirely possible that there is a heterogeneity which is influencing flow in the lateral direction. This hypothesis is supported by Figure 6 of Sudicky (1986) which shows lenses of low conductivity zones in the 10–19 m region of the

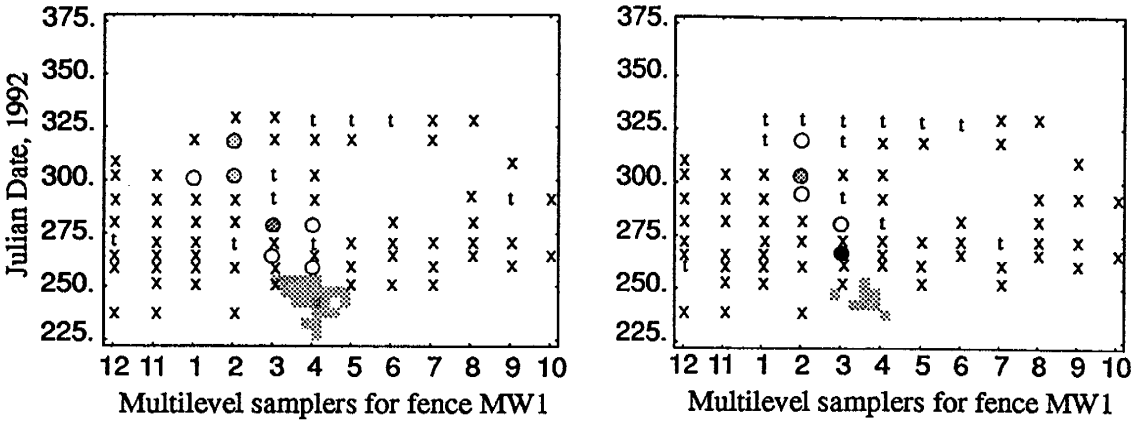

Figure 4–32. Comparison of measured and simulated breakthrough of 2,6 DFBA along fence MW1 at the 4 m (left) and 5 m (right) depth.

A–A' transect. This would correspond to the region running from about 1 m south of the pumping well (roughly the 10 m location of Sudicky's Figure 6) towards the northeast. The hydraulic conductivity data for transect A–A' is shown in Figure 4–33 for cores 1–9 and

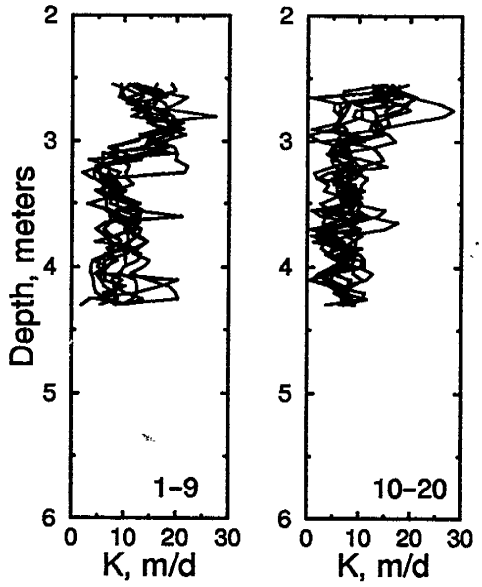

Figure 4–33. Hydraulic conductivity data for transect A–A' from Sudicky (1986); the left figure shows cores 1–9, the right figure shows cores 10–20.

10–20 separately. For these depths, it appears that there are some lower values for the 10–20 m region, but obviously there is a large amount of overlap. However, these small differences may be important considering the sensitivity of recovery for injections on the capture zone boundary. If the horizontal extent of the lenses is governed by the same statistical parameters as determined from the two transects as a whole, then the region of the aquifer between I3, I11, SW1 and MW1, or the region just to the northeast of I5, may be influencing flow either laterally or vertically. Sudicky's data is only for the upper portion of the aquifer, but even if the lenses do not extend to the bottom of the aquifer, the effect would be for flow to circumvent this region either vertically, in a manner similar to what Dagan (1989) has described for the Borden site when he refers to the Borden aquifer as a 'brick layered structure', or laterally, which could cause a larger proportion of the tracer to be captured than was determined by the simulations. Tracer from I6 may also be affected by a relatively lower hydraulic conductivity zone in this region. The simulations all give a relative recovery of zero for I6 and close to 1.0 for I15, yet the experimental results suggest that the measured recovery is about 2. g greater than what complete recovery from I15 would allow. A relative recovery of 0.033 from I6 would provide a mass balance. This would also account for the early simulated arrival times for PFBA and 2,6 DFBA at the sampling fence MW1, shown in Figure 4–31 and Figure 4–32.

The character of the capture zone is much different for a layered aquifer than for a homogeneous aquifer. For a homogeneous system, the capture zone can be easily conceptualized, and easily modeled mathematically using a two–dimensional model. With a layered system, the capture zone boundaries are no longer vertical, and the shape of the capture zone over the depth of the aquifer depends on the relative values for hydraulic conductivity for the different layers. For conductivities relatively lower at depth, and higher in the upper part of the aquifer, the capture zone will be wider at depth and narrower above. For injections extending over a 3 meter length vertically, the lower portion may be completely captured by the well whereas the upper portion may be partially captured, or not captured at all as in the

case of injection of 3,4 DFBA at I10. For simulations with higher conductivity in the upper portion of the aquifer, namely simulations 11, 12 and 13, other injection sites may begin to exhibit partial capture as well. In particular, sites I2, I5 and I12 begin to show partial capture in these simulations for the upper capture interval, P3. Partial capture at all three of these sites has significance with respect to the recovery map of Figure 4–8. As mentioned in the two–dimensional analysis of m–TFMBA, the relative recovery of 0.97 from I2 may be due to decay of the tracer. However, for simulation 13, the simulated relative recovery is 0.985. In this case, the simulated mass not captured by the well is from the upper, high conductivity regions of the aquifer. Given the error associated with the model, it may be that the measured relative recovery of 0.97 results from hydraulic conductivity variations instead of tracer decay, or it may be a combination of both.

These results are predictable if we look at the available data, such as that shown later in Figure 4–33. For a homogeneous aquifer with K=7.09 m/d, the width of a steady state two–dimensional capture zone is roughly w=5.2 m ($2w=Q/(qa*\bar{h})$; $\bar{h}$=7.3 m, qa=7.09*0.004; Q=2.16 m^3/d). For K=5.0 m/d, w=7.4 m, and for K=15.0 m/d, w=2.5 m. From Figure 2–9, it easily seen that for flow in a northerly direction, I2, I7 and I12 would be outside the capture zone for K=15.0 m/d (for a purely two–dimensional system). This scenario is further complicated due to the layering in the aquifer and the changing flow direction. The new scenario then is one where flow is initially to the northeast, and I2, I7 and I12 are within the capture zone. As the direction of flow changes towards the north, the capture zone boundary migrates towards the east such that the upper portions of the plumes from I2, I7 and I12 are located on the capture zone boundary. The lower portions of the plumes remain within the capture zone since the capture zone is wider at depth due to relatively lower hydraulic conductivities.

Finally, well recoveries for sites located on the capture zone boundary are influenced by dispersion of the plume, as was noted in Figure 4–29 for simulation of tracer injected at I10. In this case, a better fit was achieved for α_L=0.04 m. This fits well with the estimate

of vertical plume movement from I10, which was relatively large compared to that estimated for the other tracers (see Table 4–3). For 3,4 DFBA (injected at I10), it was hypothesized that the tracer was injected into the strongly convergent zone of the flow field, minimizing dispersion (thus the α_L=0.04 m) and maintaining high concentrations which produce higher density contrasts and larger vertical velocites.

Simulations 11a through 11d further examined the effect of varying the longitudinal dispersivity. Sensitivity of transport to transverse dispersivity was not tested. Tracer 3,4 DFBA was the only one that had a better fit for α_L=0.04 m. 2,6 DFBA, 3,5 DFBA, and o-TFMBA had better fits with α_L=0.10 m, while m-TFMBA, PFBA and Br had better fits with α_L=0.08 m. Best fits were determined by the smallest BTC error for the sum of individual well interval fits (see the discussion associated with Figure 4–35, below).

The relative recovery and BTC error, found from the vertical integration of the data, for these simulations is shown in Figure 4–34. The dashed lines indicate the minimum errors for purposes of comparison. There is very little difference in the model fits. Figure 4–35

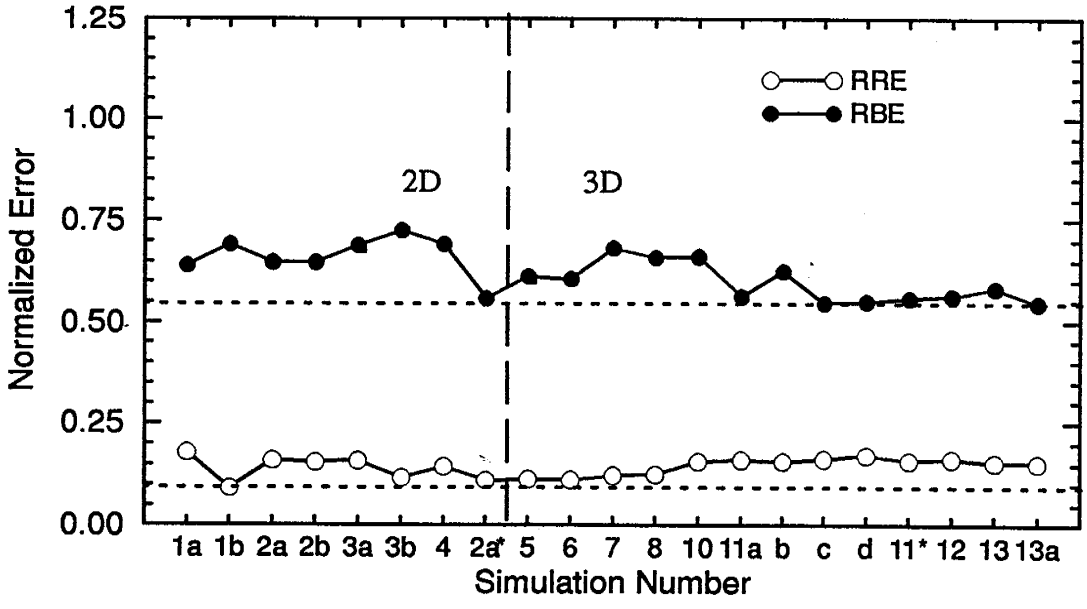

Figure 4–34. Normalized error for various vertically integrated 2D and 3D simulations.

shows the error determined from fitting recoveries and BTCs for the individual well intervals. The errors are larger than for the vertically integrated approach since breakthrough and recovery aren't averaged over all well intervals. The RBE is about 0.8 and the RRE is about 0.3. Both error values drop significantly in going from simulation 5 to 8, but then the error levels-off for the remainder of the simulations. That is, once the vertical heterogeneity is established at the 5 meter level, and buoyancy effects are applied, the error doesn't change much. Modifications in the model were primarily based on using the RBE as an objective function, while also keeping an eye on the RRE.

The relative error for each tracer individually is shown in Figure 4-36. The errors are roughly the same for all tracers. The sensitivity of 3,4 DFBA is evident as both the RRE and RBE fluctuate depending on the simulation.

It is worth noting that the values for hydraulic conductivity for simulation 10 were arrived at by trial and error, resulting from approximately 6 iterations of the 2-layer conduc-

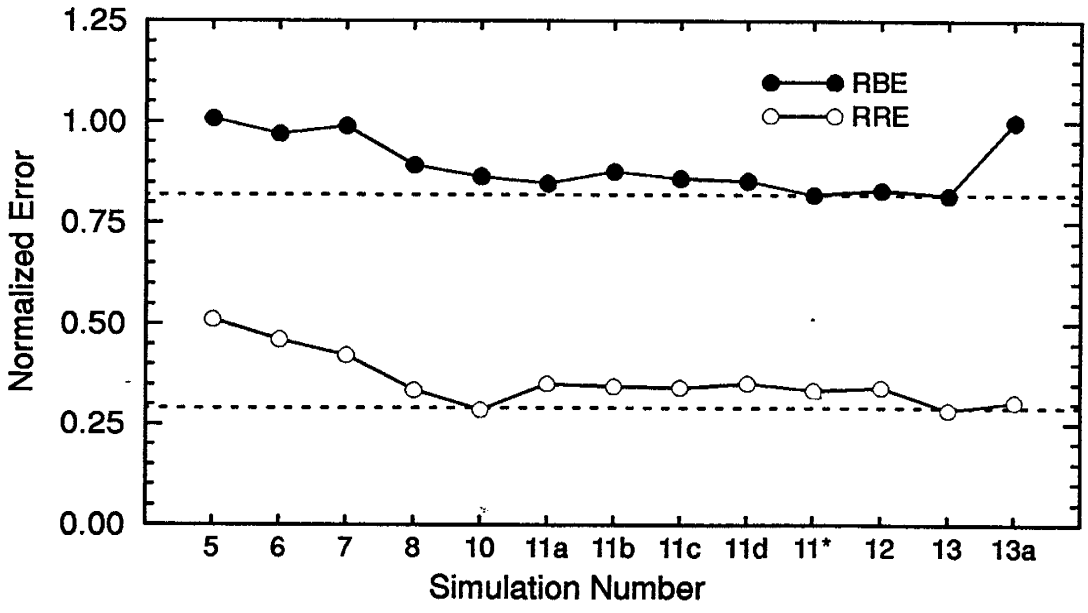

Figure 4-35. Relative recovery and BTC error for various 3D simulations. For each simulation, the errors were based on BTCs and recoveries for each well interval.

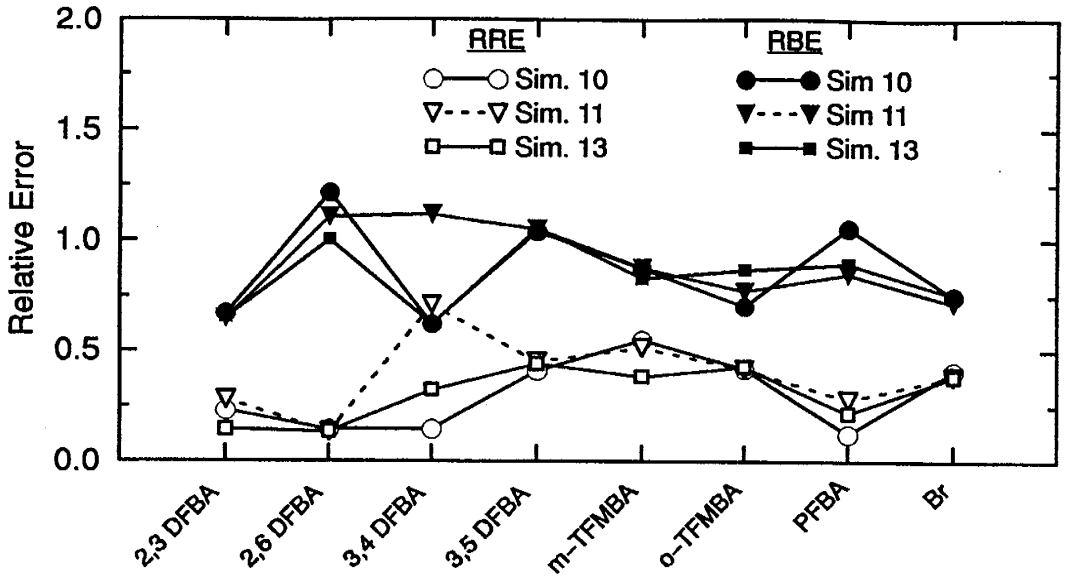

Figure 4–36. Relative error between experimental and 3 simulated breakthrough curves for the 8 tracers.

tivity field to obtain what was considered the best fit, presented here. In the end, not only were the magnitudes of hydraulic conductivity of the two layers important, but a careful balance between the two had to be achieved. If the upper values were too low, then the upper portion of the plume did not split off of the lower portion. If the lower K values were too low, then the lower layer impeded flow and too much water, and tracer, was drawn down from the upper zone.

In general, the hypothesis of vertical heterogeneity determined from the two–dimensional analysis is correct. The use of a retardation factor of 1.3 to obtain a close fit for two–dimensional breakthrough of 3,4 DFBA is not needed for the three–dimensional simulation. In the two–dimensional simulations, the retardation factor was used as a fitting parameter to account for three–dimensional effects and was not representative of a reversible sorption process as initially proposed. These results are encouraging since the tracers used in these experiments have been shown to not exhibit sorption in an aquifer with low organic–carbon content, such as the Borden aquifer.

Table 4–11 gives comparisons between estimates of vertical plume migration in the experiment, recreated here from Table 4–3, and vertical plume migration determined from simulation 13 results. Simulation results are presented as the total vertical movement, and the vertical flow due to buoyancy effects alone. The buoyancy term was calculated in the following manner. At pre-determined times during the simulation, the maximum downward vertical velocity due to density was calculated, based on the maximum density determined for the plume. This data can be plotted on a velocity versus time plot, shown in Figure 4–37 for three different simulations. This curve was then integrated to give the vertical movement of the plume due to density. The value for vertical movement determined in this way represents a maximum value since it was derived from maximum densities and velocities for the plume for each measurement time. Comparison of total simulated vertical flow to buoyancy induced vertical flow in Table 4–11 suggests that vertical buoyancy induced vertical flow accounts for approximately half of the total downward vertical flow. The remaining half of the vertical flow can be primarily attributed to a fully penetrating flux well located in a heter-

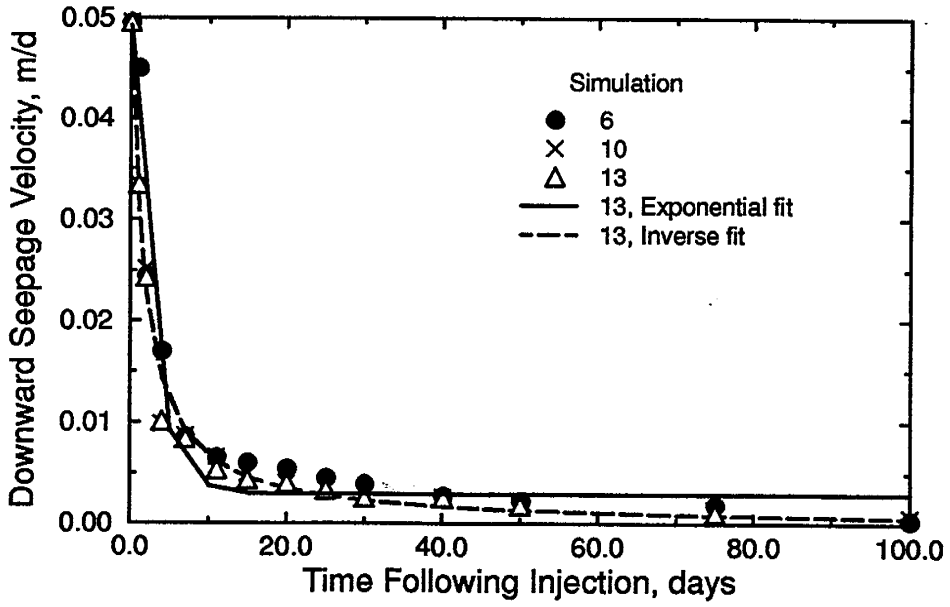

Figure 4–37. Downward seepage velocity as a function of time for simulated tracer injection at I15. Simulation numbers are in reference to Table 4–10. See text for explanation of different fits.

ogeneous aquifer with lower hydraulic conductivity at depth. Other contributing factors may include non–uniform pumping rates for each of the well intervals and vertical recharge at the water table. From Figure 4–37 it is apparent that the majority of the vertical movement attributed to density contrasts occurs within the first 10 days following injection.

Table 4–11. Estimation of vertical plume migration during Experiment 1; comparison of estimates from data and from simulations.

	Vertical Flow, meters Estimated from measured data.		Vertical Flow, meters Simulated	
Tracer	From P3	From P6	Total, m	Buoyancy Induced, m
2,3 DFBA	0.70	0.70	0.68	I5: 0.30 I8: 0.26
2,6 DFBA	0.50	0.68	0.64	I6: 0.34 I15: 0.29
3,4 DFBA	-	0.94	0.69	I10: 0.37
3,5 DFBA	0.86	0.52	0.60	I7: 0.25
m–TFMBA	0.88	0.54	0.73	I2: 0.26
o–TFMBA	0.68	0.25	0.25	I1: 0.08
PFBA	0.41	0.44	0.58	I4: 0.18 I9: 0.39 I12: 0.21
Br	0.70	0.91	0.50	I1: 0.08 I2: 0.26 I9: 0.39 I15: 0.34

A brief attempt at fitting a functional form to the simulated data in Figure 4–37 resulted in an exponential and an inverse function giving the two best fits. Of these, the inverse fit was surprisingly accurate. The exponential fit is given by

$$q_b = a_0 + a_1 * \exp(-ta_2) \qquad (4\text{–}3)$$

where q_b is the vertical seepage velocity resulting from buoyancy effects in meters per day, t is time in days, and a_0, a_1 and a_2 are fitting coefficients. For the fit shown in Figure 4–37, a_0=0.002924, a_1=0.046342 and a_2=2.5. The inverse fit is given by

$$q_b = b_0 + \frac{b_1}{(t+1)} + \frac{b_2}{(t+1)^2} \qquad (4\text{–}4)$$

where b_0, b_1 and b_2 are fitting coefficients. For the fit shown in Figure 4–37, b_0=–0.000178, b_1=0.078289 and b_2=–0.028156.

The values for total simulated vertical flow in Table 4–11 are similar to the values estimated from experimental results. The simulated value for 2,3 DFBA is essentially identical to the experimental values, while values for the other tracers are generally close. What is especially encouraging is that even if the experimental and simulated values don't coincide exactly, they appear to have the same trend. For instance, the experimentally derived values for o–TFMBA are at the smaller end of the scale, which is predicted by the model. The large vertical drop estimated from the experiment for 3,4 DFBA is not matched by an equally large value in the simulation. However, the simulated value for 3,4 DFBA is one of the larger of those values. The vertical movement calculated from density contrasts in the aquifer are listed by injection site for each tracer. They are roughly one–half, or less, of the total simulated vertical drop in most cases. For 2,3 DFBA, density flow accounts for about 0.44 of the total vertical migration. The largest buoyancy effect is seen for PFBA and Br^- injected at I9, which has 0.39 m of vertical flow. The smallest effect is for o–TFMBA injected at I1, 0.08 m, which was very close to the well and had small travel times. The difference between the total, simulated vertical flow and the buoyancy induced flow is attributed to the hydraulics of the system and the interaction of the pumping well with the layered aquifer.

Discussion.

The total tracer mass injected into the system was 963.9 g. The total tracer mass recovered was 515.3 g, or a relative recovery of 0.53. Roughly one–half of the injected mass was not captured by the well. The measured breakthrough and recovery data allowed for direct estimation of recoveries from individual injection sites. Had there been recovery from injection sites I3, I11, I13 and I14, the process of assigning recoveries may have been more

of a challenge. The lack of recovery for these 4 sites reflects the transient nature of the flow field, and the uncertainty associated with predicting the direction of flow, since some, or all, of these sites were intended to interact with the capture zone. However, in the design of the experiment, it was crucial that several sites be located outside the capture zone so that the boundary of the capture zone, using tracers, could be delineated. In this light, only one or two of the sites with zero recovery can be considered as not useful.

The relative recovery error, or RRE, for predicting recovery was determined to be about 0.10 of the mass recovered, or about 52. g in this case. An error of 10% is very reasonable. The relative breakthrough error, or RBE, was 0.50, or more, of the recovered mass, indicating the ability of the model to predict the mass recovered as a function of time is not as good. The difference between the two error terms is due to the insensitivity of simulated capture to model parameters for sites not on the capture zone boundary. The RBE is also related to the travel time of tracers recovered at the well, suggesting that prediction of time–dependent capture zones, or fronts, exhibits larger uncertainty than prediction of total mass recoveries.

Interpretations of pumping well breakthrough data for individual injection sites are shown in Figure 4–38. These interpretations, or estimations, are based on simulation results, and actual breakthrough data taken at the well and at the multilevel samplers. The low recovery of I10 is attributed to vertical plume splitting. Tracer injected at I6 was thought to be on the boundary of the capture zone and probably exhibited vertical and horizontal plume splitting. Recoveries for PFBA are uncertain since breakthrough was still occurring when the pump was shut down. Relative recovery of PFBA for I12 was listed as 0.96, but may have been 1.0 with continued pumping. Since I9 and I12 arrival times are similar, I9 may also be breaking–through near the end of the experiment, as suggested by the simulation results.

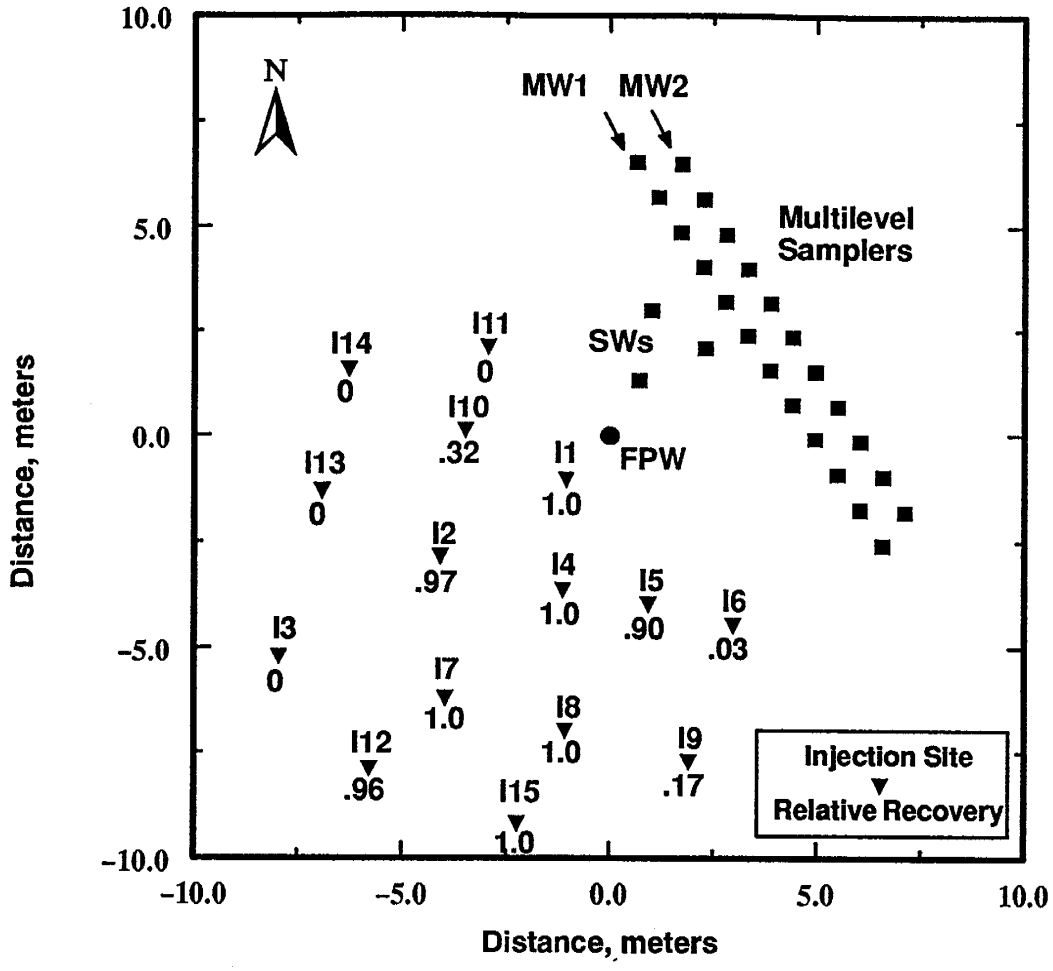

Figure 4–38. Capture zone map for the 15 injection sites in Experiment 1 as determined by comparison of model simulation results to measured data.

One of the most useful injection sites, in terms of deciphering the system, is I10. It is hypothesized that this site is on the capture zone boundary, or more precisely, it crosses the boundary vertically, and is essentially on the boundary laterally. From breakthrough of only the lower portion of the plume, we were able to deduce several important points regarding how the flow system works. First of all, the splitting of the plume vertically indicated that there was vertical nonuniformity of the flow field resulting from vertical heterogeneity of the hydraulic conductivity. The plume in the Waterloo–Stanford experiment was affected in a similar manner (Freyberg, 1986; see also Rajaram and Gelhar, 1991). Second, in using

the two-dimensional model, we determined that retardation may be important and needs to be considered when simulating the capture zone. This was contrary to what was known regarding sorption of the FBAs in aquifers similar to the Borden aquifer. The three-dimensional model strongly suggested that the sorption effect was due to the inability of the two-dimensional model to account for the vertical velocity components in the system. Third, in attempting to fit both the two-dimensional and three-dimensional model to tracer injected at I10, the sensitive nature of the model results to input parameters became evident. Clearly, for injection sites on the capture zone boundary, the uncertainty in predicting breakthrough and recovery for these sites is large. Finally, we can state in general terms that neither the flow system or the capture zone were two-dimensional as initially hypothesized. Vertical flow velocities resulted from pumping from a constant-flux well (instead of a constant-head well); heterogeneities in hydraulic conductivity; and density contrasts between the tracer plume and surrounding aquifer water. Vertical movement of the tracer plumes was in the range of 0.5 to 1.0 m, and was similar that seen by Sudicky et al. (1983) and Freyberg (1986).

Comparisons can be made of the capture zone experimentally determined for Experiment 1 to capture zones predicted using a simple model and three different sets of prior information. Figure 4-39 shows these three capture zones overlaid onto the capture zone map of Figure 4-38 determined for Experiment 1. The three capture zones based on prior data, which assume steady state conditions and do not include the effects of dispersion, were mapped using the backward approach typically used to mathematically delineate capture zones (Wilson and Linderfelt, 1991). Two of the data sets are from previous studies conducted in the sand pit at CFB Borden. The Stanford based capture zone uses the mean direction of plume migration as the mean direction of flow, taken from Mackay et al. (1986). The Barker based capture zone uses the mean direction of plume migration from an emplaced creosote source experiment conducted by Jim Barker and students at the University of Waterloo in 1991. The source location of the creosote was essentially the same location as the source of the Stanford experiment, and much of the same multilevel sampling structure

installed for the Stanford experiment was used by Barker. As is seen from Figure 4–39, the flow directions based on the two experiments are different and produce capture zones of different orientation. The third data set is based on the mean flow direction derived from gradient calculations using head measurements taken prior to the startup of Experiment 1, shown in Figure 3–3 and Figure 3–4. This capture zone is of different orientation then the other two, with the difference between adjacent capture zones being about 14°. Capture zones derived using the pre–experiment and Barker experiment data would give fairly reasonable results for the injection sites used in Experiment 1. The capture zone derived using the Stanford experiment data set, which is the oldest set of prior data, but also the most cited data

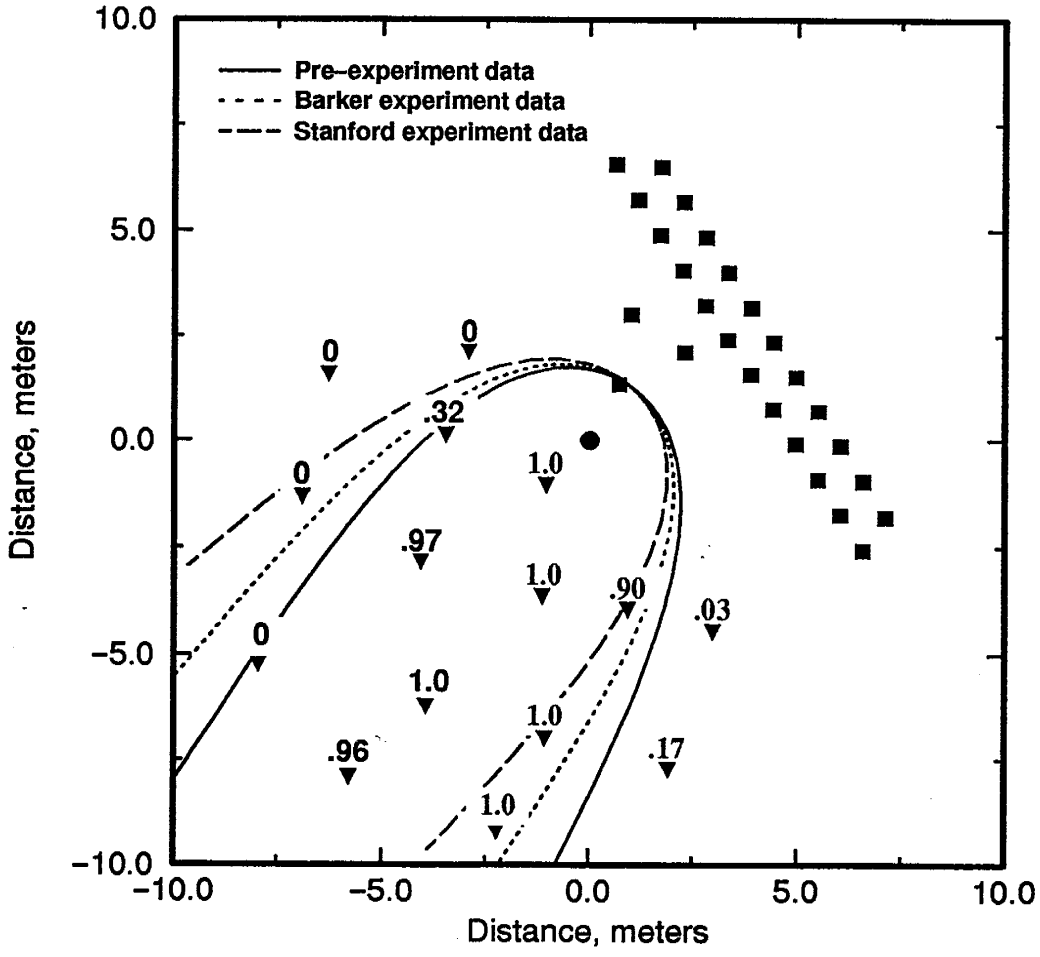

Figure 4–39. Comparison of Experiment 1 capture zone and steady–state capture zones based on three different sets of prior data.

set, would produce the largest error of the three steady-state capture zones. The relative recovery errors are 0.22, 0.22 and 0.60 for the pre-experiment, Barker experiment and Stanford experiment based capture zones, respectively. The errors for the pre-experiment and Barker data sets are reasonable, while the error for the Waterloo-Stanford data set is quite large.

The error in "predicting" the tracer mass recovered at the pumping well, using either the two- or three-dimensional transient transport models, was in the range of 0.10 to 0.15 for all simulations, regardless the data set used or the degree of calibration of the model. If it is assumed that this error represents the best model fit that can be achieved, then the error due solely to the predictive component of the simple model can be estimated by subtracting the best fit error of 0.10 (i.e. the lower of the 0.10 to 0.15 range) from the predictive model error. The error in the simple model due to prediction alone is then 0.12 (i.e. 0.22-0.10) for the pre-experiment and Barker data, and 0.50 for the Waterloo-Stanford data. The predictive model using the Barker or pre-experiment data gives a very reasonable result based on this approach, however, the predictive error associated with the Waterloo-Stanford data is still large.

The concept of a layered system was tested with the three-dimensional model, and was shown to be very effective in simulating flow and transport at the experimental site. There was noticeable improvement in the model error in going from the non-layered, or homogeneous, system to the layered system. No attempt was made to model lateral heterogeneities in the system. From previous studies at the site (Sudicky, 1986; Woodbury and Sudicky, 1991), it is clear that the system is not perfectly stratified. However, the horizontal correlation scale of 2.8 m (Sudicky, 1986) or larger (see Woodbury and Sudicky, 1991) is much larger than the vertical scale of 0.12 m (Sudicky, 1986), which supports the use of a layered model. Thorbjarnarson and Mackay (1994) used similar arguments in their analysis. As a comparison to the data they presented, and to Sudicky's data (Sudicky, 1986), estimates of hydraulic conductivity ratios were made from the results of the present experiment. The

estimates are based on peak arrival times for a given tracer at the different well depths. From Darcy's Law, travel time is inversely proportional to the hydraulic conductivity. In a linear system, the ratio of travel times provides an estimate of the ratio of hydraulic conductivities for two well intervals, and assumes the ratios of the gradients and the travel distances to be unity. The interval with which all other intervals were compared was P4, since this interval was expected to have complete breakthrough along the entire well interval vertically, and the breakthrough of 2,3 DFBA in P4 was a bimodal curve as expected from two injection sites (see Figure 4–1). Also, the vertically–integrated BTCs most resembled the BTC in P4 for most tracers. These criteria were based on the tracer 2,3 DFBA since it's recovery was very close to 1.0, and the travel paths to the extraction well for the two sites it was injected at were thought to be two of the most direct out of all the tracers.

The results of this exercise are shown in Figure 4–40 for six injection sites. These data are compared to the core data from the two transects studied in Sudicky (1986; unpublished data), and to the hydraulic conductivity ratios listed in Table 4 of Thorbjarnarson and Mackay (1994). The data for all studies are presented as depth below ground surface. The relative conductivities of the 2–3 m and 3–4 m intervals show a similar trend to both Sudicky's data and Thorbjarnarson and Mackay's data, which extend to a depth of 4 m. The data in Figure 4–40 also show a slight increase in hydraulic conductivity in the 4–5 m interval, with values in the 5–6 m interval similar to those in the 3–4 m interval for most sites. The vertical variation in relative hydraulic conductivity is similar, but not identical, for all injection sites. The ratios for I7, I4 and I12 show the largest vertical variability in hydraulic conductivity, and they also resemble each other closely. The ratios for I2 and I5 show very minor stratification. From comparison of Figure 2–9 and Figure 4–40, there is no obvious connection between the location of the injection site and vertical variability of hydraulic conductivity. This is reasonable since the minimum distance between injection sites is about 2 m, which is approaching the horizontal correlation scale of 2.8 m. Also, flow paths are generally larger than the correlation scale, but not large enough to provide a reasonable average

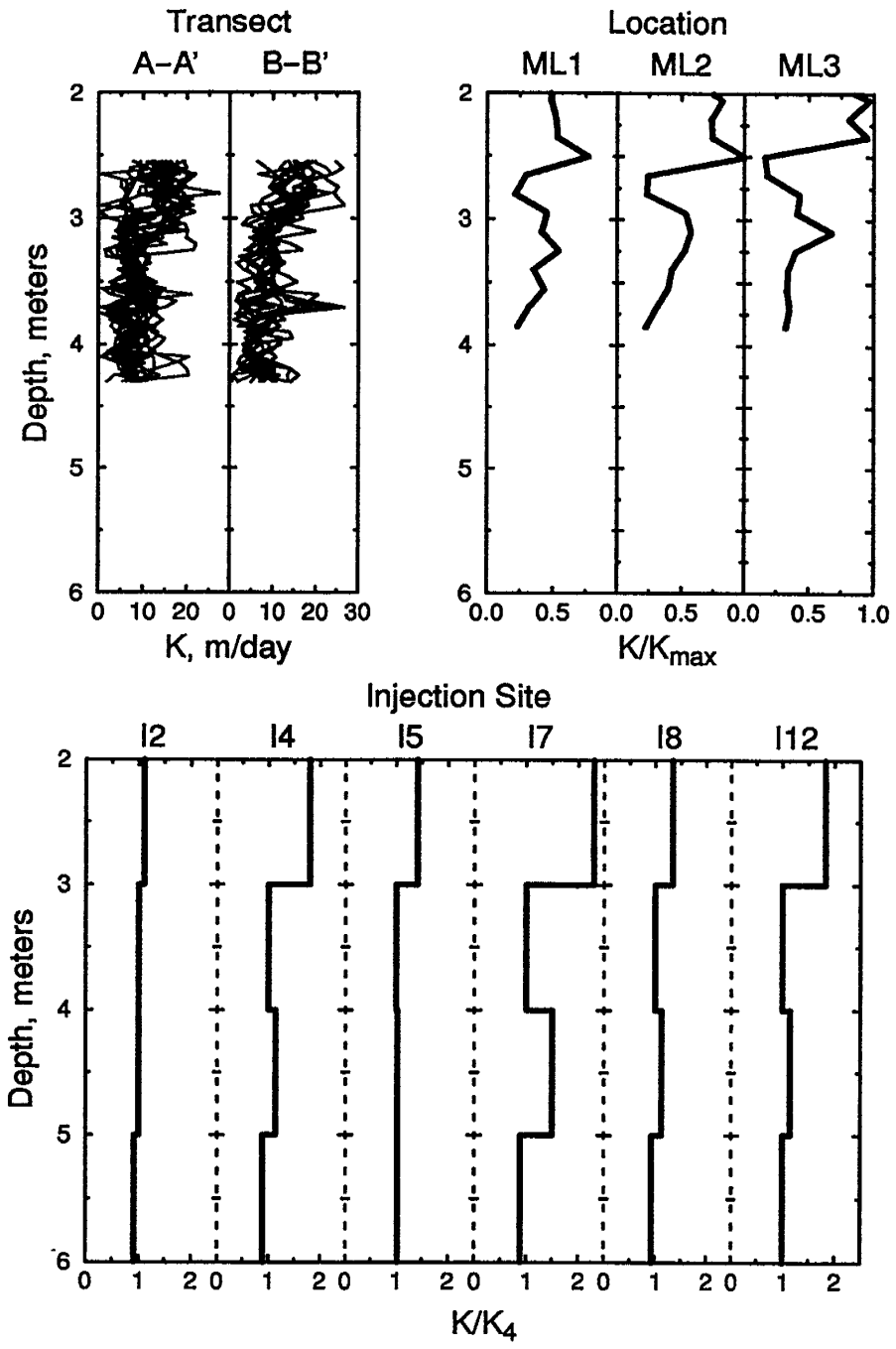

Figure 4–40. Comparison of hydraulic conductivity data from Sudicky (1986) (upper left), Thorbjarnarson and Mackay (1994b) (upper right), and this study (lower).

of the underlying structure of the aquifer such that paths for tracer injected at different sites could sample a significantly different portion of the conductivity field. The comparisons presented in this analysis must also be tempered by the fact that the actual travel paths will

vary for tracer at different levels in the aquifer due to the dimensions of the capture zone being dependent on the values of hydraulic conductivity.

The data from Sudicky (1986) and Thorbjarnarson and Mackay (1994) are valuable in evaluating the configuration of the hydraulic conductivity field. It is this data that was primarily used in determining conductivities for the 9–layer system used in simulations 13 and 13a, shown in Table 4–10. Lateral changes in conductivity would expected to be gradual over the scale of the experiment, making the use of stochastic parameters in generating the hydraulic conductivity field questionable, except when site specific data was available for conditioning of the conductivity field. However, a stochastic approach may be a useful exercise in a future analysis, since the data used for estimation of stochastic parameters (Sudicky, 1986) was collected at the site of the two experiments conducted in this study.

In terms of dispersivities used in the model, the macrodispersivities determined from analysis of Sudicky's data (Sudicky, 1986; see Section II) are not applicable to the smaller transport distances in this study. The value of 0.08 m for longitudinal dispersivity initially used in the modeling of Experiment 1 were in the range of values estimated by Sudicky et al. (1983) which were determined from 11 m of plume migration. The value of 0.001 m for the horizontal transverse dispersivity was determined after consulting a variety of sources in the literature. It has been proposed that both the vertical and horizontal transverse dispersivities are on the order of the molecular diffusion coefficient. Data from Sudicky et al. (1983), Freyberg (1986) and Sudicky (1986) confirm that the vertical transverse dispersivity is probably this small, but the horizontal transverse dispersivity has been estimated from the data to be larger, ranging from 0.0022 to 0.05 m. That the values of the horizontal transverse dispersivity are higher than the molecular diffusion coefficient is thought to reflect the inability of current models to account for time–varying velocities in the aquifer. The value of 0.0022 m is actually an estimate of the vertical macrodispersivity based on the model of Rajaram and Gelhar (1991), and it is considered to be twice the molecular diffusion coefficient and is representative of a local dispersivity. Sudicky et al. (1983) estimated the horizontal

transverse dispersivity at 0.005 after 0.75 m of plume migration at a site near the sand pit. The value of 0.001 m was used initially since it was at the lower range for a local dispersivity value and at the upper range for molecular diffusion, and with the model incorporating transients in the flow field, it was thought this value was a good place to start. The calibration fit of the two-dimensional model chose α_T=0.005 m. Both the two- and three-dimensional model were the most sensitive first to the value of hydraulic conductivity, then longitudinal dispersivity, and finally the transverse dispersivity. Time-dependent dispersivities were also tested in the two-dimensional model for various tracers, based on results on Freyberg (1986) and Thorbjarnarson and Mackay (1994). In all cases, constant values provided superior fits. Testing of a best-fit for the transverse dispersivity was not conducted for the three-dimensional model since the magnitude of the error associated with this term was considered small and expensive to determine.

V. RESULTS AND INTERPRETATION: SECOND EXPERIMENT

Pumping for the second, partially penetrating pumping well experiment was initiated on December 15, 1992. Pumping took place from the variable saturated thickness of the upper 3 meters of the aquifer. Tracer injections took place between December 17 and 28, 1992. The pumping rate was maintained at 1.0 L/min until April 15, 1993, at which time it was increased to 1.25 L/min, in order to increase the size of the capture zone. The desired design pumping rate was 1.5 L/min, but with only two lines withdrawing water from the well, resistance to fluid flow was too great and the maximum, reliable rate achievable was 1.25 L/min. The pumping rate was maintained at 1.25 L/min until July 7, 1993, at which time the pump and all experimental installations were shut down. Daily average pumping rates for Experiment 2 are shown in Figure 2–8.

Tracer Breakthrough and Recovery Analysis

In Experiment 2, only one tracer was injected within each injection interval, giving a total of 8 available tracers. The injection scheme was more complicated than that for the first experiment, with some sites having different tracers injected at different depths. The purpose of injecting more than one tracer at a site, at different depth intervals, was to help gain an understanding of the vertical flow components present during the experiment, caused by partial penetration of the pumping well or aquifer heterogeneity. The breakthrough curves for all 8 tracers for each well interval, P2 and P3, are shown in Figure 5–1. The breakthrough data can also be presented as if there were no vertical partitioning of the well, and mixing took place over the 2 m length of the well. This is accomplished by vertically integrating the data from the two well intervals, and is referred to as the vertically–integrated data for Experiment 2. None of the other sources of data represent a vertical average, unless otherwise noted. The vertically–integrated BTCs are shown in figures accompanying the write–up of each tracer which follows. The time scale reference in the following analysis is for Julian Date, 1993, with January 1, 1993 representing t=1 d, and negative times referring

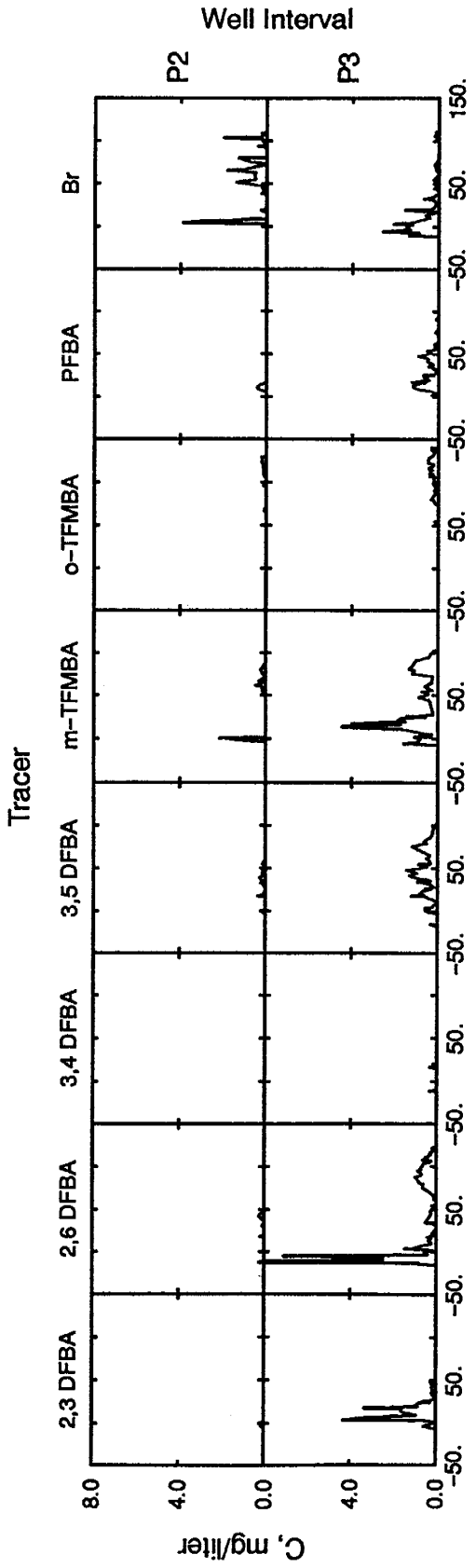

Figure 5-1. Experimental breakthrough curves for the extraction well intervals P2 and P3 for the 8 tracers used in Experiment 2.

to dates in 1992. As in Experiment 1, the breakthrough curve at the well was integrated to find the total mass recovered for each tracer. Masses for all time intervals were summed to give total mass recovered for each well interval, r_j:

$$r_j = \sum_{k}^{K} c_k \forall_k \ , \tag{5-1}$$

where K is the number of time intervals, c_k is the daily concentration for time k and $\forall_k$ is the volume pumped for the kth day. Tracer recoveries for each well interval, r_j, were summed to give total mass recovered for the ith tracer, R_i:

$$R_i = \sum_{j}^{J} r_j \ , \qquad i=1,2...,8 \tag{5-2}$$

where J, the number of well intervals, is equal to 2. Table 5–1 gives the mass released, the total mass recovered, R, and the relative recoveries (total mass recovered/mass injected for each tracer) for the 8 tracers. Figure 5–2 shows the normalized cumulative mass recoveries for the 8 tracers. From Figure 5–2, all tracers have completed breakthrough at the well except for o–TFMBA, since the slope of the curve is slightly greater than zero in the figure. Recovery for most tracers is complete within 150 d of starting the experiment. Also, most

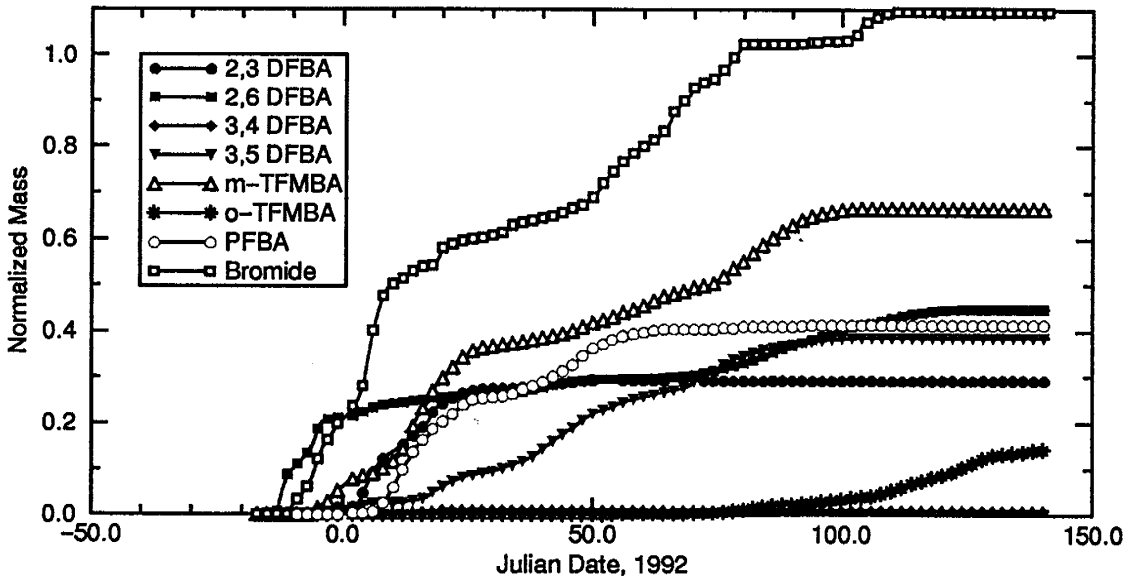

Figure 5–2. Normalized cumulative mass recoveries for the 8 tracers used in Experiment 2.

of the tracer breakthrough was complete when the pumping rate was increased from 1.0 L/min to 1.25 L/min, at t=105 d. The only tracers that are possibly affected by the increased pumping rate is Br^-, which shows a small but sudden increase in the mass recovered starting at about t=105 d, and o-TFMBA which is still arriving at the well at the time the pumping rate was increased.

Table 5-1. Mass released, mass recovered, and relative recovery for each tracer. Injection masses account for 97% purity to allow for direct comparison to mass recovered.

Tracer	Mass Injected, gm	Mass Recovered R, gm	Relative Recovery, Recovered/Injected
2,3 DFBA	117.3	34.4	0.29
2,6 DFBA	156.4	70.2	0.45
3,4 DFBA	97.7	0.9	0.01
3,5 DFBA	117.3	45.4	0.39
m-TFMBA	117.1	78.0	0.67
o-TFMBA	117.1	17.0	0.15
PFBA	97.5	24.3	0.25
KBr	39.6	41.6	1.05

The fraction of total mass recovered to that injected for each well interval is given in Figure 5-3. Recall that injections were at the 2 to 5 meter depth, with the following exceptions; 3,4 DFBA was injected from 5-7 m in I3 and I14 and from 3-4 m in I13; 2,6 DFBA was injected from 2-4 m in I12; PFBA was injected from 2-3 m and 4-5 m in I13; Br- was injected from 2-4 m in I3 and at the water table in I14 (see Table 3-3 and Figure 2-10). Except for Br^-, the majority of tracer recovered was in P3, the lower of the two pumping well intervals. The well was designed to pump at the same rate from both intervals. Anticipating significant accelerating flow upward toward the pumping intervals led us to believe that the lower interval capture zone would extend well below the 3 meter depth, and the upper interval would extend below its lowest level of 2 meters. Thus we expected significant tracer recovery in the upper interval. There are several hypotheses which help to explain why recoveries in P2, the upper interval, were lower than expected. First, our initial estimate, which depended on the estimated value of the aquifer conductivity, and conductivity anisotropy ra-

tio, and assumed a uniformly distributed pumping rate along the length of the well, may have been inaccurate. The more recent simulation results, presented later in this section, suggest that we should expect the majority of tracer breakthrough in the lower interval. Second, the initial density contrast between the plume and background water caused the plume to sink, perhaps causing the plume to migrate below the capture zone for the upper well interval. Third, during periods of vertical recharge, the lower boundary of the capture zone for the upper well interval would be relatively higher in the aquifer. Finally, there was bacterial clogging of the 1/4" tubing coming from the upper pumping interval, especially following the spring thaw which began at approximately Julian Date 100, 1993. This could have reduced the contribution of water pumped by the upper interval relative to the overall pumpage, and as the upper interval flow rate dropped off, flow from the lower interval would have increased to make up the difference. This possibility was only indirectly monitored by the visual flow indicators. One, or a combination, of these effects may have been responsible for the low recoveries seen in P2. The high Br^- recovery in P2, roughly half the total recovery, resulted from Br^- injection at the surface of the aquifer at site I14 (see Figure 5-3).

Finally, with a fully-penetrating well, the capture zone has two-dimensional properties in that it extends from the water table to the lower, impermeable boundary of the aquifer, as was the situation in Experiment 1. The lateral boundaries of the capture zone are more or less vertical with the lower boundary of the capture zone coinciding with the bottom of the aquifer. For a partially penetrating well in the upper region of the aquifer, which is the situation for Experiment 2 discussed here, the capture zone will not necessarily intersect the bottom of the aquifer, depending on the pumping rate and aquifer properties. For the simple case of a homogeneous aquifer, the shape of the capture zone in cross-section (perpendicular to the direction of ambient flow) will be approximately elliptical (i.e. for one-half of an ellipse, see Wilson and Linderfelt, 1991). Now the lower boundary of the capture zone and the lower aquifer boundary do not coincide. It is important that the distinction be made between the 'lateral' capture zone boundary, and the 'lower' capture zone boundary or 'bot-

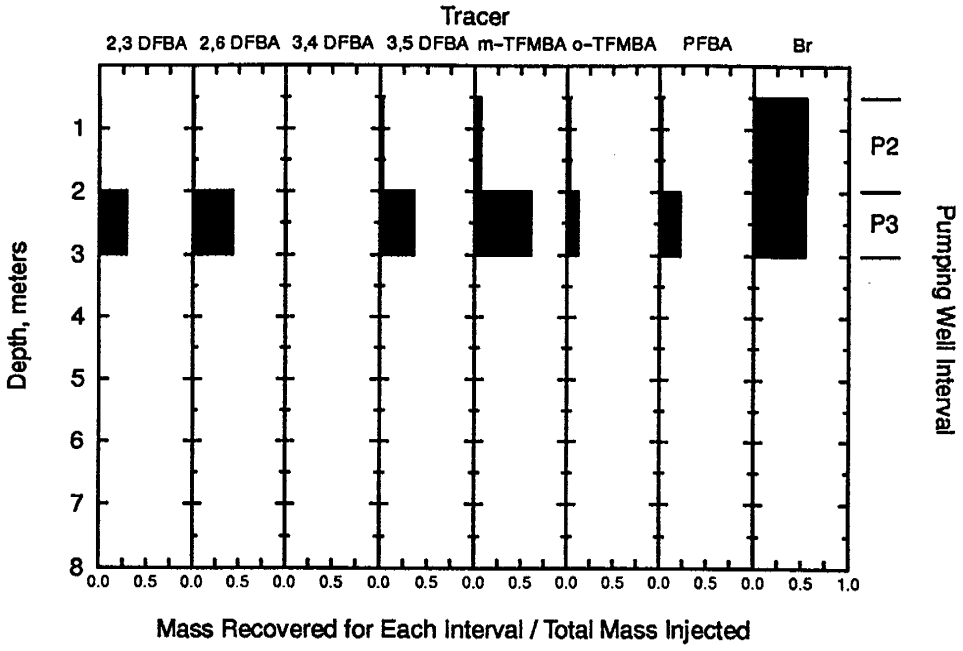

Figure 5–3. Vertical profile of mass recoveries for the 8 tracers used in Experiment 2.

tom' of the capture zone, since they grade into each other. Along the bottom of the capture zone, the slope is zero, along the sides the slope approaches infinity, and there will be a point along the curve where the slope is 45 degrees. In the discussion which follows, the lower boundary of the capture zone refers to that part where the slope is zero or close to zero, the lateral boundary is the part of the boundary where the slope is becoming large and approaches infinity. Clearly, there will be some instances when this distinction cannot be made and further descriptions will be necessary. In addition, the boundary is not a sharp, well defined feature but instead is fuzzy due to the effects of dispersion and the fluctuating flow field.

2,3 DFBA

Figure 5–4 shows the vertically–integrated, measured BTC for 2,3 DFBA. There is relatively small recovery in the top interval as compared to the lower interval. 2,3 DFBA was injected at sites I9 and I10 (see Figure 2–10). Based on the direction of ambient flow

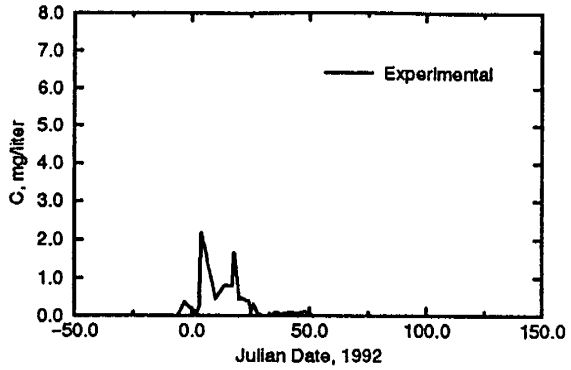

Figure 5–4. Experimental, vertically–integrated BTC for 2,3 DFBA for Experiment 2.

for Experiment 2, which changes from about N10E to N40E over the duration of the experiment (see Figure 3–4), it is likely that tracer injected at I9 is not captured by the well. This conjecture is supported by Figure 5–4, which shows one main breakthrough sequence, and Figure 5–2, which also shows only one mass recovery sequence. If all of the recovered 2,3 DFBA is attributed to I10, then the relative recovery for I10 is 34.4/58.6 (mass recovered/ mass injected), or 0.59, just under two–thirds of the injected mass for that site. In the design of Experiment 2, it was estimated that the maximum depth of the capture zone was between 5.0 m and 5.5 m below ground surface for a homogeneous, anisotropic aquifer. For a heterogeneous aquifer these results would be modified somewhat. If the plume dropped approximately 0.3 m due to density contrasts between the plume and surrounding aquifer water, based on vertical well recovery data from Experiment 1 (see Figure 4–3, Table 4–3 and Table 4–11), then it seems reasonable that about one–third of the injected mass would end up below the bottom of the capture zone. This effect may be enhanced by I10 being located fairly close to, and off to one side of, the well. Near the well, the capture zone is not as deep (Wilson and Linderfelt, 1991) as the flow is accelerating up into the well. This may have allowed some of the tracer to be injected outside the capture zone, or to migrate out of the capture zone by density effects or dispersion. It is also possible that the plume originating at I10 split vertically in the same way as described in Experiment 1 (see discussion of *3,4*

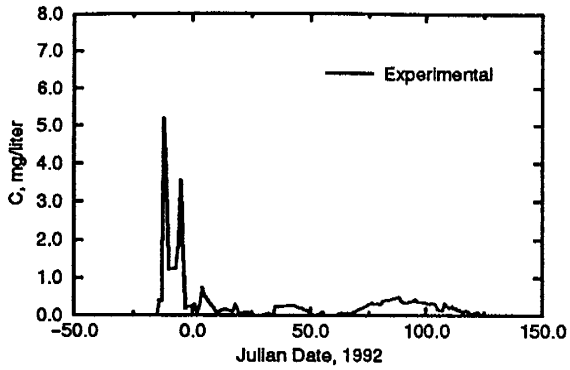

Figure 5-5. Experimental, vertically-integrated BTC for 2,6 DFBA for Experiment 2.

DFBA, Section IV) due to relatively higher hydraulic conductivity in the upper portion of the aquifer. However, with the direction of flow shifting from N10E to N40E during the experiment, it is expected that lateral splitting was not an issue in this case. Estimated relative recoveries: I9: 0.0; I10: 0.59.

2,6 DFBA

Vertically-integrated well breakthrough for 2,6 DFBA is shown in Figure 5-5. Injection sites for 2,6 DFBA were I1 (58.7 g), I11 (58.6 g), and I12 (39.1 g). Based on gradient direction data, it is assumed that I11 was not captured at the well. If all recovered mass is attributed to injection at I1 and I12, the total injection mass is 97.8 g and relative recovery for these two sites is 70.2/97.8 = 0.72. Due to the nature of the capture zone near the well, which begins to curve upward toward the stagnation point in the zone beneath the well (Wilson and Linderfelt, 1991), complete recovery of tracer injected at I1 is not a certainty since some of the tracer may have been lost at the bottom of the capture zone. Both Figure 5-2 and Figure 5-5 show that there is more than one breakthrough period. In Figure 5-2, the normalized cumulative mass curve for 2,6 DFBA begins to level off at about 25 d, and reaches a plateau of roughly 0.3 at around 50 d. If we take this as the maximum mass recovered for I1, then 46.9 g were recovered from I1, for a relative recovery of 0.8 for that injection

site. This leaves 23.5 g of mass recovered from I12, or a relative recovery of 0.6. Estimated relative recovery: I1: 0.8; I11: 0.0; I12: 0.6.

We can estimate the lower boundary of the capture zone, based on the relative recoveries for I1 and I12. Tracer injected at both sites was injected from 2–5 m below ground surface. If it is assumed that the mass that wasn't recovered was lost at the bottom of the capture zone, then about 0.6 m of the bottom part of the plume was split off in both cases. If there was no vertical flow due to density contrasts between the plume and the aquifer water, then the lower boundary of the capture zone could be positioned at about 4.4 m below ground surface. However, buoyancy effects are known to cause the plume to move vertically downward. In Table 4–11, estimates of buoyancy–induced vertical flow for site I1 in Experiment 1, based on simulation, was approximately 0.08 m. This would place the lower capture zone boundary at about the 4.5 m depth. This can be compared to the model used to design the experiment, which estimated the maximum capture zone depth at around 5.0–5.5 m for a homogeneous, anisotropic (horizontal–to–vertical anisotropy) aquifer. As a further comparison, it was noted that there wasn't any leachate in the pumpage during the first part of the experiment, when the pumping rate was 1.0 L/min, indicating that the lower capture zone boundary was within the 5–6 m interval, determined in Experiment 1 (see Section IV). The estimate of 4.5 m would place the lower capture zone boundary higher than estimated using other means, yet the heterogeneous nature of the aquifer may act to flatten–out the capture zone, thereby decreasing its maximum depth. It may also be that the capture zone is not as deep in the vicinity of I1 as suggested above for 2,3 DFBA (see also Wilson and Linderfelt, 1991).

Using similar reasoning, the depth of the lower capture zone boundary at I12 can be estimated. Since the direction of flow from I12 is in favor of complete capture of tracer injected at I12 (as flow changes from north towards the northeast, I12 ends up in the center of the capture zone laterally), the mass loss can be safely attributed to plume splitting at the lower capture zone boundary. For this site, tracer was injected from 2–4 m below ground

surface. Without any flow due to density contrasts, the lower boundary of the capture zone would be located at about 3.1 m depth. With buoyancy effects, the boundary is lowered since the plume will have migrated downward across the boundary. If the plume dropped 0.5 m, then the boundary would be at 3.6 m down. This is still higher-up in the aquifer than the 4.5 m depth estimated above, but the 4.5 m was considered an estimate of the maximum capture zone depth. The capture zone shape is concave up (i.e. an elliptical shape), and the tracer from I12 was off to one side of the longitudinal axis of the capture zone when it was injected (towards the lateral boundary), and for a short time thereafter until the flow direction changed. Based on this, a lower capture zone boundary depth of 3.6 m may be reasonable.

3,4 DFBA

Injection sites for 3,4 DFBA were I3 (5–7 m depth), I13 (3–4 m depth), and I14 (5–7 m depth). For these sites, 3,4 DFBA was used to help determine the vertical extent of the capture zone. Vertically-integrated breakthrough for 3,4 DFBA is shown in Figure 5–6. Breakthrough for individual well intervals is shown in Figure 5–1. A small amount of tracer was captured early, at about t=–15 d, in the lower well interval, P3. It is followed by a second small pulse of tracer 25 days later. Only 0.9 g of tracer was recovered for both well intervals. Based on gradient-direction data, and the relative location of the injection sites with respect to the pumping well, it is assumed that tracer injected at I13 was not captured at the well.

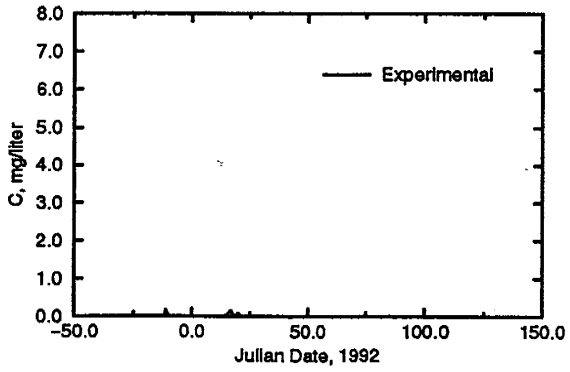

Figure 5–6. Experimental, vertically-integrated BTC for 3,4 DFBA for Experiment 2.

The early arrival is most likely an error in the analysis, or possibly a contaminated sample, since the breakthrough date and the injection date are the same. The second small arrival could be from I3 for tracer traveling on a more or less direct path to the well. It could also be from I3 for tracer from the upper part of the plume traveling beneath, and essentially past the well, then circulating upward and back into the well. The path lines leading to the well from the lower part of the capture zone would follow such a circuitous route to the well (Wilson and Linderfelt, 1991). The strongest evidence that the breakthrough for 3,4 DFBA is from I3 comes from injection at I14. Br^- was injected in the upper portion of the aquifer and 3,4 DFBA in the lower portion. The Br^- plume from I14 has arrival times of about 45 d (see Figure 5-1, the second breakthrough in P2 for Br^-). The 3,4 DFBA injected at I14 would be expected to take longer since it would take a similar path as just described for 3,4 DFBA injected at I3. The arrival time for 3,4 DFBA in Figure 5-6 is at about 15-20 d (for the second breakthrough) which is much earlier than 45 d. Based on this, it is determined that 3,4 DFBA injected at I3 had a relative recovery of 0.02, and I14 had a relative recovery of 0.0.

Estimated relative recoveries: I3: 0.02, I13: 0.0, I14: 0.0.

3,5 DFBA

Breakthrough for 3,5 DFBA is shown in Figure 5-7, resulting from injection at sites I5 and I7 (both 58.6 g). The observed breakthrough sequence does not show two distinct

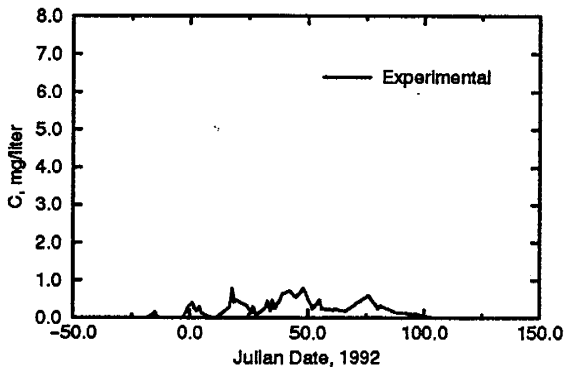

Figure 5-7. Experimental, vertically-integrated BTC for 3,5 DFBA for Experiment 2.

peaks, but instead breakthrough occurs over a broad time period with several small peaks. Recovery was 45.4 g, or 0.39 of the total mass injected, indicating that one or both tracer masses had partial recovery at the pumping well. It is possible that the first two or three peaks are from I5, while that last breakthrough is from I7, but is is difficult to differentiate contributions from each injection site from either Figure 5–7 or Figure 5–2. It also possible that plume splitting was both vertical and lateral, resulting from the heterogeneous nature of the hydraulic conductivity field, the fluctuating flow field, and the added complexity of the partially penetrating well. It was revealed (by simulation) for Experiment 1, that for higher hydraulic conductivity in the upper portion of the aquifer, tracer injected at I5 was beginning to migrate outside the capture zone in the upper part of the plume (I5 was in the same location for Experiments 1 and 2). For Experiment 2, the changing flow direction, from N10E to N40E, would enhance this effect. Site I7 is in very favorable location for capture by the well. If the recovered mass was assigned completely to injection at I7, a relative recovery of 0.77 would result, which is a slightly higher recovery than for estimated recovery of nearby injection sites (see discussion on *2,6 DFBA*, *m-TFMBA* and *PFBA*). However, the estimated relative recovery of 0.6 for nearby I12 reflected the injection from 2–4 m only, whereas the injection interval of I7 was from 2–5 m. In addition, if all the mass recovered were assigned to I7, then recovery at I5 would be zero. Recovery from I14, which is close to I5, was estimated at 1.0, but tracer at I14 was injected at the water table such that well capture was highly probable. Since recovery from I6 was estimated at zero, tracer injected at I5 may be in a vertically thinner, lateral part of the capture zone. Going back to I12, if it is assumed that the mass that was lost was from the lower part of the plume, then a recovery of 0.41 results if the tracer were injected in the 4–5 m interval as well. With I7 closer to the well, the expected recovery may be higher. From these considerations, a rough approximation of the individual recoveries for I5 and I7 can be made. If two–thirds of the mass recovered is assigned to I7 and one–third to I5, the relative recoveries become 0.52 and 0.26, respectively. This is a reasonable division when considering estimated recoveries for the other tracers, except for m–TFMBA

at I8 (see *m-TFMBA*, below). Estimated relative recovery for I8 is 0.63, with tracer injected from 2–5 m. This would require an adjustment of recoveries, with I5's recovery being lowered and I7's being increased. If relative recovery for I7 is increased to 0.65, for instance, then relative recovery at I5 is reduced to 0.12. This may still be reasonable, since as the capture zone rotates in a clockwise direction, portions of tracer from I5 may split laterally from the plume. Estimated relative recovery: I5: 0.12, I7: 0.65.

It may be that there are other important factors which have not yet been considered. So far only a layered system has been discussed. Even though the horizontal correlation length, λ=2.8 m, is relatively large compared to the scale of the experiment, (see Section II), it may be entirely possible that there is a heterogeneity which is influencing flow in the lateral direction, as first proposed in the analysis of Experiment 1 (see Section IV). This hypothesis is supported by Figure 6 of Sudicky (1986) which shows lenses of low conductivity zones in the 10–19 m region of the A–A' transect (see also Figure 4–33). This would correspond to the region running from about 1 m south of the pumping well (roughly the location of the 10 m location of Sudicky's Figure 6) towards the northeast. If the horizontal extent of the lenses is governed by the same statistical parameters as determined from the two transects as a whole, then the region of the aquifer between I3, I11, SW1 and MW1 may exhibit lower hydraulic conductivity causing flow to circumvent this region either laterally or vertically. In the first experiment, this concept was used to help explain why simulated recoveries for sites I6 and I9 were lower than what was estimated. Also, in the first experiment gradient direction was changing from the northeast to the north, causing the plume to flow to the left of this region, and towards the well. During Experiment 2, the opposite would be true since the gradient direction is shifting from the north to the northeast. These arguments support the estimates made above for relative recoveries I5 and I7, as well as account for the high simulated recoveries from I5.

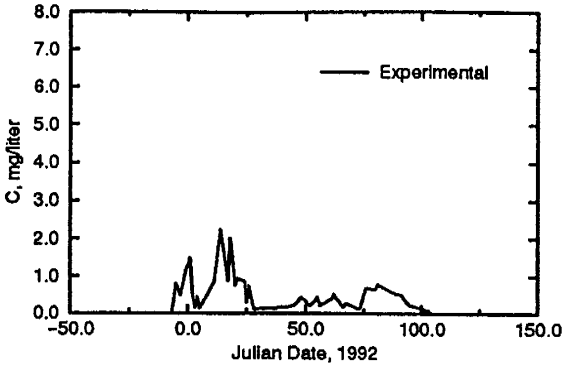

Figure 5-8. Experimental, vertically-integrated BTC for m-TFMBA for Experiment 2.

m-TFMBA

Injection sites for m-TFMBA were I4 and I8 (both with about 58.5 g). The vertically integrated BTC, shown in Figure 5-8, reflects these two separate injections. Breakthrough in P2, shown in Figure 5-1, has two distinct and separate breakthrough sequences, while P3 shows overlap of the two tracer plumes as they breakthrough at the well. The smaller concentrations seen in P3, at 40-60 d, may be due to the vertical splitting of the plume originating from I8, resulting from higher hydraulic conductivity in the upper portion of the aquifer, as was seen in Experiment 1 (see details for *PFBA* in Section IV, Three-dimensional Analysis). Total mass recovered for m-TFMBA was 78.0 g, or 0.67 of that injected, indicating that one or both of the tracer plumes were partially recovered, or that one of the plumes was entirely recovered while the other was partially recovered. In Figure 5-3, there is a strong breakthrough up until about 25 d, then the slope of the cumulative mass recovery curve lessens. Since the breakthrough profile for I4 is well defined in Figure 5-8, it may be that breakthrough from I4 is over by about 20 or 25 d when the break in slope occurs. This would give a relative recovery for I4 of about 0.70, and a relative recovery for I8 of about 0.63. The location of site I4 with respect to the well would suggest that relative recovery should be about 1.0, but portions of the injected tracer may have been injected below the capture zone boundary. Also, because of buoyancy effects, the plume most likely migrated downward

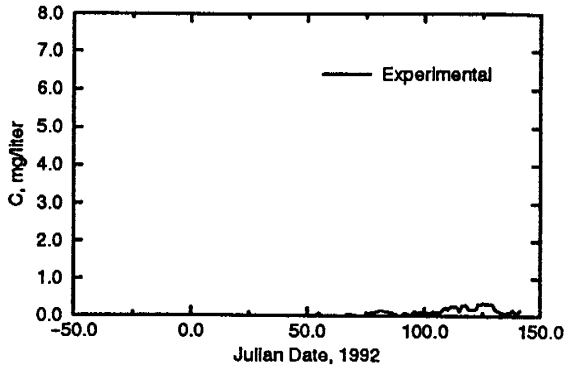

Figure 5-9. Experimental, vertically-integrated BTC for o-TFMBA for Experiment 2.

across the lower boundary of the capture zone as well. From the estimated relative recoveries of 0.70 and 0.63 for I4 and I8, respectively, it is estimated that approximately the lower 1 m of each plume was not captured. Again, if vertical flow due to density contrasts is estimated at about 0.3-0.4 m, then the lower capture zone boundary can be roughly placed at 4.5 m depth. This coincides well with other estimates for the depth of the lower capture zone boundary (given in discussions for the other tracers). Estimated relative recovery: I4: 0.70, I8: 0.63.

o-TFMBA

The vertically-integrated breakthrough curve for o-TFMBA is shown in Figure 5-9. Injection sites for o-TFMBA were I6 and I15 (both with 58.5 g injected). The mass recovered was 17.0 g, or 0.15 of the injected mass. It is difficult to assign the recovered mass to either site I6 or I15. Site I15 is roughly as far from the well as is site I12. Tracer injected at I12 (2,6 DFBA) shows breakthrough at roughly the same time (see discussion of *2,6 DFBA*, above). Also, relative recovery was estimated at 0.63 for tracer injected at I8 (see the discussion of *m-TFMBA*, above). From comparison of estimated recoveries from I8 and I12, it seems that tracer from I15 should have also been recovered. However, as the gradient direction changes towards the northeast, it is possible that the plume from I15 was not captured at all, instead migrated towards the northeast and away from the well. There

is breakthrough of o-TFMBA at the multilevel sampling fence, at sampler MW1-6 at the 3.5 m depth, for t=96 and 100 d (Julian Date, 1993). This is 111 d after injection at I6, and 104 d after injection at I15. It seems reasonable that the tracer at I6 migrated towards the north at first, and was along or near the capture zone boundary at this time. Then, as the gradient direction changed to the northeast, the plume split with some being capture by the well and some migrating towards the fence. Since the other two fence depths sampled, the 5 and 6 m depths, didn't show any breakthrough of o-TFMBA, the plume most likely split vertically, in a similar manner to 2,6 DFBA and PFBA in the first experiment. It is interesting to note that the plume appears to be less than 2 m wide as it crosses the fence, indicating that it may not be easily detected at the sampling fences, especially for flow perpendicular to the fence. As of this time, it is not clear what relative recoveries should be assigned to each injection site, so recovery will be split equally between the two sites. Estimated relative recovery: I6: 0.15, I15: 0.15.

PFBA

Injection sites for PFBA were I2 (58.5 g) and I13 (39.0 g; 2–3 m and 4–5 m depths). Breakthrough in Figure 5–10 is bimodal. As with 3,4 DFBA, it is reasonable to assume that tracer injected at I13 was not captured at the well, based on flow direction data (see Figure 3–4) and the relative location of I13 to the pumping well (see Figure 2–10). The breakthrough sequence shown in Figure 5–10 is most likely from tracer injected at I2. This may result from tracer at depth migrating below and past the well, then back up and into the well, or from other vertical or horizontal splitting of the plume such that each portion takes a slightly different route to the well, each with a different travel time. The relative recovery is 0.62 for recovery from I2 only. This value fits well with previous estimates regarding the depth of the lower capture zone boundary, in that the mass not captured by the well was from the lower portion of the plume, and that the lower boundary of the capture zone is near the 4.5 m depth for buoyancy effects of roughly 0.5 m. Estimated relative recovery: I2: 0.62, I13: 0.0.

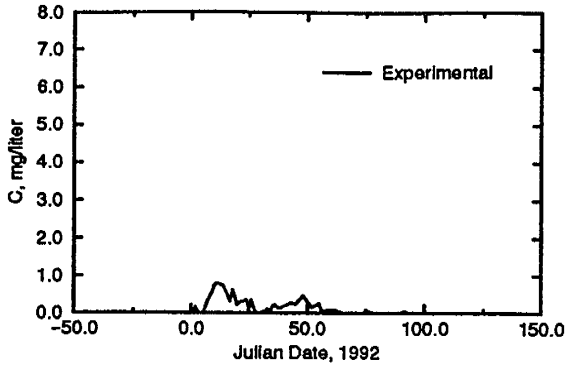

Figure 5-10. Experimental, vertically-integrated BTC for PFBA for Experiment 2.

Br^-

Injection sites for Br^- were I3 (19.5 g; 2–4 m depths) and I14 (20.1 g; applied at the water table). Vertically integrated breakthrough of Br^- is shown in Figure 5–11. The mass recovered is estimated at 1.05 of the mass injected. It is very likely that tracer injected at both sites was fully recovered based on their spatial locations and the tracer injection depths. Slightly larger than expected recoveries for Br^- has been noticed in other studies using HPLC analysis (e.g. Bowman and Rice, 1986). The observed breakthrough sequence for both P2 and P3, shown in Figure 5–1, can be easily separated into tracer originating from I3 and I14. For P2, the early peak is from I3 while the larger tracer mass arriving at a later time is from the application of tracer at the water table. On the other hand, breakthrough in P3 shows the

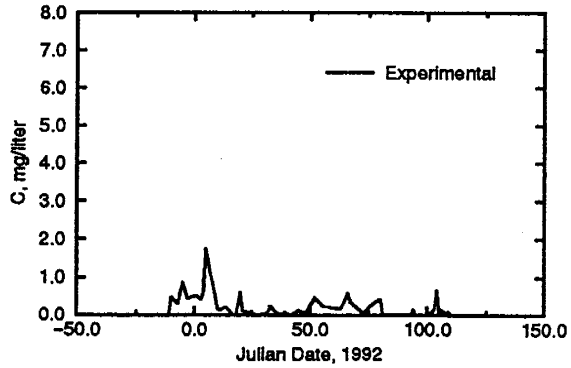

Figure 5–11. Experimental, vertically–integrated BTC for Br for Experiment 2.

opposite breakthrough profile with a larger mass breakthrough for early times from I3, and a small, late arrival which would be from I14. Notice that breakthrough for I3 and I14 appears to occur simultaneously within the separate intervals, over a portion of the experiment. Estimated relative recoveries: I3: 1.0, I14: 1.0.

Three-dimensional Model Analysis

The finite difference grid discretization used in simulating the second experiment is the same as that used in the first experiment. The input parameters, gradient direction and magnitude, aquifer thickness and pumping rate were taken from measurements of these parameters during the course of Experiment 2. Three simulations were generated for three of the conductivity fields used in Experiment 1, simulations 6, 10 and 13. In addition, an equivalent of simulation 13a was also conducted which allows for linear interpolation between numerically generated velocity fields.

Instead of examining some of the features of the different model fits first, as was done for Experiment 1, the model error for the 4 simulations will be reviewed first, with more detailed interpretation following. Table 5–2 compares simulated and measured recoveries along with error analysis results. Figure 5–12 shows the relative error for the 4 simulations used to model Experiment 2. The 'VI' curves are the errors derived from comparison of the well breakthrough masses averaged, or vertically–integrated, over the two well intervals. The '3D' refers to the error found by summing the error for the individual well intervals, P2 and P3. Their similarity is due to the majority of tracer recovered in the lower well interval, P3. For the breakthrough error (the upper two curves), there is little change in going from the homogeneous system, simulation 6, to the 2–layer system, simulation 10. There is significant improvement in going to the 9–layer model, simulations 13 and 13a. For recoveries, the improvement going from simulation 6 to 10, and from 10 to 13 is roughly the same. There is essentially no difference in the error for simulation 13 and 13a, with the only differ-

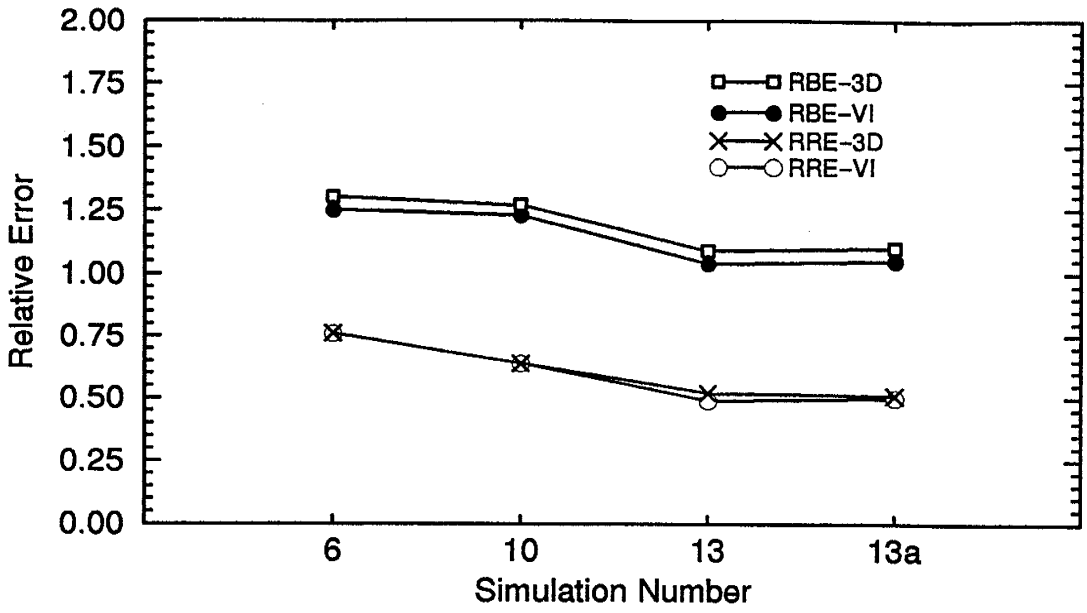

Figure 5-12. Relative recovery and breakthrough error for three-dimensional simulations. VI refers to comparison of vertically-integrated, 3D refers to comparison of separate well intervals.

ence between the two simulations being the velocity interpolation method. All remaining reference to model comparisons will be to simulation 13 unless otherwise noted.

Table 5-2. Comparison of experimental and simulated mass recoveries and breakthrough curves for Experiment 2.

	Tracer Mass Recovery		Recovery Error		Breakthrough Error	
Tracer	*Experimental* R_E	*Simulated* R_S	Recovery Error ε_R	Relative Recovery Error RRE (Absolute value)	Breakthrough Error ε_{BTC}	Relative Breakthrough Error RBE
2,3 DFBA	34.4	42.9	8.48	0.25	27.02	0.79
2,6 DFBA	70.2	92.0	21.86	0.31	60.74	0.87
3,4 DFBA	0.01	0.0	-0.94	1.00	0.94	1.00
3,5 DFBA	45.4	98.1	52.74	1.16	98.26	1.27
m-TFMBA	78.0	105.9	27.92	0.36	78.31	1.00
o-TFMBA	17.0	53.2	36.16	2.13	49.68	2.93
PFBA	24.3	36.7	12.47	0.51	28.56	1.18
Br	39.7	36.8	-2.90	0.07	41.94	1.06

Figure 5–13 shows the measured and simulated breakthrough curves for 7 of the 8 tracers used in Experiment 2. There was zero simulated recovery of 3,4 DFBA at the well (for all simulations), so a comparison plot for 3,4 DFBA is not included in Figure 5–13. The conductivity field was that used for simulation 13 for Experiment 1 (see Section IV, Table 4–10). Longitudinal dispersivity was 0.08 m, horizontal and vertical transverse dispersivities were 0.001 m. Model input parameters are shown in Figure 5–14 for hydraulic gradient, aquifer thickness and pumping rate. Interpretation of the modeling analysis below first briefly treats each tracer separately, then evaluates the modeling results from an overall perspective.

2,3 DFBA

The model fits shown in Figure 5–13 are better for some tracers and worse for others. The fit for 2,3 DFBA is very good. Arrival times for the simulated and measured breakthrough are very close. The shape of the two curves is different however, indicating a more complex flow system for the real aquifer. The RRE is moderate at 0.25 (see Table 5–2), with the simulated recovery higher than the measured recovery, as is the case for all tracers except Br^- (both measured and simulated recovery for 3,4 DFBA is effectively zero). Breakthrough of 2,3 DFBA was attributed to I10, above, with an estimated relative recovery of 0.59 for this site. Simulated relative recovery for I10 was 0.75 (for simulation 13), giving a difference in recovered mass of 9.6 g. If the plume split vertically at the lower part of the plume, 9.6 g translates into roughly 0.5 m difference in the capture zone boundary location, with the experimental capture zone boundary being shallower. This suggests that either buoyancy effects were not large enough in the simulation, or the hydraulic conductivity field is incorrect. Lower conductivities would lower the bottom of the capture zone, and also reduce vertical flow due to density contrasts. If the conductivities are increased, the capture zone narrows both laterally and vertically, bringing the lower capture zone boundary up and also increasing downward, density induced flow, which also raises the lower capture zone boundary.

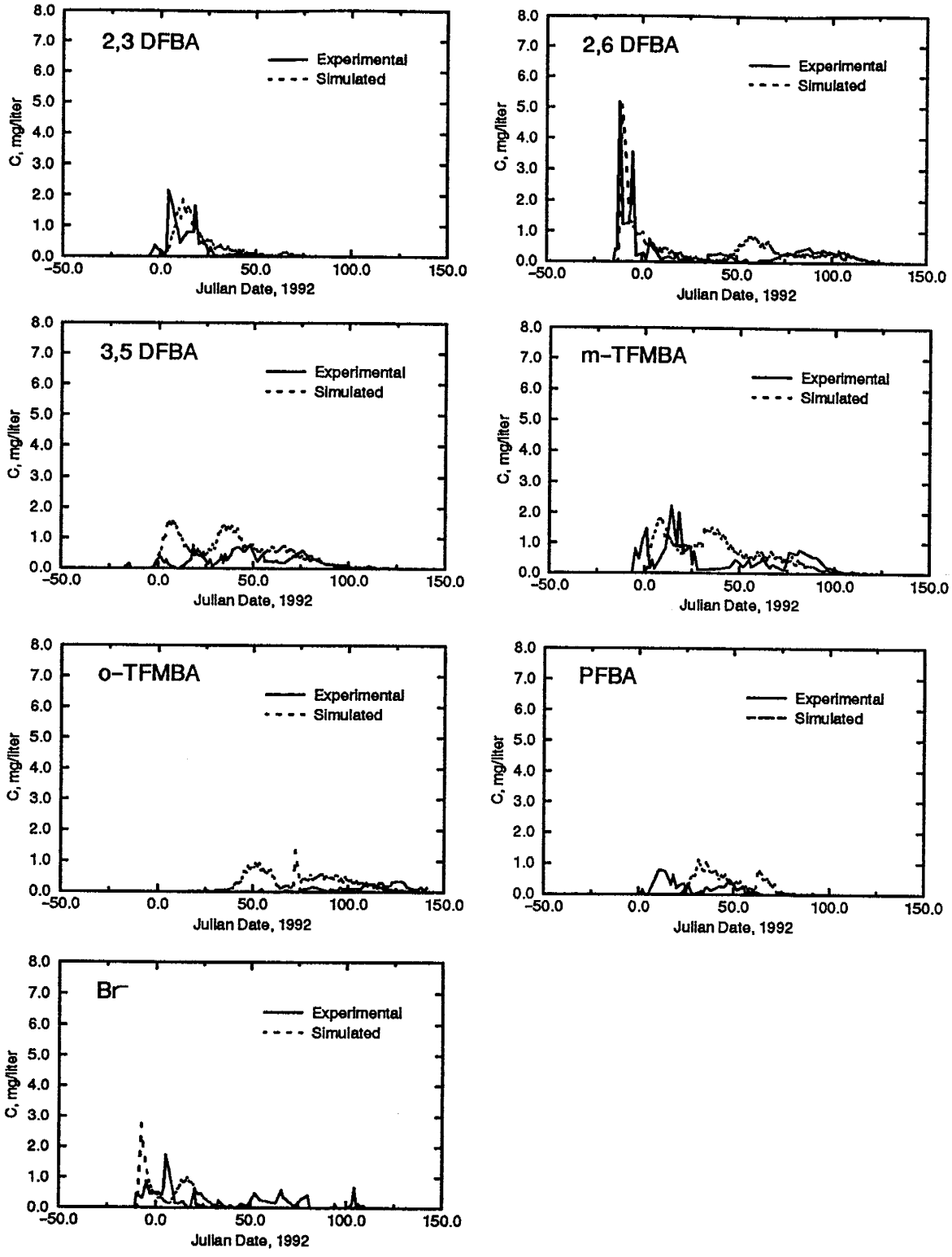

Figure 5-13. Measured and simulated breakthrough curves for Experiment 2. The simulated BTC is from simulation 13. Simulated breakthrough for 3,4 DFBA was zero, so the figure for 3,4 DFBA is not shown.

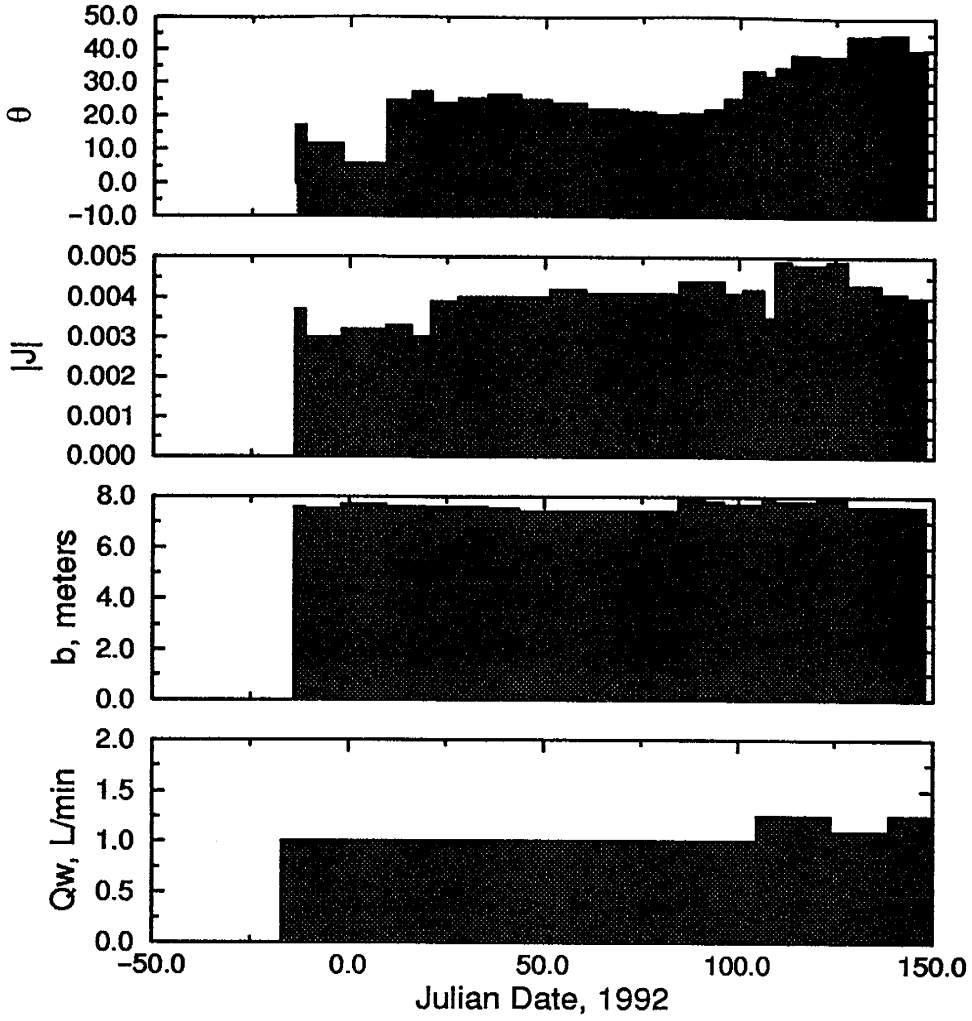

Figure 5–14. Input parameters for three-dimensional analysis of Experiment 2. Q_w is pumping rate, b is aquifer thickness, |J| is magnitude of hydraulic gradient, and θ is directional component of hydraulic gradient.

2.6 DFBA

The model fit for 2,6 DFBA, shown in Figure 5–13, is also very good, however there is an unmatched portion of the simulated breakthrough curve at t=50 to 75 d. 2,6 DFBA was injected at I1, I11 and I12 with estimated recoveries of 0.8, 0.0 and 0.6, respectively. The early measured breakthrough is attributed to I1 which is very close to the well. Later arrivals are believed to come from I12. The simulated recovery is larger than the measured recovery

by RRE=0.31. Simulated recoveries for sites I1, I11 and I12 are 0.92, 0.0 and 1.0, respectively. If loss of tracer is attributed to vertical splitting of the plume, the measured recovery translated to a 0.8 m loss from the lower part the plume from I12, and this is the difference in locations of the capture zone boundary for the experiment and the simulation (since the simulated recovery was 1.0). The mass not captured from I1 in the experiment is 11.7 g, which translates into 0.6 m of the lower portion of the plume not recovered. Simulated mass not captured for I1 (simulation 13) is 5.4 g, or 0.24 m of the lower part of the plume not captured. The difference is 0.36 m, with the experimental capture zone boundary location (with respect to the vertical plume length) being shallower, or, in other words, the model simulated the lower boundary as being too deep.

3.4 DFBA

Simulated recovery for 3,4 DFBA was zero. The measured recovery for 3,4 DFBA was 0.01 g. The simulated recovery would seem close to the measured recovery, yet it is impossible to tell whether the simulated plume was close to being recovered as is suggested by the measured data.

3.5 DFBA

Simulated recovery for 3,5 DFBA is more than twice the measured recovery, with RRE=1.16. The simulated first and last arrival times at the well for 3,5 DFBA are similar to the measured arrival times, as shown in Figure 5–13. The overall shape of the two curves are very similar, yet the size and arrival time of the peaks is not the same, with simulated arrivals earlier. The RRE is large, which indicates that tracer injected at one or both of the injection sites, I5 and I7, were very sensitive to the capture zone boundary. The relative recovery is 0.81 for I5 and 0.85 for I7, estimated measured relative recoveries are 0.12 and 0.65, respectively. There is a significant amount of uncertainty in the estimates of measured recoveries. Assuming the mass not captured was from the lower part of the plume, the difference in the lower capture zone boundary location between the experiment and the simulation

for I7 is 0.6 m, with the experimental boundary being shallower. An error 0.6 m in the simulated lower boundary location is similar to values calculated for some of the other tracers.

m-TFMBA

The overall fit for m-TFMBA is not that good. There are two early measured peaks, shown in Figure 5-13, evidently from site I4, and then a series of smaller peaks presumably from I8. The simulated first arrival time for I8 is at about 25 d, which is at about the same time as the measured arrival times. However, the simulated peak arrival time for I8 is earlier (compare 35 d to 80 d for simulated to measured peak arrival times, respectively) and at higher concentrations (compare 1.5 mg/L to 0.8 mg/L for simulated to measured peak concentrations, respectively) than for the measured BTC for I8. Estimated relative recoveries for I4 and I8 are 0.70 and 0.63, respectively. Simulated relative recoveries for I4 and I8 are 0.98 and 0.85, respectively, with the mass not captured hypothesized to originate from the lower part of the plume in each case. The difference in vertical capture zone boundary location for I4 and I8, with respect to the injection plume, is 0.84 m and 0.66 m, respectively. The boundary location in the experiment is estimated to be shallower in each case.

o-TFMBA

Simulation results indicate roughly 3% of tracer injected at I6 is captured at the well, and 87% of I15 is captured. The simulated BTC in Figure 5-13 arrives earlier than the measured BTC, and has higher concentrations and mass recovered. The measured relative recovery is 0.15 (overall), the simulated relative recovery is 0.45. The difference in the two recoveries is 36.2 g, which is about 0.62 of the mass injected at I15 or I6 alone. Due to the location of I6, it is reasonable to assume that recovery would be very small, and most likely zero, for this injection site. This suggests that the error in simulated recovery is largely attributable to I15. From the analysis conducted for Experiment 1 (see Section IV, above), large discrepancies between simulated and measured recoveries usually meant that the injection site was located on the capture zone boundary. For Experiment 2, it appears that tracer from most

injection sites interact with the lower capture zone boundary. This resulted in RREs of, for example, 0.25, 0.31 and 0.36 for 2,3 DFBA, 2,6 DFBA and m-TFMBA, respectively. The RRE for o-TFMBA is 2.13, which is much larger than the three values just listed. This large error suggests that o-TFMBA injected at I15 is on the lateral edge of the capture zone, a reasonable conjecture given its location and estimated recovery.

The difference in the magnitude of error for sites on the lateral boundary versus the lower boundary is directly related to the source of uncertainty in the model. The largest source of uncertainty during the experiments was the directional component of the gradient. The other large source of uncertainty arises from the estimation for hydraulic conductivity. However, once estimated, the uncertainty in hydraulic conductivity does not change with time and, for a layered system as portrayed here, is uniform in lateral extent. The error in predicting the lower boundary of the capture zone would be predominantly influenced by the uncertainty in gradient magnitude and hydraulic conductivity. This would account for the similar RREs for injection sites with plumes that interact primarily with the lower boundary of the capture zone, such as 2,3 DFBA, 2,6 DFBA and m-TFMBA. Sites on the lateral boundary, however, interact with the part of the capture zone which is influenced by the largest source of uncertainty, the directional component of gradient. Note that this doesn't help explain the large RRE for 3,5 DFBA. In that case, the error was attributed to low conductivity lenses in the aquifer which were not represented in the capture zone model. But, the source of error for 3,5 DFBA still had to do with defining the lateral movement of the tracer plume. This further suggests that the error is not only associated with the large uncertainty of the gradient direction, but that the high sensitivity of recovery has to do with character of the injection site itself. We can speculate that the lateral extent of the plume, and how its size compares with the magnitude of the uncertainties, are both important factors. In the vertical dimension, the plume is 3 m long in most cases, and the uncertainties associated with the lower capture zone boundary are on the order of 1 m or less. In the horizontal dimension, the plume dimension is about 0.2 m, making it very sensitive to all of the uncertainties, espe-

cially the uncertainty in location of the lateral capture zone boundary which is influenced by the large uncertainty in the flow direction and also, the horizontal hydraulic conductivity distribution which hasn't been taken into account in the model. If the lateral extent of the injection plume were larger, the error in predicting recoveries at the well would be smaller.

In estimating recoveries, the model suggests that the potential for recovery for tracer from I15 is greater from I6. Based on this, the recoveries estimated from the initial analysis above can be modified such that I6 has zero recovery and I15 has a relative recovery of 0.30, and that these values have significant uncertainty associated with them.

PFBA

The simulated arrival times for PFBA are later than the measured arrival times. The shape of the two curves is similar, though, each with two peaks separated by approximately 30 d. The simulated recovery is larger then the measured recovery. Since I13 doesn't show any simulated well recovery, based on the analysis of the measured data above, the model appears to be simulating the major components of the flow system fairly well in that simulated recovery was only from I2, as was determined for the measured data, and the overall shape of the BTCs are very similar. Estimated relative recovery was 0.62. Simulated relative recovery is 0.63.

Br^-

The simulated recovery for Br^- is very close to the measured recovery, with RRE=0.07 as shown in Table 5-2. This is the only tracer with simulated and measured recoveries this close. This is because Br^- was injected from 2-4 m for one site (I3), instead of the 2-5 m for most of the other injection sites, and at the water table for the other site (I14). In the analysis of the other tracers, it was determined that the tracer plumes intersected the capture zone boundary in the lower 1 m of the plume, for tracers injected from 2-5 m, and that this was where the primary source of error in simulated tracer migration occurred. Simulated arrival times for tracer injected at the water table at site I14 appear to be much earlier

than measured arrival times in Figure 5-13 (i.e. the second breakthrough mass for each curve; see also Figure 5-1). In the simulation, tracer from I14 arrives at about 15-20 d, whereas the measured arrival time starts at around 50 d. The reason for the early simulated times may be that the simulated hydraulic conductivities are too high in the shallow part of the aquifer near the water table. Also, the tracer solution may have been caught up in the low velocity zone of the capillary fringe for at least a portion of it's residence time in the aquifer.

Discussion

The total mass injected during Experiment 2 was 876.5 g. The total mass recovered was 310.9 g, giving a relative recovery of 0.36. The relative recovery error, or RRE, is roughly 0.50, or, put another way, the error in predicting the mass recovered at the pumping well is 50% of the mass recovered at the pumping well. The relative breakthrough error, or RBE, is roughly 1.0, indicating the ability of the model to predict the mass recovered as a function of time is not very good. Both the relative recovery error and the relative breakthrough error are much larger for Experiment 2 than for Experiment 1. The model in Experiment 2 had difficulty in matching the three-dimensional aspects of the system, which was made apparent by the poor fit of the model at the lower capture zone boundary.

Observed breakthrough in the upper well interval, P2, was less than expected. There are several possible explanations. Injection of the tracer solution caused local mounding of the water table which would have given the plume a small, initial downward velocity. Also, tracer plume densities would cause the injected plume to migrate vertically downward. This effect is largely substantiated from Experiment 1 breakthrough results. A third possible reason for reduced tracer recoveries in P2 is that the water table extends above the top of the well during much of the experiment, producing a source of water above the well which would create downward vertical flow to the well, and also decrease effective pumping rate per unit aquifer thickness for the upper well interval. One, or a combination, of the above three ef-

fects could contribute to low tracer mass recoveries in well interval P2. In addition, it should be noted that the lower boundary of the upper well interval and the upper boundary of the injection wells are both at 2 m below ground surface. This would enhance any of the above three effects, producing lower mass recoveries in P2.

The simulated recovery for 6 of the 8 tracers are higher than the measured recovery. The 2 tracers that didn't fit this trend were 3,4 DFBA and Br^-. 3,4 DFBA was injected in the lower portion of the aquifer, from the 5–7 m depth, which was determined to be below the capture zone, or at the very edge of the capture zone boundary. On the other hand, Br^- was injected in the upper part of the aquifer. Injection of Br^- at I14 was at the water table, most of which was recovered in the upper well interval. Injection at I3 was from 2–4 m, and was injected very close to the pumping well so that the lower part of the tracer plume did not intersect the capture zone boundary at depth. This accounts for the complete recovery of Br^- by the well. The remaining 6 tracers all had injection intervals from 2–5 m, except for 2,6 DFBA injected at I12 which was from 2–4 m. The lower capture zone boundary along the long–axis of the capture zone (for a steady state system, this would be along a line through the stagnation point and the well, parallel to the direction of flow) was estimated at the 5.0 m to 5.5 m depth by the experiment design model, without considering plume density effects, and somewhere above the 6 m depth based on the lack of leachate in the pumpage during the first part of the experiment when the pumping rate was 1.0 L/min.

The depth of the capture zone boundary decreases with distance from the center axis. Also, the width of the surface expression of the capture zone is larger for a partially penetrating well near the surface of the aquifer than for a fully penetrating well. These factors suggest that the loss of mass for many of the tracers was at the bottom of the plume. Since the simulated recoveries (for the 6 tracers) were larger than the measured recoveries, it would appear that the model did not accurately predict the location of the lower capture zone boundary. This may have been due to misrepresentation of the hydraulic conductivity field, or it could be due to an incorrect conceptualization of density induced flow in the model. Not

only are the density-induced velocities thought to be conservatively high, based on comparison to Yih's work (Yih, 1965; see Section III), but the initial concentrations in the aquifer are probably lower than the corresponding tracer solutions prior to injection since mixing of tracer solution with aquifer water will occur during injection. Also, mounding did take place when the tracers were injected which would impart a small downward vertical velocity to the plume. The act of injecting the tracer may also cause the injected plume to be pushed upward, which would counteract the vertical velocities. Although it's not clear what the relative magnitudes of the these two effects would be, they are probably both relatively small in comparison to other forces acting on the plume.

The later arrival of PFBA injected at I2 is a function of site location, conductivity and changing flow direction. Site I2 is probably on, or near, the lateral boundary of the capture zone. This would put it on a longer flow path than if it were, say, closer to the well. If the simulated conductivity were too high, as may be the case for simulations in this study, this would have the effect moving the boundary of the capture zone inward such that I2 would now be positioned on these longer flow paths and simulated breakthrough would have larger arrival times. This effect would be enhanced by the changing flow direction.

Simulated arrival times are too early for some tracers, as is the case for 3,5 DFBA, m-TFMBA, o-TFMBA and Br^-. This possibly suggests that the conductivities in the model were too high. If the hydraulic conductivity were reduced for the entire aquifer, the capture zone would become broader and deeper. The seepage velocities would decrease, but the overall travel time could increase since the path taken by the plume to the well may be more direct. Also, with lower hydraulic conductivity, the vertical flow resulting from density contrasts would decrease, reducing the amount of tracer migrating across the lower capture zone boundary. These effects could all act to increase mass recoveries at the pumping well, which make the model less compatible with the experimental results.

If conductivities were reduced in the lower part of the aquifer only, the lower boundary of the capture zone may move upward, and possible laterally outward, as water would be more accessible in the upper reaches of the aquifer. This will have two effects in the simulations. First, with the lower boundary higher, the simulated recoveries will be reduced for the 6 tracers discussed above. Second, the flow paths to the well are longer, and travel times larger, for pathlines closer to the boundary. This would help increase travel times for many of the tracers arriving at the well too early. A flatter, wider capture zone may also help explain why many of the tracer plumes from individual sites appear to have similar recoveries, or more importantly, why similar amounts of each tracer haven't been captured. For I2, widening and flattening the capture zone would place the boundary further out and place it on shorter pathlines to the well. For tracers with reasonable simulated arrival times, this modification in the flow field would most likely not effect their breakthrough profiles. The three tracers that show reasonable fits for arrival times are 2,3 DFBA, 2,6 DFBA and Br. The good fits are for the first tracers to arrive in each case (except 2,3 DFBA which appears to only have one breakthrough), which in all three cases are for injections sites very close to the well (I10, I1 and I3, respectively). Plume migration for tracer injected at these sites would be the least affected by a change in the conductivity field. As was pointed out during the three-dimensional modeling phase of Experiment 1, the relative values for conductivities in the different layers is very important such that lowering the conductivity in the lower portion of the aquifer would require adjustment of the conductivities in all the layers. Related to this, the anisotropy ratio of K_h to K_v of 1.3 may be too low, which would have the affect of flattening the capture zone and raising the lower boundary. Also, it was noted that the data from Sudicky (1986) and Thorbjarnarson and Mackay (1994) did not compare horizontally, shown in Figure 4–40. The layered model, simulation 13, relied more on Sudicky's data. Slightly different results may be obtained if conductivities more close reflected Thorbjarnarson and Mackay's data set.

There are other possible mechanisms that could be affecting simulated recoveries, and controlling measured recoveries. The conceptualization of vertical flow due to density contrasts could be wrong, yet from considerations of analytic solutions for buoyancy induced flow examined in Section III, the simulations overestimate vertical flow. A reduction in downward plume migration would only act to increase the error in model fit. Also, for a partially penetrating well near the upper surface of the aquifer, as is the case in Experiment 2, the capture zone could be sensitive to the boundary condition imposed at the upper boundary, and the method by which the model characterized the aquifer there. However, from Figure 5–14, the aquifer thickness doesn't change much during the experiment. Vertical flow from surface recharge is also considered minimal during most of the experiment since there was a frozen layer of sand at the surface preventing recharge. Sensitivity of model results to dispersivity was not tested during simulation of Experiment 2. However, from simulation 11 in Experiment 1, the values of dispersivity used in the model doesn't seem to matter that much in most cases and the effect is considered small. Finally, for sites near the lateral boundary of the capture zone, the changing flow field may also have an important effect on the recovery at the well such that a more accurate and detailed formulation of these transients may improve model fit. This is unlikely, however, since there is little difference in model error between simulations 13 and 13a which examine the affect of the transient nature of the flow field on model behavior in a crude manner.

Based on the preceding analysis, a relative recovery, or capture zone map was constructed for Experiment 2, shown in Figure 5–15. The map is similar to the capture zone map of Experiment 1 (see Figure 4–8) in that tracers injected at sites along one side of the experiment were not recovered, except in this case sites exhibiting zero recovery were on the east side compare to the west side for Experiment 1. This resulted from the flow direction for each experiment. It is interesting to note that two of the injection sites were moved from the west side to the east side following the first experiment (I11 and I13), to accommodate what was at that time a more northerly flow direction. However, flow shifted back to the

northeast during the second experiment. Not only is it hard to predict the transport of tracers in such a transient system, but it was difficult to predict where to install portions of the experiment in order to obtain useful results.

Based on the above analysis and discussion, the concept of the capture zone boundary is not one of a static feature of the flow system, but instead a dynamic feature which depends not only on the hydraulics of the pumping well and the hydraulic conductivity of the system, but on the transient nature of the flow system boundaries, the dynamics of the plume itself,

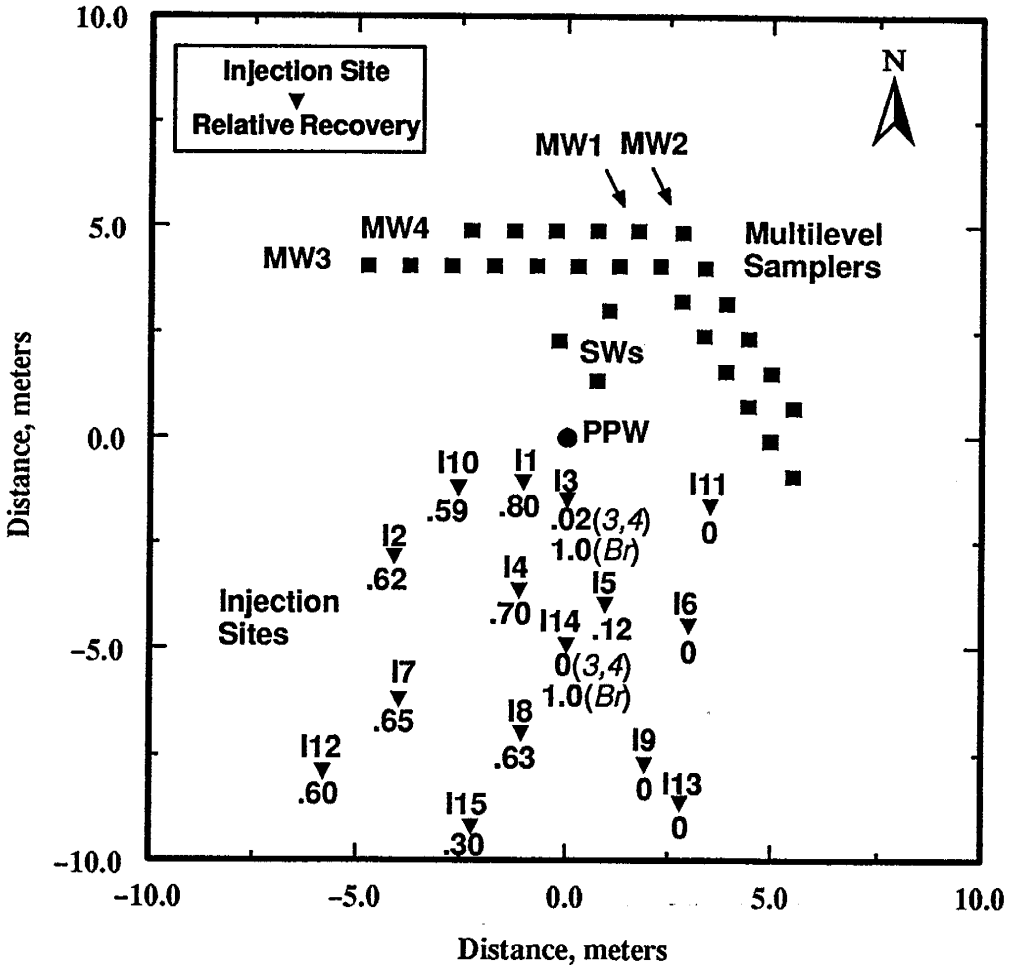

Figure 5–15. Experiment 2 capture zone map based on relative recoveries for 15 injection sites. For each site, the top number is injection site location, the bottom number is the estimated relative recovery (tracer mass recovered at the pumping well / tracer mass injected at that site).

and the time-dependent interaction of the plume with the pumping well-induced capture zone. The density of the plume was seen to play a vital role in determining the location of the actual capture zone. If the boundary were considered static, then the boundary of the capture zone, based on capture of the injected tracer, would be positioned near the 4 m depth at many of the injection well sites since approximately one-third of the injected mass was not captured in many cases. However, the actual boundary of the capture zone, based solely on well and aquifer hydraulics, was estimated to be deeper than this, perhaps near the 4.5 m depth for many of the injection sites due to the vertical movement of the plume resulting from density contrasts. Yet this is still a slightly static view, since both the capture zone and the plume are moving laterally, as well as vertically, in response to fluctuations in the flow field.

VI. SUMMARY AND CONCLUSIONS

The results and findings presented in this report represent new and original research regarding the delineation of capture zones in the field, and the usefulness of various models in delineating capture zones. These research activities are summarized below, with conclusions and recommendations for further work following:

- Delineation of a capture zone in the field based on tracer breakthrough and recovery for both a fully penetrating and a partially penetrating pumping well located in a shallow sand aquifer with essentially lateral ambient flow;
- The simultaneous use of multiple tracers to delineate a capture zone;
- The simultaneous use of 7 fluorinated benzoates in one experiment;
- Direct testing of simple, two-dimensional steady state capture zone predictive models, based on the tracer delineated capture zone, to evaluate model accuracy;
- Direct testing of two- and three-dimensional transient flow and transport capture zone models calibrated to various subsets of data, based on the tracer delineated capture zone, to evaluate model accuracy;
- Comparison of the simple predictive model to the more complex calibrated models to ascertain the practical applicability of the models in predicting capture zones;
- Detailed evaluation of the transient nature of the hydraulics in the Borden aquifer.

The first step in evaluating capture zones in this study was to conduct field tracer experiments in an aquifer exhibiting relatively simple flow characteristics. Field delineation of the capture zones depended on assigning tracer mass recoveries to individual injection sites. This task was potentially difficult since individual tracers were injected at two or more sites such that overlap of breakthrough curves was possible. Fortunately, with tracer at some sites showing zero capture at the well and other tracers showing distinct and separate breakthrough from each injection site, it was possible to assign

recoveries to individual sites with a high level of confidence for most of the tracers in both experiments. The estimated tracer recoveries provided a direct estimate of the capture potential at those sites. The maps of the relative recoveries at each site allowed direct delineation of the capture zone in the field.

Vertical flow components, and vertical variability of horizontal flow components, present in both experiments, made interpretation of the capture zone more difficult, especially for injection sites located near the capture zone boundary. The estimated vertical tracer plume migration ranged from 0.25 m to 0.94 m for tracers injected in Experiment 1. Model simulations gave similar results and suggested that buoyancy induced flow accounted for approximately one-half of the total plume vertical sinkage. In the second experiment, buoyancy effects most likely enhanced vertical plume splitting as the tracer plumes migrated downward across the capture zone boundary at depth.

The two experiments were significantly influenced by transient conditions. The transient nature of the flow system was apparent in water-table measurements at individual piezometers, and also from the resulting gradient calculations based on these measurements. Previous analyses of the natural gradient plume experiments, such as in Freyberg (1986) or Sudicky (1986), assumed steady flow. Our initial experimental design followed this approach, with the initial design of the first experiment oriented at an angle of N52E. After construction and installation of the experiment, it became apparent that flow was in a more northerly direction than suggested by previous studies. This resulted in modification of the original installation before start-up of Experiment 1. Prior to start-up of the second experiment, additional modifications were made to account for the more northerly flow. However, once the second experiment was under way, flow then rotated back to the northeast, so that, again, some of the injection sites and multilevel samplers in the downgradient monitoring fence were not optimally placed. The magnitude of the transient exceeded all expectations, with the range in flow direction approaching 90 degrees (compared to about 14 degrees estimated in previous studies). The mean flow direction, based on data collected during the course of this study, was approximately N20E, which is substantially different than the direction of N45E observed in the nat-

ural gradient plume experiment conducted by Mackay et al. (1986). Clearly, if unanticipated transients occur in the best studied site in North America, they can be expected anywhere.

The orientation of the capture zone in Experiment 1 was approximately N25E to N30E, which is close to the direction flow when the experiment was started, while the mean flow direction was N15E to N20E. The more easterly capture zone orientation is due to the interacting dynamics of the migrating plumes and the nearly linear change in flow direction from N38E to N5W. This suggests that steady–state capture zone models which use the mean flow direction may be in error in predicting the true capture zone orientation in a transient system. The width of the capture zone in the first experiment was estimated at approximately 2.5–3.0 m, which is smaller than the 5 m width estimated during the design of the experiment. The narrower measured capture zone was due to the changing flow direction and also higher hydraulic conductivity than was used to originally estimate the capture zone width. Steady–state capture zone models would predict a wider capture zone which would be conservative in terms of wellhead protection. The capture zone width–to–depth ratio in the first experiment, 3 m to 7 m, was perhaps unrealistically small when compared to wells used in practical applications (e.g. water supply wells, aquifer remediation wells). For larger capture zones, the changing flow field would not have had as much of an affect on the capture zone orientation and width. Also, the fuzziness of the capture zone boundary was large compared to the width of the capture zone for the small capture zones considered here. For a larger capture zone, the lateral movement of the capture zone boundary would be comparatively smaller with respect to the capture zone width, reducing the uncertainty associated with a transient system. However, the pumping–induced velocities would be larger, and flow paths for captured tracers or contaminants would be larger (since the capture zone is itself larger), both effects which would increase dispersion and the fuzziness of the capture zone.

The hydraulic conductivity of the aquifer in the Borden sand pit has been described stochastically by Sudicky (1986) and others as a stationary random field, yet for the present study, vertical stratification of hydraulic conductivity is believed to have had a larger impact on the results in a manner similar to that described by Thorbjarnarson and Mackay (1994). Significantly, the data collected

by Sudicky, and Thorbjarnarson and Mackay, is in the upper, faster part of the aquifer. Their data did not extend downward into the slow zone, where there is also evidence of vertical plume splitting. The vertical plume splitting occurring at depth compares very well with that seen in the experiments by Sudicky et al. (1983) and Mackay et al. (1986). The vertical splitting of the plume resulted from the strongly layered hydraulic conductivity in the aquifer. The layering translates into a nonuniform shape and size of the capture zone with depth, and can also be expressed as partial capture of tracer that interacts with the capture zone boundary, as was the case for 3,4 DFBA injected at I10 in the first experiment. Also, the relatively short flow paths and small horizontal tracer plume dimensions in the experiments minimized the spatially averaged effects of heterogeneities, such that longitudinal dispersion was small, yet larger than a local-scale dispersion coefficient. The transverse dispersivity was also small, yet estimated to be non-zero and larger than the molecular diffusion coefficient, suggesting that the higher frequency hydraulic gradient fluctuations not accounted for in the model calibrations may have had a small but noticeable effect on the results.

The tracer delineated capture zones determined in the two experiments provided a means with which to directly test mathematical capture zone delineation methods. The simplest model was based on potential flow theory and was applied as a predictive model to the first experiment capture zone using three *a priori* input data sets. These data sets differed primarily in the estimated flow direction, with the oldest data from the Waterloo-Stanford experiment in 1986 indicating a mean flow direction of N45E, the Barker data set from 1991 indicating a mean flow direction of N38E, and the mean flow direction derived from gradient calculations taken prior to the experiment indicating a flow direction of N24E. The data most often cited, from the Waterloo-Stanford experiment (Mackay, 1986), gave a relative recovery error of 0.60 in predicting the tracer mass recovered at the pumping well while the other two predictions gave relative recovery errors of 0.22 each. One of the most important factors influencing the capture zone in the first experiment was the fluctuating flow field, the oldest estimate of which was based on the Waterloo-Stanford data. Clearly, the most well known data was not the best data to use in predicting the capture zone.

Further modeling included two- and three-dimensional transient flow and transport modeling using various subsets of data. All simulations based on these models were calibrated to the transient hydraulic gradient data calculated from head measurements taken during the experiments, and used the random walk method to solve for dispersive transport. In addition, some simulations were calibrated to hydraulic conductivity, dispersivity, and aquifer thickness such that the degree of calibration varied between simulations. The calibrated model results were used to test hypotheses regarding the hydraulics of the flow system, to better evaluate the experimental tracer breakthrough and recovery data used to delineate the capture zone in the field, and to provide best fit models with which to compare results from the simple, predictive model.

Application of the two-dimensional model in evaluation of two of the tracers provided a close fit to measured data when a retardation factor and decay constant was applied, respectively. However, the three-dimensional model results were favorably compared to the measured data without including any retardation or decay mechanisms, which agreed with the experimental results indicating that the aquifer was heterogeneous with vertical flow components. In addition, the two-dimensional model simulated lateral plume splitting at the capture zone boundary for one injection site which was shown to be vertical plume splitting by the measured data. The three-dimensional model was capable of simulating this vertical plume splitting along the capture zone boundary by allowing for hydraulic conductivity to vary with depth and incorporating buoyancy effects into the model.

Even though the three-dimensional model was better able to simulate flow and transport, effectively accounting for apparent retardation and decay effects and lateral plume splitting in the two-dimensional model, it did not provide an improvement in capture zone delineation based on tracer recovery and breakthrough comparisons. The relative recovery error, or RRE, associated with these models, using vertically-averaged breakthrough and recovery data ranged from 0.10 to 0.15 in Experiment 1, and was at least 0.50 in Experiment 2. The RRE derived from comparison of mass recoveries for the individual well intervals in the first experiment was a minimum of 0.30, roughly twice that for the vertically-integrated result. The difference in model fits for the vertically-inte-

grated results and the fully three-dimensional results in the first experiment indicates the error in simulating the vertical distribution of tracer mass. The larger RRE for Experiment 2 reflects the interaction of many of the tracer injections with the lower capture zone boundary, and the inability of the model to accurately simulate this boundary location. These results suggest that the largest potential source of uncertainty in the model is the variable vertical hydraulic conductivity, once the transient nature of the system has been accounted for.

The relative breakthrough error, or RBE, was in all cases higher than the associated RREs, but with similar trends to the results. The RBE represents the error associated with the ability of the model to predict the time-sequence of mass breakthrough at the well which is also related to the prediction of tracer travel time which represents time-dependent capture zone locations. The RBE is approximately 0.55 in the first experiment, using vertically-averaged data, and over 1.00 in the second experiment. Clearly, the model is more robust in predicting the mass recovered independent of time which results from the insensitivity of simulated recoveries to model input parameters except for sites located on the capture zone boundary. In addition, these results agree with theoretical results presented by Gutjahr et al. (1994) suggesting that heads convey information regarding outflow locations while transmissivities convey information regarding travel times. By including transient gradients in the models used here, comparisons of time-independent tracer recoveries were more accurate than comparisons of breakthrough curves, which are time-dependent and influenced more strongly by hydraulic conductivities than by heads or the associated gradients.

In the first experiment, the error in "predicting" the tracer mass recovered at the pumping well (i.e. matching the calibrated model with the experimental results) was in the range of 0.10 to 0.15 for all simulations, regardless of the type of model (i.e. the two- or three-dimensional transient transport models), the input data set, or the degree of calibration of the model. If it is assumed that this error represents the best model fit that can be achieved, then the error due solely to the predictive component of the simple model can be estimated by subtracting the relative error of 0.10 (i.e. the lower of the 0.10 to 0.15 range), which represents the best fit simulation, from the predictive model error. The error in the simple model due to prediction alone is then estimated at 0.12 (i.e. 0.22 - 0.10)

for the pre-experiment and Barker data, and 0.50 for the Waterloo-Stanford data. The predictive model using the Barker or pre-experiment data gives a very reasonable result based on this approach. However, the predictive error associated with the Waterloo-Stanford data is still significant. The error in choosing the simple model over the transient transport models is 0.12 (using either of the two data sets with errors of 0.22), while the error in choosing the data set used in the simple model is 38% (0.60-0.22), indicating there is a larger error associated with the fluctuating flow field than with the choice of the model in this case. From a practical standpoint, a prediction error of 0.12 can be considered quite reasonable, such that the total error of 0.22 for the simple model makes it acceptable as a predictive tool (assuming that a suitable input data set is selected). In addition, if the simple capture zone model were used as a decision making tool, it would either be accompanied by an uncertainty analysis, or it would be applied with some type of safety factor which effectively accounts for the uncertainties in the system. These two approaches would improve the effectiveness of the model prediction, making this model more appealing and giving it a higher "usefulness" rating.

If the simple two-dimensional model provides a reasonable prediction of the capture zone, then we can ask what is the usefulness, or practical application, of the two- and three-dimensional transient transport models. The usefulness of these models can be viewed in terms of the extra resources invested in the development and simulation of these models, and collection of the data needed to calibrate the models. Since the two-dimensional flow and transport model is straightforward to develop, data requirements are minimal, and simulation time is reasonable, then it makes sense to use this type of model since the fit it provided was as good or superior to the other models tested. However, this assumes that a reasonable prediction of future flow transients can be made. On the other hand, the three-dimensional model did not provide a significant reduction in error over the two-dimensional transient transport model in delineating the capture zone, even though it clearly simulated the flow system much better than the two-dimensional model. In this case, construction of the three-dimensional model would not be worth the added investment in time to collect the data, construct the model, and perform the simulations. Under what circumstances would a three-dimensional model be applicable? The first impulse is to apply a three-dimensional model to a more "com-

plex" system than the Borden aquifer. However, given the relative simplicity of the Borden aquifer, the large amount of pre-existing data available from previous experiments, and the inability of the three-dimensional model to improve on the results of the two-dimensional model, it is speculated that three-dimensional simulations of an aquifer more complex than the Borden aquifer would be even less successful, and that the two-dimensional model would probably provide equally good, or even better, results. These results are in agreement with results presented by Bair and Roadcap (1992) in comparing analytical and semi-analytical flow models to a three-dimensional finite difference flow model which were used to delineate capture zones.

A fully three-dimensional treatment of the flow system would be required when vertical flow components are significant and on the order of, or larger than, the horizontal flow component. This would be the case where there are partially penetrating flow boundaries, a large component of vertical recharge, or where there are variations in hydraulic conductivity causing significant vertical flow. The second experiment was an example of a system with fully penetrating lateral flow boundaries and essentially no vertical recharge, but the extraction well is partially penetrating, causing large vertical flow gradients near the well. Both the recovery and breakthrough errors were large resulting from three-dimensional simulation of the second experiment. This was for a relatively simple flow system with the model calibrated to all available data collected during the experiment. From evaluation of the model fit for individual injection sites, it is apparent that the primary source of error arose from simulating splitting of the tracer plumes at the lower capture zone boundary. Had the system been more complex, the error would have been even larger. The significance of this error can be viewed from two perspectives. First, it is suggested that a three-dimensional model would never provide a reasonable prediction of the capture zone. However, had this model actually been applied as a purely predictive model, an uncertainty analysis could be conducted which would aid in the decision making process. Also, from an engineering standpoint, it would make sense to include the entire saturated thickness as part of the capture zone in order to obtain a conservative prediction regarding a well head protection area. Second, it should be noted that, often times, the location of a spill is at the ground surface with the contaminant intersecting the aquifer at the upper

boundary (e.g. the water table). In situations such as this, the model would not be simulating the interaction of the contaminant with the lower capture zone boundary where the largest source of model error exists.

One of the important conclusions regarding capture zone modeling, and delineation of wellhead protection areas, is that regardless of the model, uncertainties will always exist and have to be dealt with accordingly. The largest sources of uncertainty in the present study arose from the transient nature of the flow field, and the vertical variability of hydraulic conductivity. As Gutjahr et al. (1994) point out, heads are important in determining particle flow direction, while transmissivities, or hydraulic conductivity, are important in determining particle travel times. In delineation of wellhead protection areas, both factors are important since a capture zone conveys information about the direction a particle moves, or where a particle that is extracted by the well originates, and the time it takes for a particle to travel to the well. In the modeling study presented here, knowledge of heads at specific locations throughout the experimental area was very important due to the highly transient nature of the flow filed, and knowledge of hydraulic conductivity greatly improved the time-sequence of mass recovery at the well using the three-dimensional model. The greatest challenge in modeling the system was when both the heads and the hydraulic gradient influenced the capture zone prediction. This occurred when tracers interacted with the capture zone boundary. When delineating a wellhead protection area, a boundary is specified, whether it is the boundary of a time-dependent front or the boundary of the entire capture zone. Both information concerning heads and hydraulic conductivity, and information about the uncertainty associated with these parameters, would be necessary in making an accurate prediction of these capture zone boundaries.

Recommendations for Further Work

The design and implementation of the experiment can be considered successful on virtually all accounts. However, it is useful to evaluate the performance of the different components of an experiment in order to improve on future applications. The following is a brief critique of particular aspects of the two experiments.

- As was noted above, the orientation of the experiment had to be modified to account for the migrating flow field. This was due to a lack of prior knowledge of the flow system, and is brought up here to make the point that the success of a field project, whether it be a research experiment, or the actual delineation of a well head protection area for a municipal supply well, depends on careful parameter estimation.

- In terms of gathering data during the experiment, most procedures worked as designed. Some of the problems with noisy vibrating-wire piezometer data could probably be eliminated by running the lines from the VWPs to the data logger either underground or through conduits. Some potential problems cannot be circumvented easily however, as brought to mind by the lightening strike which either damaged or destroyed all the VWPs and the data logger one week prior to initiating the first experiment. The location of the piezometers could be modified to better reflect the local conditions of the capture zone by moving VWPs from the edge of the sand pit inward closer to the pumping well, or preferably by adding more piezometers to the array.

- In future experiments, where tracer is injected in an aqueous solution, it is recommended that peristaltic pumps, or an equivalent device, be used instead of gravity feed as was done for Experiment 1. Injecting the tracers at a fairly constant rate, and perhaps more uniformly along the injection well, at all sites would give better control of initial conditions.

- The pumping well and associated apparatus performed exceedingly well. The one weakness in this part of the experiment design was the uncertainty associated with the pumping rate of individual flow lines from the pumping well. There was gradual clogging of some of the visual flow spinners and well lines from precipitation of iron oxide originating in the leachate, while the upper flow line period-

ically clogged due to bacterial buildup. These lines were periodically cleaned out, yet the reduced flow rate in any one interval would change the vertical distribution of pumping rate for the entire well. During the three-dimensional modeling phase of the study, pumping was assumed uniform for all well intervals. The hypothesis of variable well-interval pumping rates, and the effect this would have on the simulations results, has not yet been tested. The clogging and cleaning of the well lines was accepted as integral parts of the experiment, yet the visual flow spinners provided little control on the effects of these processes and activities. As of this time, it is not clear what solution could be applied to remedy the situation if a similar experiment were conducted. Part of the problem is associated with the very low pumping rate for each well line, which would require very accurate, and expensive flow meters, which in turn are very sensitive to particulate matter in the water.

The following are suggestions for further field experiments, or components of field experiments.

- More rigorous approaches to evaluation of breakthrough curve separation using, for example, signal processing techniques, may allow for more complex injection schemes where multiple tracers, combined in predetermined ratios, are injected at multiple sites. In principle, these types of approaches show much promise in extending the number of available tracers for a given experiment.

- With respect to the modeling of the experiments, we assumed that aquifer storage effects were negligible and used a linear, quasi steady-state approach in our preliminary models. This implies an instantaneous response of the aquifer to changes in heads, a valid assumption if the changes are slow and/or small, such that re-equilibration of the flow field is of short duration. We feel this assumption was largely substantiated from comparison of observed and simulated results.

Weekly head measurements, used to describe the hydraulic gradient, appear to represent the general trend of the flow field. However, high frequency fluctuations, which were recorded with vibrating wire piezometers, do occur and may require full treatment of the transients in the system. Examination of the transient nature of the flow system in more detail is currently under way. In addition, processes and factors that could be important and worth including in future capture zone analyses include capillary fringe effects, vertical recharge, and atmospheric and biological processes. To this date, a regional or local flow model at Borden has not been constructed. Based on observations made during this study, it is felt that many, if not all, of the processes just listed have significant influence on flow in the sand pit area.

- In a system influenced by transients, the time scale of the study must be taken into account when predicting flow behavior. For an experiment of short duration, such as the experiments conducted in this study, mean flow behavior based on previous data can provide inadequate information for prediction (i.e. design of the experiment). This was exacerbated by the occurrence of an above normal year for precipitation in 1992. Even for an experiment running over several time periods, the mean behavior will not adequately take into account extreme events or previously undetected trends. A partial solution to this problem, when designing a WHPA for instance, is to represent flow direction by a probability density function. This would lead to an output PDF of the capture zone, or WHPA, on which zoning regulations could be based. However, even capture zones with low probability of occurrence must be further weighted by the risk associated with certain types of hazardous chemicals.

- In the present study, the water table was modeled in a very simple manner, and vertical recharge effects on the capture zone were considered negligible. Careful estimates of vertical recharge, based on measurements of precipitation, infiltra-

tion, and the water table response, would provide further data for experimental capture zone analysis and model comparisons.

- The experiments conducted in the present study were designed to delineate a capture zone. An important next step would be to conduct a real wellhead protection experiment. This would involve first predicting a capture zone, or well head protection area. Once the capture zone is predicted, the pump is installed and turned on, and tracers are injected outside this area with sampling at the pumping well to determine the accuracy of the prediction.

- The capture zone width-to-depth ratios in the present study were not directly comparable to typical capture zones, such that larger-scale experiments, similar in design to the experiments presented here, would help address any scale related issues not addressed in this study.

The following are suggestions for further capture zone analysis and flow and transport modeling.

- Simulated breakthrough at the multilevel sampling fences is very sensitive to variations in hydraulic conductivity, and may also be sensitive to other parameters, making this data especially valuable in model calibration. Further modeling of fence breakthrough in the first experiment may lend additional insights regarding the capture zone, as well as the hydraulics of the Borden aquifer in general, should the remaining multilevel water samples become available.

- Curve fitting was done by trial and error. Better fits, and more accurate parameter estimation, would be obtained with the use of an automated optimization procedure. This would require specification of a suitable objective function, and may also require refinement of error estimation techniques.

- Variable hydraulic conductivity was portrayed as a layered system in the three-dimensional model. A stochastic approach in both the two- and three-dimensional models may improve the capture zone model fits.

- The transient flow modeling assumed storage effects were negligible. Further testing of this assumption is warranted, especially with respect to the sensitive nature of the capillary fringe and its influence on saturated thickness and hydraulic gradient.

- The transient in the present study was based on hydraulic gradient calculations derived from weekly head measurements. Head measurements taken every 10 minutes with vibrating wire piezometers were not used in the gradient calculations. Incorporation of the 10 minute data into the model would lend provide insights into whether these higher frequency fluctuations would provide a better model fit, and estimates of the associated uncertainties of these fluctuations obtained when they are not included in the model.

- In the present study, recharge was assumed to be horizontal. The vertical recharge, which was evident from the head measurements taken in the sand quarry, were input into the model in the simple manner of changing saturated thickness and direction and magnitude of ambient flow. However, the shape of a capture zone changes depending on the source of recharge. It was estimated that the magnitude of vertical recharge was small compared to the magnitude of lateral recharge, however, these relative effects were not tested.

- Only the simple capture zone model was applied as a purely predictive model. Further modeling using the two- and three-dimensional transient models to predict the capture zone would provide valuable insights into the predictive capabilities of models in a highly transient system. A variety of approaches predicting the transient behavior of the aquifer would be developed and tested.

- To date, a flow model of the Borden aquifer, either at the scale of the sand quarry, or at a larger regional scale, has not been developed. As a result, concrete conclusions have not always been obtained in previous plume migration studies conducted in the Borden aquifer. The complexities of the aquifer presented in the present study suggest that a comprehensive model of the sand quarry, based on the hydraulics of the flow system as a whole, incorporating information from previous studies as well as newly collected data, would provide valuable insights into the hydraulics of a complex flow system, as well as help address unexplained phenomena from previous studies.

VII. REFERENCES

Akindunni, Festus F., and R.W. Gillham. 1992. Unsaturated and saturated flow in response to pumping of an unconfined aquifer: Numerical investigation of delayed drainage, Ground Water, 30(6): 873–884.

Atlas, R.M. and R. Bartha. 1987. Microbial Ecology: Fundamentals and Applications, Benjamin/Cummings Publ. Co.: 352–353.

Aziz, K. and A. Settari, 1979, Petroleum Reservoir Simulation, Elsevier, New York.

Bair, E.S., C.M. Safreed, and B.W. Berdanier. 1991a. CAPZONE–An analytical flow model for simulating confined, leaky confined, or unconfined flow to wells with superposition of regional water levels. International Groundwater Modeling Center, Colorado School of Mines, Golden, Colorado, 193 pp.

Bair, E.S., A.E. Springer and G.S. Roadcap. 1991b. Delineation of traveltime-related capture areas of wells using analytic flow models and particle tracking analysis, Ground Water, 29(3); 387–397.

Bair, E.S. and G.S. Roadcap. 1992. Comparison of flow models used to delineate capture zones of wells: 1. Leaky–confined fractured–carbonate aquifer, Ground Water, 30(2): 199–210.

Bair, E.S., C.M. Safreed, and E.A. Stasny. 1991c. A monte carlo–based approach for determining traveltime–related capture zones of wells using convex hulls as confidence regions, Ground Water, 30(6): 849–855.

Ball, W.P., CH. Buehler, T.C. Harmon, D.M. Mackay and P.V. Roberts. 1990. Characterization of a sandy aquifer material at the grain scale, J. Contam. Hydrol., 5: 253–295.

Barry, D.A., J. Coves, and Garrison Sposito. 1988. On the Dagan model of solute transport in groundwater: Application to the Borden Site, Water Resour. Res., 24(10): 1805–1817.

Barry, D.A. and Garrison Sposito. 1990. Three-dimensional statistical moment analysis of the Stanford/Waterloo Borden tracer data, Water Resour. Res., 26(8): 1735-1747.

Bear, J. 1972. Dynamics of Fluids in Porous Media, American Elsevier, New York, 764 pp.

Bear, J. 1979. Groundwater Hydraulics, McGraw-Hill, New York.

Bear, J. and M. Jacobs. 1965. On the movement of water bodies injected into aquifers, J. of Hydrol., 3: 37-57.

Benson, C. and Robert S. Bowman. 1994. Tri- and tetrafluorobenzoates as nonreactive tracers in soil and groundwater, Soil Sci. Soc. Am. J., 58, 1123-1129.

Boggs, J.M. and E.E. Adams. 1992. Field study of dispersion in a heterogeneous aquifer 4. Investigation of adsorption and sampling bias, Water Resour. Res., 28(12): 3325-3336.

Bonn, B. and S. Rounds. 1990. DREAM-Analytical Groundwater Flow Programs. Lewis Publishers, Inc., Chelsea, Michigan, 109 pp.

Boulton, N.S. 1963. Analysis of data from non-equilibrium pumping tests allowing for delayed yield from storage, Proc. Inst. Civil Engr., 26: 469-482.

Bowman, R.S. 1984a. Analysis of soil extracts for inorganic and organic tracer anions via high performance liquid chromatography, J. Chromatogr., 285: 467-477.

Bowman, R.S. 1984b. Evaluation of some new tracers for soil water studies, Soil Sci. Soc. Am. J., 48, 987-993.

Bowman, Robert S. and Robert C. Rice. 1986. Transport of conservative tracers in the field under intermittent flood irrigation, Water Resour. Res., 22(11): 1531-1536.

Bowman, R.S. and J.F. Gibbens. 1992. Difluorobenzoates as nonreactive tracers in soil and ground water, Ground Water: 30(1), 8-14.

Brusseau, Mark L. 1993. The influence of solute size, pore water velocity, and intraparticle porosity on solute dispersion and transport in soil, Water Resour. Res., 29(4): 1071–1080.

Chow, J. and J .L. Wilson. 1988. Induced Infiltration from a Partially Penetrating Stream in an Aquifer with Ambient Flow, presented at Spring Mtg., Amer. Geophy. Union, Baltimore.

Dagan, G. 1982. Stochastic modeling of groundwater flow by unconditional and conditional probabilities. 2. The solute tranport, Water Resour. Res., 18(4): 835–848.

Dagan, G. 1984. Solute transport in heterogeneous porous formations, J. Fluid Mech., 145: 151–177.

Dagan, G. 1988. Time–dependent macrodispersion for solute transport in anisotropic heterogeneous aquifer, WAter Resour. Res., 24(9): 1491–1500.

Dagan, Gedeon. 1989. Comment on "A note on the recent natural gradient tracer test at the Borden Site", by R.L. Naff, T.–C. Jim Yeh, and M.W. Kemblowski, Water Resour. Res., 25(12): 2521–2522.

Environmental Protection Agency. 1987. Guidelines for the Delineation of Wellhead Protection Areas, Rpt. EPA 440/6–87–010, Office of Ground–water Protection, Washington, D.C.

Environmental Protection Agency. 1990. WHPA: An integrated semi–analytical model for the delineation of wellhead protection areas (1st release), Office of Ground–Water Protection, Washington, D.C.

Environmental Protection Agency. 1991. WHPA: An integrated semi–analytical model for the delineation of wellhead protection areas (2nd release), Office of Ground–Water Protection, Washington, D.C.

Farrell, D.A., A.D. Woodbury, E.A. Sudicky, and M. Rivett. 1992. A geostatistical analysis of fluctuating water-levels at the Borden tracer-test site, Waterloo Centre for Groundwater Research, University of Waterloo, Canada, unpublished document E-66.

Farrell, D.A., A.D. Woodbury, E.A. Sudicky, and M. Rivett. 1994. Stochastic and deterministic analysis of dispersion in unsteady flow Borden tracer-test site, J. Cont. Hydrology, 15, 159-185.

Freyberg, David L. 1986. A natural gradient experiment on solute transport in a sand aquifer 2. Spatial moments and the advection and dispersion of nonreactive tracers, Water Resour. Res., 22(13): 2031-2046.

Frind, E.O., G.B. Matanga and J.A. Cherry. 1985. The dual formulation of flow for contaminant transport modeling 2. The Borden aquifer, Water Resour. Res., 21(2): 170-182.

Frind, E.O., E.A. Sudicky and S.L. Schellenberg. 1987. Micro-scale modelling in the study of plume evolution in heterogeneous media, Stochastic Hydrol. Hydraul., 1: 263-279.

Gelhar, L.W., and C.L. Axness. 1983. Three-dimensional stochastic analysis of macrodispersion in aquifers, Water Resour. Res., 19(1): 161-170.

Gibbens, J.F. 1989. An evaluation of several fluorinated benzoic acids for use as soil and ground water tracers, Unpublished M.S. thesis, Hydrology Program, New Mexico Inst. of Mining and Tech., Socorro, NM.

Gutjahr, A., B. Bullard, S. Hatch and L. Hughson. 1994. Joint conditional simulations and the spectral approach for flow modeling, Stochastic Hydrol. Hydraul. 8, 79-108.

Jacob, C.E.. 1950. Flow of Groundwater, Chap. 5 of Engineering Hydraulics, John Wiley & Sons, New York.

Javendel, I. and C-F Tsang. 1984. Capture-zone type curves: A tool for aquifer cleanup, Ground Water, 24(5): 616-625.

Keeley, J.F. and C-F. Tsang. 1983. Velocity plots and capture zones of pumping centers for ground-water investigations, in Proceedings of the Third National Symposium on Aquifer Restoration and Ground-Water Monitoring, Natl. Water Well Assoc.

Kinzelbach, W. 1990. Simulation of pollutant transport in groundwater with the random walk method, Groundwater Monitoring and Management (Proceedings of the Dresden Symposium, March 1987). IAHS Publ. no 173.

Lee, K. 1986. Pollution capture zones for pumping wells in aquifers with ambient flow, M.S. Independent Study, Hydrology Program, New Mexico Institute of Mining and Technology, Socorro, New Mexico.

Lee, K. and J.L. Wilson. 1986. Pollution capture zones for pumping wells in aquifers with ambient flow, presented at Fall Mtg., Amer. Geophy. Union, San Francisco.

Lerner, David N. 1992. Well catchments and time-of-travel zones in aquifers with recharge, Water Resour. Res., 28(10): 2621-2628.

Leppert, S.C. 1990. Capture zones in transient flow fields,: simulations and analysis, M.S. Independent Study, Hydrology Program, New Mexico Institute of Mining and Technology, Socorro, New Mexico.

Linderfelt, William R. and John L. Wilson. 1991. Three-dimensional capture zone analysis: partially penetrating well and stream effects and two-dimensional model comparisons, presented at Fall Mtg., Amer. Geophy. Union, San Francisco.

MacFarlane, D.S., J.A. Cherry, R.W. Gillham and E.A. Sudicky. 1983. Migration of contaminants in groundwater at a landfill: A case study 1. Groundwater flow and plume delineation, J. Hydrol., 63: 1-29.

Mackay, D.M., D.L. Freyberg, P.V. Roberts and J.A. Cherry. 1986. A natural gradient experiment on solute transport in as sand aquifer 1. Approach and overview of plume movement, Water Resour. Res., 22(13): 2017-2029.

Mackay, Douglas M., Gino Bianchi-Mosquera, Andrew A. Kopania, Homayoon Kianjah and Kathryn W. Thorbjarnarson. 1994. A forced-gradient experiment on solute transport in the Borden aquifer 1. Experimental methods and moment analysis of results, Water Resour. Res., 30(2): 369-383.

McDonald, M.G. and A.W. Harbaugh. 1983. A Modular Three Dimensional Finite Difference Ground-Water Flow Model, U.S.G.S. Open File Report 83-875.

Morrisey, D.J. 1987. Estimation of the recharge area contributing to a pumped well in a glacial drift river valley aquifer, USGS Open File Rpt. 86-543.

Muskat, M. 1937. The Flow of Homogeneous Fluids Through Porous Media, McGraw-Hill Book Co., New York.

Naff, R.L., T.-C. Jim Yeh and M.W. Kemblowski. 1988. A note on the recent natural gradient tracer test at the Borden site, Water Resour. Res., 24(12): 2099-2103.

Naff, R.L., T.-C. Jim Yeh and M.W. Kemblowski. 1989. Reply, Water Resour. Res., 25(12): 2523-2525.

Nelken, L.H., and J.C. Birkett. 1982. Dipole moments, Handbook of Chemical Property Estimation Methods; (eds.)W.J. Lyman, W.F. Reehl, and D.H. Rosenblatt, McGraw-Hill, N.Y., 17-1 to 17-25.

Nelson, William R. 1978. Evaluating the environmental consequences of groundwater contamination 2. Obtaining location/arrival time and location/outflow quantity distributions for steady flow systems, Water Resour. Res., 14(3): 416-428.

Neuman, S.P. 1972. Theory of flow in unconfined aquifers considering delayed response of the water table, Water Resour. Res., 8(4): 1031-1044.

Newsom, J.M. and J.L. Wilson. 1988. Flow of groundwater to a well near a stream: Effect of ambient groundwater flow direction, Ground Water, 26(6), 703-711.

Nicholson, R.V., J.A. Cherry, and E.J. Reardon. 1983. Migration of contaminants in groundwater at a landfill: A case study 6. Hydrogeochemistry, J. Hydrol., 63: 131-176.

Nwankwor, G.I., J.A. Cherry and R.W. Gillham. 1984. A comparative study of specific yield determinations for a shallow sand aquifer, Ground Water, 22(6): 764–772.

Nwankwor, G.I., R.W. Gillham, G. van der Kamp, and F.F. Akindunni. 1992. Unsaturated and saturated flow in response to pumping of an unconfined aquifer: Field evidence of delayed drainage, Ground Water, 30(5): 600–700.

O'Hannesin, S.F. 1981. Spatial variability of grain–size parameters and hydraulic conductivity at a dispersion test site, Bachelor of Environmental Studies Honours Report, 46 pp., Univ. of Waterloo, Waterloo, Ontario.

Rajaram, Harihar, and Lynn W. Gelhar. 1991. Three–dimensional spatial moments analysis of the Borden tracer test, Water Resour. Res., 27(6): 1239–1251.

Rehfeldt, Kenneth R. and Lynn W. Gelhar. 1992. Stochastic analysis of dispersion in unsteady flow in heterogeneous aquifers, Water Resour. Res., 28(8): 2085–2099.

Schafer–Perini, A. 1990. Numerical study of the influence of permeability heterogeneity in non–uniform steady–state flow systems, Ph.D. thesis, New Mexico Institute of Mining and Technology, Socorro, New Mexico.

Schafer–Perini, A. and J.L. Wilson. 1991a. Three–dimensional stochastic flow and displacement in a five–spot pattern, SPE Paper 21243, Proc. 11th SPE Sym. on Reservoir Simulation, Soc. of Petro. Engr.:405–423

Schafer–Perini, A. and J.L. Wilson. 1991b. Efficient and accurate front tracking for two–dimensional groundwater flow models, Water Resour. Res., 27(7): 1471–1485.

Shafer, J.M. 1987a. Reverse pathline calculation of time related capture zones in non–uniform flow, Ground Water, 25(3): 283–289.

Shafer, J.M. 1987b. GWPATH: Interactive ground–water flow path analysis, Bulletin 69, Illinois Department of Energy and Natural Resources.

Shafer, J.M. 1990. GWPATH–Version 4.0. Illinois State Water Survey, Champaign, Illinois.

Slichter, C.S. 1899. Theoretical investigation of the motion of ground waters, U.S. Geol. Survey Ann. Rpt., 19: 295–384.

Springer, A. E. and E. Scott Bair. 1992. Comparison of methods used to delineate capture zones of wells: 2. Stratified–drift buried–valley aquifer, Ground Water, 30(6): 908–917.

Sudicky, E.A., J.A. Cherry and E.O. Frind. 1983. Migration of contaminants in groundwater at a landfill: a case study 4. A natural–gradient dispersion test, J. Hydrol., 63: 81–108.

Sudicky, E.A. 1986. A natural gradient experiment on solute transport in a sand aquifer: Spatial variability of hydraulic conductivity and its role in the dispersion process, Water Resour. Res., 22(13): 2069–2082.

Sykes, J.F., S.B. Pahwa, R.B. Lantz, and D.S. Ward. 1982. Numerical simulation of flow and contaminant migration at an extensively monitored landfill, Water Resour. Res., 18(6): 1687–1704.

Tchelepi, H.A. and F.M. Orr, Jr. 1993. Dispersion, permeability heterogeneity, and viscous fingering: Acoustic experimental observations and particle–tracking simulations, Phys. Fluids A 5(7): 1558–1574.

Teutsch, G. 1989. A variable scale approach for the delineation of groundwater protection zones using field and numerical modelling techniques, IAH–Volume. 28th International Geological Congress, Washington D.C.

Teutsch, G. and B. Hofmann. 1990. The delineation of groundwater protection zones using forced gradient tracer tests: A model validation case study. Model CARE 90: Calibration and Reliability in Groundwater Modelling, IAHS Publ. no. 195.

Theis, C.V. 1935. The relation between the lowering of the piezometric surface and the rate and duration of discharge of a well using groundwater storage, Trans. Amer. Geophys. Union, 2: 519–524.

Thiem, G. 1906. Hydrologische Methoden, J.M. Gebhardt, Leipzig, 56 p.

Thorbjarnarson, Kathryn W., and Douglas M. Mackay. 1994. A forced-gradient experiment on solute transport in the Borden aquifer 2. Transport and dispersion of the conservative tracer, Water Resour. Res., 30(2): 385-399.

Tompson, Andrew F.B. and Lynn W. Gelhar. 1990. Numerical simulation of solute transport in three-dimensional, randomly heterogeneous porous media, Water Resour. Res., 26(10): 2541-2562.

Tucker, W.A. and L.H. Nelken. 1982. Diffusion coefficients in air and water, Handbook of Chemical Property Estimation Methods; (eds.) W.J. Lyman, W.F. Reehl, and D.H. Rosenblatt, McGraw-Hill, N.Y.: 17-1 to 17-25.

Turner, J.S. 1973. Buoyancy Effects in Fluids, Cambridge University Press, New York.

Uffink, Gerard J.M. 1988. Modeling of solute transport with the random walk method, in Groundwater Flow and Quality Modeling, eds. E. Custodio, A. Gurgui and J.P. Lobo Ferreira, D. Reidel Publishing, Boston.

Varljen, M.D. and J.M. Shafer. 1991. Assessment of uncertainty in time-related capture zones using conditional simulation of hydraulic conductivity, Ground Water, 29(5): 737-748.

van Kooten, Jaco J.A. 1994. Groundwater contaminant transport including adsorption and first order decay, Stochastic Hydro. Hydrau. 8, 185-205.

Wang, H. 1987. Charles Sumner Slichter - an engineer in mathematician's clothing, History of Hydrology, 3: 103-112.

Wilson, J .L. 1981. Analytical methods in groundwater hydrology. Groundwater Hydrology, Boston Society of Civil Engineers, GeoTechnical Lecture Series, Boston, Massachusetts.

Wilson, J .L. 1986. Induced Infiltration in Aquifers with Ambient Flow, presented at Fall Mtg., Amer. Geophy. Union, San Francisco.

Wilson, J .L. 1993. Induced infiltration in aquifers with ambient flow, Water Resour. Res., 29(5): 3503-3512.

Wilson, John L. and William R. Linderfelt. 1991. Groundwater quality in pumping wells located near surface water bodies. WRRI Technical Completion Report 261, Water Resources Research Institute, Lac Cruces, New Mexico, 145 pp.

Woodbury, Allan D. and E.A. Sudicky. 1991. The geostatistical characteristics of the Borden aquifer, Water Resour. Res., 27(4): 553-546.

Yih, C.S. 1965. Dynamics of Nonhomogeneous Fluids, MacMillan Co. N.Y., 330 pp.

APPENDIX 1: TRACER INJECTION EXPERIMENT 1

Each tracer solution consists of tracer chemical and 10.67 liters of de-ionized water. Potassium hydroxide was added to the fluorinated benzoic acid tracer solutions, to neutralize the acidic nature of the tracer and to facilitate dissolution. The amounts of chemical used for each sample are listed in Table A1-1. All chemicals were measured by weight (0.0005 grams). The 10.67 liter volume of water was also measured by weight, with an accuracy of 0.125 lb., and stored in individual plastic containers.

To make an injection solution, approximately 1 liter of de-ionized water was removed from a container and mixed with the chemical tracer, along with an equivalent molar amount of potassium hydroxide. For almost all solutions, the additional potassium hydroxide was added to bring the pH up to 7.0. This may have been due to impurities in the system, and also de-ionized water is acidic to begin with. Potassium bromide was also added to the solution for 4 injection site solutions (see Table A1-1). When a pH of 7.0 was achieved and the solution visually appeared to be free of particulate matter, the tracer was considered to be dissociated. The measuring and combining of chemicals with the deionized water took approximately 30 minutes. The mixing process, until dissociation was achieved, took between 30 minutes and 20 hours. After mixing was completed, the 1 liter solution was poured back into the original container. Through mixing was assumed to take place during the transport of solutions to the field site, which took approximately 2 hours.

The dates of tracer injection are given in Table 3-2.

Injection Procedure

Prior to injection of tracer, 20 ml samples were collected from each container for HPLC analysis at NMT. Tracer solution was injected into the aquifer by gravity feed. The containers were placed on stands approximately 1 meter high, giving approximately 2 meters of injection head. The tubing from the injection well was connected to the container outlet with a 'Y' connector. A 60 cc syringe was used to draw aquifer water up into the injection

line in order to purge the line of air, preventing the injection of air into the aquifer. Once the containers were drained, they were shaken to ensure all of the solution was injected. Following injection, 30 ml of de-ionized water per meter of injection tubing below the water table was injected into the lines in order to purge them of tracer solution.

The majority of injection took approximately 20 minutes, while some took up to one hour. Two injections took 2 hours; the 4-5 m interval for both I3 and I12. It is not clear why. Clogging of the screened injection ports may have been responsible, or these intervals may have been in a low permeability zone.

APPENDIX 2: TRACER INJECTION EXPERIMENT 2

The preparation and injection of tracer solution for the second experiment took place from December 17 to December 28, 1993. The injection program was carried out in 4 injection sessions, each session taking 2–3 days to complete. A total of 45 injections were performed over 15 injection well locations. Table A1–3 gives the date, location and depth of each injection. As Table A1–3 shows, all but 2 locations had 3 different injection depths. The exceptions were; 1) injection well I3 with 4 injection depths and 2) injection well I12 with only 2 injection depths.

All solutions were injected with a peristaltic pump except the top level of injection well I14. Here, the solution was poured onto the surface of the water table, which was approximately 0.5 meters below ground surface.

Tracer Solution Preparation

Each tracer solution consists of tracer chemical and 10.67 liters of de–ionized water. To all the Fluorinated Benzoic Acid tracer solutions, potassium hydroxide was added to neutralize the acidic nature of the tracer and to facilitate dissolution. The amounts of chemical used for each sample are listed in Table 1. All the chemicals were measured by weight ($\pm$.0005 grams). The 10.67 liter volume of water was also measured by weight ($\pm$0.125 lb.) and stored in individual containers.

To make an injection solution, 1 liter of de–ionized water was removed from a container and then mixed with the chemical tracer along with an equivalent molar amount of potassium hydroxide. When a pH of 7 was achieved and the solution visually appeared to be free of particulate matter, the tracer was considered to be dissociated. The measuring and combining of the chemicals with the de–ionized water took approximately 30 minutes. The mixing process (until dissociation was achieved) took between 30 minutes and 20 hours.

After the mixing process was completed, the 1 liter solution was poured back into the original container and mixed.

The Injection

Prior to the injection of the solution, the pump was used to draw aquifer water up into the injection lines to avoid the injection of air into the aquifer. A 20 ml sample bottle was filled with tracer solution from each injection container and then refrigerated until analyzed. The solution sample represent the initial concentration of the tracer injection solution. Once the sampling was completed, the remainder of the solution was pumped into the aquifer. A peristaltic pump was used to introduce the tracer into the aquifer for two reasons. Firstly, the rate of injection was controlled and all injection times would be uniform. Secondly, forcing the tracer down the injection tube also distributes the tracer more uniformly over the injection interval. Before the container was disconnected from the injection lines, it was shaken to ensure removal of all tracer solution. Immediately after the tracer injection, 30 ml of de-ionized water was injected per meter of tubing length to force all the tracer solution out

The only exception to the above process was the surface tracer emplacement at injection well I14. Here, a hole, 30 cm in diameter and 0.5 m deep, was dug to the top of the water-table and the tracer solution was slowly poured into the hole to avoid losing tracer to the unsaturated zone.

After each batch of injections, the containers including the valves were rinsed three times, each with one liter of de-ionized water. As well, all the injection connectors and fittings were flushed three times with de-ionized water.

APPENDIX 3: LABORATORY TRACER ANALYSIS

Samples from the pumping well and multilevel samplers were analyzed for the tracers using an HPLC separation technique developed by Bowman (1984; see also Bowman and Gibbens, 1992; Benson and Bowman, 1994). The basic methodological components of the isocratic HPLC separation include a phosphate-based mobile phase, constant pump rate, 25 μL sample injection, silica–based chromatographic column with Strong Anion eXchange (SAX) bonded phase, and UV detection. The separation mechanism uses mobile phase pH, ionic strength, and organic modifier content, to differentiate tracer retentiveness on an anion exchange column, by their degree of deprotonation, or acid dissociation constants (pK_a's).

The retentive property of an FBA in an anion exchange column can be related, by the Henderson–Hasselbalch equation, to mobile phase pH and the degree of dissociation for that given FBA:

$$K_a = \frac{[H][A]}{[HA]} \; ; \qquad pK_a - pH = \log[HA] - \log[A] \quad . \tag{A3–1}$$

An acid with a pK_a greater than mobile phase pH will remain mostly in undissociated form, while an acid with pK_a less than mobile phase pH will be largely dissociated,

$$\begin{array}{lll} pH < pK_a & pH = pK_a & pH > pK_a \\ [A] < [HA] & [A] = [HA] & [A] > [HA] \end{array} \quad . \tag{A3–2}$$

pK_a's for the FBA's are given in Table 3–1. At a mobile phase pH far in excess of the highest tracer pK_a, the FBA tracers are largely deprotonated and, since they are all monovalent in anionic form, largely undifferentiable on an anion exchange column. Thus, effective mobile phase pH is limited to suggested column manufacturer limits for silica-based columns ($2 > pH > 8$) and tracer pK_a range (2.7–3.8).

Previous Analyses of FBA Tracers

Pearson *et al.* (1992) used ion chromatography with conductivity detection in the separation of bromide, a difluorobenzoic acid, a trifluoromethyl-benzoic acid, and penta-

fluorobenzoic acid. The isocratic method included carbonate/bicarbonate-based mobile phase, constant pump rate, 25 μL sample injection, polyvinyl styrene IC chromatographic column, and UV detection. Although advantages of low detection limit capability were evident, lateral peak resolution suffered from very close elution times and coelution of the trifluoromethyl-benzoic acid with chloride. This method is a standard EPA sanctioned procedure for detecting bromide, since it is very effective in maintaining separation of bromide from chloride and nitrate. In fact, the New Mexico Bureau of Mines and Mineral Resources (NMBMMR) Chemistry Lab used this method to cross-verify our bromide recoveries.

Howe (1988; see also Boggs and Adams, 1992) employed an isocratic methodology in the separation of bromide, a difluorobenzoic acid, a trifluoromethyl-benzoic acid, and pentafluorobenzoic acid. A phosphate-based mobile phase was used, in conjunction with a constant pump rate, 25 μL sample injection, a silica-based SAX chromatographic column, and UV detection. Mobile phase pH was 4.0, notably in excess of the highest tracer pK_a. The separation was successful and stable because the tracers were unique enough in carbon atom content, net electron density, or hydrophobicity, to separate in spite of the fact they were largely deprotonated and all monovalent in anionic form. The principle difference between Howe's method (1988) and that of Bowman (1984) was the incorporation of a silica pre-column of the same size as the analytical column. The silica pre-column presaturated the mobile phase with silicate ions so as to protect the analytical column from acidic mobile phase induced dissolution. Both methods incorporated small guard columns packed with the same material as the analytical column. Bowman (personal comm., 1993) found that a silica pre-column did not significantly increase column life.

Stensrud *et al.* (1990) evaluated tracer data from 1988 field experiments at the Waste Isolation Pilot Plant (WIPP) site, near Carlsbad, NM. Four fluorobenzoic acids were used including one difluorobenzoic acid, two trifluoromethyl-benzoic acids and pentafluorobenzoic acid. An isocratic separation was used with a phosphate-based mobile phase containing tetrabutylammonium phosphate to induce ion pairing with the FBA, constant pump rate, 50

μL sample injection, octadecyl silane (C18) chromatographic column, and UV detection. The mobile phase pH was 6.4. The C18 column differentiated ion pairs on the basis of polarity.

Methods and Materials in the Chromatographic Analysis

The instrumentation sequence included the following: Waters Model 501 pump (1.0 to 2.0 mL/min), Perkin-Elmer ISS–200 Autosampler (25 μL sample injections), 4.6 mm × 250 mm stainless steel SAX column, Waters Model 481 UV variable wavelength detector (wavelength set at 205 nm), HP 3396II integrator, and a real-time linked Chrom-Perfect data management program in an Everex 386 PC. The SAX column brands were: Phenomenex, with Spherex 5 μm SAX particles; and Regis, with 5 μm Spherisorb S5SAX particles. Both the Phenomenex and the Regis SAX packings had 10-nm average pore size and were preceded upstream by an Alltech SAX guard cartridge. The differences between column and guard cartridge packing bonded phases had no distinguishable influence on comparative separation sequences and elution times.

The tracers were carried through the instrumentation sequence by a mobile phase with a given molarity of potassium dihydrogen phosphate buffer, a pH adjusted by an equimolar solution of ortho-phosphoric acid, and an addition of acetonitrile as an organic modifier. Increased phosphate anion concentration competes with the deprotonated tracers to invoke shorter tracer retention times on the column. Notably, phosphate concentration affects all tracers including bromide in the same way. Thus differences in mobile phase concentration would not rearrange elution sequence, but only have the effect of compressing or expanding the elution sequence. The acetonitrile organic modifier affects FBA retention time in a consistent manner, tending to cause more rapid elution of high pK_a FBA's, but has little effect on bromide. The interaction of pH with the anionic tracers involves degree of acid dissociation. Thus FBA elution is strongly affected by pH while bromide elution is not.

Sample Filtration

Samples were filtered because aquifer water invariably contained particles in excess of the 0.45 μm maximum threshold permitted in HPLC analysis. Before samples were routinely analyzed, a sample of aquifer water from the vicinity of the field experiment was filtered through a 13 mm in diameter, 0.45 micron nylon mesh filter, which was subjected to scanning electron microscopy (SEM) analysis. The NMT Materials and Metallurgical Engineering Dept. carried out the SEM analysis on a Hitachi HiScan HHS-2R, at 20 kv accelerating power. After applying a gold-palladium plasma coating to the filter, analysis of the filter element found abundant calcium carbonate, silica particles, as well as flocculated masses of iron hydroxides and clay minerals, all of which corresponded to previous findings (Nicholson *et al.*, 1983). Additionally, early background samples from wells of previous experiments had gelatinous masses of precipitate stained to a rusty brown color, derived from iron-oxidizing bacteria metabolism.

In comparing HPLC response peak-height based recoveries of standard and filtered standard solutions, the best response came from positive displacement filtration systems with low dead-volume. A 3 mm diameter syringe filter provided better tracer conservation than an 8.5 mm diameter centrifugal filter (all 0.45 μm nylon mesh). The 3 mm filters were set in hard plastic molds, while the 8.5 mm filters were hand-installed in re-usable flexible translucent polyethylene assemblies. 13 mm - and 25 mm - diameter syringe filters simply had more dead volume to facilitate solute retention upstream of the filter element.

Table A3-1 shows the mean detector responses, in terms of peak height, to an eight-component standard. One fifth of the milligram amount listed in Table A3-1 was dissolved in 100 mL of distilled-deionized water. A 25 mL subset was diluted on a 1:1 ratio to make 50 mL. From the 50 mL standard, 2 mL were analyzed without filtration, 2 mL using an 8.5 mm centrifugal filter, and 2 mL were analyzed after filtration through a 3 mm syringe filter. A centrifuge was used to spin the centrifugal filter assemblies until all the fluid had passed

through the filter membrane. The 3 mm syringe filters were used in conjunction with 2 mL polyethylene syringes. Each of the 2 mL standards was analyzed in triplicate, providing the bases for the reported means. The 100+% PFBA recovery illustrates detection imprecision.

Table A3–1. Mean response for filtrations of standards.

Tracer	3,4-DFBA	m-TFMBA	3,5-DFBA	2,3-DFBA	o-TFMBA	bromide	2,6-DFBA	PFBA
mg/L	14.4	10.6	10.1	10.2	10.8	11.2	10.2	17.2
8.5 mm centrifugal filt.	306481. (92.8%)	186573. (88.1%)	161009. (84.7%)	122973. (90.9%)	92362.4 (90.1%)	43040.1 (90.4%)	60888.2 (91.1%)	32304.0 (94.7%)
3.0 mm syringe filt.	328452. (99.4%)	211555. (99.9%)	172019. (90.5%)	130309. (96.4%)	97141.5 (94.8%)	45046.7 (94.6%)	63267.8 (94.6%)	34202.0 (100.%)
unfiltered	330349.	211801.	190025.	135234.	102507.	47603.4	66863.4	34104.7

Peak Height vs. Peak Area

The sample filtration experiments yielded several other subsidiary findings, specifically pertinent to calibration. Because of baseline noise, flow deviations, peak–tailing (inherent for very late eluting compounds or the use of an old column), or peak shouldering with interference effects, peak area integration was less consistent for analytical quantification than peak height. The greater degree of variation in reference points from which peak area could be integrated from run to run produced more variation in peak area. For this reason, peak height was used exclusively as the basis for quantifying detector response.

Sensitivity to pH

Table A3–2 summaries some separation sensitivity analysis results, in which the principal variable between different separation methods was mobile phase pH. Acetonitrile content was held at 18%, while phosphate concentration was tailored to column conditions. For the mobile phases with pH's: 2.60, 2.80, 3.47, and 3.52, the mobile phase molarities were 0.01, 0.02, 0.008, and 0.02, respectively. Again, phosphate concentration only had the effect of compressing or expanding the elution sequence.

At a mobile phase pH of 2.60 to 2.70, for instance, common ion effects inhibited fluorobenzoic acid dissociation and most of the FBAs were largely undissociated. The most significant exception was PFBA, about 50% was undissociated at pH 2.7. The elution sequence (see Table A3-2) reflected pK_a progression, in that the tracer with the highest pK_a yielded the earliest elution time. Only bromide could react with the column exclusively by anion exchange, and accordingly, it was the longest retained tracer. The problem with this mobile phase was the lack of adequate separation between 3,4-DFBA and m-TFMBA. Even if 3,4-DFBA and m-TFMBA were initially separated, they would be coeluting after 24 hours of analysis.

Table A3-2. Elution sequences as a function of pH.

Tracer	3,4-DFBA	m-TFMBA	3,5-DFBA	2,3-DFBA	o-TFMBA	KBr	2,6-DFBA	PFBA
pK_a	3.83	3.8	3.59	3.29	3.0	N/A	2.85	2.72
pH=2.60	1	2	3	4	5	8	6	7
pH=2.80	1	2	3	4	5	6	7	8
pH=3.47	1	2	3	4	6	5	8	7
pH=3.52	1	2	3	5	7	4	8	6

Between a pH of 2.70 and 2.80, bromide and 2,6-DFBA were very difficult to separate. When mobile phase pH was 2.80 to 2.85 (Gibbens, 1989), elution order again reflected pK_a progression. Bromide, however, eluted before 2,6-DFBA and PFBA, with pK_a's of 2.85 and 2.72 respectively. The problem with this mobile phase was, again, the lack of adequate separation between 3,4-DFBA and m-TFMBA. Bromide and nitrate were similarly affected. Column changes induced apparent coelution of bromide and nitrate after 12 hours and coelution of 3,4-DFBA and m-TFMBA after 24 hours.

Between a pH of 2.9 and 3.4, bromide and o-TFMBA were very difficult to separate. At a pH of 3.47, the pK_a progression was no longer adhered to, except by those tracers with pK_a's greater than 3.0. As the dissociated and ionic character of the FBAs increased, the pK_a-related retention mechanism decreased in influence, while polarity (see Table 3-1) appears to have increased in influence. After bromide the elution sequence was o-TFMBA,

PFBA, and 2,6-DFBA (see Table A3-2). From Table A3-2, it is apparent that the higher polarity of o-TFMBA may be responsible for it's longer retention time. Similarly, the longer retention of 2,6-DFBA vs. PFBA may indicate that the higher polarity of 2,6-DFBA has more influence on the retention mechanism than pK_a. This method was unfortunately used only as a first-time screening method on samples because it coeluted chloride and nitrate over o-TFMBA. The separation was found to be considerably more stable than the two previous methods. Identical mobile phases could be used in succession over 48 hours, before bromide would start coeluting with o-TFMBA, and apparently chloride, and nitrate.

At a pH of 3.52, bromide eluted ahead of 2,3-DFBA and the remaining elution sequence was rearranged to the following: 2,3-DFBA, PFBA, o-TFMBA, 2,6-DFBA. This method also apparently coeluted chloride and nitrate over o-TFMBA. But, identical mobile phases could be used in succession over 48 hours, before PFBA would start coeluting with o-TFMBA, chloride, and nitrate. At mobile phase pH's greater than 3.55, bromide and 3,5-DFBA coeluted, as well as 2,3-DFBA and PFBA.

Separation Optimization

Column deterioration, over extended periods of analysis and exposure to mobile phase, was most evident in gradual coelution of tracers with similar pK_a's, late elution times, or low pK_a's. Specifically, 3,4-DFBA and m-TFMBA have very similar high pK_a values, while bromide, 2,6-DFBA, and PFBA had late elution times and low pK_a values. Transient column conditions demanded different mobile phases over time, and frequent recalibration.

Column retention time drift was addressed by focussing on flow rate and pH of the mobile phase. At pH's <2 or >8.5, the silica beads and bonded phase in an SAX column break down (Snyder and Kirkland, 1979), the silica beads more so at pH's greater than 8.5. No separations were observed at pH > 3.55, since the FBAs were largely deprotonated and thus undifferentiable by degree of dissociation, nor, as mentioned earlier, by polarity differences. At pH's of 2.6-2.8, downward adjustments in mobile phase concentration were required af-

ter 24 hours of analysis, in order to re-expand shrinking and potentially overlapping retention times. Hence, pH was increased from 2.8 to 3.5. The separations at pH<2.85 were optimized with a flow rate of 2.0 mL/min. A flow rate of 1.0 mL/min or less did not induce appreciable separation between 3,4–DFBA and m–TFMBA, while increasing analysis time for the complete tracer suite from 15 min to 30 min. Unfortunately, most SAX columns deteriorate prematurely at high flow rates (Phenomenex recommendation: 0.6 mL/min; Regis recommendation: 0.4 mL/min). At a pH of 3.5, a flow rate of 1.0 mL/min, and a relatively lower starting molarity, downward adjustments in mobile phase concentration were usually required after 48 hours of analysis. As mentioned before, these advantages were nullified by the apparent coelution of chloride and nitrate with o–TFMBA.

Single component tracer standards were tested before each mobile phase was used. Secondly, our HPLC analysis involved external calibration. A detector response to a calibration standard suite under one mobile phase condition would thus be exclusively applied to the five samples directly preceding and following that suite. Trying to impose the condition of exact reproducibility at the status quo would have effectively shortened column life to one batch of mobile phase.

To minimize column costs, a discount manufacturer (Phenomenex) was chosen that recycled column bodies. As mentioned previously, differences between column bonded phases had no distinguishable influence on comparative separation sequences or elution times.

Other Issues in Separation Analysis

Other aspects tested over the course of routine analysis were: analytic accuracy, replicate analyses, biodegradation of tracers, and misidentification of tracers. Most of these issues are covered in Section 3. Part of that discussion refers to bromide cross–verification analysis using ion chromatography (IC) and phenol colorometric analyses, performed independently by the NMBMMR Chemistry Lab. The phenol colorometric analysis were eventually quali-

fied by NMBMMR as unreliable due dilution error and inadequate sample volume. The IC method, involved a carbonate/bicarbonate mobile phase (1.8 mM Na_2CO_3 and 1.7 mM $NaHCO_3$), 88 μL sample injections, a Dionex 4000i pump (2.0 mL/min) and UV detector (set at 208 nm), in conjunction with a 4.6 × 100 mm Hamilton PRP–X100 polyvinyl styrene column, and a Millipore–Waters 745 integrator. The method successfully separated chloride and nitrate from bromide by 2 and 3 minutes of retention time, respectively. The IC results for bromide measurement appear to be consistently 50–60% lower than the SAX–HPLC results. This issue is still under investigation. The IC results did not appear to increase the resolution of the separate bromide arrivals or resolve the interference effects at the 6, 7, and 8 m pumping well intervals.

References

Benson, C. and Robert S. Bowman. 1994. Tri- and tetrafluorobenzoates as nonreactive tracers in soil and groundwater, Soil Sci. Soc. Am. J., 58, 1123–1129.

Boggs, J.M. and E.E. Adams. 1992. Field study of dispersion in a heterogeneous aquifer 4. Investigation of adsorption and sampling bias, Water Resour. Res., 28(12): 3325–3336.

Bowman, R.S. 1984a. Analysis of soil extracts for inorganic and organic tracer anions via high performance liquid chromatography, J. Chromatogr., 285: 467–477.

Bowman, R.S. and J.F. Gibbens. 1992. Difluorobenzoates as nonreactive tracers in soil and ground water, Ground Water: 30(1), 8–14.

Gibbens, J.F. 1989. An evaluation of several fluorinated benzoic acids for use as soil and ground water tracers, Unpublished M.S. thesis, Hydrology Program, New Mexico Inst. of Mining and Tech., Socorro, NM.

Howe, L. 1988. Tennessee Valley Authority - Quality Assurance Procedure, No. NRS–LB–AP–30.418.8, Section 8.3.

Nicholson, R.V., J.A. Cherry, and E.J. Reardon. 1983. Migration of contaminants in groundwater at a landfill: A case study 6. Hydrogeochemistry, J. Hydrol., 63: 131–176.

Pearson, R.J., S.D. Comfort, and W.P. Inskeep. 1992. Analysis of fluorobenzoate tracers by ion chromatography, Soil Science Society of America Journal, 56(6), 1794–1796.

Snyder, L.R. and J.J. Kirkland. 1979. Introduction to Modern Liquid Chromatography, 2nd ed., John Wiley & Sons Inc., New York, 863 pp.

Stensrud, W.A., M.A. Bame, K.D. Lantz, and G.J. Saulnier, Jr. 1990. WIPP Hydrology Program, Waste Isolation Pilot Plant, southeastern New Mexico, Hydrologic Data Report #8. Sandia National Laboratories, Contractor Report SAND89–7056

This dissertation is accepted on behalf of the faculty of the Institute by the following committee:

John L. Wilson
Adviser

12/2/94

Fred M. Phillips

William C. Hanson

Date

I release this document to New Mexico Institute of Mining and Technology.

William R. Kinsfather — December 2, 1994

Students Signature — Date